Loughborough University

Loughborough University
Institutional Repository

Optimisation and control of thermal recovery for a hybrid vehicle

This item was submitted to Loughborough University's Institutional Repository by the/an author.

Citation: © Sandra Hounsham

Additional Information:

- A Doctoral Thesis. Submitted in partial fulfillment of the requirements for the award of Doctor of Philosophy of Loughborough University.

Metadata Record: https://dspace.lboro.ac.uk/2134/6129

Please cite the published version.

Loughborough University

This item was submitted to Loughborough's Institutional Repository (https://dspace.lboro.ac.uk/) by the author and is made available under the following Creative Commons Licence conditions.

creative commons

COMMONS DEED

Attribution-NonCommercial-NoDerivs 2.5

You are free:

- to copy, distribute, display, and perform the work

Under the following conditions:

Attribution. You must attribute the work in the manner specified by the author or licensor.

Noncommercial. You may not use this work for commercial purposes.

No Derivative Works. You may not alter, transform, or build upon this work.

- For any reuse or distribution, you must make clear to others the license terms of this work.
- Any of these conditions can be waived if you get permission from the copyright holder.

Your fair use and other rights are in no way affected by the above.

This is a human-readable summary of the Legal Code (the full license).

Disclaimer

For the full text of this licence, please go to:
http://creativecommons.org/licenses/by-nc-nd/2.5/

Optimisation and Control of Thermal Recovery for a Hybrid Vehicle

By

Sandra Hounsham

Doctoral Thesis

Submitted in partial fulfillment of the requirements for the award of Doctor of Philosophy of Loughborough University

December 2008

© by Sandra Hounsham 2008

Abstract

The automotive industry is currently driven to reducing fuel consumption in internal combustion (IC) engines and hence much research is being done into alternative fuels and power sources. Thermal energy recovery from IC engines has proved to be of considerable interest within the automotive industry. The motivation is that fuel consumption can be reduced with a minimal effect on the "host" technology of the vehicle.

This thesis reports on a project that aimed to investigate the architecture and control of a thermal energy recovery system, working towards proving this novel system concept. This was achieved by the use of software modelling techniques and experimental tests on various components of the system, namely heat exchangers and steam expanders. Various modelling toolboxes were used to model a) a hybrid vehicle configuration and b) steam expanders. The hybrid vehicle modelling began as a basic model to demonstrate the hybrid application and configuration of the steam system, and was further developed to control and optimise the system in such a way that the fuel economy, the overall efficiency of the IC engine and the heat recovery system were all maximised. Standard drive cycles were used to run the hybrid vehicle models. The steam expander modelling was performed in order to validate the results from a series of experimental tests and also to deduce if the expander models could be scaled up to predict results for larger expanders.

The fuel consumption for the initial modelling showed a reduction of between 8% and 36%, depending on drive cycle and modelling toolbox used. With the development of a simple PID controlled system, the fuel consumption was further reduced resulting in a range of 26% to 41%, again depending on drive cycle and modelling tool box. The experiments on steam expanders point to a uni-flow configuration being the most suitable. The expander modelling presents the groundwork for developing expander models to be used for validating the experimental results; again the uni-flow arrangement gave the most promising results.

This thesis presents the results and draws conclusions from each project step; these conclusions are summarised together with some recommendations for future work.

Contents

Nomenclature

APU	Auxiliary Power Unit
BDC	Bottom Dead Centre
CVT	Continuously Variable Transmission
DISI	Direct Injection Spark Ignited
ECMS	Equivalent Consumption Minimization Strategy
EM	Electric Motor
FCEV	Fuel Cell Electric Vehicles
FHDS	Federal Highway Driving Scheme
FTP	Federal Test Procedure
FUDS	Federal Urban Driving Scheme
GPS	Global Positioning System
GT	Gamma Technologies
GT-SUITE	Gamma Technologies modelling software suite
HEV	Hybrid Electric Vehicles
HP	High Pressure
IC Engine	Internal Combustion Engine
LP	Low Pressure
LQ	Linear Quadratic
LQR	Linear Quadratic Regulator
MPC	Model Predictive Control
MIMO	Multiple Input Multiple Output
m_dot_exhaust	mass flow rate of exhaust gas
m_dotw_pred	mass flow rate of water, predicted value
m_dots	mass flow rate of steam
NEDC	New European Drive Cycle
n	Speed
PID	Proportional Integral Differential (Controller)
PRBS	Pseudo Random Binary Sequence
PSAT	Powertrain Systems Analysis Toolkit
P_act	Actual pressure
P_dem	Pressure demand

P_downs	Pressure downstream of the expander
P_ups	Pressure upstream of the expander
Q_{in}	Heat input
Q_{out}	Heat output
QSS-TB	Quasi-Static Simulation ToolBox
RTC	Real-Time Control
SI	Spark Ignited
SISO	Single Input Single Output
SIT	System Identification Toolbox
SOC	State Of Charge
SQA	Steam Quality Analyser
T_{ci}	Temperature of cold fluid, input (heat exchanger)
T_{co}	Temperature of cold fluid, output (heat exchanger)
TDC	Top Dead Centre
TGT	IC Engine torque demand (N m)
T_{hi}	Temperature of hot fluid, input (heat exchanger)
T_{ho}	Temperature of hot fluid, output (heat exchanger)
Torq_act	Actual torque
Torq_dem	Torque demand
T_cond	Condenser working temperature
T_exhaust	Exhaust gas temperature
T_sat/T_{sat}	Saturation temperature
T_ueb	Gearbox torque (N m)
T_w	Water temperature
UDDS	Urban Dynamometer Driving Schedule
US06	United States Highway Drive Cycle
W_{in}	Work input
W_{out}	Work output
w_ueb	Gearbox speed (rad/s)
α	expander valve cut-off ratio
α_pred	expander valve cut-off ratio, predicted value

Publications

"The Controllability of Vapour Based Thermal Recovery Systems in Vehicles"
R. Stobart, S. Hounsham, and R. Weerasinghe, *SAE paper*, vol. 2007-01-0207.
Presented at the SAE World Congress 2007, Detroit, USA.

"Modeling heat recovery systems for hybrid vehicle applications"
S. Hounsham, R. Weerasinghe, and R. Stobart, *IMechE, VTMS8 paper*, vol. 2007.
Presented at IMechE, Vehicle Thermal Management Systems 8 conference, 2007, Nottingham, UK.

"Energy Recovery Systems for Engines"
S. Hounsham, R. Stobart, A. Cooke and P. Childs, *SAE paper*, vol. 2008-01-0309.
Presented at the SAE World Congress 2008, Detroit, USA.

"Thermal recovery of I.C. Engines: A Research Overview"
A. Cooke, P. Childs, R. Stobart and S. Hounsham
Submitted to the *International Journal of Energy* 2008. Under review at time of submission of this thesis.

Acknowledgements

This project was supported by the UK Engineering and Physical Sciences Research Council under Grant reference GR/T19810/01.

I would like to start by thanking my supervisor Professor Richard Stobart whose knowledge and guidance had an enormous impact on this work. Also many thanks to my second supervisor Professor Peter R.N. Childs, who made an important contribution to the project and always provided sound advice on the planning and development of this thesis. Thanks also go to Dr. Adam Cooke, who came into the project late, but certainly made up for it by being a breath of fresh air and someone who would finally explain those pesky thermodynamic issues to me! Richard, Peter and Adam all motivated me in different ways over the course of my studies and I am indebted to them all.

Additionally, a big shout of thanks to the University of Sussex technicians that worked with me on this project - Ian Wallis and Barry Jackson. As well as being a fountain of knowledge on engine test facilities and experiments they were also fun to work with. Also thanks to Spirax Sarco ltd in Cheltenham for the use of their steam generator for the early experiments and also for providing us with support and valves for the heat exchanger tests.

On to my non-academic acknowledgements; I would like show my appreciation to my family and friends for their continued support and encouragement and finally, but most importantly to my partner, Mary, who supported me, emotionally and financially, and gave me the extra strength and motivation needed to complete these studies.

I would like to dedicate this work to my late father, Anthony Robert Hounsham.

1 Introduction and literature review

1.1 Introduction and outline of the thesis

The research that forms the foundation for this thesis was carried out as part of a joint project between the University of Sussex and Loughborough University called the HYSTOR project. This project was supported by the UK Engineering and Physical Sciences Research Council under Grant reference GR/T19810/01.

This chapter aims to give an overview of the project. The background and the motivation for the research will be discussed along with a basic introduction to the HYSTOR system concept. The technologies and theoretical background are also covered. A literature review of the current research relating to the fields of thermal recovery, hybrid vehicle modelling and control will be presented. Finally the aims and objectives of the thesis will be detailed.

Chapter 2 details the simulation tools and architecture that were used to model various hybrid configurations. The different configurations, developed using two software modelling toolboxes, QSS-TB and PSAT, are presented along with a description of how the components of the HYSTOR system were developed and verified using the Matlab and Simulink environment. Details of the drive cycles used to run the simulations are also presented in this chapter. Results for fuel consumption are tabulated for each of the modelling tools used.

A detailed study of the expander testing is presented in Chapter 3; small (circa 4 cc) expanders were tested with compressed nitrogen and steam to determine a suitable expander for the system.

The development of expander simulations using an engine modelling toolbox, GT-SUITE, is described in Chapter 4. The results of the expander tests are graphically presented along with a discussion on how the results could be verified using GT-SUITE simulations and if they could be used to a) predict results for larger expanders and b) predict results for different media sources.

Chapter 5 describes the development of a control system for the thermal recovery and energy management of the HYSTOR concept.

Optimisation strategies are presented and discussed in Chapter 6.

Finally Chapter 7 presents a summary of the thesis conclusions, along with a review of the thesis objectives ending with some discussion on future recommendations for further work.

1.2 Reducing automotive emissions and fuel consumption

There are increasing environmental concerns with respect to exhaust emissions from internal combustion (IC) engines, such as particulate matter and nitrogen oxides that both damage air quality and contribute to the greenhouse effect. The total effect of IC engine emissions and emissions from other sources, such as industrial plants, is potentially contributing to global warming.

Environmental concerns have led to the development of strict governmental regulations for restricting emissions of carbon monoxide (CO), carbon dioxide (CO_2), nitrogen oxides (NO_x), and unburned hydrocarbons (HC). In Europe the Euro framework of regulation of test specifications regulates tailpipe emissions through the Emission Standards for the European Commission [1].

The Commission has recently proposed legislated limits on CO_2 emissions as a reaction to the failure of the voluntary agreement. The industry responded well by increasing diesel production. However, the progress towards the 120 g/km fleet average had evidently stalled by early 2006. The Commission is currently formulating the new legislation that will impose limits and fines on car companies that fail to comply.

A further reason for lowering IC engine emissions is due to their contribution to air pollution in urban areas which has been cited as having a detrimental effect on public health (for example asthma). The Californian Air Resources Board (CARB - [2]) gives a good overview of what causes air pollution and what effect it can have on public health. CARB cites that asthma cases in California have risen by 75% since 1980 and it is thought that some of this increase is attributed to a decrease in air quality. CARB has a research division that is attempting to discover the real nature of the connection between air pollution and asthma, especially with respect to children’s health.

1.2 Reducing automotive emissions and fuel consumption

There is also a drive towards reducing oil dependence and hence, a reduction in fuel consumption. This is due to the depletion of available oil supplies, commonly known as 'the oil crisis'. There is a lack of obtainable oil fields/reserves left in the world with many fields either hard to exploit (for example Siberia) or found in countries of a volatile political nature (for example Iraq) and so cannot be relied on with robust confidence. British Petroleum (BP) provides a statistical review of world energy [3]. In this report the world's oil reserves, production and consumption are presented. It is particularly interesting to note that the areas consuming large amounts of oil and the areas producing large amounts are not necessarily the same, meaning vast amounts of oil are imported and exported everyday, which is leading to more fuel consumption and emissions involved with the transportation. The production/consumption data for 2007 is visualised in Figure 1-1.

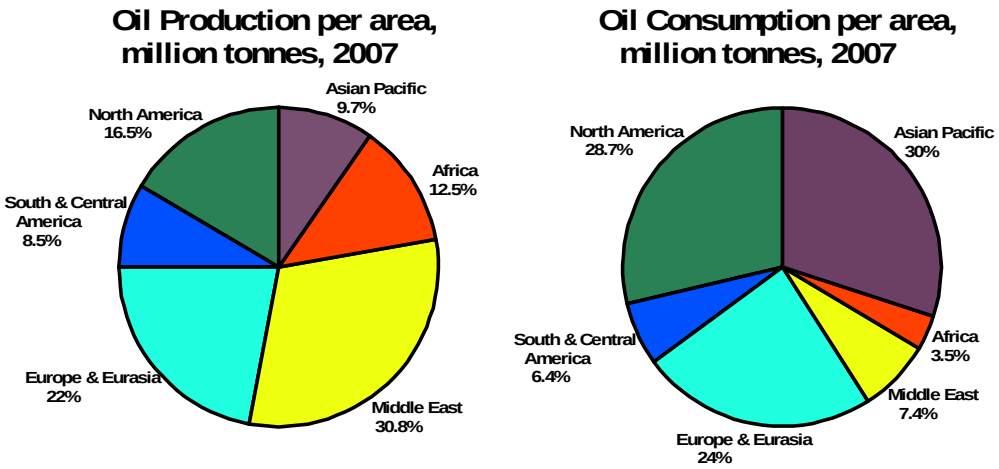

Figure 1-1 Oil production and consumption, million tonnes, per area, 2007 [3]

The need to reduce oil dependence and fuel consumption is particularly relevant within the current climate with the increasing concern over the rising price of barrels of oil and is an important driver in reducing use, and size, of passenger vehicles, even in America, previously seen as a gas-guzzling nation.

With these combined issues of the need to cut fuel consumption and reduce emissions from IC engines, the majority of the automotive industry is currently investing in research for alternative energy sources and technologies that address these issues. The Energy Foundation is a partnership that funds research into fuel efficiency and renewable energy and their 2002 annual report [4] provides reasons for cutting emissions and fuel consumption.

For automotive applications, the main research into recovering energy is electrical via a motor/generator/battery configuration in the shape of Hybrid Electric Vehicles (HEVs). Examples of HEVs that are now available on the market are the Toyota Prius and the Honda Civic Hybrid, additionally other automotive companies are planning development and production of HEVs, for example Ford, BMW, Nissan, Mazda. A HEV configuration uses less fuel than a conventionally fuelled vehicle and, when running on electric power only, cuts emissions, and consumption, to zero.

Alternative fuel research includes fuel cell technology and fuel cell electric vehicles (FCEV). Both HEV and FCEV technologies use electrical storage via battery, flywheel or super capacitor. The HEV configuration is heavily reliant on the electric battery as energy storage and research is being carried out to improve the performance, life and reduce the cost of the battery to make HEVs more desirable and affordable. Lithium-ion batteries are currently of great interest and a number of announcements by car manufacturers have been made. General Motors (GM) Volt series hybrid concept is typical. The use of fuel cells is an emerging technology and with increasing research, could prove to be a cost effective and efficient alternative to HEVs. Some of the research presented in the literature review of Sections 1.4 and 1.5 has been carried out on fuel cell hybrid applications. As well as HEVs and FCEVs, there is a drive to research further alternatives; one of the emerging technologies is heat recovery from the IC engine exhaust waste. The energy recovered can be turned into electric energy, using thermo-electric devices, or to use the recovered heat to generate thermal energy in the form of steam. It is this latter idea that the HYSTOR system concept, and hence this thesis, is based upon.

1.3 Heat recovery and the HYSTOR system concept

The HYSTOR system concept explored in this project utilises the heat that is rejected through the IC engine exhaust. A typical IC engine can waste up to 70% of the fuel energy as heat, with up to 44% of this is via the exhaust [5]. Figure 1-2 shows the distribution of heat in a small (1.4 litre) IC engine.

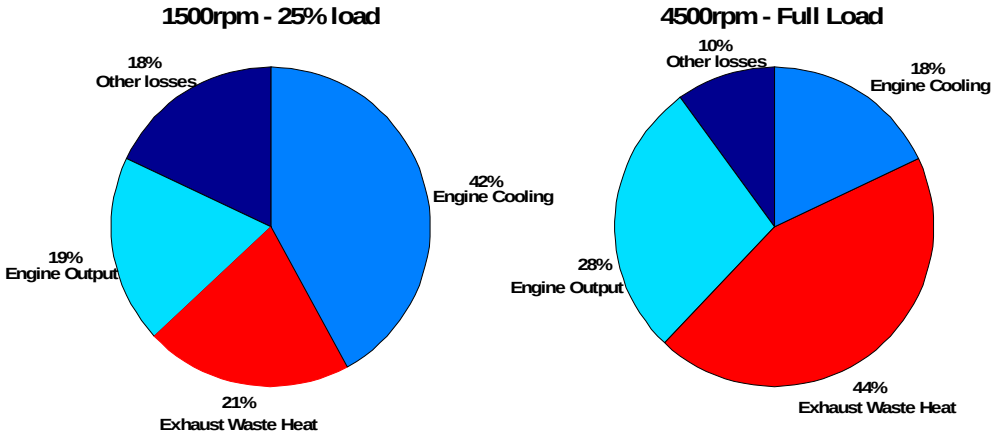

Figure 1-2 Heat balance of a 1.4l spark ignition engine [5]

As can be seen in Figure 1-2, the available heat for recovery is in between 20% and 44%, depending on speed and load. If the system were to be part of the cooling system for the IC engine, then this could increase to around 60%.

The recovered energy will be stored in the form of both hot water at saturation conditions and water vapour, which has been generated by recovering the heat from the exhaust gas waste. A heat exchanger was developed by the project for this purpose. The steam will then either be used (expanded) immediately or stored in an accumulator and expanded, when required, to generate work. A suitable expander to be used for this purpose was investigated during the project.

The initial HYSTOR system concept was presented by Bayley [6]. The merits of using a vapour expander in a hybrid configuration are explained and the paper details the use of a steam accumulator and vapour expander in a parallel hybrid vehicle. The overall system configuration for the original concept is shown in Figure 1-3.

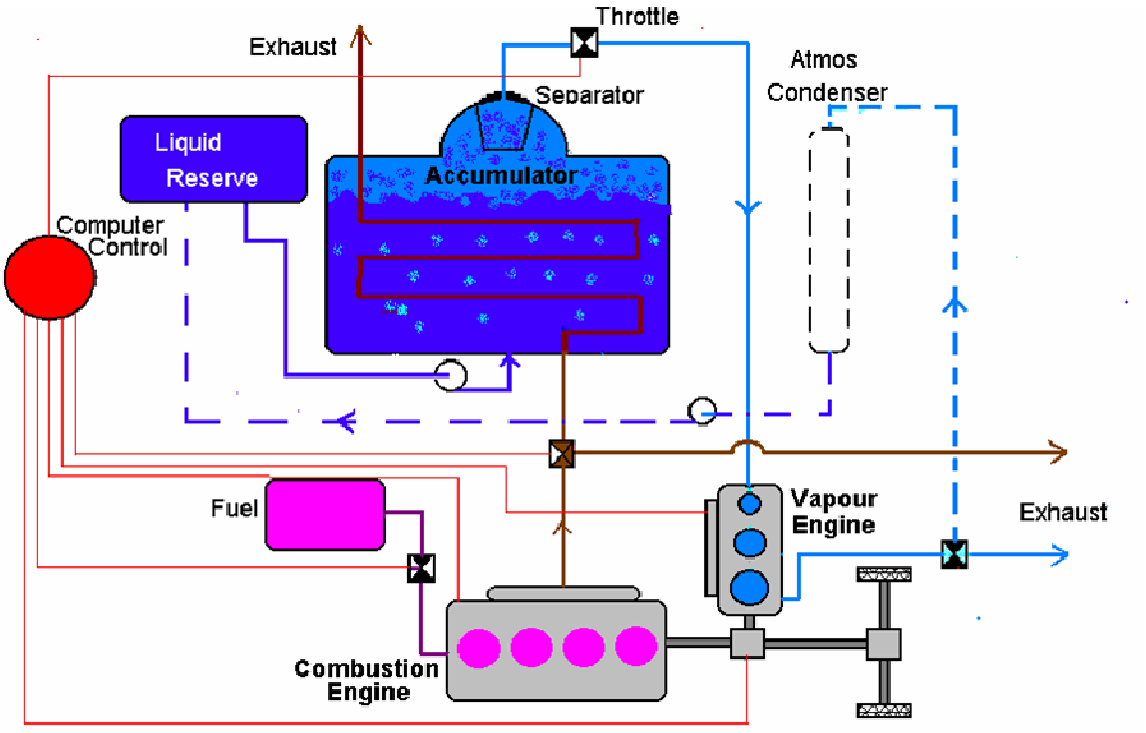

Figure 1-3 Concept configuration of a parallel steam hybrid vehicle [6]

The main points for this system are the parallel coupling of the IC engine and vapour expander, and also the computer control which performs overall, supervisory control, and individual control of the system components. This paper uses drive cycles to predict the fuel consumption reduction for such a system; the drive cycles are FUDS (US Federal Urban Driving Scheme) and FHDS (US Federal Highway Driving Scheme), which are now replaced by FTP-75 [7] and US06 [8], respectively. The paper compares the vapour system with a gas turbine system, a diesel system and a diesel hybrid system, using these comparisons it is suggested that there will be a considerable reduction in fuel consumption

for the FUDS cycle (up to 75% when comparing gas turbine to vapour) but little reduction for the FHDS cycle (approximately 12.5% reduction).

Stobart & Weerasinghe [9] further review techniques for recovering heat from exhaust gases using a bottoming cycle such as the Rankine cycle. Devices used for such a process are presented – expanders and condensers, for example. This paper goes on to develop a simple model using QSS-TB (Quasi Static Simulation ToolBox, see Section 1.5 for more information). This simple model was used to demonstrate the expected fuel consumption reduction when implementing the heat recovery system. The basis of the heat recovery system uses the closed loop power cycle based on the evaporation and expansion of a working fluid commonly known as the Rankine cycle, a T-s diagram and a system diagram are presented, in Figure 1-4.

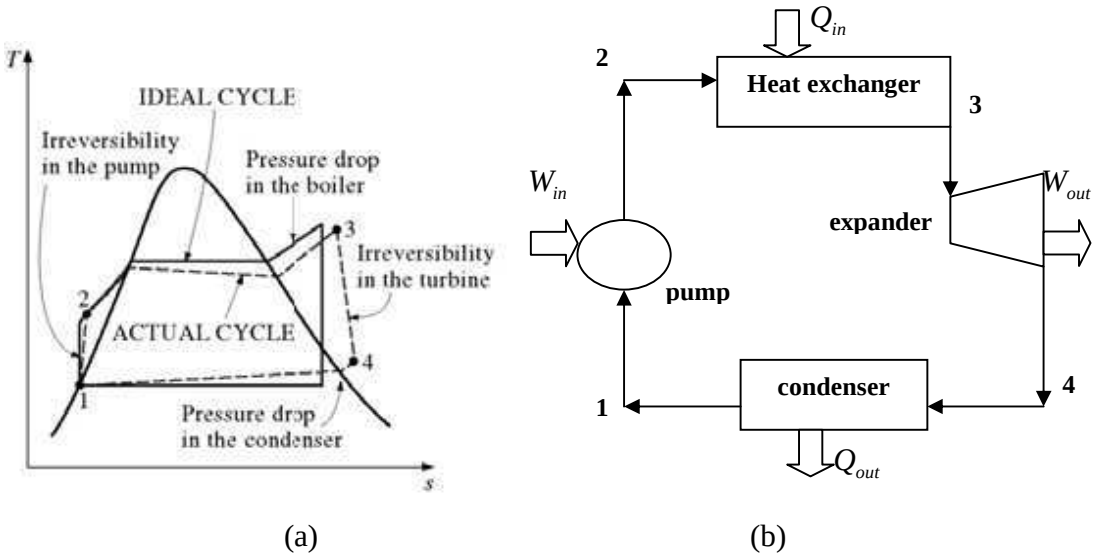

(a) (b)

Figure 1-4 Rankine cycle, (a) T-s diagram from [10], (b) schematic

This thermodynamic cycle will further be investigated and modelled in this thesis. An ideal Rankine cycle is made up of four sequential processes, these are:

1-2: Isentropic compression, this takes place in the pump;

2-3: Constant pressure heat addition in the boiler/accumulator;

3-4: Isentropic expansion, this takes place in the expander;

4-1: Constant pressure heat rejection in the condenser.

1.3 Heat recovery and the HYSTOR system concept

The control issues for the HYSTOR concept are discussed by Stobart et al. [11] using the notions of availability and exergy for the system. This paper develops the availability using a system with the temperature points as shown in the temperature distribution diagram illustrated in Figure 1-5.

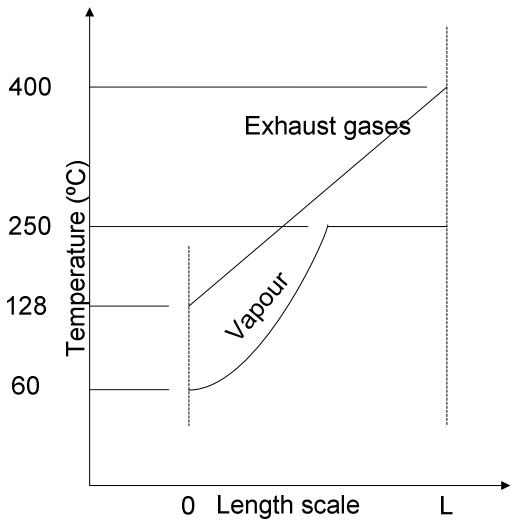

Figure 1-5 Temperature distribution for the heat exchange process [11]

Referring to Figure 1-5, the exhaust temperature enters the heat exchanger at 400°C, and falls to 128°C on exit, the water is heated to saturation temperature of 250°C, corresponding to a working pressure of 40 bar. The availability for such a temperature distribution, with an isentropic efficiency of 80%, is calculated to be 150 kJ/kg. The paper concludes that the expected steam sub-system efficiency should be within 20%. Stobart [12] further investigates the availability approach to thermal recovery concluding that acceptable efficiencies are available at safe operating pressures – nominally 32% at 20 bar.

El Chammas & Clodic [5] also discuss the use of bottoming cycles for recovering thermal energy from an exhaust pipe. The expander of choice was a steam turbine. Different fluids, along with water, were investigated for their suitability. Whereas alternative thermodynamic fluids may give better efficiencies, there were instability and environmental issues with them. This paper also defines a new factor called “Achievable Carnot Factor”

(ACF) in order to compare different fluids. The ACF calculates, for each fluid, the ratio of a standard Rankine cycle efficiency to the maximum ideal Carnot efficiency. In this way the ACF provides a better analysis than efficiency on its own when analysing the performance of the various working fluids considered within the paper. The example given is for and organic fluid R-245ca (also known as 1,1,2,2,3-pentafluoro-propane) with an efficiency of 16% when used in a Rankine bottoming cycle, but when calculating the ACF, the result is that the Rankine cycle can deliver up to 53% of the maximum possible work, which can lead to a different conclusion on the suitability of the working fluid.

Publications from the automotive industry, such as Honda and BMW indicate the interest in this area. From his keynote address at the Institute of Mechanical Engineers (IMechE), VTMS8 (Vehicle Thermal Management Systems) conference, Rump [13] announced that fuel consumption can be improved by up to 20% using the BMW turbo-steamer concept. Endo et al. [14] presented Honda's concept for a heat management system, including heat exchanger design and choice of expander. This paper reports a thermal efficiency increase from 28.9% to 32.7%, which equates to an overall improvement of 13.2%. Exact fuel consumption improvements were not given.

The initial system configuration shown in Figure 1-3 was superseded by the configuration shown in Figure 1-6 which has some small, but important alterations. This configuration shows the high pressure (HP) and low pressure (LP) water feeds and also includes the system as part of the engine cooling control.

1.3 Heat recovery and the HYSTOR system concept

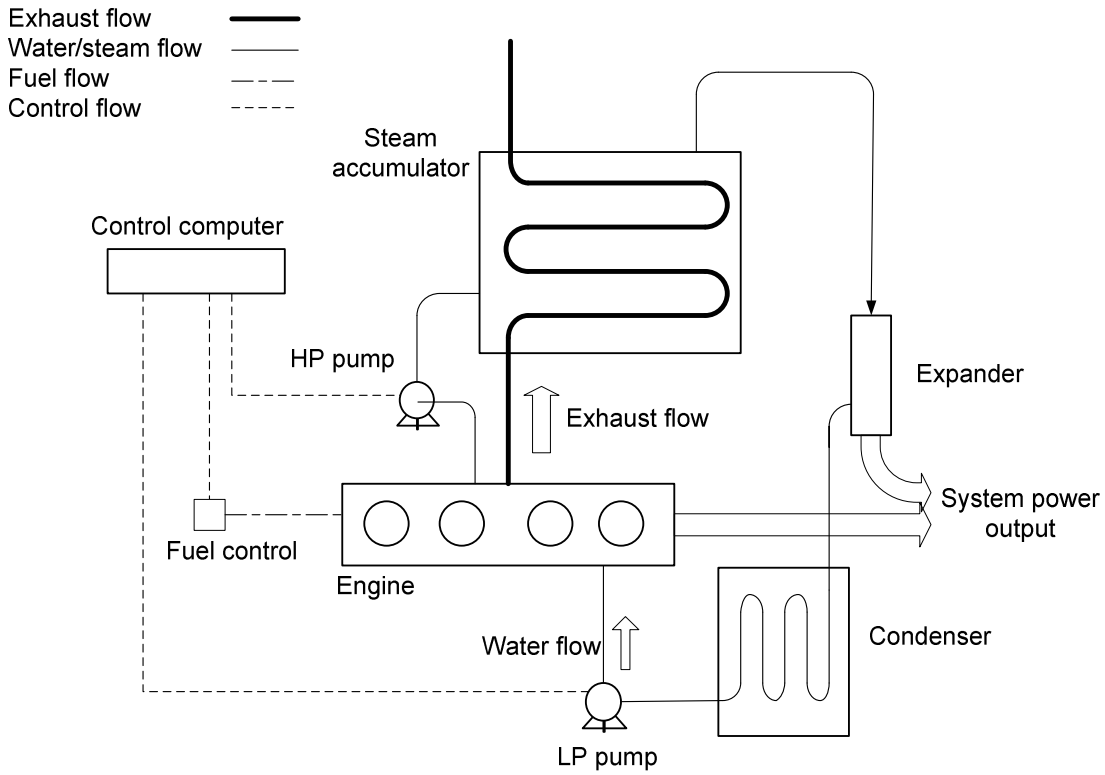

Figure 1-6 Overall HYSTOR system concept

The overall HYSTOR system concept is described as follows; heat is recovered, via a heat exchanger, from the IC engine exhaust and stored in the form of accumulated hot water and steam. Shaft work is produced by the steam expander and used to either:

(a) Assist the IC Engine driven vehicle, by adding torque to the driveshaft, thereby reducing fuel consumption and emissions, accumulating any excess energy as required;

(b) Drive an auxiliary power unit (APU), if the energy is not required by the vehicle (for example the vehicle is braking or idling) to ensure the energy is not wasted, any excess energy can be used generate electricity and charge an electric storage device;

(c) Provide all the required torque to the drive shaft resulting in emissions free driving for inner-city areas.

The exhausted, expanded, steam will then be condensed and passed through the engine cooling system or circulated directly to a pump before being fed back into the heat exchanger.

The choice of how best to utilise the steam expander generated work, items (a), (b) or (c) in the previous list, will depend upon the architecture developed or the mode that the vehicle is being driven in. Possible labels for these modes, corresponding to the previous list, are:

(a) Motor Assist Mode;
(b) Charge Mode;
(c) Steam Only Mode.

These modes correspond to the HEV operating modes detailed in the next section.

1.4 Control and optimisation strategies for hybrid vehicles

Much research has been documented on the topic of HEV energy management and control of the powertrain and energy management. As stated previously, the HYSTOR system concept is the use of a steam system as an alternative power source in a hybrid vehicle. The storage (battery) and driver (electric motor) of the HEV configuration is analogous with the accumulator and expander, respectively, of the steam hybrid configuration.

Some of the methods for controlling HEVs and FCEVs mentioned in this section could be applied to the HYSTOR concept and so are further researched for their applicability to the heat recovery concept.

An overview of the power management and control requirements of HEVs is given by Chau & Wong [15], the four main HEV configurations were presented and discussed. These configurations are:

(a) Series Hybrid;
(b) Parallel Hybrid;
(c) Series-Parallel Hybrid;
(d) Complex Hybrid.

These configurations were discussed in detail within the paper, along with the power control strategies that need to be employed for each configuration. This paper also highlights some key issues that need to be considered when designing the control strategy for a hybrid vehicle, these issues are related to HEVs, but can be considered for the HYSTOR configuration, the issues are as follows:

(i) Optimal Engine Operating Point – on the torque/speed plane;
(ii) Optimal Engine Operating Line – for different power demands;
(iii) Optimal Engine Operating Region – with respect to fuel efficiency;
(iv) Minimum Engine Dynamics – to regulate the engine speed to avoid fast fluctuations;

(v) Minimum Engine Speed – low speeds usually mean low fuel efficiency so a threshold should be derived to avoid this;

(vi) Minimum Engine Turn-on Time – to avoid repeated turning on and off on the IC engine as this could result in low fuel efficiency;

(vii) Proper Battery Capacity – so that the battery is used efficiently (this could relate to steam accumulator capacity for the HYSTOR concept);

(viii) Safety Battery Voltage – to prevent damaging the battery (this could relate to steam pressure for the HYSTOR concept, the pressure should be kept at a safe level not just for the steam accumulator, but also for passenger safety);

(ix) Relative Distribution – of power generated by the IC engine and the electric motor correctly distributed over drive cycles (this could relate to the steam expander for the HYSTOR concept);

(x) Geographical Policy – if electric only driving is required for emissions free driving (this could relate to steam only driving for the HYSTOR concept).

On a similar note, Walters et al. [16] gave an overview of various powertrain configurations either in production (at the time of writing – 2001), for example the Toyota Prius and Honda Insight, or under development, the GM Precept, Ford P2000 and DaimlerChrysler ESX3. These HEV configurations are compared with conventional vehicle configurations, namely the Chevrolet Impala, DaimlerChrysler Concorde, Ford Taurus, Honda Accord and Toyota Camry.

Hochgraf et al. [17] introduce and discuss two different control strategies for a series HEV configuration, these control strategies are:

- *Power-tracking* where the engine/alternator output follows the power demand from the road/driver;
- *Load-Levelling* where the output of the engine/alternator is constant and any excess power is used to charge a battery.

The characteristics and efficiencies were examined for each strategy and it was concluded that the Load-Levelling strategy yields better fuel efficiency. This could relate to the

HYSTOR concept in that the output from the IC engine and steam expander, coupled, is constant and any excess energy is used to generate steam which is stored in an accumulator for use when the power demand increases.

These strategies are also mentioned by Waltermann [18], who additionally presents a hierarchical control structure, with respect to a series HEV configuration, which consists of an upper level of outer, or global, control loops cascading down to inner, or local, control loops. The local control loops are faster than the global control loops because the dynamics are higher. The upper level structure, the global loop(s), is used for developing optimisation. The lower, local, levels consist of the real components, for example IC engine, generator, battery and so on, whilst the upper levels include the energy management and drivetrain management. This thinking could easily be applied to the HYSTOR concept, with the local controls relating to control of the system components, for example, the pump and expander. The global control will relate to supervisory control of the overall system and this will include optimisation algorithms.

Wittmer et al. [19] discuss operating modes with respect to a parallel HEV configuration. A set of clutches were employed within the drivetrain which determine how the IC engine and the Electric Motor (EM) are connected within the powertrain, to the flywheel or directly to the transmission. This paper also discusses control strategies that are as follows:

(a) Electric Based;
(b) Fuel Based;
(c) Combination of Fuel and Electric Based.

These control strategies were developed and used to determine which strategy is the best for achieving the optimum fuel efficiency for the HEV vehicle.

Zhang et al. [20] also discuss operating modes which have slightly different titles, these modes are:

(a) Electric Motor only;
(b) IC Engine only;

(c) Combined Electric Motor / IC Engine;
(d) Electric CVT;
(e) Energy recovery (charging);
(f) Standstill.

The control issues discussed were to optimise fuel consumption and emissions with respect to which modes are used. Operational modes (a), (b), (c) and (e) were also investigated by Schouten et al. [21], who introduced an additional mode for regenerative braking. These operating modes could be considered for controlling the HYSTOR concept; the system should be able to operate in modes (a), (b), (c), (e) and (f).

Real Time Control Strategy (RTCS) was discussed by Johnson et al. [22] and was used to optimise both fuel efficiency and emissions, with respect to a parallel HEV configuration, by considering the dynamic vehicle operating conditions such as recent events, relating to torque demands, and battery status. A set of control variables were detailed which relate to the battery state of charge (SOC), torque thresholds and battery status. A stepwise algorithm was presented for the RTCS.

Another strategy introduced by Montazeri-Ghi et al. [23] is Electric Assist Control Strategy (EACS) where a genetic algorithm was developed with a cost, or fitness, function to minimise fuel consumption and emissions. This related to a parallel HEV configuration.

One of the goals in the control of hybrid vehicles, and the HYSTOR concept, is to reduce fuel consumption, a strategy that has been developed to assist this goal is the Equivalent Consumption Minimization Strategy (ECMS) which was introduced by Paganelli et al. [24] and further developed by Paganelli et al. [25]. This strategy converts power flow into an equivalent fuel cost for parallel HEV configurations. The basis of the strategy is that when the HEV is charging the electric battery as well as providing mechanical power to the vehicle, more fuel will be consumed than when the battery is being discharged and hence the electric motor is contributing to the power for the vehicle. The following diagrams are

re-created from [24]. Figure 1-7 shows the energy flow for when the HEV is discharging the battery and Figure 1-8 shows the energy flow for when the HEV is charging the battery.

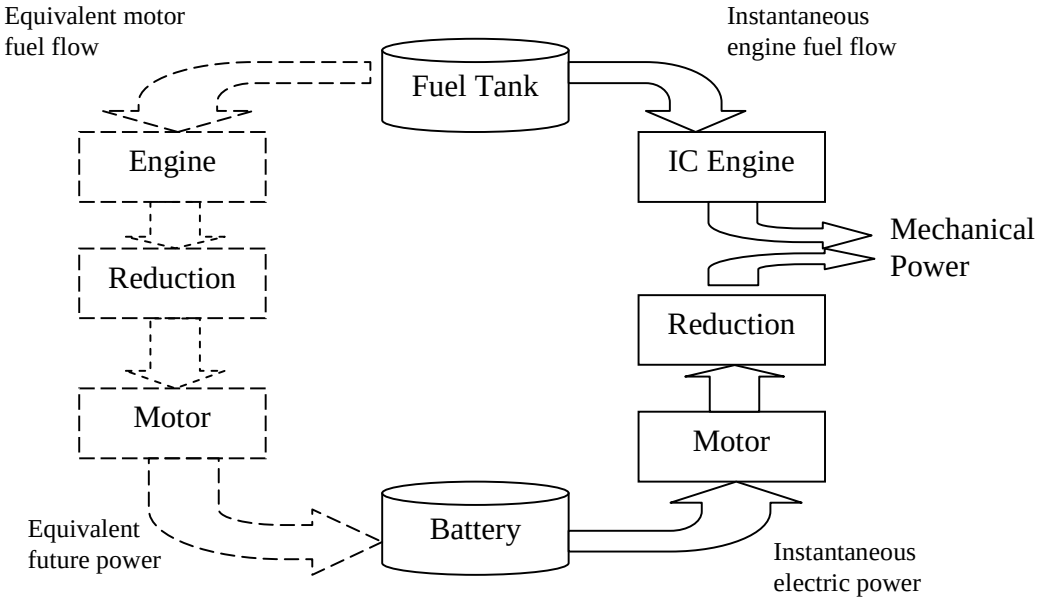

Figure 1-7 Energy route for the equivalent fuel flow consumption of the electric motor for a positive current (discharge case) [24]

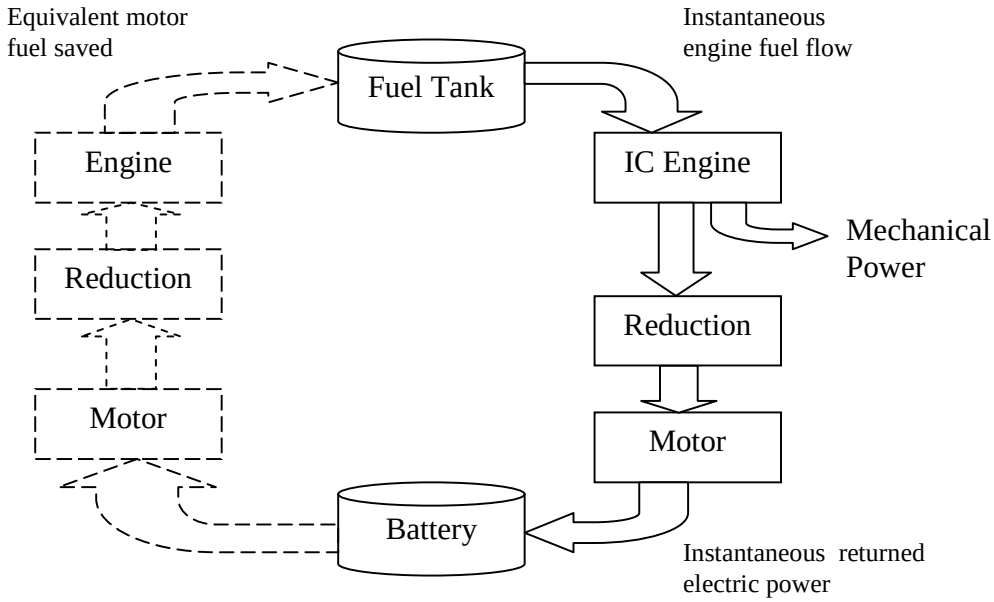

Figure 1-8 Energy route for the equivalent fuel flow consumption of the electric motor for a negative current (charge case) [24]

Rodatz et al. [26] investigates the ECMS strategy further for fuel cell vehicles as does Paganelli et al. [27], the latter states that ECMS can be used for other hybrid configurations. Sciarretta et al. [28] validates the ECMS strategy against previous strategies and cost functions. Guezennec et al. [29] compare ECMS with an *a priori* method of control and optimisation to determine the best strategy for controlling Fuel cell and FCEV models. A later article from Sciarretta [30] gave an overview of HEV control and optimisation techniques including ECMS, the article concludes by stating that feedback control and ECMS provide good optimisation, compared to dynamic programming techniques, which primarily use drive cycles for optimisation. This article also suggests that future control and optimisation will use outside information from, for example, a GPS system to gain knowledge on the possible drive cycle for each journey and make adaptations to the control accordingly.

Results reported for the ECMS system are between 17% and 30% fuel economy improvement compared to a conventional vehicle, with a 5% improvement when compared

to an HEV using SOC control algorithm. The ECMS is an instantaneous control configuration and hence does not use an *a priori* knowledge when calculating the cost function, hence it is highly suitable as a real-time controller.

The ECMS could be investigated for the HYSTOR concept. As stated previously the charging of the electric battery can be likened to the storing of the generated, excess, steam in an accumulator, in this way the 'charging' and 'discharging' of the steam accumulator can be considered when developing an optimisation algorithm for the system that would employ the techniques of ECMS. A possible configuration is shown in Figure 1-9.

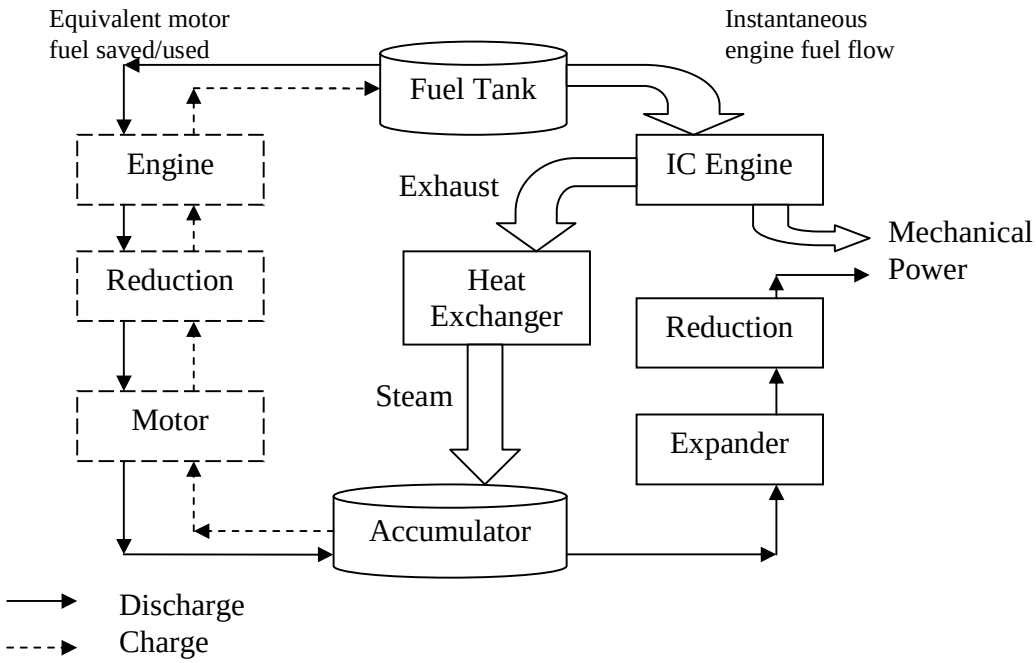

Figure 1-9 Possible configuration for the HYSTOR system using the ECMS control strategy

When the system is in discharge mode, and steam is being used by the expander, the equivalent fuel is being consumed, and when the system is in charge mode, steam is being accumulated and fuel is being saved.

The use of fuzzy logic to control and manage a hybrid powertrain has been investigated by Kheir et al. [31], this paper also uses the ECMS idea as part of its engine management approach. Tzeng et al. [32] and Huang et al. [33], also used fuzzy logic. These papers are linked in using an integrated mechanism for energy management. Schouten et al. [21] also used fuzzy logic to control the different operating modes that are presented in the paper. Lin et al. [34] compared two different control algorithms, one rule based (i.e. using fuzzy logic) the other a dynamic control algorithm, it is concluded that the dynamic control algorithm resulted in a lower fuel consumption than the fuzzy logic based algorithm.

Musardo et al. [35] developed an adaptive control strategy that uses ECMS to improve fuel economy and reduce emissions. The resulting performance of the adaptive control is lower than the global optimum, but it is claimed that the strategy developed gives a more robust real time solution. Another adaptive control scenario is presented by Jiang et al. [36] which presents control strategies related to maximum output of the alternative energy source (for example a battery power source) or maximum efficiency or a combination of the two, which adapts with respect to the state of the energy storage (e.g. State of Charge - SOC), this creates a power sharing control strategy.

A Model Predictive Control (MPC) method is discussed by Vahidi et al. [37], this method does not use drive cycles or *a priori* knowledge. This paper states that the power demands can be split into rules based for instant demands and optimisation based for long-term demands.

A key discussion point in much of the research, for example Paganelli et al. [25] and Musardo et al. [35], is whether to base control actions on global, or local commands. Global refers to use of *a priori* knowledge for example the use of driving cycles to control and optimise, whilst local refers to current system variables for example, SOC. Global, or *a priori*, actions or commands are not really suitable for a Real Time Control scenario, but are useful for investigating fuel consumption. During the modelling phase of a project this control is usually via a Map Based Control strategy. Local optimisation and control requires a cost function to be developed with respect to certain system variables, such as

fuel consumption and, for HEVs, SOC. This results in a real-time algorithm being developed.

Delprat [38], investigated and developed two optimisation algorithms to be used in controlling an HEV. Both algorithms use torque and gear ratio as decision variables, taking into consideration the SOC of the battery. Whilst this technique could be applied to the HYSTOR system concept, it is probably beyond the scope of this thesis, but should be considered for future work. The reason for this being that the scope of the HYSTOR project is primarily concerned with the development and control of the components of the steam system, the components of the vehicle (such as the gearbox) will be observable, but not controllable at this stage.

In a paper by Suh & Stephanopoulou [39] the coordination of control issues for a fuel cell system is discussed, which states that lack of communications between inner control loops, in this case a fuel cell converter and compressor, leads to low system performance with respect to optimisation. When communications are introduced and with good supervisory control, the performance improves. This is an issue that should be considered when developing the supervisory control architecture for the HYSTOR system, it is important to get the level (global or local) of communication between the IC engine system and the expander system correct to get the best performance.

In Scordia [40], an optimisation tool was developed, arbitrarily called ‘KOALA’ by its developer, using dynamic programming and is a good base to predict the possible fuel consumption reductions for HEVs using drive-cycles, comparisons of different HEV configurations are possible using the method.

In Stobart [11], an overview of the control concepts for the HYSTOR concept were investigated and presented. The design of the heat recovery system was examined through the use of energy/heat balance theories. The availability was discussed and the variables that affect the availability and overall system performance were considered, these variables are:

Exhaust gas temperature;
Exhaust gas mass flow rate;
System operating pressure;
Steam dryness, or quality, fraction.

It is anticipated that these variables will form the basis of control dynamics so that the energy production and storage can be controlled in such a way as to ensure the vehicle is operating at its optimal efficiency, with respect to both the IC engine and steam expander.

1.5 Software modelling tools used for hybrid vehicles

Many different modelling tools have been developed and utilised in the process of modelling hybrid configurations and control strategies. A common link between all the modelling tools, presented in this section, is that they have all been developed in a Matlab/Simulink environment. This is because the Matlab environment is ideal for creating and developing mathematical models for engineering applications and solutions, the Simulink toolbox components include specific items for developing controls, signal processing and real-time programming.

Guzzella et al. [41] and Rizzoni et al. [42] used the Quasi Static Simulation ToolBox (QSS-TB), developed at the ETH University in Zurich, Switzerland [43]. QSS-TB is a backward looking simulation toolbox, this means that the 'cause and effect' calculations are reversed so that rather than calculating the speed from the known acceleration and force, the speed is used to calculate the acceleration and force required to meet the demands made upon the vehicle. The drive cycle is fed into vehicle and gearbox components that calculate the torque required from the engine component in order to meet the drive cycle requirements. The engine component then calculates the fuel consumption. The HYSTOR project began the software modelling process by using QSS-TB. A conventional (no-hybrid) configuration is shown in Figure 1-10. How QSS-TB was used to model HYSTOR Hybrid models will be further investigated in Chapter 2.

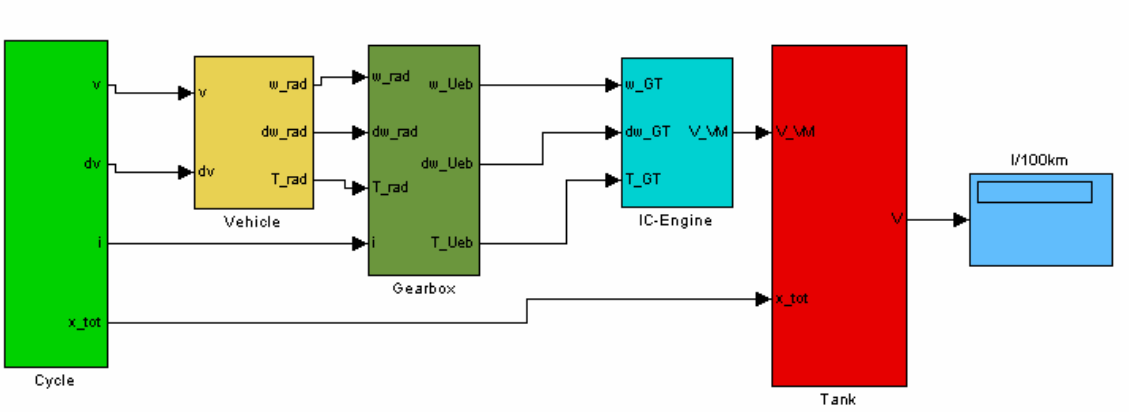

Figure 1-10 Conventional vehicle model using QSS-TB

An alternative method of calculating the fuel consumption is for the drive cycle to be fed into an engine component which uses acceleration and force calculations to determine the speed and load required and in turn feeds these results forward to the gearbox and vehicle components, this is how forward looking simulation tools operate. An example of a forward looking simulation modelling tool is Powertrain Systems Analysis Toolbox, PSAT [44], which was used in research by Kheir et al. [31]. PSAT was developed by the Argonne laboratories in Chicago. Argonne hosts the Department of Energy support group for hybrid and electric vehicle research in the USA. This modelling tool was also used within the HYSTOR project. PSAT uses the forward looking concept and is suited to the dynamic system of the HYSTOR configuration. Further details are given in Chapter 2.

Another forward looking simulation tool is ADVISOR, used by Johnson et al. [22], Zhang et al. [20] and Montazeri-Ghi et al. [23]. This simulation tool was developed by the National Renewable Energy Laboratory (NREL) and is an advanced vehicle simulator. It has now been commercialised and is available on the website from AVL [45]. ADVISOR is used to develop models for light and heavy weight vehicles in conventional configurations and also using hybrid and fuel cell configurations.

Other examples of modelling tools used in previous research include VP-SIM and PSIM. VP-SIM, used by Rodatz et al. [26] is a modular scalable forward simulation tool box developed by Ohio State University. PSIM is another forward looking simulation tool and was used by Tzeng et al. [32] and Huang et al. [33].

In a paper produced as part of the HYSTOR project, Hounsham et al. [46], discuss how both the QSS-TB and PSAT were used to develop the HYSTOR Hybrid vehicle models and some early results for the system when running different lightweight driving cycles with the models. More detail for the development of the HYSTOR system using software modelling tools can be found in Chapter 2. This paper also discusses the expander test setup and results which is further discussed in Chapter 3.

1.6 Objectives of the thesis

As stated in Section 1.3, the novel heat recovery concept utilises the heat that is otherwise wasted from the IC engine exhaust by recovering energy in the form of heat and this is used to raise steam from water. The HYSTOR project aims to establish scientific aspects of this novel energy storage through analysis and by using software modelling techniques supported by experimental validation. The end product for the project, as well as test results and discussion, is to present the strategy and architecture to control such a system, with a view to optimising fuel consumption whilst retaining vehicle performance.

Two hybrid vehicle modelling toolboxes, QSS-TB and PSAT, were used to develop and test different hybrid configurations and also were used as a building block to develop and model the different components for the system, for example heat exchanger and expander. Background for these toolboxes is detailed in Chapter2, the reason for using two separate toolboxes for the modelling was so that a comparison of results could be made, which would validate any possible fuel consumption improvements. Also, for reasons given in Chapter 2, QSS-TB tended to be easier to adapt and fast to execute, whereas PSAT, although slower, was more suited to the dynamics of the HYSTOR system, and hence would provide more realistic results. Both modelling tools are capable of working with drive cycles, such as NEDC – New European Drive Cycle [47], hence, the results from both modelling tools were compared and presented.

The MatLab/Simulink environment was used to develop the controls required for the system. Initially the individual components of the system were modelled, for example the heat exchanger, and individual controls were developed for each component that required control. Progressing on from this, overall, or supervisory, control dynamics were developed for the system. Simulink was used to develop both the individual and overall control, with the model being validated using the QSS-TB and PSAT models when the control dynamics performed satisfactorily.

1.6 Objectives of the thesis

GT-SUITE, developed by Gamma-Technologies [48], is a software modelling tool that can be used to model engine configurations. The HYSTOR project used GT-SUITE to initially model the expander configurations used in the expander testing phase. This had two purposes, (i) it can validate the results the HYSTOR project obtained from the expander testing; (ii) the results can be used to scale up the expander models and then be compared to the medium expander test results; hence proving, or disproving, the scalability of the expander models. GT-SUITE was also used to compare results using different media, for example steam and compressed air at various pressures.

A mini test facility was developed to test three different expander configurations (uni-flow, rotary and counter-flow) to determine which configuration was most suitable for use as a steam expander. The test facility for the mini test bed will be presented along with details of how the required test data was acquired. The results of the tests will also be presented in this thesis.

The main objectives of this thesis are as follows:

1) give a review of the expander testing completed, including discussions of the results;
2) present an overview of the software modelling performed for the project;
3) discuss, in detail, how the control architecture was developed, designed and tested;
4) discuss possible optimisation strategies and how they could be applied to the system concept;
5) summarise the project progress, draw conclusions and discuss future work in this area.

These items will fulfil the aims of the research project to develop a robust and controllable system that will optimise the fuel consumption of the HYSTOR system, whilst retaining the performance of the vehicle and also ensuring that the efficiencies of both the IC engine and steam expander systems are optimised.

The overall aim of this thesis is to fully investigate optimal control architectures for the system and to demonstrate how such a configuration can be applied to the hybrid vehicle scenario as specified by the system concept.

2 Software modelling and simulation of the HYSTOR concept

2.1 Introduction to software modelling

This chapter discusses the two modelling toolboxes, QSS-TB and PSAT, which were used to create models of the HYSTOR concept in a hybrid vehicle application. An in depth description is given for each of the toolboxes along with how the HYSTOR models were developed. The reason for using two separate toolboxes for the modelling was so that a comparison of results could be made, which would assist in validating any fuel consumption improvements.

This initial phase of modelling was used to develop and test different heat recovery systems within a hybrid vehicle configuration. The conventional vehicle models that were available with the modelling toolboxes were used as a building block to develop and model the different components for the heat recovery system, for example heat exchanger and expander. The two modelling toolboxes allowed the use of standard drive cycles to run the models and, hence, compare results, which was a good way to determine the performance of the heat recovery systems. Once the models were verified, they were used to further develop the control strategy, as detailed in Chapter 5

The main difference between the two modelling toolboxes is the way that they handle the cause-and-effect relationship of the system being modelled. The conventional strategy is to calculate the vehicle acceleration from given forces. Having knowledge of the vehicle acceleration, the wheel, gearbox and engine accelerations can also be calculated and hence the fuel consumption required to meet these accelerations. This conventional strategy will be referred to as a forward looking model. Forward looking modelling is more suited for modelling dynamic systems, i.e. system models that involve changing dynamics of a system using differential equations. The alternative to the forward looking model is a backward looking model, this strategy reverses the cause-and-effect relationship and uses the acceleration data, from given speeds at discrete times, to calculate and the forces required to provide these accelerations, the calculations then work back to use engine maps that relate speed and load to fuel consumption. The

backward looking model strategy is a fast modelling technique which makes use of such “non-causal” models.

The first toolbox used was the Quasi Static Simulation ToolBox (QSS-TB) [43], which is a backward looking hybrid simulation tool developed by Eidgenössische Technische Hochschule (ETH) in Zürich. The models developed using QSS-TB are further discussed in Section 2.2.

The second toolbox used was Powertrain Systems Analysis Toolbox (PSAT) [44], which is a forward looking toolbox developed by Argonne National Laboratories (that hosts the Department of Energy support group for hybrid and electric vehicle research). How the hybrid model components were adapted from being used in the QSS-TB model to the PSAT model is presented in Section 2.3. Section 2.4 presents the drive cycles that were used to run the software models.

The results for each of the model runs are presented in Section 2.5 for QSS-TB and PSAT. The results are summarised and conclusions are presented in Section 2.6.

2.2 Software modelling of the HYSTOR hybrid using QSS-TB

This section will detail the software modelling strategy employed when using the QSS-TB as a modelling tool.

2.2.1 Introduction to QSS-TB

The QSS-TB is a toolbox developed by ETH in Zurich, or more specifically, the Measurement and Control Laboratory at the Swiss Federal Institute of Technology in Zurich, Switzerland.

The toolbox uses the Matlab/Simulink platform, and was developed with the intention of creating a flexible, easy to use toolbox that simulates different powertrains in order to determine the fuel consumption, moreover the toolbox is freely downloadable [43] and has various different powertrain components such as fuel cell, battery storage, electric motors and generators, that can easily be applied to a hybrid vehicle configuration. As stated in the introduction to Chapter 2, the QSS-TB is a backward looking simulation toolbox.

A conventional vehicle model using QSS-TB is shown in Figure 2-1.

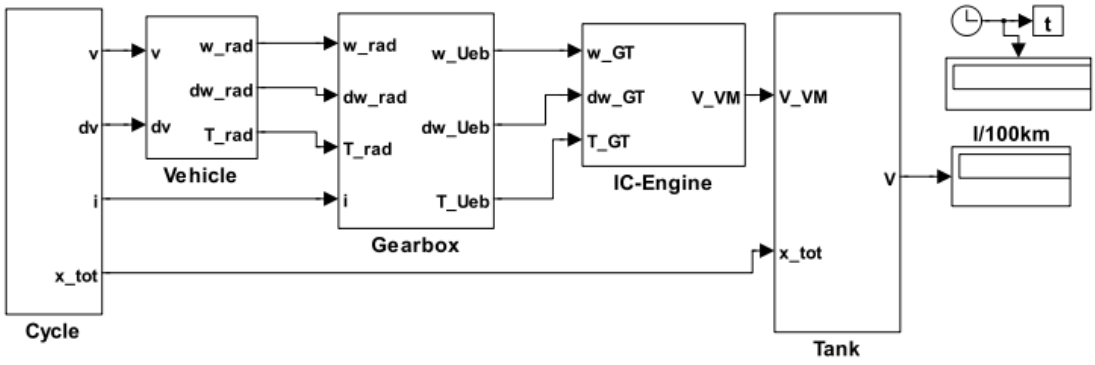

Figure 2-1Conventional ICE driven vehicle model using QSS-TB

As can be seen in Figure 2-1, the model is driven by a component, or Simulink function block, called *Cycle*. The standard drive cycle consists of a time vector, speed vector (v)

and a gearbox vector (i), on initialising the data, these vectors are loaded into the Matlab workspace and the acceleration vector (dv) is calculated as follows:

$$dv = (v(n) - v(n-1)) / h$$

Where h is the step size used in the simulation model. The *Cycle* block accesses these vectors, and outputs the vector elements for each step, additionally the distance is calculated (x_tot) using the speed and step data. The outputs of this block are vector elements representing the following parameters:

v	speed (m/s);
dv	acceleration (m/s²);
i	gear number;
x_tot	total distance (m).

The speed and acceleration parameters are fed into a function block representing the *Vehicle*; this block uses these input parameters along with vehicle data stored in the Matlab workspace, representing the inertia and resistance parameters, to calculate the torque on the wheel. The block also uses the wheel radius to convert the speed from m/s to rad/s and the acceleration from m/s² to rad/s². The outputs of the *Vehicle* block are as follows:

w_rad	speed of wheel (rad/s);
dw_rad	acceleration of wheel (rad/s²);
T_rad	torque on the wheel (N m).

The next function block in the model is the *Gearbox*; this block uses the outputs from the *Vehicle* block and the gear number from the *Cycle* block and calculates the speed and acceleration of the gearbox. Additionally the block calculates the power direction – engine to wheel or wheel to engine and in this way the positive or negative torque, respectively, on the gearbox is calculated. The outputs of the *Gearbox* box are the following parameters:

w_Ueb	speed of the gearbox (rad/s);
dw_Ueb	acceleration of the gearbox (rad/s²);
T_Ueb	torque on the gearbox (N m).

The penultimate block in the conventional vehicle model chain is the *IC-Engine* block, this block uses all the outputs from the *Gearbox* block and calculates the fuel consumption required by the *IC-Engine* in order the meet the speed and load requirements determined by the *Vehicle* and *Gearbox*. This calculation is done by using an engine map, or a look up table, that uses the speed and load as inputs to find the corresponding fuel consumption. This map has either been calculated, using the Willans parameter [49], or is a result of real engine data. The *IC-Engine* block takes into consideration idle, deceleration and fuel cut-off points before using the fuel consumption map. The output from the *IC-Engine* block is simply:

V_Vm consumption (kg/s).

The final block for the model is the *Tank* block, which uses the consumption information from the *IC-Engine* and the distance (x_tot) from the *Cycle* block to determine the fuel consumption over the drive cycle, the output is presented as litres/100 km.

The conventional model is used to compare the different fuel consumptions obtained from the HYSTOR Hybrid vehicles in order to determine if the hybrid configuration improves the fuel consumption, or not.

2.2.2 HYSTOR hybrid model using QSS-TB

The QSS-TB contained some functions for Hybrid electric vehicle and fuel cell vehicle configurations, but not for a steam system hybrid configuration, hence new function blocks were developed to represent a *Hybrid Interface* and the *Steam System*, this configuration is shown in Figure 2-2.

2.2 Software modelling of the HYSTOR hybrid using QSS-TB

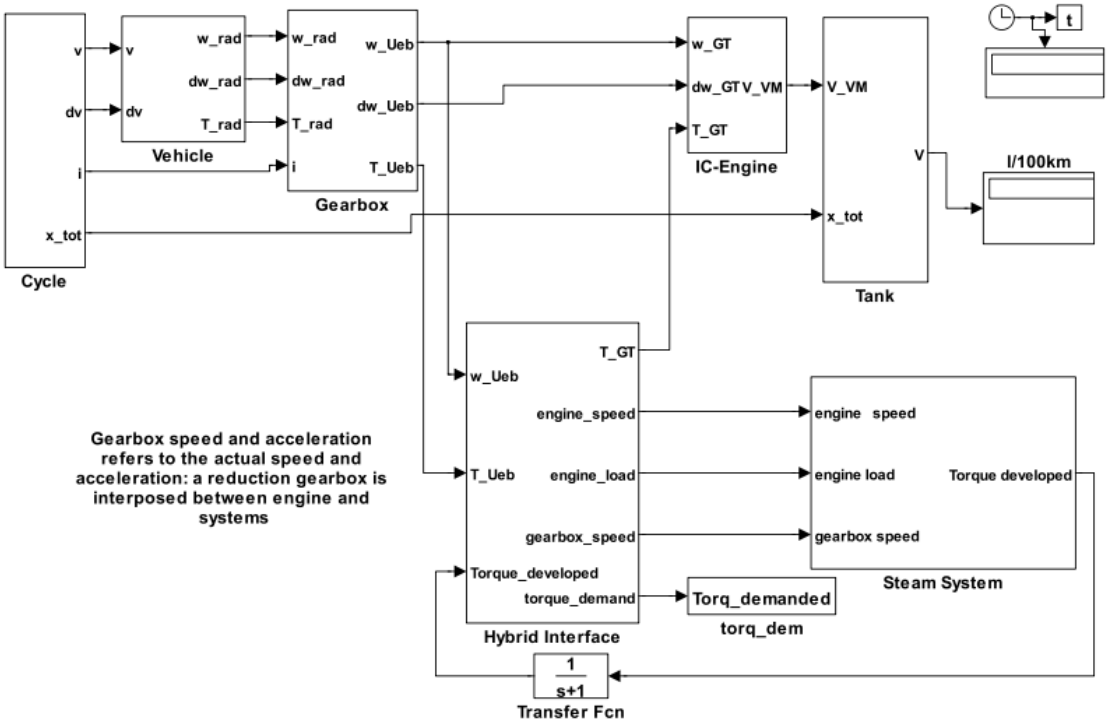

Figure 2-2 The HYSTOR hybrid vehicle model using QSS-TB

The *Hybrid Interface* block is shown in detail in Figure 2-3.

2.2 Software modelling of the HYSTOR hybrid using QSS-TB

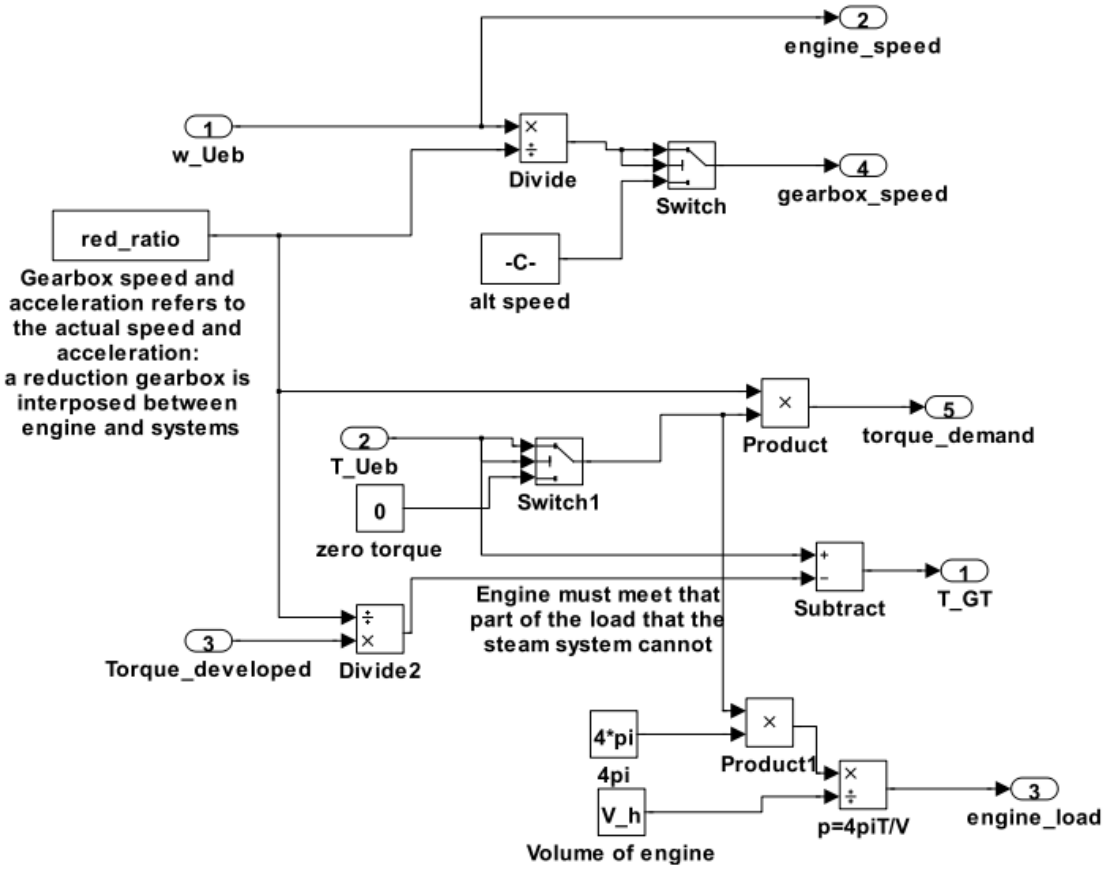

Figure 2-3 Hybrid interface block

The *Hybrid Interface* block uses the gearbox speed (w_Ueb) and load (T_Ueb) parameters from the *Gearbox* block, a reduction ratio was used in order to provide the *Steam System* block with the engine speed in revolutions per second. The gearbox speed is passed along to the steam system as received. The gearbox load is converted from torque (N m) to mep (Pa) using the displacement volume to give the engine load. The *Steam System* returns the torque developed which the *Hybrid Interface* subtracts from the *Gearbox* Torque and presents the remaining torque (T_GT) to the *IC-Engine*. The outputs from the *Hybrid Interface* are as follows:

T_GT	torque demand on IC engine (N m);
engine_speed	speed of the gearbox (rad/s);
engine_load	load on gearbox (mep Pa);
gearbox_speed	speed of expander (revs/s);
torque_demand	torque demand from gearbox (N m).

The *Steam System* block uses the engine speed and load data from the *Hybrid Interface* to determine the exhaust properties in order to perform heat transfer calculations, the gearbox, or expander, speed is used to calculate the maximum possible work from the steam expander given the heat transfer. The output from the *Steam System* is the torque developed by steam system (N m).

The *Steam System* block contains two sub-blocks as can be seen in Figure 2-4.

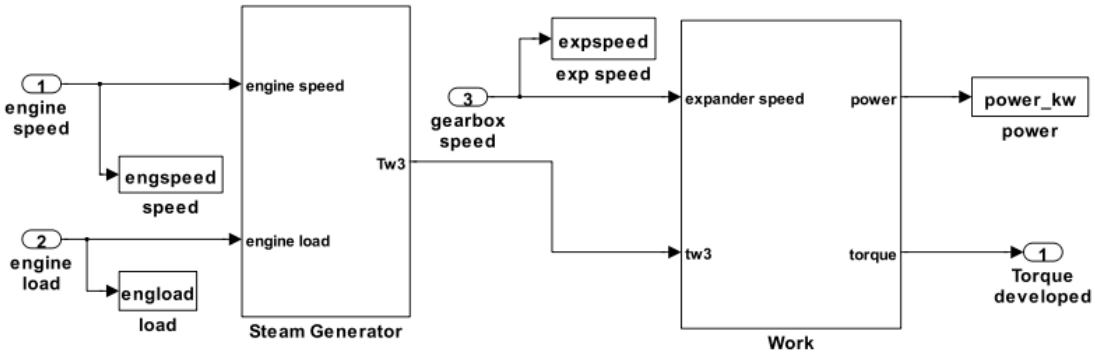

Figure 2-4 Steam system block for a basic steam system

The *Steam System* consisted of a simple heat exchange calculation block – *Steam Generator* which uses the engine load and speed data from the *Hybrid Interface* block to determine the exhaust temperature and mass flow rate via look-up tables. Using this data a simple heat transfer calculation was performed which resulted in a heat output; this parameter was then used by the *Work* block along with the expander speed, to calculate the maximum possible work a conceptual expander could provide. This was calculated using the given enthalpies for the upper and lower system pressures (18 bar and 1 bar, respectively), the different between the two enthalpies results in the ideal isentropic work, allowing for expander efficiency, set at 0.8, the expander work can be calculated. The work was then converted to torque for the *Hybrid Interface*. The *Steam Generator* used a simple boiler model which is visualised in Figure 2-5.

2.2 Software modelling of the HYSTOR hybrid using QSS-TB

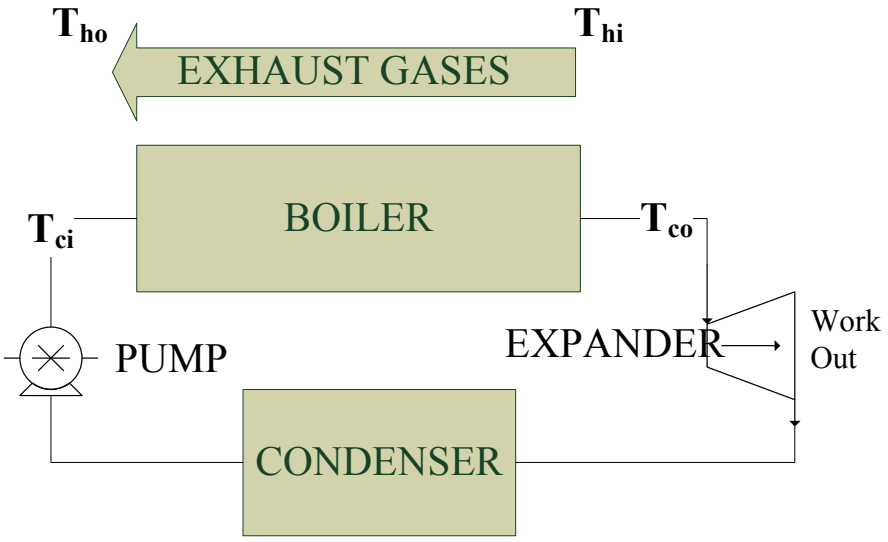

Figure 2-5 Simple boiler model

The calculations for the *Steam Generator* were based on a three phase heat transfer between the exhaust gases and the water/vapour; this is shown in Figure 2-6.

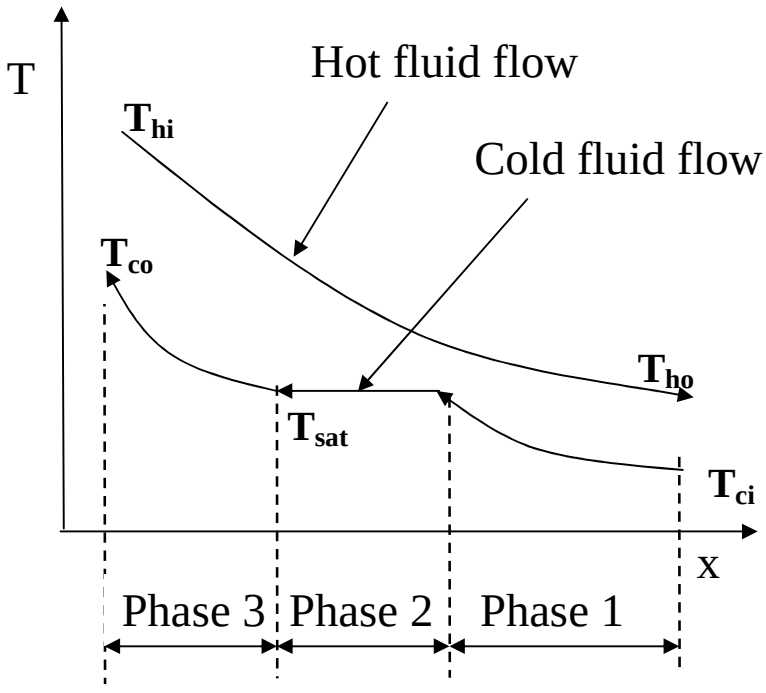

Figure 2-6 Three phase heat transfer for the heat exchanger model

During phase one the water flows into the heat exchanger at ambient temperature (T_{ci}) and is heated to saturation point, phase two moves the saturated water to saturated vapour (evaporated, T_{sat}) and finally, phase three superheats the vapour to reach T_{co} at the output of the heat exchanger. Referring to the temperatures labelled in Figure 2-6, the equations used are as follows:

$$Q_{total} = \dot{m}_e . c_{pe} . (T_{hi} - T_{ho}) \quad (2.1)$$

$$Q_{total} = Q_1 + Q_2 + Q_3 \quad (2.2)$$

$$Q_1 = \dot{m}_w . c_{pw} . (T_{sat} - T_{ci}) \quad (2.3)$$

$$Q_2 = \dot{m}_s . h_{fg} \quad (2.4)$$

$$Q_3 = \dot{m}_w . c_{ps} . (T_{co} - T_{sat}) \quad (2.5)$$

Where:

$\dot{m}_e$ is the mass flow rate of the exhaust gas, kg/s;

c_{pe} is the specific heat of the exhaust gas, kJ/kg K;

$\dot{m}_w$ is the mass flow rate of water, kg/s;

c_{pw} is the specific heat of water, kJ/kg K;

h_{fg} is the latent heat of vaporization at boiler pressure (18 bar), kJ/kg;

c_{ps} is the specific heat of steam at boiler pressure (18 bar), kJ/kg K.

T_{ci} was assumed to be at ambient temperature and T_{ho} was assumed to be equal to T_{sat}. This is referred to as the boiler model. The complete Simulink model files for the boiler model can be found in Appendix B.1.

Using this model, a simple optimisation task was carried out using different values for the boiler pressure and to compare the work/torque output for each, the optimum value was chosen to be 18 bar as this gave the best result, at higher pressures the work output was not increased, this is due to the larger temperature differences, and hence less heat transfer.

The initial boiler model used the instantaneous steam as it was generated; hence there was no control over the steam use. An improvement for the control in the model was to add a simple mechanism when using the steam in the *Work* block. This used the torque information from the *Hybrid Interface* and coupled with the following algorithm:

```
if  IC-Torque Required =< 0
        accumulate steam
else
        if IC-Torque Required < Steam-Torque
                only develop IC-Torque
                accumulate any un-used steam
        else
                develop Steam-Torque
        end-if
end-if
```

This is referred to as the accumulator model as it is simulating the accumulation of steam, whereas the previous models instantaneously used all the available steam, whether it was required or not. The complete Simulink model files for this model can be found in Appendix B.2.

2.2.3 Running the QSS-TB models

For each of the models created using QSS-TB, initialisation files were required in order to run the model. These files can be found in Appendix B.3.

There were two sets of data used, one of which represented the vehicle data for a Volkswagen (VW) Golf 1.6 litre; the other represented a conceptual small car using a Ford I3 engine, both of which used a mass=1181 kg, this is nominally the weight of a VW Golf, no data for an I3 car was available. The VW Golf data was chosen due to this vehicle being used as a European standard for research. The Ford I3 engine data was obtained experimentally at the test facilities in the University of Sussex. The Ford I3 engine is a 3-cylinder, in-line, Direct-Injection Spark-Ignition (DISI) engine with a

capacity of 1.1 litres, the engine was supplied by the Ford Motor Company. The Ford I3 engine was used most recently in the research by Vulli [50].

For the Golf, the engine maps used to relate the speed and load of the engine to exhaust gas temperature and exhaust mass flow rates were created using scaled down data from a 7.2 litre Caterpillar diesel engine. This data had been recorded during an earlier research project, at the University of Sussex, and the temperature and mass flow rates were scaled down to represent a smaller passenger vehicle engine. For the I3 data real engine data was obtained, at different speed and loads, from the Ford I3 engine, again at the University of Sussex, and the engine maps for exhaust gas temperature and exhaust mass flow rate were created from the recorded data.

2.2.3.1 VW Golf exhaust data maps

Figure 2-7 shows exhaust maps for the VW Golf. The exhaust temperature and mass flow rate maps that were used as 2-D lookup tables in the HYSTOR steam system models, the access vectors are speed (rad/s) and load (brake mean effective pressure, BMEP, in Pa). These maps were derived from data acquired for a 7.2 litre, Caterpillar diesel engine, which was scaled down to represent a smaller passenger vehicle engine.

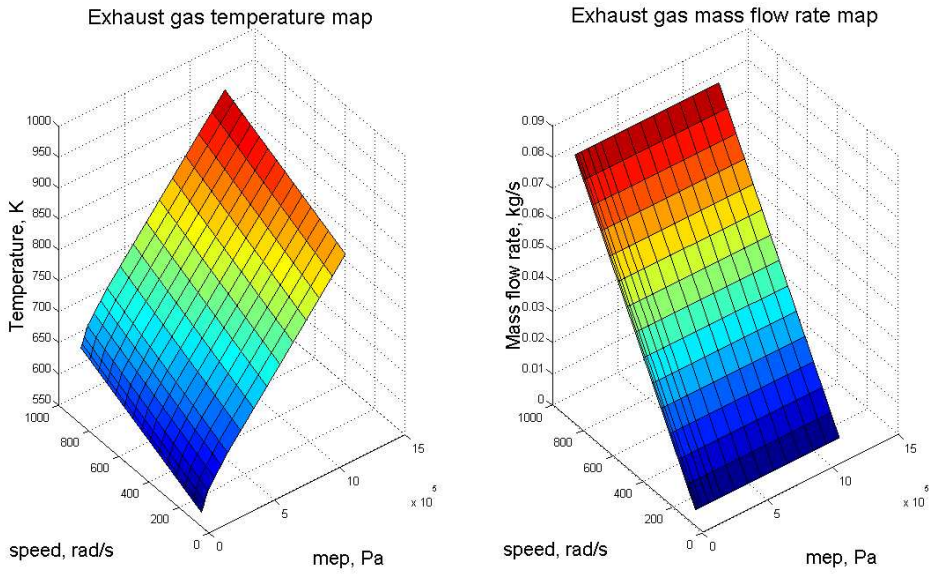

Figure 2-7 Exhaust gas maps used for the VW Golf models

2.2.3.2 Ford I3 engine tests

The Ford I3 engine at the University of Sussex was available for the HYSTOR project to run at varying speeds and loads in order to obtain exhaust gas temperature and mass flow rate data. This data was used to create the exhaust data maps for lookup tables in the HYSTOR steam system model. Table 2-1 shows the speed and load steps used along with the data acquired for exhaust temperature and exhaust mass flow rate. The recording was done using the INCA measuring and calibration tool [51] system which communicates with the engine management system.

Engine speed		**Engine load**		**Exhaust gas temperature**	**Exhaust gas mass flow rate**
rpm	**rad/s**	**N m**	**bar**	**°C**	**kg/s**
1000	104.72	13	1.5	229.7	0.0060
		35	4.0	403.4	0.0053
		64	7.3	596.1	0.0098
2000	209.44	13	1.5	311.8	0.0121
		35	4.0	550.0	0.0098
		70	8.0	747.6	0.0177
		84	9.6	816.0	0.0197
3000	314.16	13	1.5	397.0	0.0214
		35	4.0	621.7	0.0160
		70	8.0	800.0	0.0250
		89	10.4	888.9	0.0316
4500	417.24	13	1.5	752.4	0.0162
		35	4.0	822.2	0.0258
		70	8.0	872.2	0.0442
		89	10.4	883.8	0.0488
6000	628.31	13	1.5	833.8	0.0224
		35	4.0	883.3	0.0360
		66	8.0	883.8	0.0560
		73	8.1	888.9	0.0610

Table 2-1 Ford I3 engine test results

Figure 2-8 shows the exhaust maps for the Ford I3 engine. The exhaust temperature and mass flow rate maps that were used as 2-D lookup tables in the HYSTOR steam system models, the access vectors are speed (rad/s) and load (BMEP in Pa). These maps were created from the Ford I3 engine test results data.

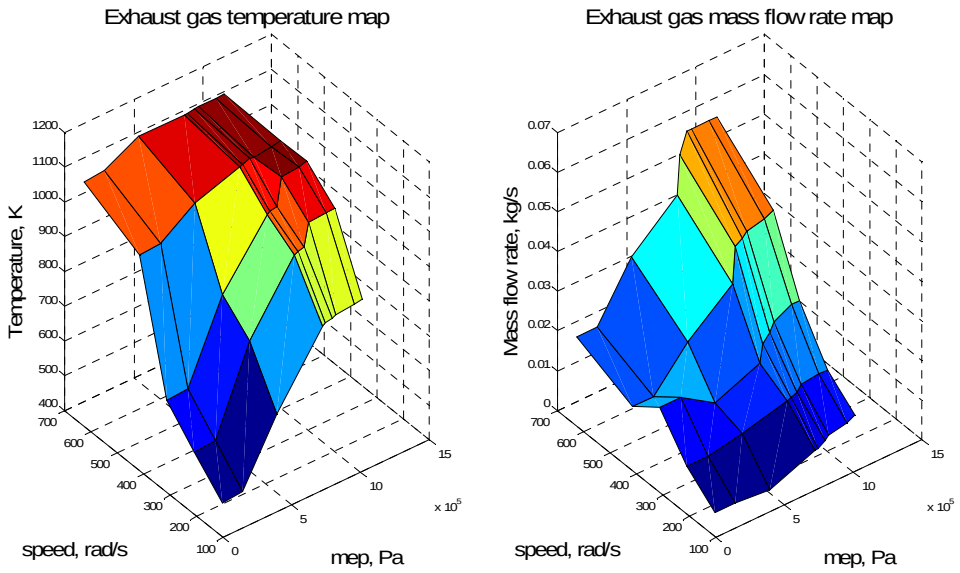

Figure 2-8 Exhaust gas maps used for the Ford I3 models

2.3 Software modelling of the HYSTOR hybrid using PSAT

Whilst the QSS-TB model was easy to use and develop the HYSTOR model with, because it is a backward looking model, it could not represent the effects of realistic dynamics. By using PSAT, which is a forward looking, dynamic modelling tool, the results generated would be more realistic. This section will detail the software modelling strategy employed when using PSAT as a modelling tool.

2.3.1 Introduction to PSAT

The PSAT modelling toolbox was developed by Argonne National Laboratories (that hosts the Department of Energy support group for hybrid and electric vehicle research). The toolbox is written using Matlab and Simulink and has a wide range of vehicle applications from small passenger vehicles to large heavy duty vehicles. The model contains a library of vehicle components to choose from and also some pre-configured vehicles to base the models on. The modelling tool also uses several different powertrain configurations, for example series hybrid and parallel hybrid electric vehicles.

When using the PSAT tool, the first step was to either load one of the pre-configured vehicles to use as a baseline. Examples of the pre-configured vehicles are a Honda Civic 1.6 litre parallel hybrid, Ford Focus 1.9 litre and a SUV (Sports Utility Vehicle) Explorer 4 litre series hybrid. The powertrain configurations available are as follows:

Conventional;
Electric;
Fuel cell;
Parallel hybrid;
Series hybrid (IC eng / electric motor);
Series hybrid (Fuel Cell / electric motor);
Power-split.

For each of these configurations there are further choices for two or four wheel drives, manual or automatic transmission and for hybrid configurations a choice of where the secondary mover is positioned, for example, pre-transmission. The configuration for a conventional vehicle used for comparison for fuel consumption purposes, is shown in Figure 2-9.

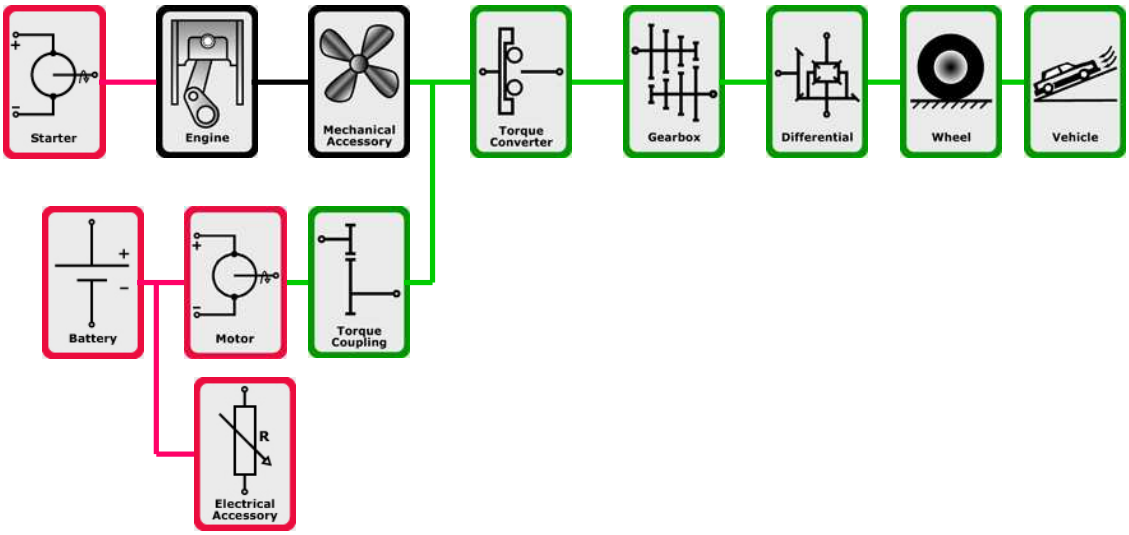

Figure 2-9 Conventional vehicle model using PSAT

For each vehicle configuration, there is a choice of components available. Each component has its own Simulink library. The Simulink libraries can be adapted to change the behaviour of the model. The engine components come with a selection of engine maps, representing a hot engine or a hot and cold engine. The models developed all used a hot and cold engine map, as this is similar to the maps used within QSS-TB. Figure 2-10 shows an example of a Simulink library for the engine library component.

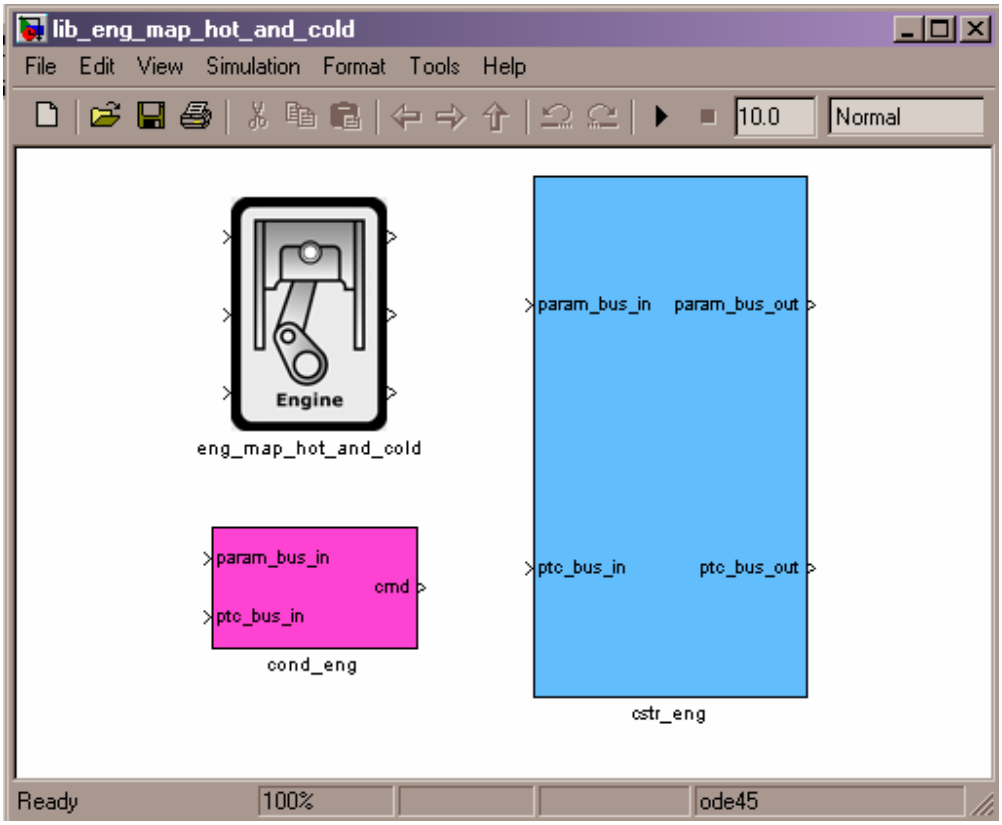

Figure 2-10 PSAT Simulink library for the engine component

The *eng_map_hot_and_cold* block is the actual component Simulink block that is compiled into the vehicle configuration. The *cond_eng* block sets out the signal conditioning for the component which means it is responsible for obtaining the inputs, data and commands, to the component block. The *cstr_eng* block deals with any constraints, or operating limits, that the component has, for example maximum or minimum speeds.

The conventional vehicle used was for a Honda Civic 1.6 litre, the specification for the vehicle is summarised as follows:

Engine: SI, 1600, engine map hot and cold;

Wheel: two wheel drive;

Transmission: automatic;

Vehicle Mass: 1230 kg.

2.3.2 HYSTOR hybrid model using PSAT

The HYSTOR project team worked closely with Argonne to develop a new configuration for the HYSTOR system. A new component was developed called *steam system.* This enabled the development of the steam models, using the models developed using QSS-TB as a baseline, then updating them so that they would work with the PSAT model. The new configuration for the HYSTOR system that was developed by Argonne is shown in Figure 2-11.

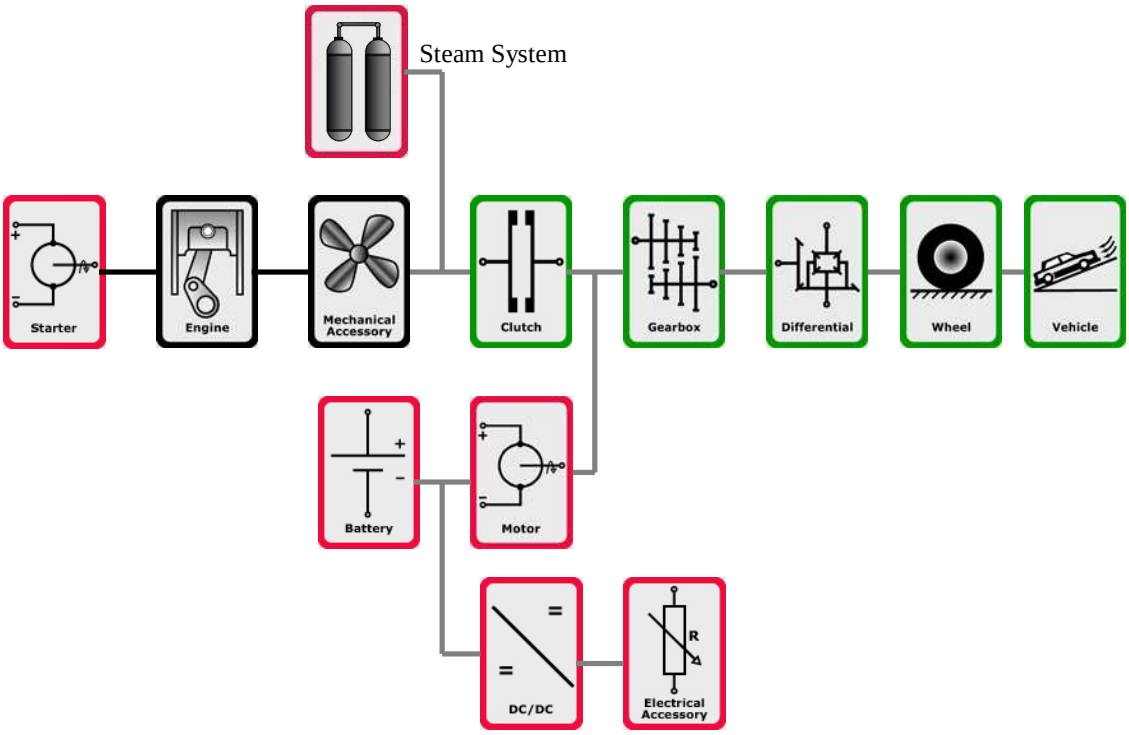

Figure 2-11 The HYSTOR hybrid vehicle model using PSAT

The Simulink blocks developed for the QSS-TB models were adapted so that they could be used for the PSAT models. The main changes were how the variables are handled between the Simulink blocks. QSS-TB simply has signal links between each block, but with PSAT, each variable that is either to be used by the model, for example torque, or any variable that needs to be recorded, for example mass steam generated, needs to be multiplexed together into one structure. The PSAT steam system component is shown in Figure 2-12.

2.3 Software modelling of the HYSTOR hybrid using PSAT

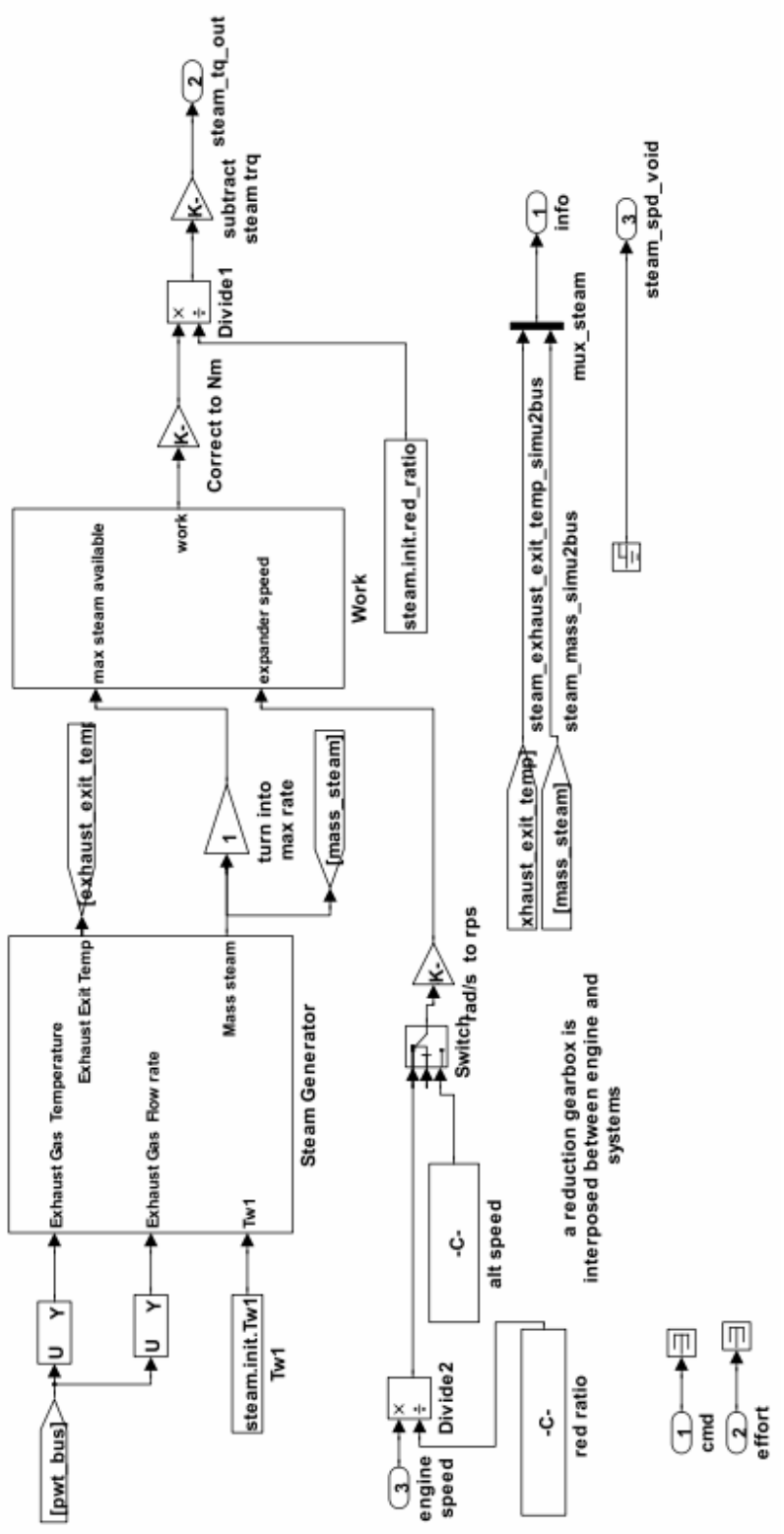

Figure 2-12 PSAT steam system component

The model is almost the same as the one used for the QSS-TB model, the Simulink blocks *Steam Generator* and *Work* are the same blocks as for the QSS-TB boiler model. The main difference is that there is no *Hybrid Interface* block, instead the reduction ratio and subtraction of torque is dealt with inside the S*team System* block. The complete Simulink model files for the QSS-TB boiler model can be found in Appendix B.1.

For the accumulator model some additional changes were necessary to the PSAT engine component so that the torque developed by the steam system was subtracted within the engine component rather than in the steam system, this change created a closer simulation of the HYSTOR hybrid. The same Simulink *Control* block used in the accumulator QSS-TB model was substituted so that the accumulator algorithm was included in the PSAT model. The changes made to the engine component are shown in Figure 2-13, this is just a section to show the addition of an input for the steam developed torque – *steamtrq*.

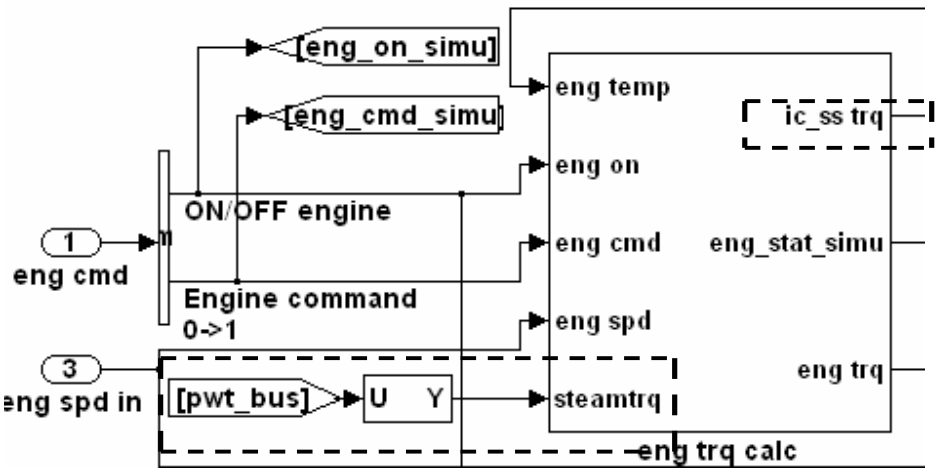

Figure 2-13 Section of the adapted PSAT engine component

The adaptations are shown within the dotted boxes. The Simulink *From* block reads the pwt_bus and the *Selector* block (U to Y) identifies which parameter is to be read, in this case *steam_torque_developed_simu*. This parameter is a new input into the *eng_trq_calc* block. The result of IC engine torque minus the steam system torque is output as *ic_ss_trq*, this is passed to the *fuel rate* calculation block (not shown in figure).

Figure 2-14 shows the Simulink block *eng_trq_calc* and how the output has been adapted to subtract the steam developed torque.

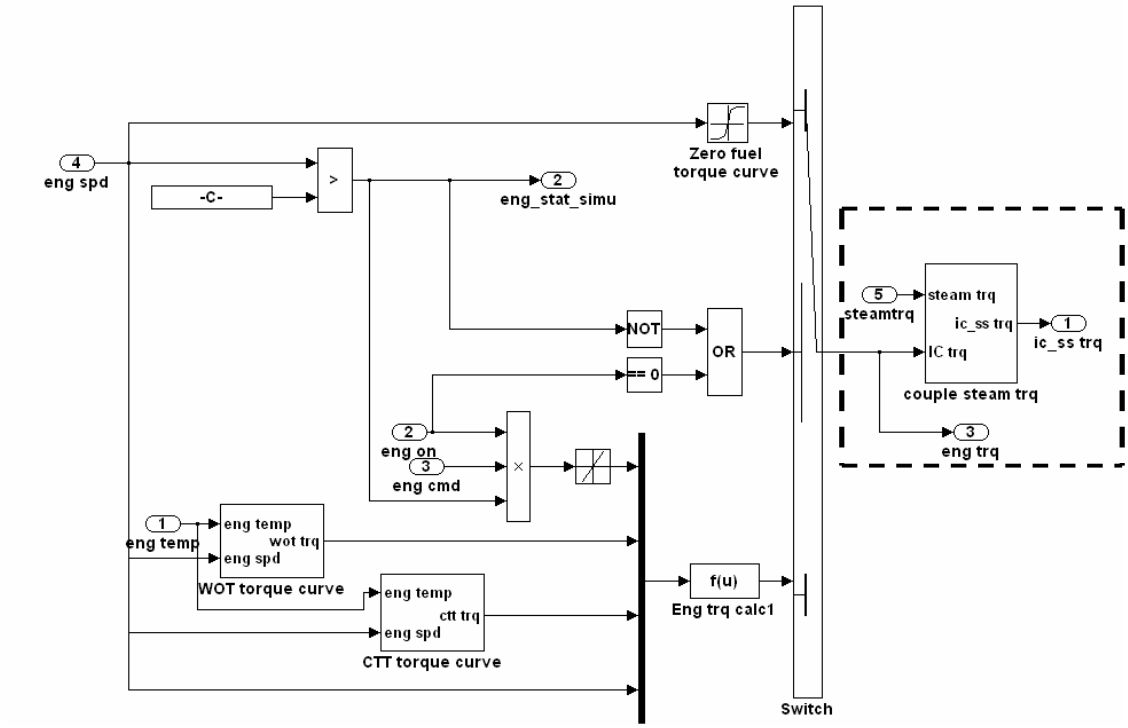

Figure 2-14 Adapted PSAT block 'eng_trq_calc'

The adaptations are shown within the dotted box. The new input *steamtrq* is subtracted from the final calculated torque. A Simulink block, *couple steam trq*, was added so that the steam is only subtracted when the vehicle torque is positive. The algorithm is summarized below:

if IC-Torque Required =< 0
IC-Torque out = IC-Torque Required
else
IC-Torque out = IC-Torque Required – Steam-Torque
end-if

The new Simulink block, *couple steam trq*, is shown in Figure 2-15.

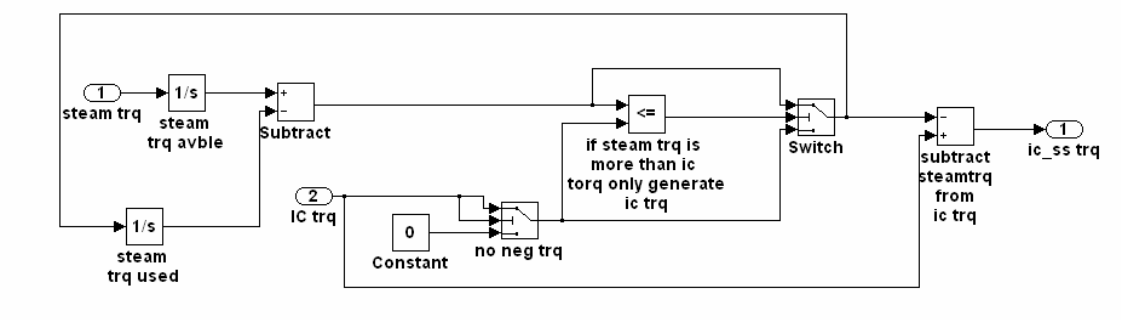

Figure 2-15 Simulink block *couple steam trq* within the PSAT engine model

As can be seen from Figure 2-15, the algorithm is similar to the algorithm found in the *Control* block of the QSS-TB accumulator model which can be found in Appendix B.2.

2.3.3 Running the PSAT models

In order to run the PSAT models, a set of files associated with each component is requires, these are:

initialisation;

scaling;

calculation.

The initialisation file contains all the initial settings for the component. The initialisation file used for the new *Steam System* component was used to set the parameters and variables used by the *Steam System* function blocks. Thermodynamic properties were set for the working pressures of the system along with the variable that sets the reduction gearbox variable and an alternative speed for when the engine speed goes below a nominal value. Additionally the volumes and masses are set for the HYSTOR steam system. The PSAT initialisation file can be found in Appendix B.4.

The scaling file can be used to set different sizes of components, for example engine size, the different scales can then be selected when running the model to compare the results for different engine sizes, but with the same configuration. For the *Steam System* component, no scaling file was used.

The calculation file is used to perform additional calculations using the value set in the initialisation file; one component can use various calculation files to set up the characteristics of the chosen component. For the *Steam System* component, no calculation file was used.

The engine component is supplied with various graphs representing the engine maps, an example is shown in Figure 2-16.

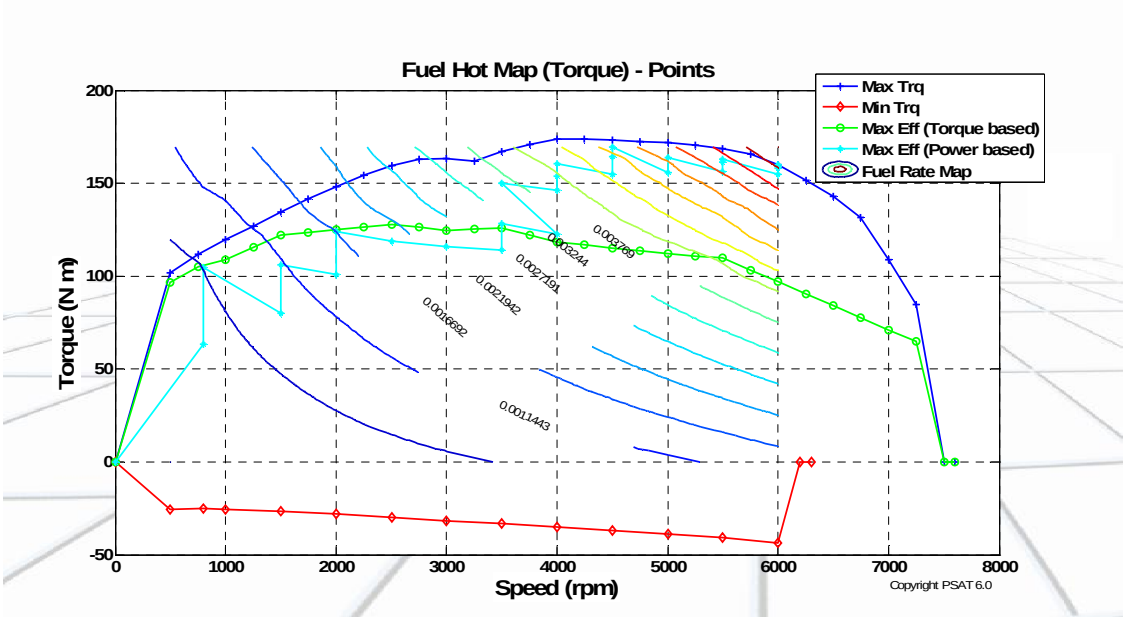

Figure 2-16 PSAT engine map, fuel using torque points

The vehicle file specification that was used a base for the *Steam System* components is summarised as follows:

Engine: si, 1800, engine map hot and cold;

Wheel: two wheel drive;

Transmission: manual;

Vehicle Mass: 1525 kg;

Hybrid configuration: parallel hybrid, pre-transmission.

2.4 Drive cycles used for the models

Drive cycles were required to run the models created using QSS-TB and PSAT. There are many standard drive cycles available. They contain data over a period of time that specifies the required speed, acceleration and gear number. The drive cycle simulates a typical driving scenario, for example on-highway driving where there are high speeds but not much acceleration or gear change, or urban driving where there are frequent gear changes and changes in acceleration but low speeds. These drive cycles are used throughout the automotive industry in a variety of test scenarios, for example emissions testing of passenger vehicles.

Three different, standard drive cycles were used to run the QSS-TB and PSAT models, these were:

NEDC – New European Drive Cycle [47];
FTP-75 – Urban Drive Cycle [7];
US-06 – US Highway Drive Cycle [8].

The details for these drives cycles can be found in Appendix A.

2.5 Results from software modelling of the HYSTOR hybrid

This section presents the results from running the QSS-TB and PSAT software models with the drive cycles. The fuel consumption is presented in tabular form followed by graphs that compare the torque demanded on the vehicle, from the gearbox, with the torque developed by the steam system and the torque developed by the IC engine. Additionally, graphs of the speed/load point for each drive cycle are presented.

The published data [52] for a VW Golf 1.6 on a combined (NEDC) cycle is between 6.7 and 7.2 l/100 km. The published data [52] for a Honda Civic 1.8l on combined (NEDC) cycle is between 6.4 l/100 km and 6.6 l/100 km.

2.5.1 Results for the boiler model

The boiler model is the model which consisted of a simple heat transfer calculation and no control over how much steam is used, and hence torque generated. Table 2-2 compares the fuel consumption for the conventional vehicles with (a) QSS-TB model with the VW Golf configuration, (b) QSS-TB model with I3 configuration, and (c) the PSAT model with the Honda Civic configuration. The percentage of improvement in fuel consumption for each vehicle/drive cycle combination is also shown. Fuel consumption is given in litres per 100 km, with the percentage improvement in brackets.

	NEDC (European)	**FTP-75 (Urban)**	**US-06 (Highway)**
QSS Golf, conventional vehicle	6.51	6.56	6.69
QSS Golf, hybrid vehicle	5.65 (13.1%)	5.46 (16.7%)	6.23 (6.89%)
QSS I3, conventional vehicle	5.54	5.59	6.02
QSS I3, hybrid vehicle	4.68 (15.6%)	4.58 (17.9%)	5.52 (8.30%)
PSAT Civic, conventional vehicle	6.70	6.69	7.28
PSAT Civic, hybrid vehicle	5.40 (19.4%)	4.61 (32.0%)	6.74 (7.42%)

Table 2-2 Fuel consumption, litres per 100km, for the boiler model

The results in Table 2-2 show that there is a reduction in fuel consumption ranging from 7% to 32% for the boiler model. This is a promising result for a simple model; the best

results are for the FTP-75 drive cycle with NEDC being second best, US-06 shows the least improvement. This is due to the US-06 cycle operating at higher temperatures during the high speed section of the cycle whilst the mass flow rate of water through the steam system model remains constant, if the water mass flow rate were varied in proportion with the exhaust gas temperatures, then more heat would be transferred, more steam would be generated and hence more work available to assist the IC engine. These results agree with the findings of Bayley [6] where earlier versions of the FTP-75 and US-06 drive cycles were used, FUDS and FHDS respectively.

The results for the PSAT model give an overall improvement when compared to the QSS-TB equivalent model. This is due to PSAT being a forward looking modelling toolbox and, as stated in the introduction to this chapter, a forward looking model is more suitable for modelling dynamic systems, such as the HYSTOR steam system.

The graphs contained in Figure 2-17 through Figure 2-22 show the power data recorded for each of the drive cycles, using the boiler model. For the QSS-TB model, only the VW Golf results are given and the results are calculated using the following three variables:

1) power demanded on the vehicle (T_ueb * w_ueb from the *Gearbox* block);
2) power developed by the steam system (Torque developed * expander speed from *Steam System* block);
3) power developed by the IC engine (T_GT * w_ueb from *Hybrid Interface* block).

For the PSAT model, the results are calculated using the following three variables:

1) power demanded on the vehicle (accmech_pwr_out from the *Mechanical Accessory* block);
2) power developed by the steam system (steam_torque_developed multiplied by eng_spd_out_simu from *Steam System* and *Engine* blocks respectively);
3) power developed by the IC engine (cpl_pwr_in from *Clutch* block).

2.5 Results from software modelling of the HYSTOR hybrid

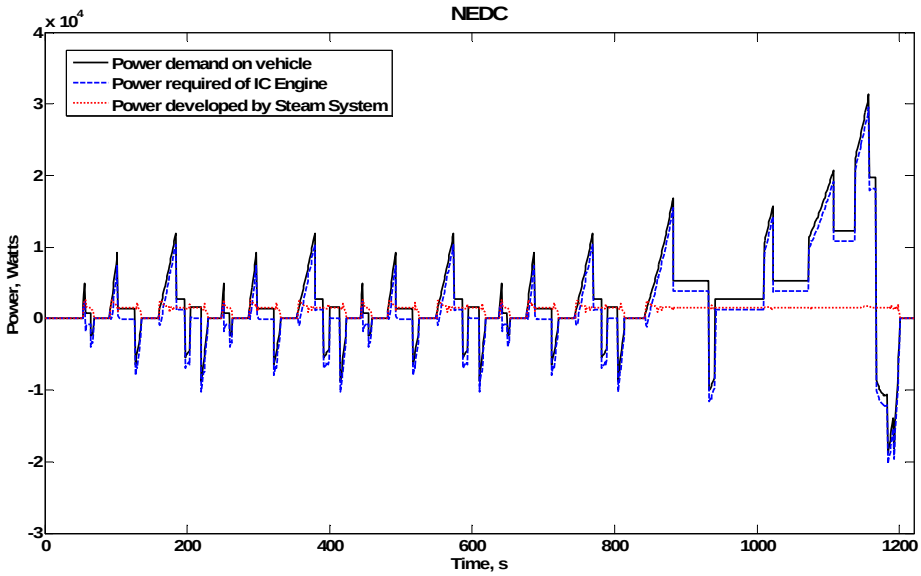

Figure 2-17 Power comparison for QSS-TB boiler model, NEDC

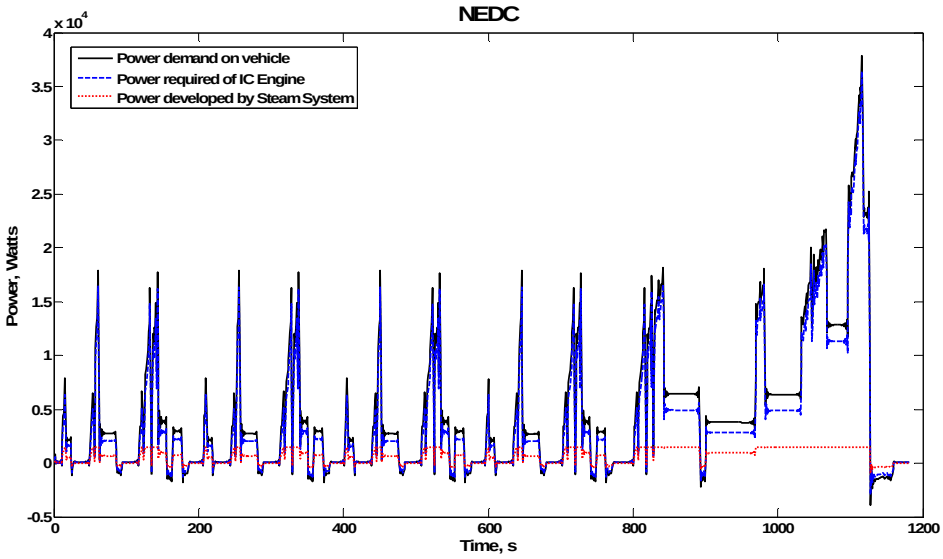

Figure 2-18 Power comparison for PSAT boiler model, NEDC

2.5 Results from software modelling of the HYSTOR hybrid

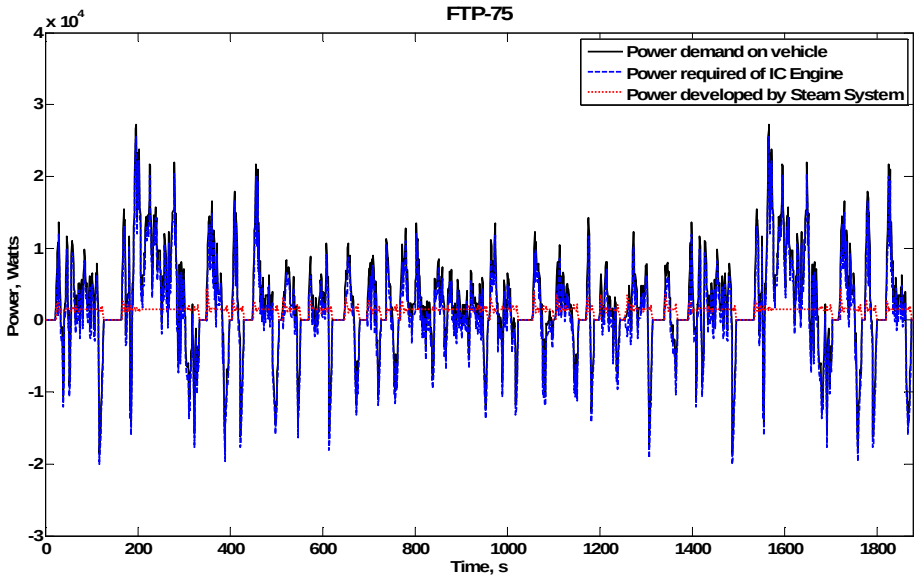

Figure 2-19 Power comparison for QSS-TB boiler model, FTP-75

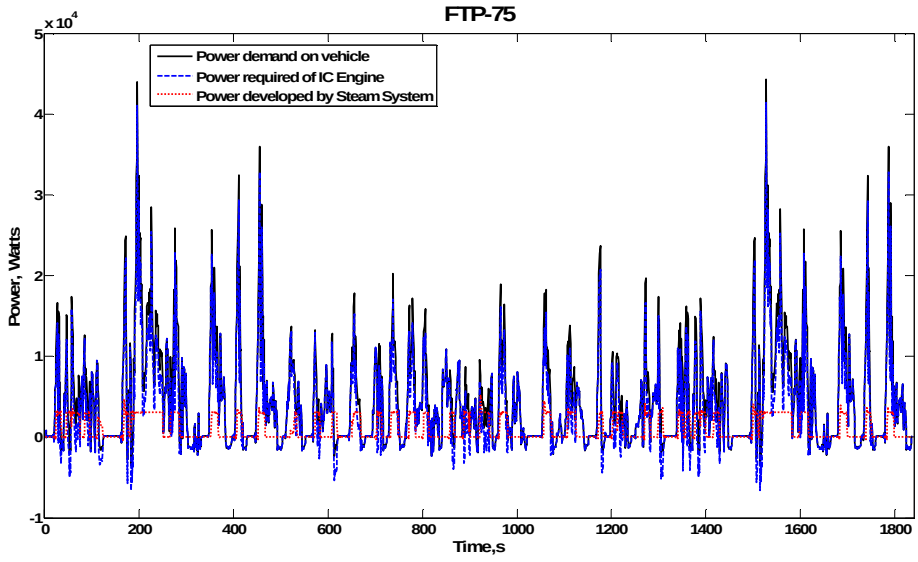

Figure 2-20 Power comparison for PSAT boiler model, FTP-75

2.5 Results from software modelling of the HYSTOR hybrid

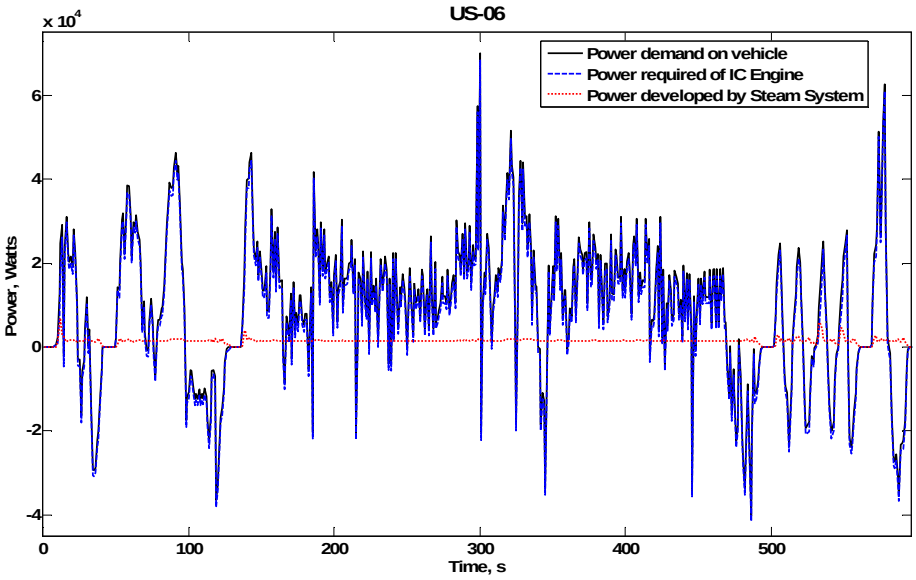

Figure 2-21 Power comparison for QSS-TB boiler model, US-06

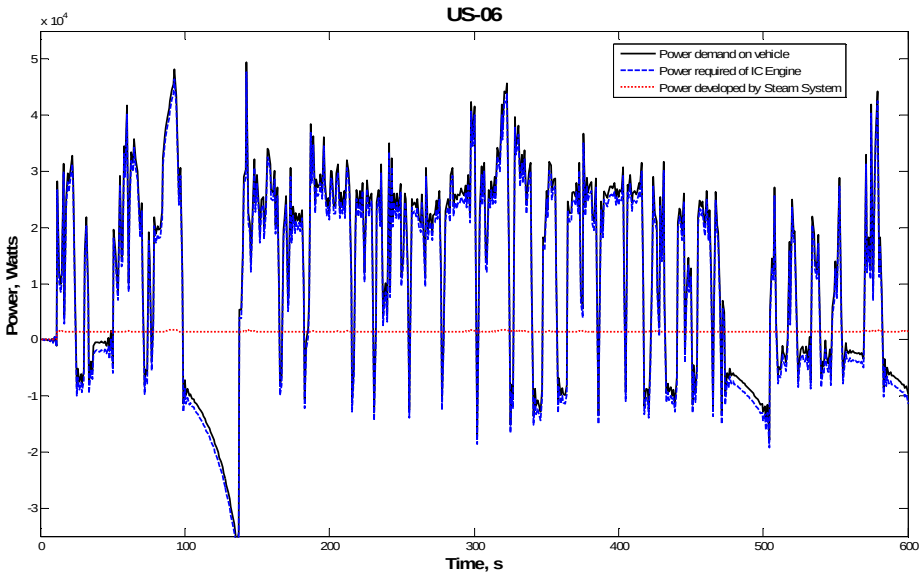

Figure 2-22 Power comparison for PSAT boiler model, US-06

The graphs presented in Figure 2-17 through Figure 2-22 show that the power developed by the steam system was a small percentage of the power demanded; hence, the IC engine provided the majority of the torque. The small percentage of power developed explains the reduction of fuel consumption shown in Table 2-2.

Additionally, the graphs show that positive power was developed by the steam system even when there was a negative power demand on the system (due to braking for example), this indicates that the developed power was wasted and did not contribute to the fuel consumption reduction.

Comparisons of the speed/load points, for each of the model/drive cycle combination are shown in Figure 2-23 through Figure 2-28.

2.5 Results from software modelling of the HYSTOR hybrid

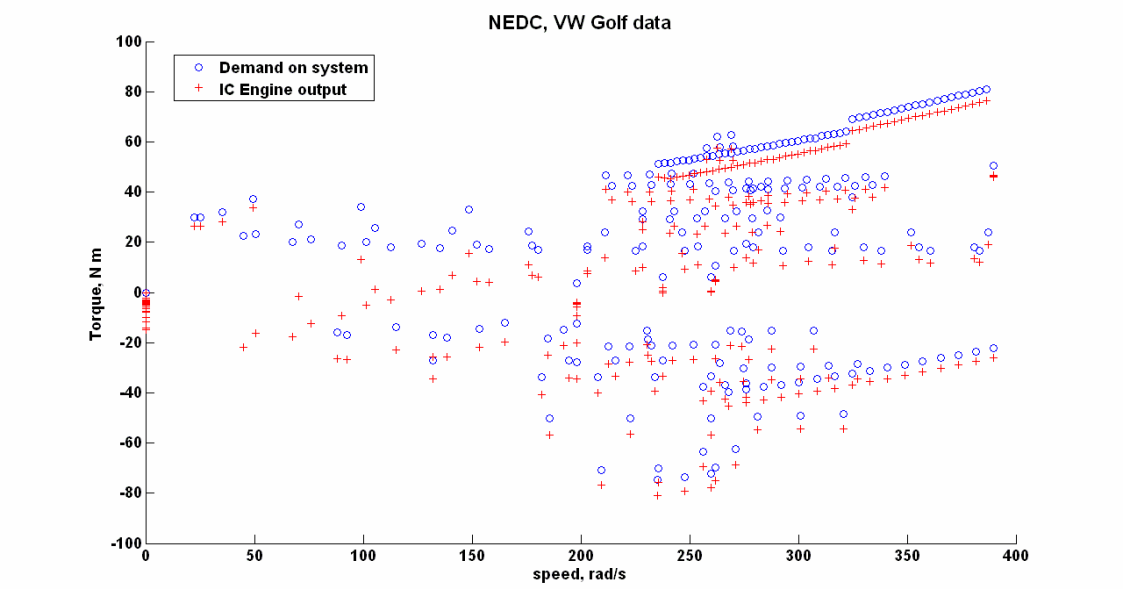

Figure 2-23 Speed and load points for the NEDC drive cycle, QSS-TB boiler model

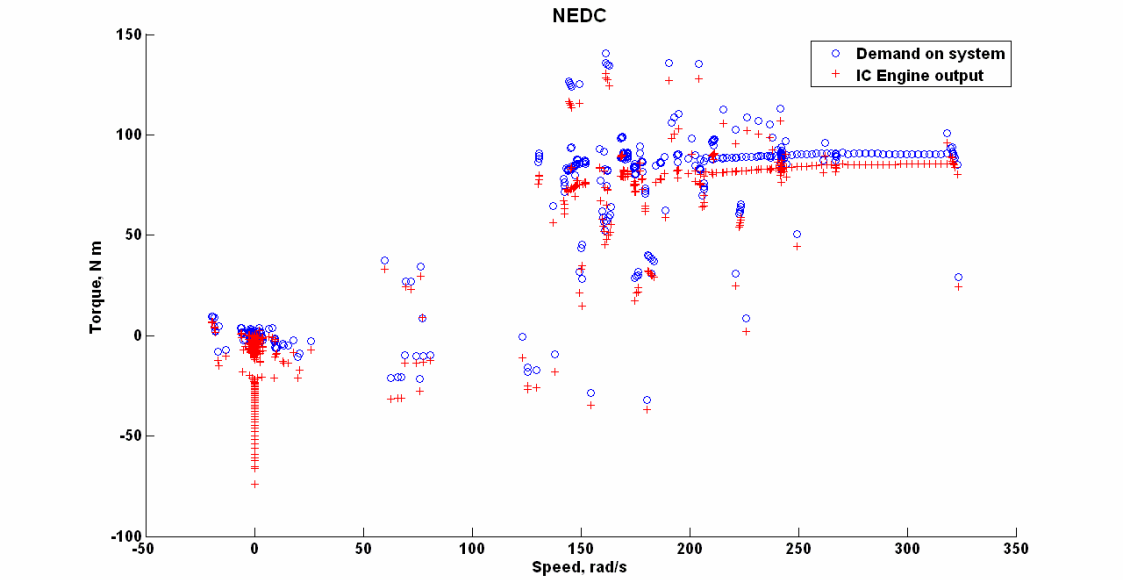

Figure 2-24 Speed and load points for the NEDC drive cycle, PSAT boiler model

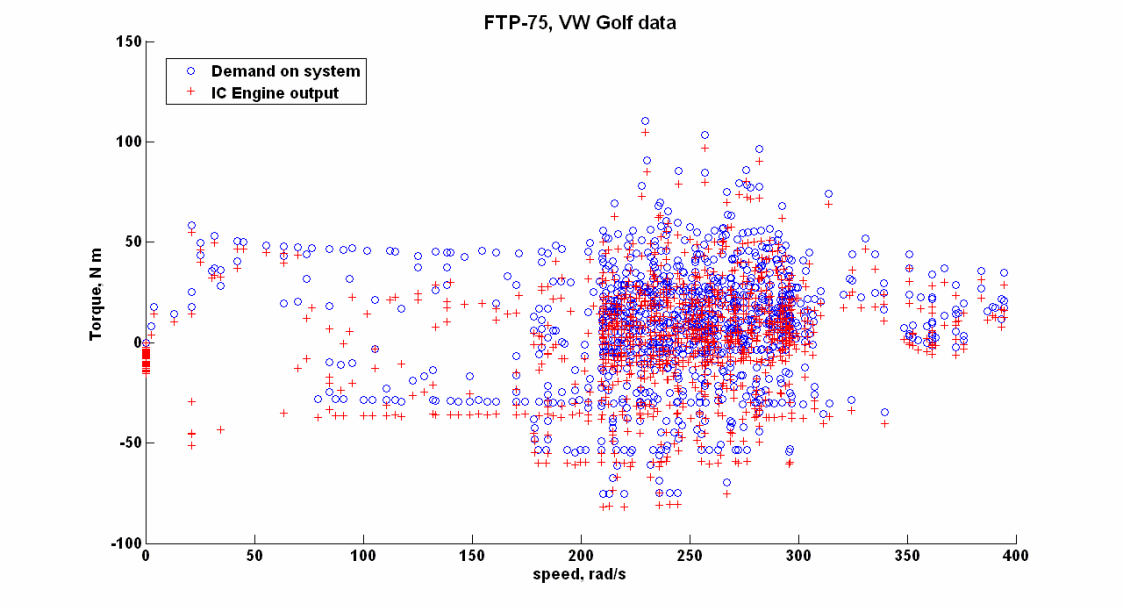

Figure 2-25 Speed and load points for the FTP-75 drive cycle, QSS-TB boiler model

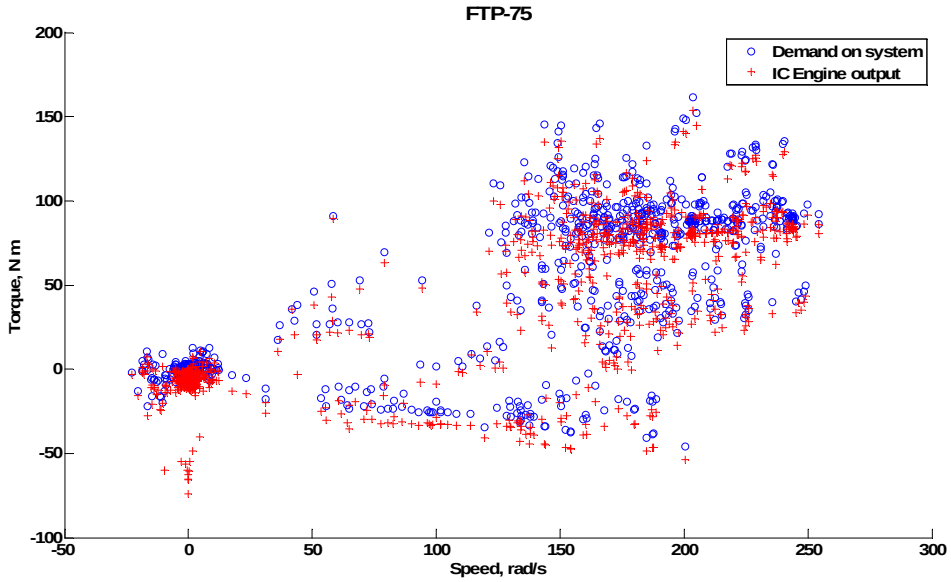

Figure 2-26 Speed and load points for the FTP-75 drive cycle, PSAT boiler model

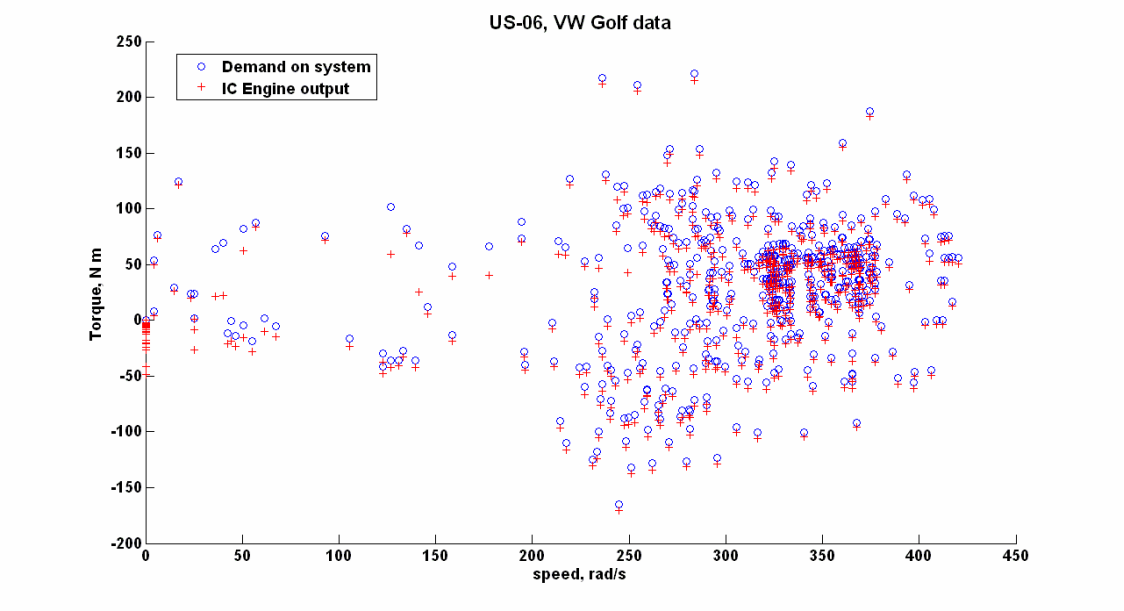

Figure 2-27 Speed and load points for the US-06 drive cycle, QSS-TB boiler model

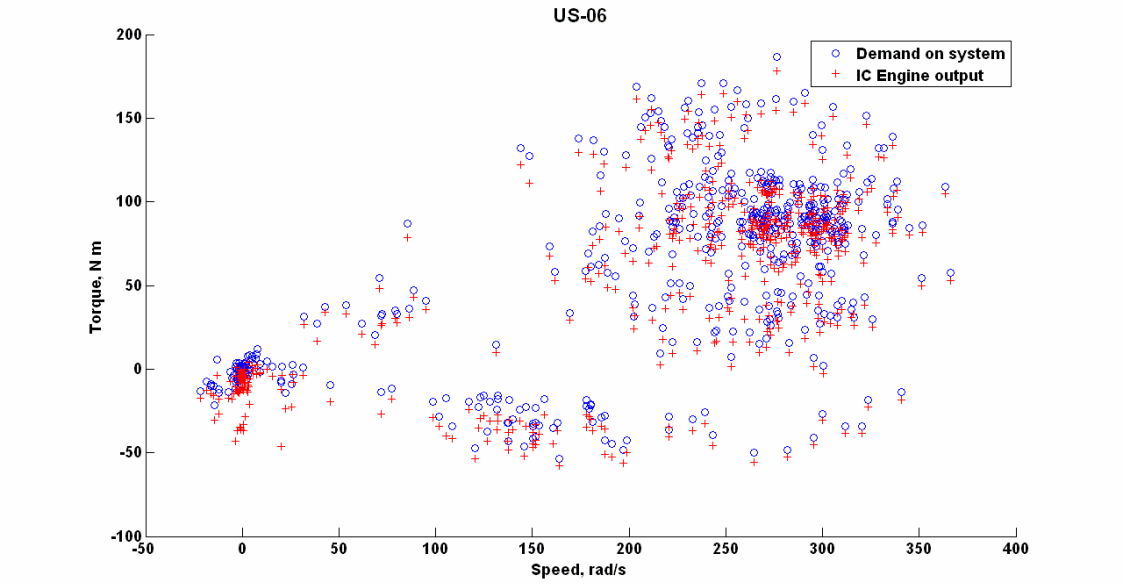

Figure 2-28 Speed and load points for the US-06 drive cycle, PSAT boiler model

As can be seen in Figure 2-23 through Figure 2-28 the positive load on the IC engine is decreased compared with the demand, this contributes to the fuel reduction. Conversely, it can also be seen that the negative loads are also increased, this is due to lack of control on the torque generation, and this indicates wasted torque. An improvement will be

visible when comparing the speed load points for the accumulator model in the next section.

2.5.2 Results for the accumulator model

The accumulator model adds the control algorithm which minimises the instances where steam is used and hence only torque is generated when positive torque is required of the IC engine. Table 2-3 compares the fuel consumption for the conventional vehicles with (a) QSS-TB model with the VW Golf configuration, (b) QSS-TB model with I3 configuration, and (c) the PSAT model with the Honda Civic configuration. The percentage of improvement in fuel consumption for each vehicle/drive cycle combination is also shown. Fuel consumption is given in litres per 100 km, with the percentage improvement in brackets.

	NEDC (European)	**FTP-75 (Urban)**	**US-06 (Highway)**
QSS Golf, conventional vehicle	6.50	6.56	6.69
QSS Golf, hybrid vehicle	5.25 (19.4%)	5.07 (22.6%)	6.16 (7.96%)
QSS I3, conventional vehicle	5.54	5.59	6.02
QSS I3, hybrid vehicle	4.27 (22.8%)	4.18 (25.1%)	5.45 (9.5%)
PSAT Civic, conventional vehicle	6.70	6.69	7.28
PSAT Civic, hybrid vehicle	4.93 (26%)	4.24 (36%)	6.60 (9.4%)

Table 2-3 Fuel consumption, litres per 100km, for the accumulator model

The results in Table 2-3 show that there is a further reduction in fuel consumption ranging from 8% to 36% for this model, compared with 7% to 32% for the boiler model. This is a promising improvement for the simple control algorithm. As was seen with the boiler model, the best results are for the FTP-75 drive cycle with NEDC being second best, US-06 shows less improvement. Again, this is due to the US-06 cycle operating at higher temperatures during the high speed section of the cycle whilst the mass flow rate of water through the steam system model remains constant, if the water mass flow rate were varied in proportion with the exhaust gas temperatures, then more heat would be transferred, more steam would be generated and hence more work available to assist the IC engine. These results continue to back up the findings of Bayley [6], where the FTP-75 and US-06 drive cycles correspond to FUDS and FHDS respectively. results agree

with the findings of Bayley [6] where earlier versions of the FTP-75 and US-06 drive cycles were used, FUDS and FHDS respectively.

The graphs contained in Figure 2-29 through Figure 2-34 show the power data recorded for each of the drive cycles, using the QSS-TB and PSAT models. This data is calculated using the same variables as for the boiler models.

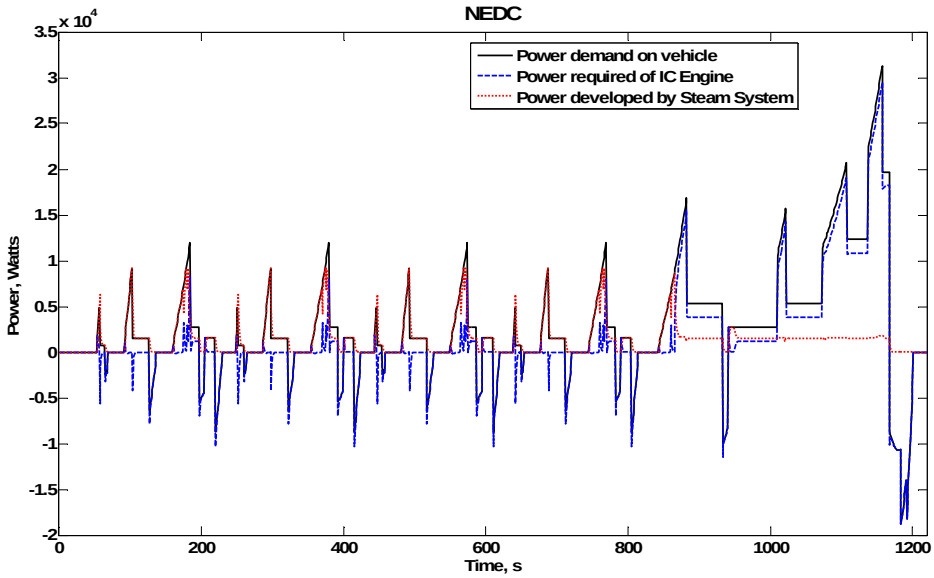

Figure 2-29 Power comparison for QSS-TB accumulator model, NEDC

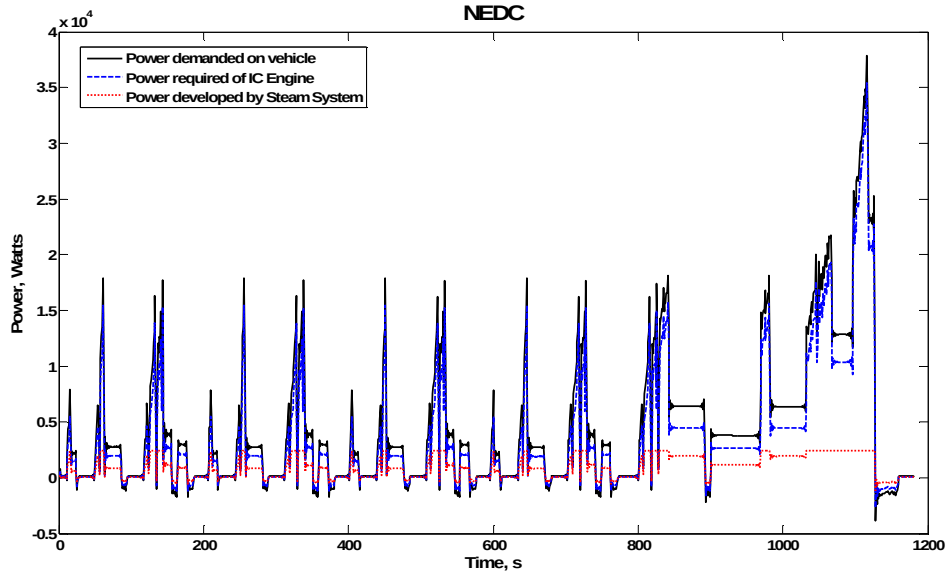

Figure 2-30 Power comparison for PSAT accumulator model, NEDC

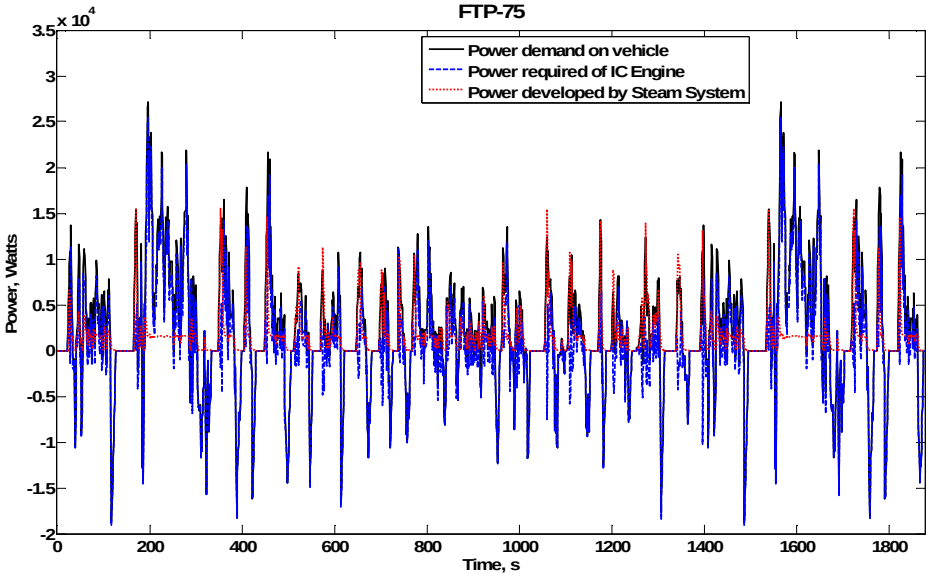

Figure 2-31 Power comparison for QSS-TB accumulator model, FTP-75

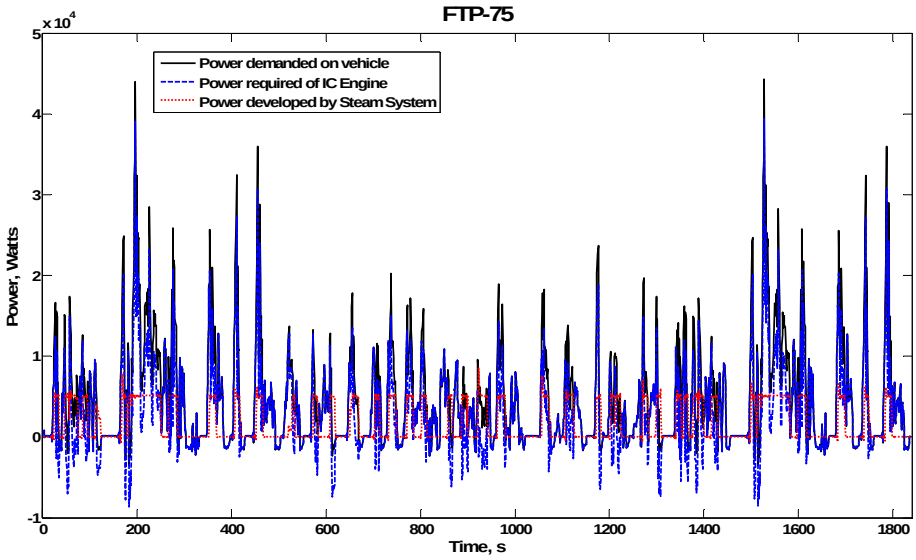

Figure 2-32 Power comparison for PSAT accumulator model, FTP-75

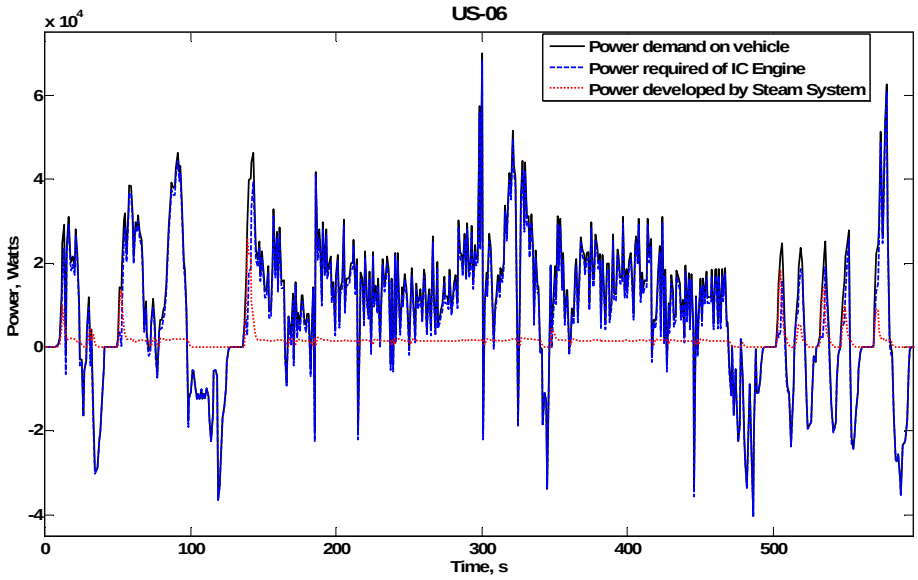

Figure 2-33 Power comparison for QSS-TB accumulator model, US-06

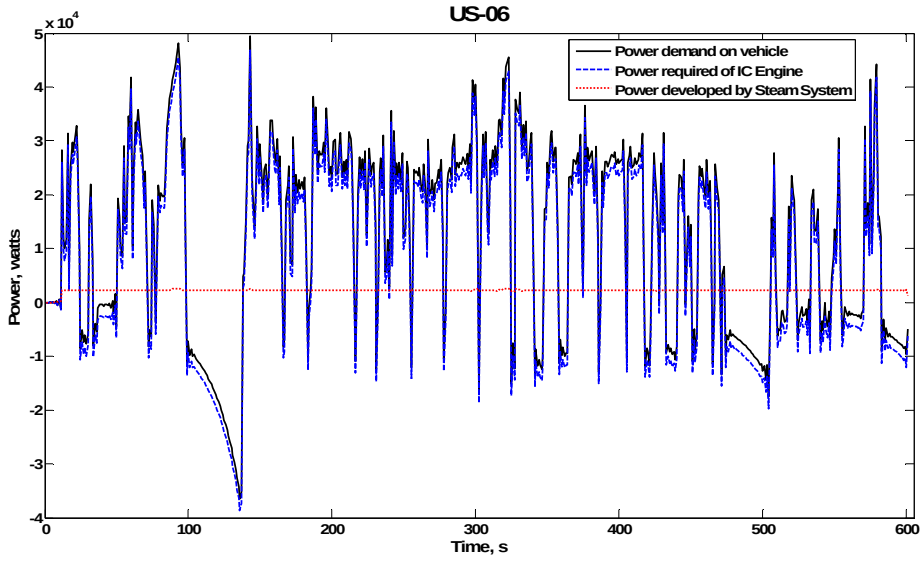

Figure 2-34 Power comparison for PSAT accumulator model, US-06

The graphs presented in Figure 2-29 through Figure 2-34 show that the power developed by the steam system was a noticeably larger percentage of the power demanded, when compared to the power developed by the boiler model, in some instances the power developed by the steam system was more than the power developed by the IC engine. This increase in power developed by the steam system explains the increase in the reduction of fuel consumption shown in Table 2-3.

The graphs also show that positive power was predominantly developed by the steam system when there was a positive power demand on the system and very little power was developed by the steam system when there was a negative power demand on the system (due to braking for example). This indicates that a very small percentage of the developed power was wasted; moreover the fuel consumption was further reduced.

Comparisons of the speed/load points, for each of the model/drive cycle combination are shown in Figure 2-35 through Figure 2-40.

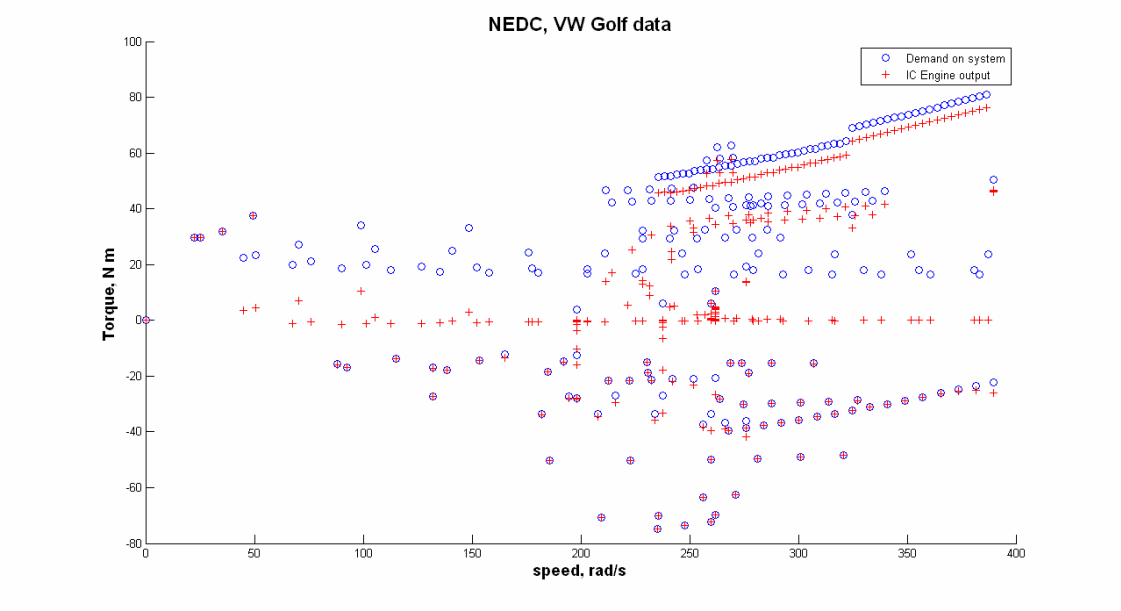

Figure 2-35 Speed and load points for the NEDC drive cycle, QSS-TB accumulator model

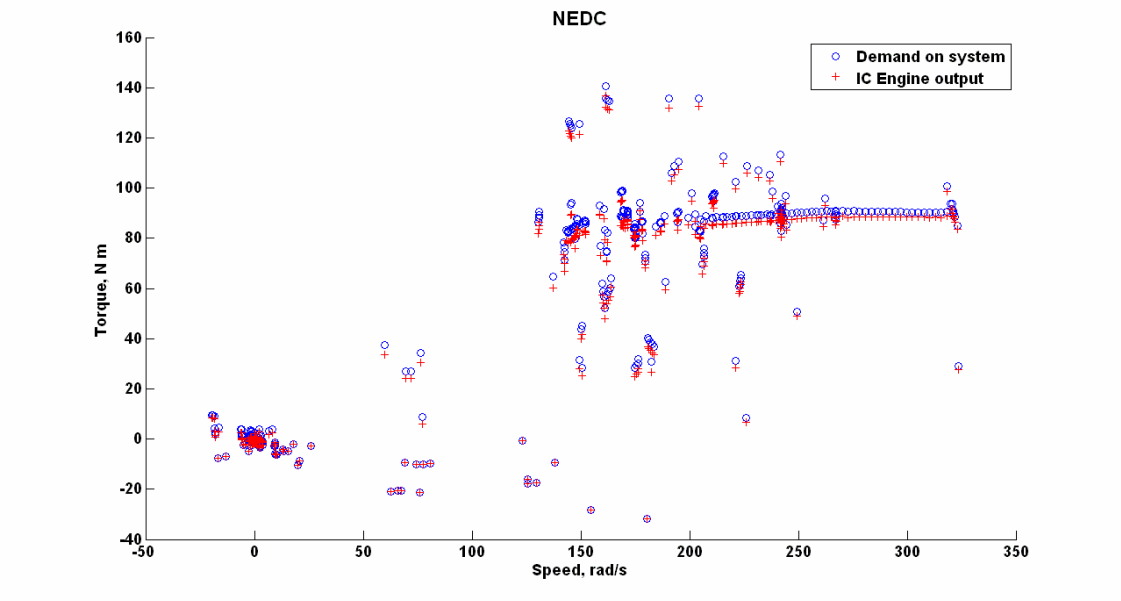

Figure 2-36 Speed and load points for the NEDC drive cycle, PSAT accumulator model

2.5 Results from software modelling of the HYSTOR hybrid

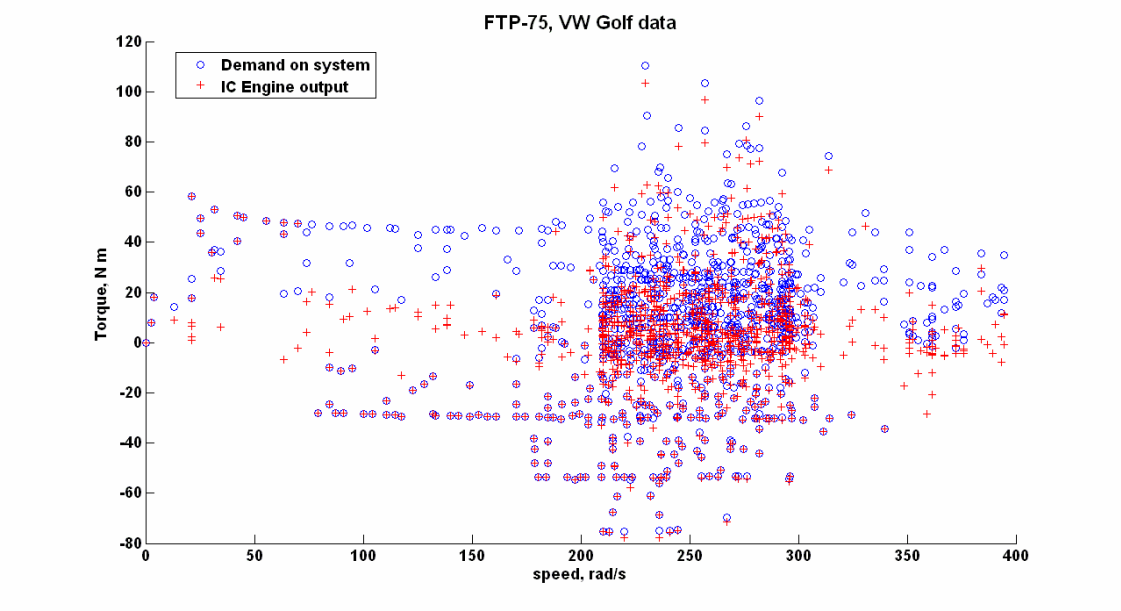

Figure 2-37 Speed and load points for the FTP-75 drive cycle, QSS-TB accumulator model

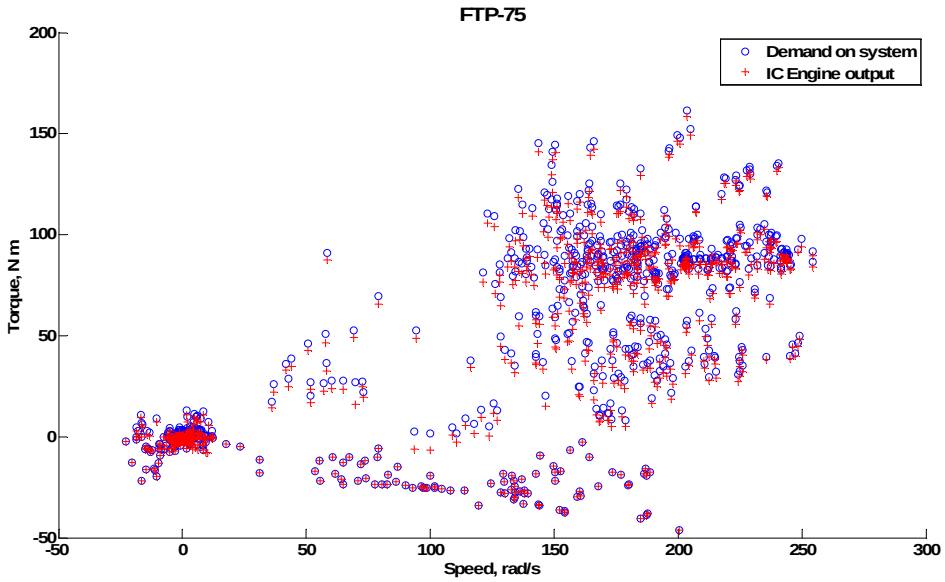

Figure 2-38 Speed and load points for the FTP-75 drive cycle, PSAT accumulator model

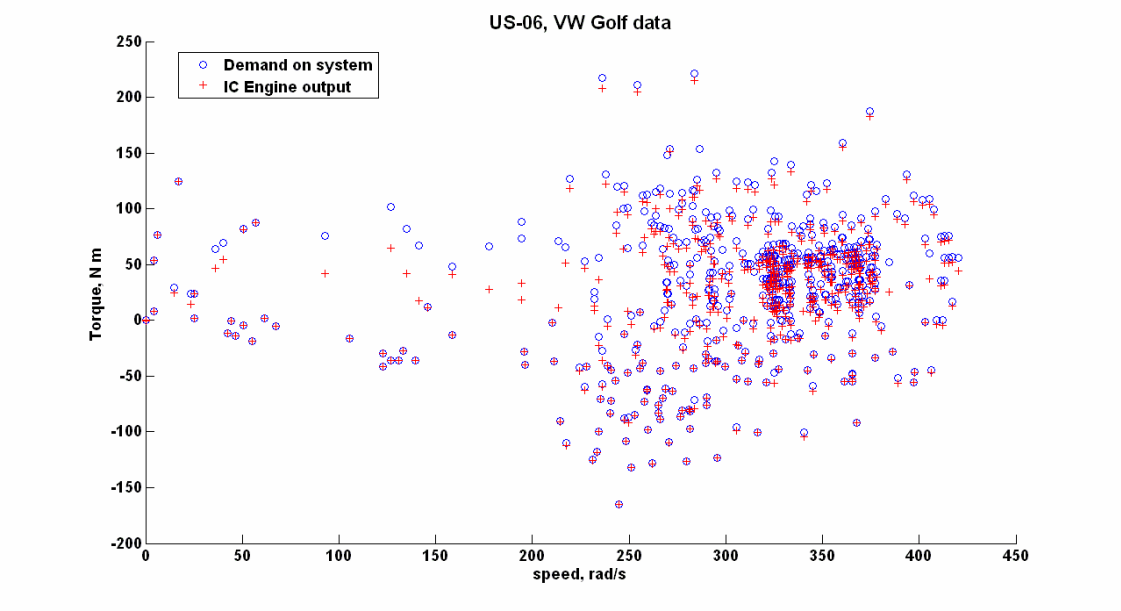

Figure 2-39 Speed and load points for the US-06 drive cycle, QSS-TB accumulator model

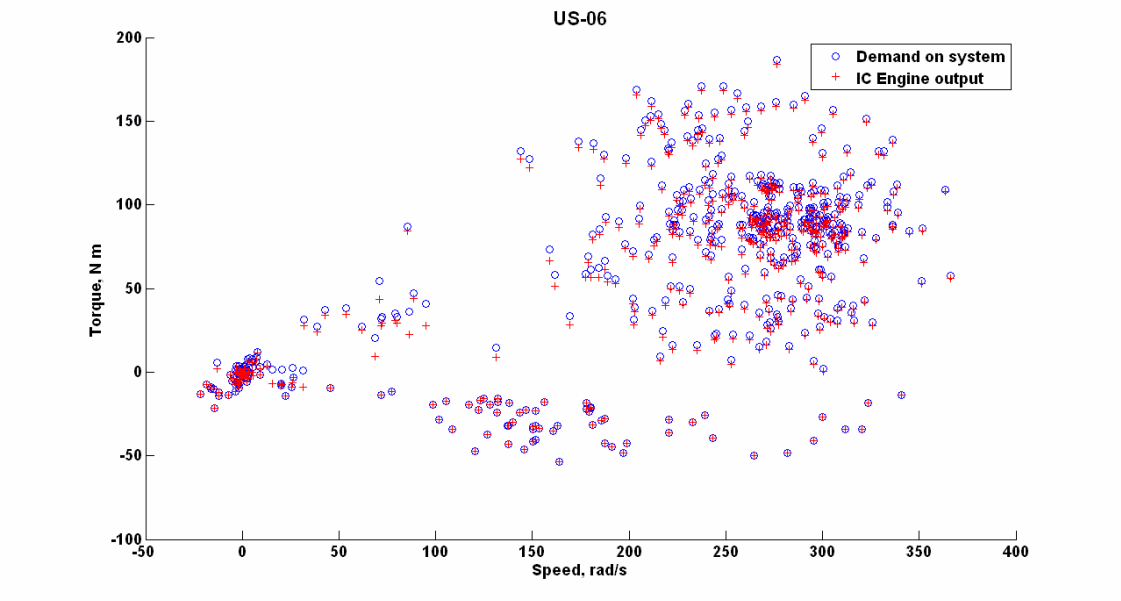

Figure 2-40 Speed and load points for the US-06 drive cycle, PSAT accumulator model

As can be seen in Figure 2-35 through Figure 2-40 the positive load on the IC engine is decreased compared with the demand, this contributes to the fuel reduction. Additionally, it can also be seen that the majority of the negative loads are the same, this was due to the improvement of control on the torque generation, this indicates there was less wasted

power when compared to the boiler model, and that the simple algorithm implemented was an improvement. When comparing the graphs with Figure 2-23 through Figure 2-27 in the previous section it can be seen that the IC engine load points have been bought closer to the zero axis indicating that less steam torque has been wasted.

2.6 Summary and conclusions for software modelling and simulation

The results for the software modelling showed that the addition of the thermal recovery system, in a hybrid vehicle application, leads to a reduction in fuel consumption with both modelling toolboxes for the three drive cycles used.

Table 2-4 summarises the fuel consumption for all the software models developed with QSS-TB and PSAT. The results are shown in litres per 100 km, for each drive cycle, with the percentage of improvement in brackets.

Configuration		**NEDC l/100 km (%)**	**FTP-75 l/100 km (%)**	**US-06 l/100 km (%)**
Conventional	QSS-TB/Golf	6.51	6.56	6.69
	QSS-TB/I3	5.54	5.59	6.02
	PSAT	6.70	6.69	7.28
Boiler	QSS-TB/Golf	5.65 (13.1)	5.46 (16.7)	6.23 (6.89)
	QSS-TB/I3	4.68 (15.6)	4.58 (17.9)	5.52 (8.30)
	PSAT	5.40 (19.4)	4.61 (32.0)	6.74 (7.42)
Accumulator	QSS-TB/Golf	5.29 (19.4)	5.07 (22.6)	6.16 (7.96)
	QSS-TB/I3	4. 27 (22.8)	4.18 (25.1)	5.45 (9.50)
	PSAT	4.93 (26.0)	4.24 (36.0)	6.60 (9.40)

Table 2-4 Summary of fuel consumption for the software models

As can be seen from Table 2-4 the results improve at a similar rate as the thermal model is improved from the boiler model to the accumulator model. Interestingly, looking at the NEDC and FTP-75 results, the PSAT model fuel reduction is substantially larger than for the QSS model. This is due to the dynamic properties of the PSAT tool being more suited to the thermal energy recovery system. This can be attributed to PSAT being a forward looking modelling toolbox and, as stated in the introduction to this chapter, a forward looking model is more suitable for modelling dynamic systems, such as the HYSTOR steam system.

A different picture appears for the US-06 results, with the improvement being similar for QSS and PSAT. This agrees with the conclusions made by Bayley [6] who reported that

the FUDS drive cycle gave a better performance than the FHDS drive cycle with respect to fuel consumption reduction; FUDS and FHDS are earlier versions of FTP-75 and US-06, respectively. This is due to the US-06 cycle operating at higher temperatures during the high speed section of the cycle whilst the mass flow rate of water through the steam system remains constant causing saturation conditions to be met more readily than for the NEDC and FTP-75 cycles. If the water mass flow rate were controlled in such a way that any fluctuations in exhaust gas conditions caused a proportional fluctuation in mass water flow rate, then more heat would be transferred, more steam would be generated and hence more work available to assist the IC engine. It will be seen in Chapter 5, where the control of the system is further developed, and the mass flow rate of water was taken into consideration, that an improvement and further reduction in fuel consumption was observed.

The improvement from implementing the simple accumulator algorithm can be visualised by comparing the US-06 results. Figure 2-21 and Figure 2-22 are for the boiler model, during the negative power sections, the steam system is still generating power, however looking at the accumulator model results in Figure 2-33 and Figure 2-34, the power developed is only by the steam system in the positive power sections, which decreases the fuel consumption.

This is confirmed by looking at the speed/load comparison graphs. For the boiler model results, the loads are reduced for both positive and negative points, whereas for the accumulator model the loads are only reduced for the positive points and these reductions are larger. This type of control could be improved and optimised further with knowledge of the IC engines economy line so that the IC engine is operating at its most efficient load whenever possible. This optimisation is discussed further in Chapter 6.

The results from the hybrid modelling show that there are significant fuel economy advantages (up to 36% improvement from the PSAT simulation results) and that this can be achieved at practical operating pressures (18 bar boiler pressure was used in the simulation models).

2.6 Summary and conclusions for software modelling and simulation

As expected, the PSAT models yielded better results than QSS-TB, for the NEDC and FTP-75 cycles, due to its dynamic properties which are better suited for heat transfer calculations and applications.

However, as good as the results are for the models, the question of whether the results are realistic must be considered. The model components at this stage were simple, for example the expander model was a representation of ideal isentropic expansion, the modelling of an accumulator was a simple set of integrators carrying the overall net steam used and generated, that did not take into consideration the quality of the accumulated steam, which may deteriorate over time, depending on environment condtions. Additionally, the weight of the added components were not taken into consideration, neither were possible friction losses due to mechanically coupling the steam expander and IC engine work outputs. Finally, the models assumed heat was available instantaneously, and did not consider the dynamics of the system over time. Some of these issues will be considered in Chapter 5, whilst others will be considered for further work in Chapter 7.

The models developed in this phase of the project were used to develop control models in Chapter 5 and to further compare fuel consumption between different control algorithms and architectures.

3 Test facility, data acquisition and results for expander testing

3.1 Expander test introduction

This chapter presents a brief overview of the expander test facility setup, data acquisition requirements and summarises the results for the expander testing.

Although the use of steam as an energy provider is a concept that has existed for a long time, with the advent of electricity usage and development of the internal combustion expander, the current use is limited to large power plants and the process industry, hence recent research and results are sparse and restricted to specialist areas. Consequently there was a need to conduct investigations into steam expansion and power production, with respect to smaller applications. The philosophy behind the HYSTOR research plan was to begin the expander testing with small expanders. Working on a small scale had a number of advantages; the experiments were more manageable and the use of steam and gases was made possible without the need for specialist facilities.

The expander configurations used are presented in Section 3.2. A description of test plan is given in Section 3.4. In Section 3.5 the expander test results are presented in the form of graphs and tables generated from the data acquired during testing.

There is some discussion in Section 3.6, which will validate the data acquired during expander testing and summarise the results.

3.2 Expander configurations

The expander tests were run using adapted miniature expanders, O.S. model aircraft engines, as detailed in the following sections, more detail on the expander data can be found in Appendix C.

The three expander configurations used were as follows:

1) Rotary – modified with two inlet ports and two exhaust ports;
2) Uni-flow – in this configuration the flow is in one direction and the inlet is physically positioned in a different part of the working cylinder to the outlet;
3) Counter-flow – in this configuration the flow is around the cylinder and the inlet and outlet are physically positioned in the same part of the working cylinder.

This chapter will focus on the rotary and uni-flow expanders, as the results for the counter-flow expander were poor compared to the other two. A description of the counter-flow expander and the test results can be found in Appendix E (nitrogen) and Appendix F (steam).

3.2.1 Rotary configuration

A 4.97 cc Wankel expander was modified to run as a Wankel steam expander. There were two inlet ports and two exhaust ports, positioned to obtain optimum performance. The inlet port was positioned at 20° to the minor symmetric line of the expander and the exhaust valves were adapted to be positioned on the side of the expander casing rather than the perimeter of the rotor housing.

For early tests, only one pressure sensor was used, positioned at 90° to the minor symmetric line of the expander. However, as this did not give a full picture of what was happening inside the moving chamber, two pressure sensors were obtained and placed as shown in Figure 3-1.

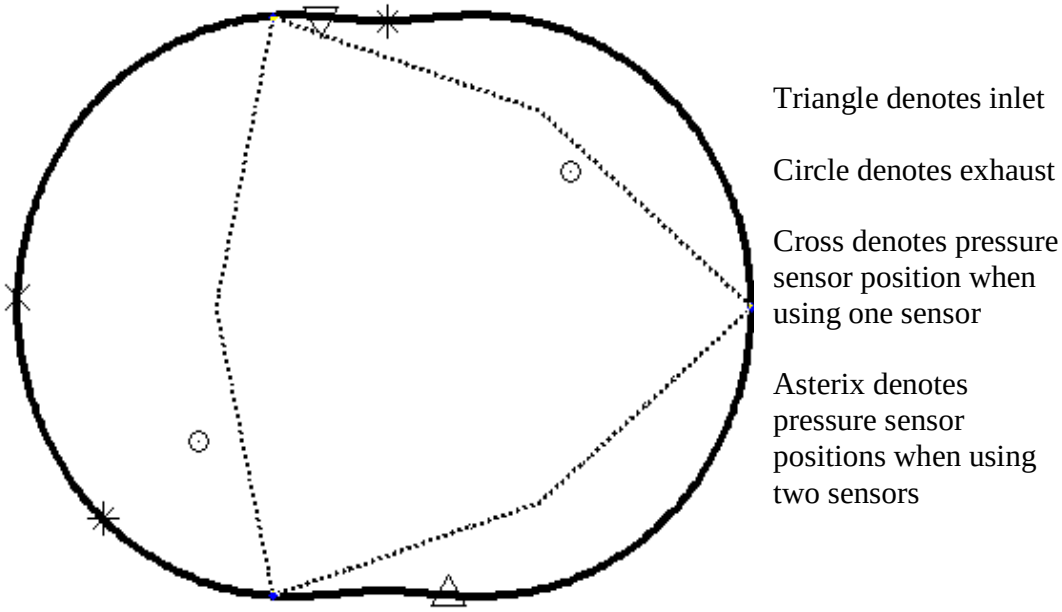

Figure 3-1 Outline drawing of the rotary expander showing position of pressure sensors

For the initial tests, inlet flow was not controlled so the mass flow rate was constant into both inlet ports as shown in Figure 3-2. This is referred to as a port valve configuration.

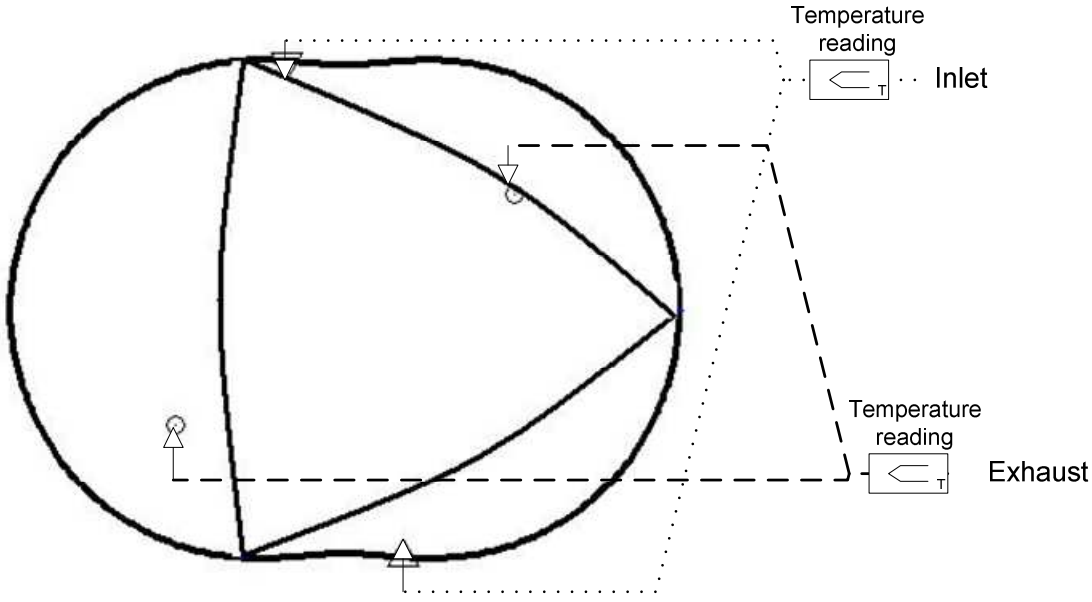

Figure 3-2 Outline of rotary expander showing inlet and exhaust configuration and thermocouple positions when no control valves were used

To improve control of the expander, the inlets had mechanical solenoid valves attached so that the mass flow rate could be altered and hence improve controllability of operation and efficiency, this can be visualised in Figure 3-3.

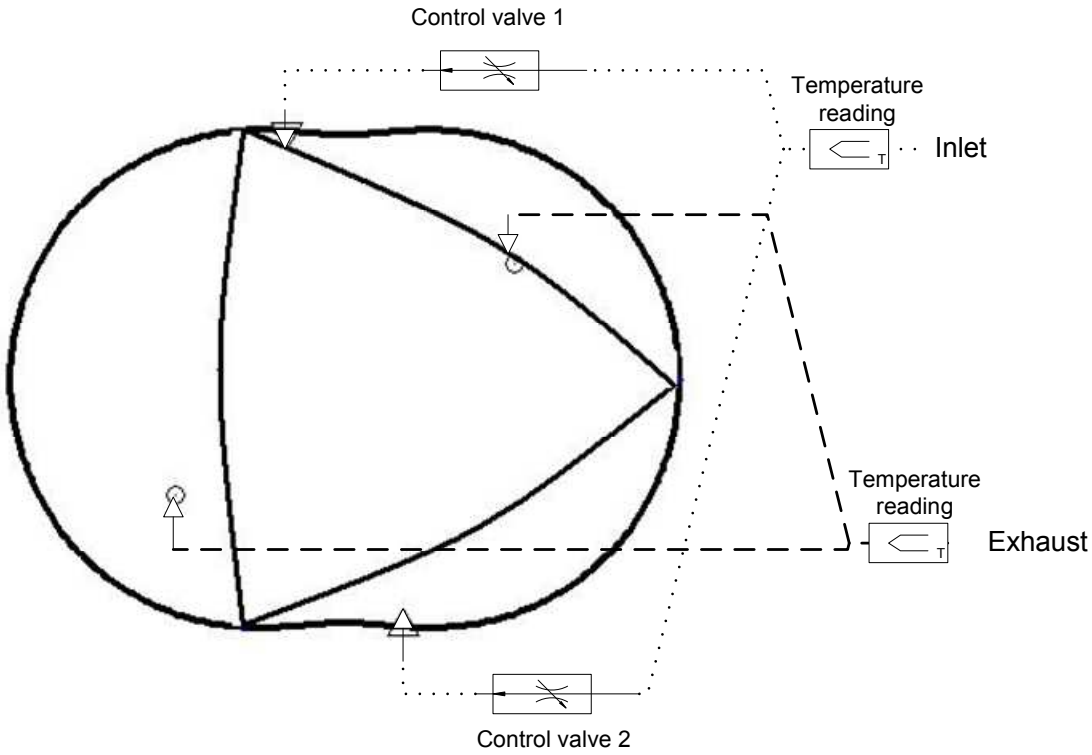

Figure 3-3 Outline of rotary expander showing inlet and exhaust configuration and thermocouple positions with control valves attached to the inlets

The rotary expander had three working chambers as shown in Figure 3-4.

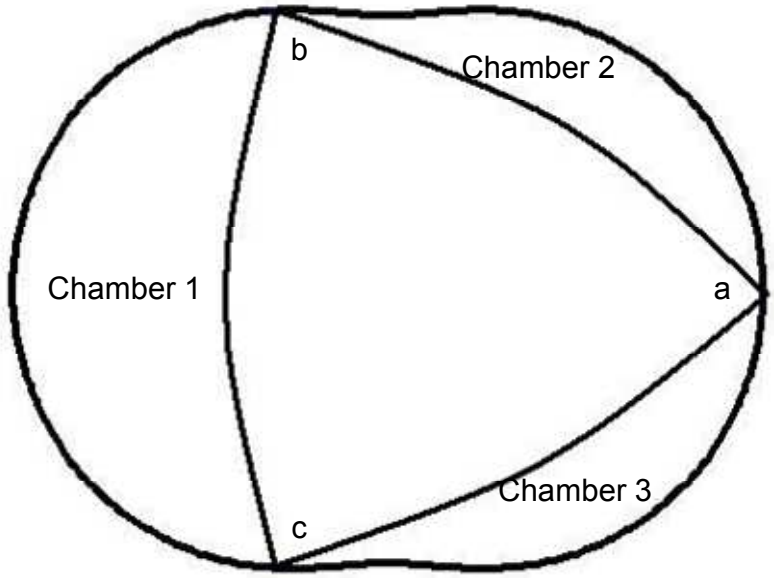

Figure 3-4 Rotary expander chambers and rotor tip labels

The rotor rotates anti-clockwise so that chamber 1 leads chamber 2 followed by chamber 3, the tips are also labelled to aid understanding of the pressure data and development of the GT-POWER models, further described in Chapter 4. Figure 3-5 shows the timing diagram for the rotary expander with respect to chamber one when there were no control valves attached.

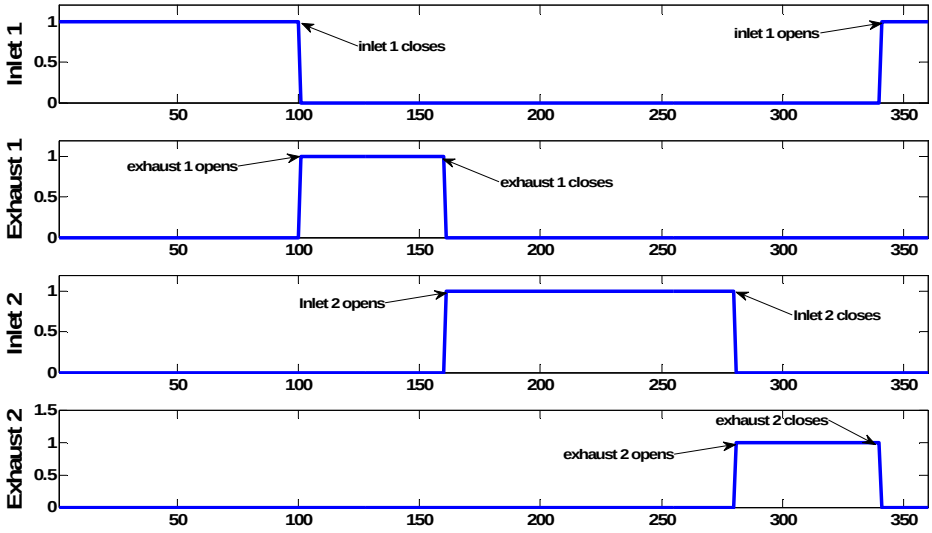

Figure 3-5 Rotary expander timing diagram for chamber 1

Figure 3-5 represents one complete rotor turn, and hence three shaft turns, with the start point as represented by Figure 3-4. The inlets are exposed for 120 rotor degrees and the exhausts are exposed for 60 rotor degrees, zero represents closed and one represents open. When the control valves are attached the inlet open time was varied, this is further discussed in Appendix D.3.

3.2.2 Uni-flow configuration

The expander used for the uni-flow tests was a 4.3 cc two-stroke reciprocating expander operating with a uni-flow configuration. Initially the inlet was controlled by a fuel injector valve; this was later replaced by a solenoid valve to improve the mass flow rate. The configuration and flow is shown in Figure 3-6.

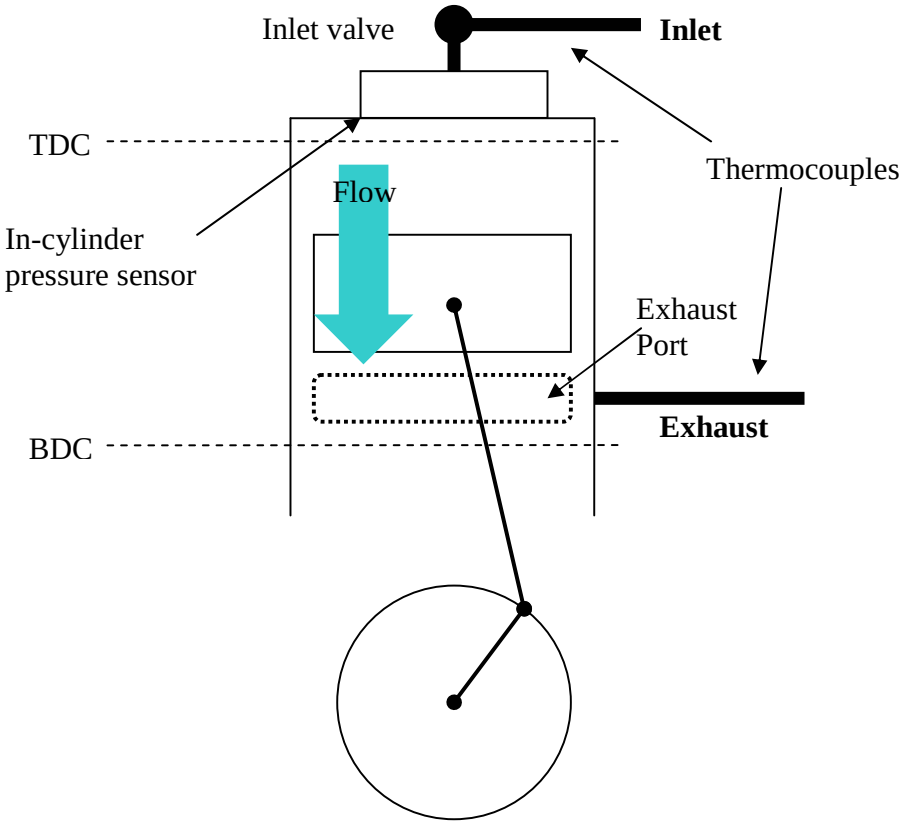

Figure 3-6 Outline of the uni-flow expander and sensors

The flow can be visualised in Figure 3-6, as the cylinder position is constant there was only one pressure sensor utilised.

3.3 Expander test setup and specification

The experimental set-up, referenced in Chapter 3, is shown in Figure 3-7 and consisted of a dynamometer, a data acquisition system controlled by National Instruments LabVIEW software, steam/air supply and a condenser unit.

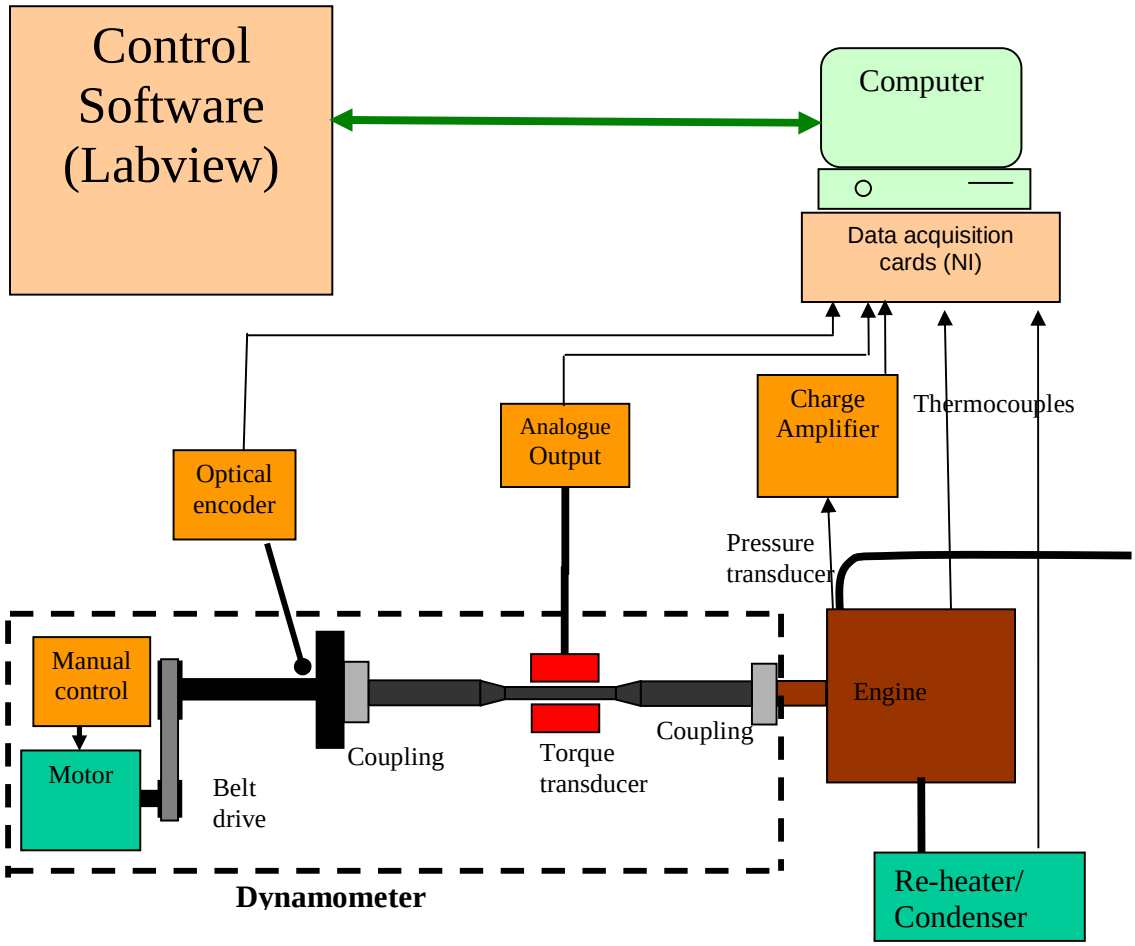

Figure 3-7 Experimental setup

The dynamometer was derived from a model maker's lathe (the WM180 from Warren Machine Tools [53]) and the drive train was modified to absorb power and to motor at a fixed speed when necessary. The expander output shaft was mounted inline with the lathe shaft through the torque transducer arrangement. A 400 W DC motor drove the main

shaft and also absorbed power. Using the motor drive enabled speed control of the main shaft and hence stable speeds were possible during data acquisition.

The sensor inputs were fed to the logging system via multi channel data acquisition cards; NI DaQ card, type 6251 and type 6259. The end of the drive shaft was fitted to an optical encoder that generated three pulse streams, namely (i) pulse per revolution; (ii) pulse per revolution -90° (directional indicator); and (iii) pulse per crank angle degree.

When the expanders were operating in steam mode, the exhaust was fed into a re-heater section (SQA - steam quality analyser - which was used to determine the quality of the steam, see Appendix D for more information) then into a condenser, after which the weight of the condensed steam was recorded to calculate the mass flow rate.

3.3.1 Data acquisition

The PC used had one internally connected NI DaQ card, type 6251, and an externally connected type 6259 USB box, both of which had the following specifications.

Resolution: 16 bits;
Sampling rates: 1 to 1.25/1.0 (MS/s) (single/multiple channel);
Absolute accuracy (full scale): ±1920 µV;
Input voltage range: ±10 V.

The NI-6259-USB was used for the thermocouple data acquisition and the NI-6251 was used for all other data acquisition.

3.3.2 Inputs to LabVIEW

Table 3-1 lists the various inputs to the PC and LabVIEW, what unit the inputs were measuring and how they were connected.

3.3 Expander test setup and specification

Quantity (Unit)	Connection to expander	Connection to PC	Range
Input temperature (°C)	K-type thermocouple	Direct connection to NI-6259-USB box (2 channels)	Temp: 0°C to 300°C
Exhaust temperature (°C)	K-type thermocouple	Direct connection to NI-6259-USB box (2 channels)	Temp: 0°C to 300°C
SQA inlet temperature (°C)	K-type thermocouple	Direct connection to NI-6259-USB box (2 channels)	Temp: 0°C to 300°C
SQA outlet temperature (°C)	K-type thermocouple	Direct connection to NI-6259-USB box (2 channels)	Temp: 0°C to 300°C
In-cylinder pressure (Pa)	Pressure sensors	Charge amplifier into NI-6251 card voltage reader (2 channels max)	Pressure: 0 bar to 250 bar Voltage: ±10 V
Source pressure (Pa)	Pressure sensor	Charge amplifier into NI-6251 card voltage reader (1 Channel)	Pressure: 0 bar to 100 bar Voltage: ±10 V
SQA inlet pressure (Pa)	Pressure transducer	NI-6251 card voltage reader (1 channel)	Pressure: 0 bar to 1 bar Voltage: 0-5 V
SQA outlet pressure (Pa)	Pressure transducer	NI-6251 card voltage reader (1 channel)	Pressure: 0 bar to 1 bar Voltage: 0-5 V
Speed (rpm)	Torque transducer	NI-6251 card voltage reader (1 channel)	Speed: 0 rpm to 20,000 rpm Voltage :±10 V
Torque (N m)	Torque transducer	NI-6251 card voltage reader (1 channel)	Torque: 0.1 N m to 20 N m Voltage: ±10 V
Revolutions	Optical encoder	NI-6251 card digital input (1 channel)	1 pulse per revolution used as a trigger to start sampling data
Crank angle	Optical encoder	NI-6251 card digital input (1 channel)	1 pulse per degree crank angle rotation to trigger sampling

Table 3-1 Inputs to data acquisition software, LabVIEW

3.3.3 Outputs from LabVIEW

The NI data acquisition cards were used to output digital pulses in order to control the opening and closing of the fuel injectors and solenoid valves that were attached to the inlet and exhausts of the expanders. Two pulse streams were utilized from the optical encoder by the data acquisition card. The pulse per revolution (ppr) pulse was aligned with the top dead centre of the piston. This pulse triggered a counter that used the pulse per crank angle degree (ppc) pulse as a source of clock ticks. The counter used two variables, a delay which represented the delay from ppr pulse to the start of the pulse to open the injector valve and a pulse width which represented the amount of time the valve was to be open.

Initially, fuel injector valves were used to control the inlet/exhaust to the two/four stroke expanders, due to the injectors' ability to operate at high speeds. However, it became apparent that the injectors could not offer full mass flow rate and additionally could not operate at high temperatures, i.e. 175°C for 10 bar steam. Mechanical solenoid valves were used instead and more favorable results were obtained, however this was at the expense of higher speeds with the maximum speed possible being 600 rpm. The solenoid valves also introduced a response time delay of between 6 and 9 ms, 6 ms with no pressure, 8 ms with 10 bar pressure and 9 ms with 15 bar pressure.

For the uni-flow expander the inlet valve opening times were optimized for each speed step, this was achieved by altering the valve opening time and closing time, separately, in steps of approximately 2 crank angle degrees, then recording the average torque at these settings. The optimum settings are as shown in Table 3-2, Top Dead Centre (TDC) is assumed at 0°.

Speed (rpm)	10 bar Steam		10 bar Nitrogen		15 bar Nitrogen	
	Open before TDC	Closed after TDC	Open before TDC	Closed after TDC	Open before TDC	Closed after TDC
150	4	26	22	8	16	15
200	6	28	18	16	12	24
300	9	36	18	23	16	11
400	19	31	33	9	28	12
500	21	33	36	8	33	12
600	25	32	39	7	36	14

Table 3-2 Timings for the uni-flow expander, in crank angle degrees

The data shown in Table 3-2 can be visualised by in the example timing diagram as shown in Figure 3-8.

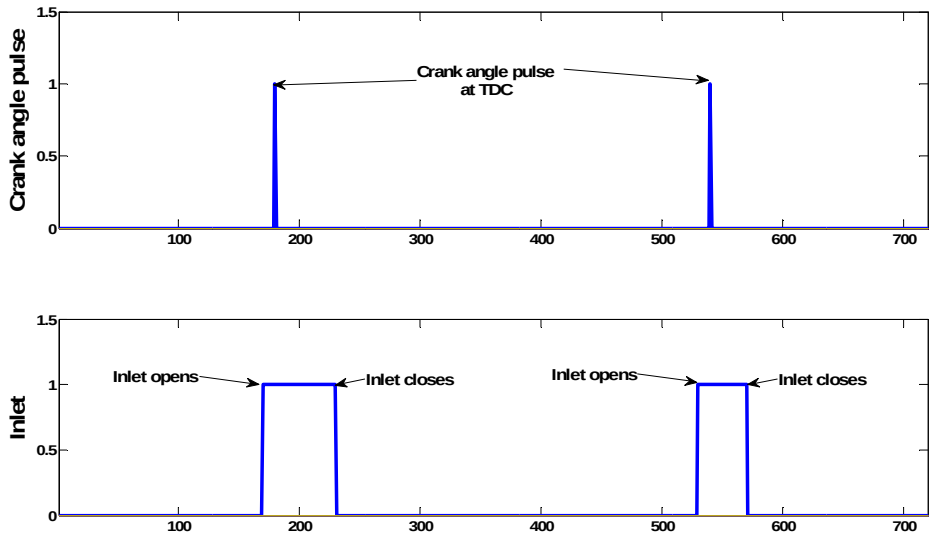

Figure 3-8 TDC, inlet valve and outlet valve pulse shown over two revolutions

As stated in Section 3.2.1, for initial testing of the rotary expander, no inlet control was employed, however as it became apparent that control was required to improve the efficiency, both the inlets had solenoid valves attached and hence these were controlled by the output pulses of the NI data acquisition cards.

3.3.4 Measurements

In addition to the inputs to LabVIEW, power was calculated as a product of speed and torque (Power = $2\pi NT$) and the mass flow rate of water was measured using a timer and a weighing scale.

The measurements were recorded by LabVIEW at the sampling rate given by the ppc pulse from the optical encoder to a Labview measurement file. This, in turn, was used as an input to MatLab where the results were collated and plotted.

3.4 Expander tests conducted

The working fluids used for the expander testing were steam and compressed nitrogen. The reasoning behind using both steam and nitrogen for the tests was to provide a balanced set of results. Additionally, the advantage of using nitrogen is that it removes the complexities of, for example, steam condensing during expansion.

The test plan initially was to test each expander with steam and compressed nitrogen at 7, 10, 15 and 20 bar, however it soon became apparent that not all the tests were feasible with the expander configurations. This was because the in-cylinder pressure, at the top of the compression stroke, for the uni-flow and counter-flow expanders was approximately 7 bar, hence, very little positive torque was recorded due to the friction torque cancelling out the positive torque.

The rotary expander worked well at 7 bar and 10 bar for both steam and compressed nitrogen, however when higher pressures of steam were used, the higher temperatures caused the sealing tips on the rotors to expand and jam the rotor.

Although the fuel injector valves could cope with the high speeds, up to 2300 rpm, they had some disadvantages. The injectors contained a small plastic filter, which melted when steam was used, this was removed but results were still poor, due to the small cross-sectional area, restricting mass flow rates. When solenoid valves were employed, the results were more favourable, however the trade-off was a limit to speed steps, the valves could not be successfully controlled over 600 rpm.

The 7 bar compressed air tests were run using shop air, the 10 bar and 15 bar compressed nitrogen tests were run using bottled compressed nitrogen. The steam tests were run using a re-commissioned steam generator. It was planned to use steam at between 7 bar and 25 bar. However due to the limitations of the expander configurations leading to the fact that anything above 10 bar steam could not be utilised (expansion within the rotary expander and the solenoid valves were only rated for 10 bar at 100°C) only 10 bar tests were feasible.

Tests involving the fuel injectors and solenoid valves were preceded by a set of optimising tests. During these tests different opening times and length of opening (pulse start and pulse width) were recorded, then the results collated and the points giving the best torque/power were recorded in full.

Table 3-3 shows the combination of expander configurations and source type and source pressure that were tested along with some explanatory notes.

Expander	Source Type	Source Pressure (bar)	Note
Rotary expander, port valves	Compressed Air	7	1
	Compressed Nitrogen	10, 15	-
	Steam	10, 15	2
	Steam	10	3
Uni-flow expander with fuel injector	Compressed Air	7	1
	Compressed Nitrogen	10, 15	-
Uni-flow expander, with solenoid valves	Compressed Nitrogen	10, 15	-
	Steam	10	3
Counter-flow expander, with solenoid valves	Compressed Nitrogen	10, 15	4
	Steam	10	5
Rotary expander, with solenoid valves	Compressed Nitrogen	10, 15	-
	Steam	10	3

Table 3-3 Expander and source combinations tested

Note 1 – As the in-cylinder pressure for the uni-flow was around 7 bar, no useful results with 7 bar compressed air were obtained, so it was decided not to use these results.

Note 2 – For these results the torque transducer was faulty so torque and power were calculated from the current and voltage used by the dynamometer motor, however as the voltage was not constant, these results may be unreliable.

Note 3 – The solenoid valves used were not rated high enough for the temperatures and pressure experienced with 15 bar steam.

Note 4 – See Appendix E for these results.

Note 5 – See Appendix F for these results.

3.5 Expander test results using steam

As the HYSTOR concept is based on the use of steam, this section concentrates on the results using steam, with the exception of a validation of the experimental setup using the nitrogen results given in section 3.4.1. The full set of nitrogen test results, for all expander configurations, can be found in Appendix E.

3.5.1 Results details

Sections 3.5.2 through 3.5.5 show the results, graphically, for the variation of specific power over speed, the variation of torque over speed, the variation of pressure over crank angle and pressure-volume (p-v) diagrams. The power was calculated from the speed and torque data, the specific power was then calculated by dividing the power by the expander capacity, for example 4.97 cc for the rotary expander.

Additionally, a calculation of torque using the pressure/volume data was performed and compared with the measured torque for all expander configurations except the uni-flow with injector valves. For the uni-flow and counter-flow configurations this was calculated using the pressure and volume data. The work per cycle was calculated using Equation 3.1:

$$W = \oint P \partial v \tag{3.1}$$

The work per cycle was then converted to torque by dividing the result by 2π.

The torque for the rotary expander was calculated using Equation 3.2 from [54].

$$T(\alpha) = Ae\left[P_1 \sin 2\alpha + P_2 \sin\left(\frac{\pi}{3} - 2\alpha\right) - P_3 \sin\left(\frac{\pi}{3} + 2\alpha\right)\right] \tag{3.2}$$

Where:

A is the area of the rotor flank, length=0.0377m, width=0.0145m,

A = length.width = 0.000546m²;

α is the rotor angle degree (with respect to tip a in Figure 3-4, Section 3.2.1);

e is the eccentricity = 0.0029m, of the radius of the inner rotor shaft;

P_1, P_2 and P_3 are the pressures on the rotor flank for chamber 1, chamber 2 and chamber 3 (as in Figure 3-4, Section 3.2.1), respectively.

As stated in the previous section, the nitrogen tests were used to balance the results and hence validate the experimental setup and data acquisition. To highlight this, the results for 10 bar compressed nitrogen with the uni-flow, solenoid valve configuration are now considered. The variation of torque over speed is shown in Figure 3-9.

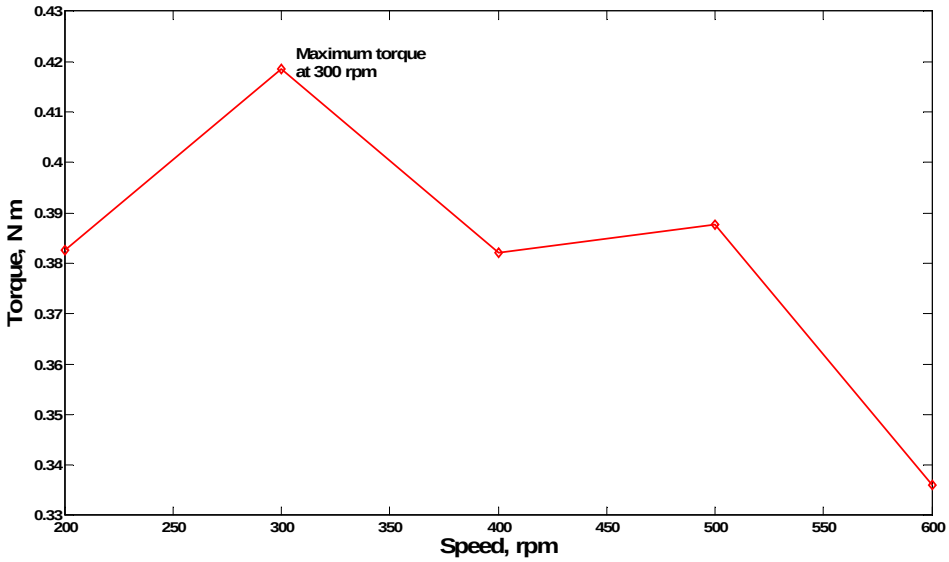

Figure 3-9 Torque, uni-flow expander, 10 bar compressed nitrogen

As can be seen in Figure 3-9 the maximum torque is observed at 300 rpm, this is a low speed for a maximum torque, this could be attributed to the limitations of the solenoid valves used in these tests. For this speed step the pressure volume data is obtained, the variation of pressure over volume is shown in Figure 3-10.

3.5 Expander test results using steam

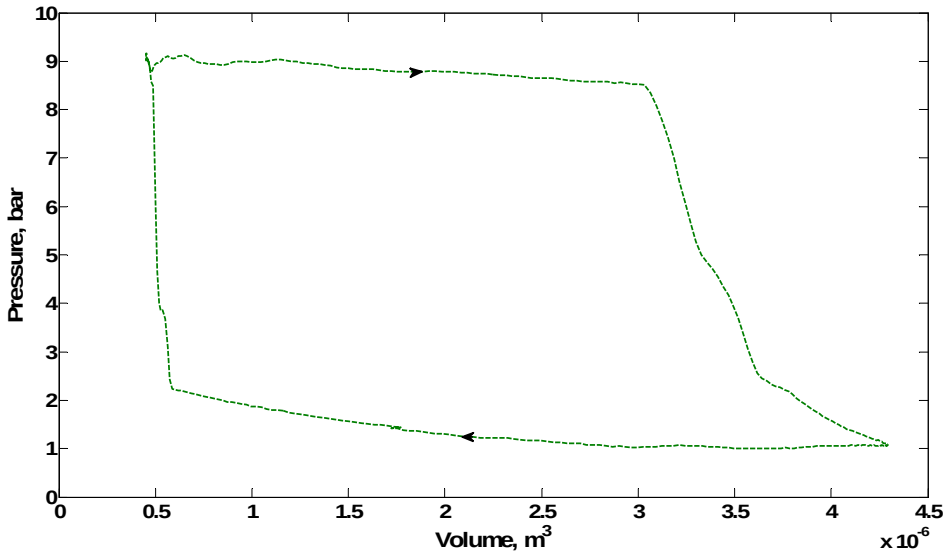

Figure 3-10 P-v diagram, uni-flow expander, 10 bar compressed nitrogen, 300 rpm

Using the pressure volume data and Equation 3.1 the work is calculated and hence the torque obtained, Table 3-4 compares the two torque results.

Speed (rpm)	Measured Torque (N m)	Calculated Torque (N m)	Percentage Difference
300	0.4186	0.4008	4.45

Table 3-4 Uni-flow expander, 10 bar nitrogen, torque comparison at 300 rpm

As can be seen from Table 3-4, the torque values are within ±5% of each other. In general ±5% is standard figure for an acceptable comparison range of values when comparing and validating results, therefore the nitrogen results have validated the experimental setup. These comparisons are calculated for each set of results to continue the validation process.

The friction torque was recorded for each expander configuration in order for the actual torque to be calculated from the test results by subtracting the friction torque from the recorded torque. The friction torque curves are shown in Figure 3-11.

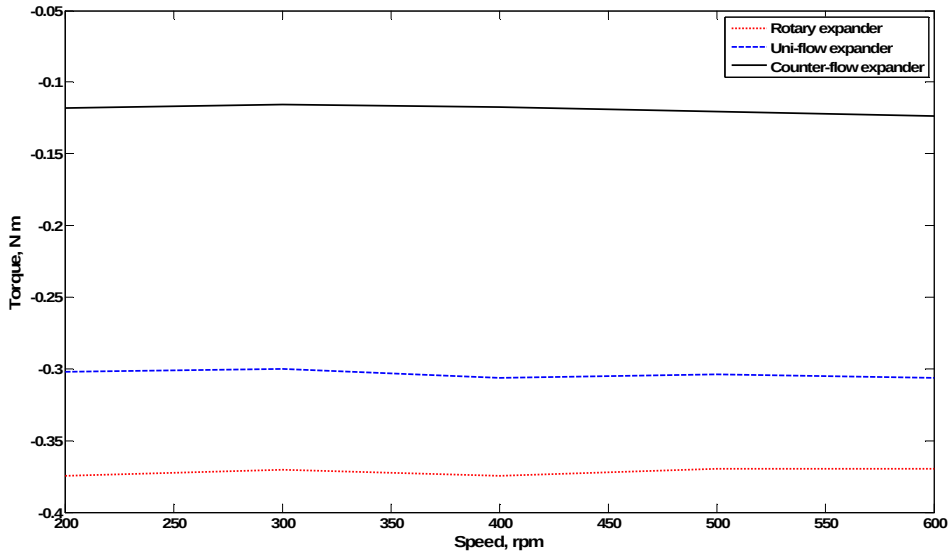

Figure 3-11 Friction torque curves for the expander configurations

As can be seen in Figure 3-11, the friction torque for the uni-flow expander is, on average, -0.3 N m, this equates to an friction mean effective pressure (fmep) of 7.2 bar, explaining why not much positive torque was recorded for the tests using compressed air at 7 bar.

Section 3.5.6 contains tables for the maximum specific torque and maximum specific power recorded for each expander configuration. Mass flow rates and calculated efficiencies are presented in Section 3.5.7.

3.5.2 Rotary expander with port valves

The results contained in this section are for the rotary configuration illustrated in Figure 3-2, Section 3.2.1. For this configuration the rotary expander was equipped with ports that create fixed inlet and exhaust timings.

Speed steps (rpm) for these tests were 200, 300, 500, 700, 900, 1100, 1300, 1500, 1700 and 2000 (maximum). Figure 3-12 shows the variation of specific power and torque over speed.

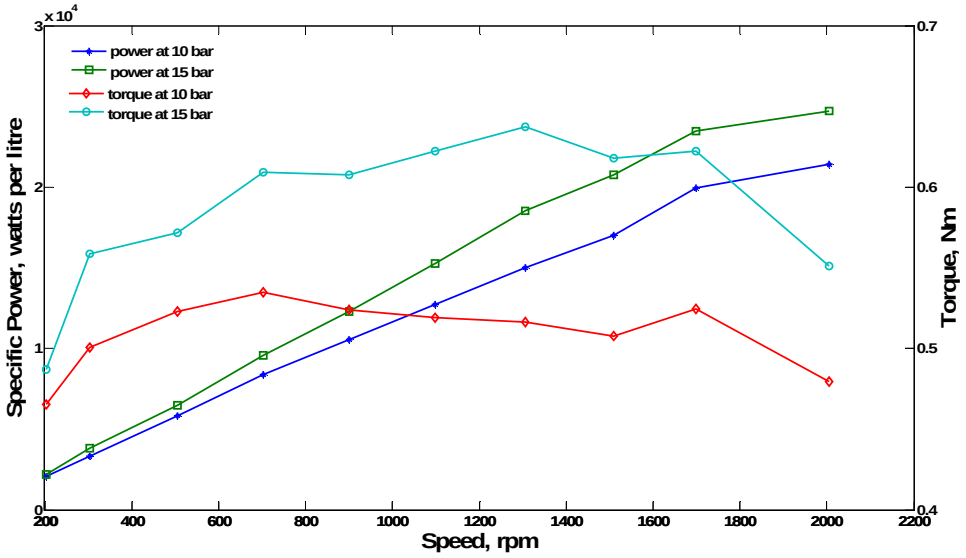

Figure 3-12 Specific power and torque, rotary expander, 10 bar and 15 bar steam

As can be seen from Figure 3-12, higher torques and specific power were recorded at the higher pressure setting; maximum torque for 10 bar was obtained at 1700 rpm, maximum torque for 15 bar was obtained at 1300 rpm and maximum specific power occurred at 2000 rpm for both pressures. Figure 3-13 shows the variation in pressure over one crank shaft rotation with 10 bar steam.

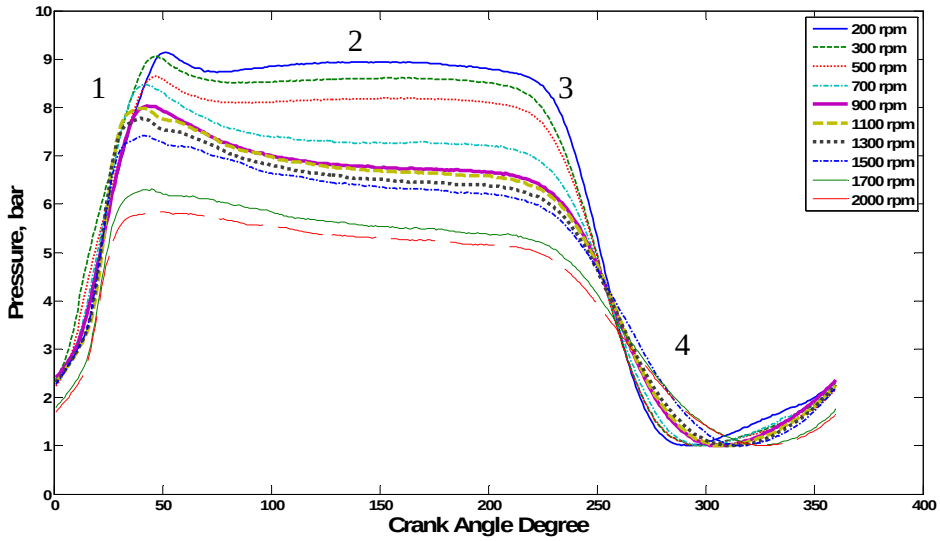

Figure 3-13 Pressure per cycle, rotary expander, 10 bar steam, with one pressure sensor

The pressure data is explained as follows:

1. Inlet port opened, pressure rises to boiler pressure;
2. Pressure held at boiler pressure whilst inlet is closed;
3. Exhaust port is opened and pressure drops to atmospheric pressure;
4. Slight rise in pressure here is due to some compression in the chamber as the volume decreases just before the inlet is opened in the next cycle.

For the pressure data acquisition at 15 bar, fewer speed steps were used due to the high temperature conditions making the setup unstable. This was because the rotary expander had separate seals attached to each rotor tip, these tended to expand when using steam and after a time would expand so much they began to bind with the surface of the rotary chambers and eventually the expander would seize.

The speed steps (rpm) were 200, 300, 500, 900, 1300 and 1700 (maximum). Figure 3-14 shows the variation in pressure over one crank shaft rotation with 15 bar steam.

3.5 Expander test results using steam

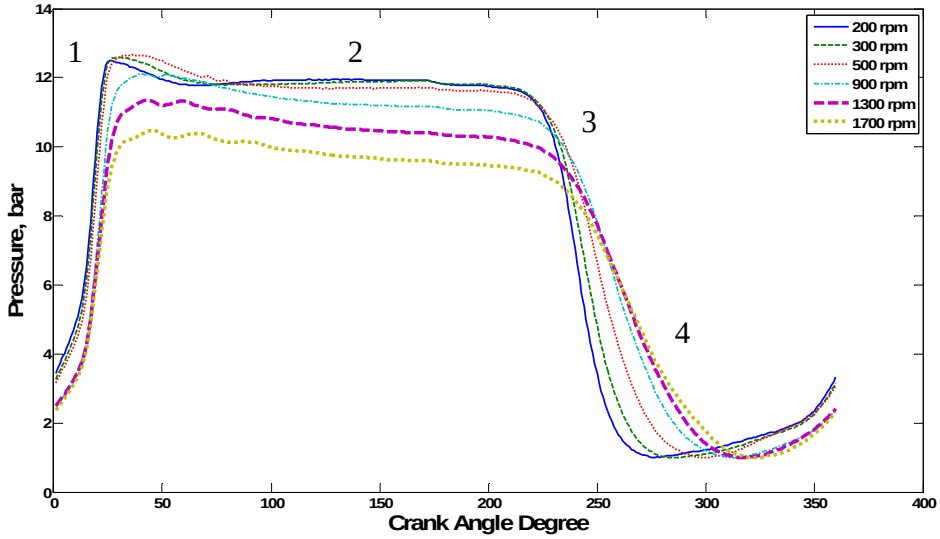

Figure 3-14 Pressure per cycle, rotary expander, 15 bar steam, with one pressure sensor

The pressure data is explained as follows:

1. Inlet port opened, pressure rises to boiler pressure;
2. Pressure held at boiler pressure whilst inlet is closed;
3. Exhaust port is opened and pressure drops to atmospheric pressure;
4. Slight rise in pressure here is due to some compression in the chamber as the volume decreases just before the inlet is opened in the next cycle.

Figure 3-15 shows the pressure volume diagram using 10 bar steam for each speed step.

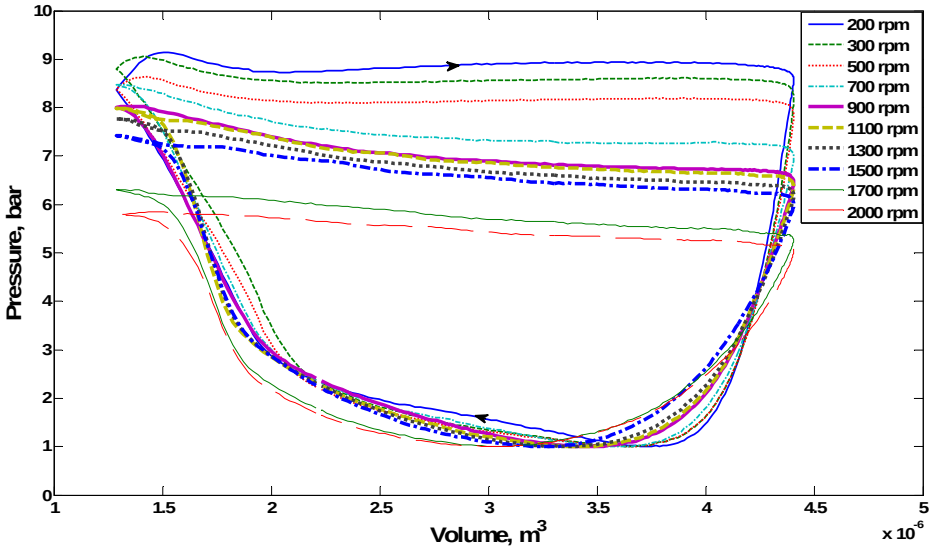

Figure 3-15 P-v diagram, rotary expander, 10 bar steam, with one pressure sensor

Figure 3-16 shows the pressure volume diagram using 15 bar steam for each speed step.

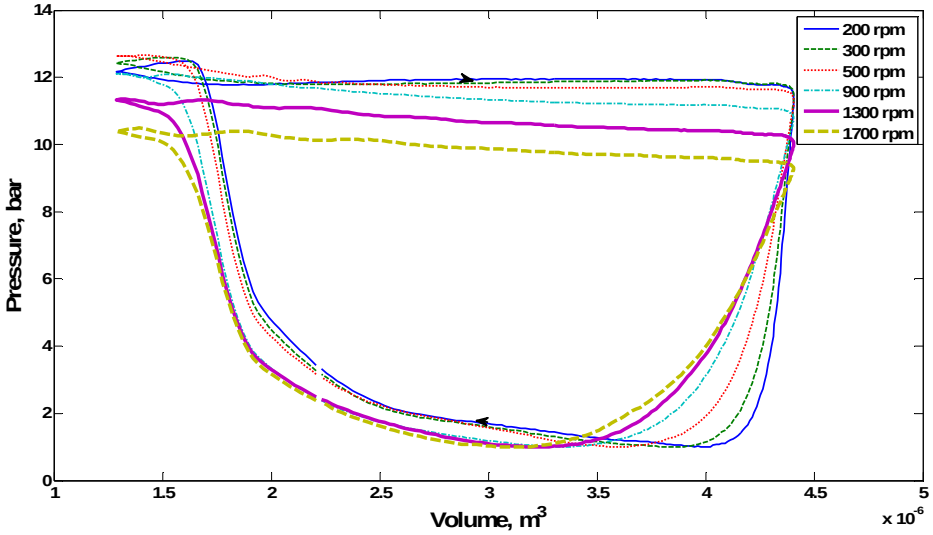

Figure 3-16 P-v diagram, rotary expander, 15 bar steam, with one pressure sensor

The rotary expander in the port valve configuration was not very efficient, as can be seen from the pressure diagrams, there was no expansion and all the work was done at boiler pressure. The inlet closes as the exhaust opens, so the steam does not have a chance to expand and perform work through expansion. The next step was to attach control valves

to the inlets so that the opening time could be controlled. The results for the improved configuration are shown in Section 3.5.5.

The data obtained for the pressure volume diagram was used to form a comparison between calculated torque (using Equation 3.2, Section 3.5.1) and measured torque, at selected speeds, and is shown in Table 3-5.

Speed (rpm)	Measured Torque (N m)	Calculated Torque (N m)	Percentage Difference
200	0.460	0.5398	+14.78
300	0.500	0.5579	+10.37
500	0.528	0.5177	-1.99
700	0.530	0.4881	-8.58

Table 3-5 Comparison of measured torque and calculated torque, 10 bar steam

The difference in values shown in Table 3-5 could be due to the fact that only one pressure sensor was used to obtain the pressure data and hence did not give a complete picture of the pressure within the chamber, this was improved by using two pressure sensors and better results can be seen in Section 3.5.5.

3.5.3 Uni-flow expander with an injector valve

These results are not available as the injectors did not perform under steam temperatures. See Section 3.5.4 for uni-flow results using steam with solenoid valves used to control the inlet rather than injectors.

3.5.4 Uni-flow expander with a solenoid valve

The results contained in this section are for the uni-flow expander in uni-flow configuration using solenoid valves to control the inlet. Speed steps (rpm) for these tests were 200, 300, 400, 500 and 600 (maximum).

Figure 3-17 shows the variation of specific power and torque over speed.

3.5 Expander test results using steam

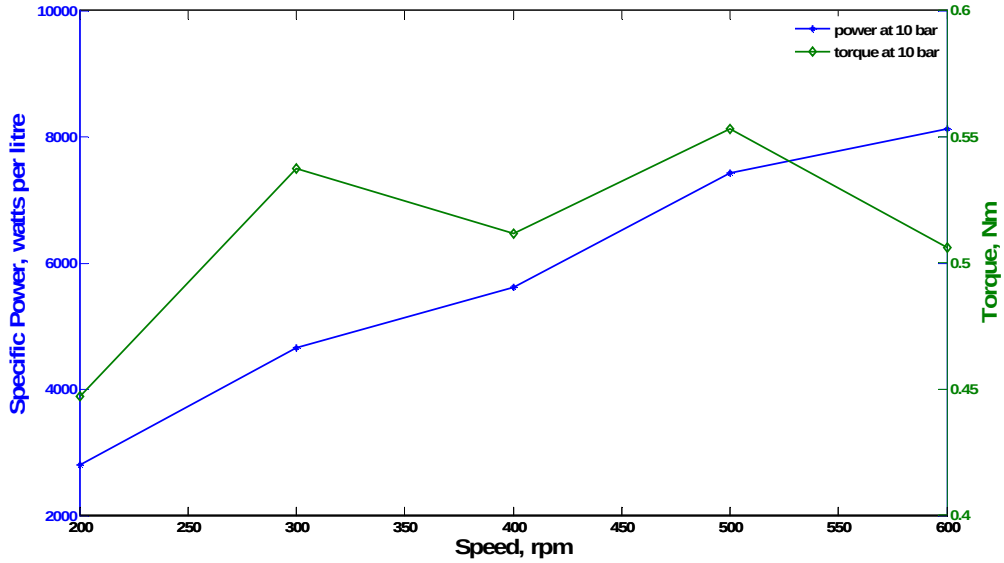

Figure 3-17 Specific power and torque, uni-flow expander, 10 bar steam

As can be seen from Figure 3-17, maximum torque was obtained at 500 rpm, and maximum specific power occurred at 600 rpm, maximum speed was 600 rpm for this configuration, limited by the use of the solenoid valves. Figure 3-18 shows the variation in pressure over one crank shaft rotation with 10 bar steam.

3.5 Expander test results using steam

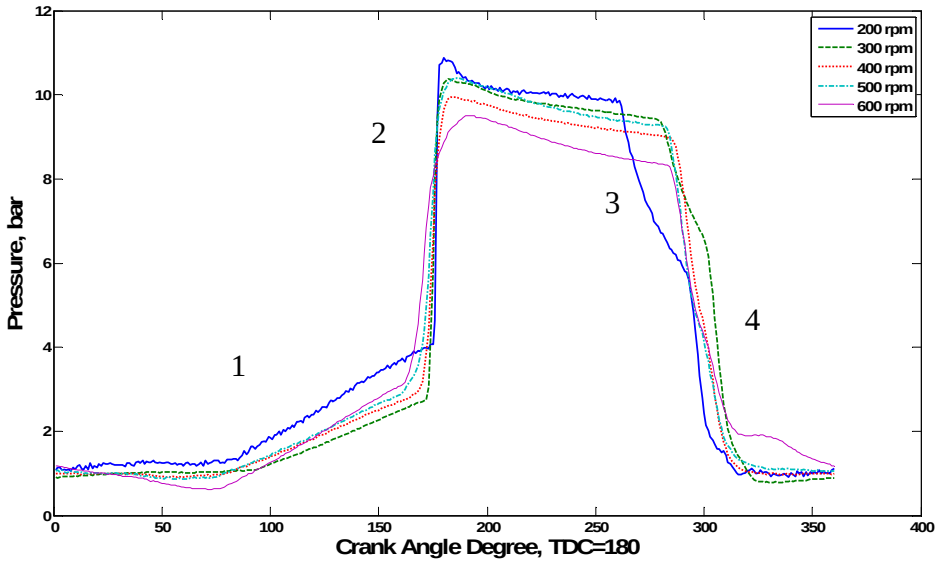

Figure 3-18 Pressure per cycle, uni-flow expander, 10 bar steam, with solenoid inlet valve

The pressure data is explained as follows:

1. Small compression witnessed as piston rises and volume decreases;
2. Inlet valve opens, pressure rises to boiler pressure;
3. Inlet valve closes, some expansion occurs;
4. Exhaust port is opened, pressure falls to atmospheric.

Figure 3-19 shows the pressure volume diagram using 10 bar steam for each speed step.

3.5 Expander test results using steam

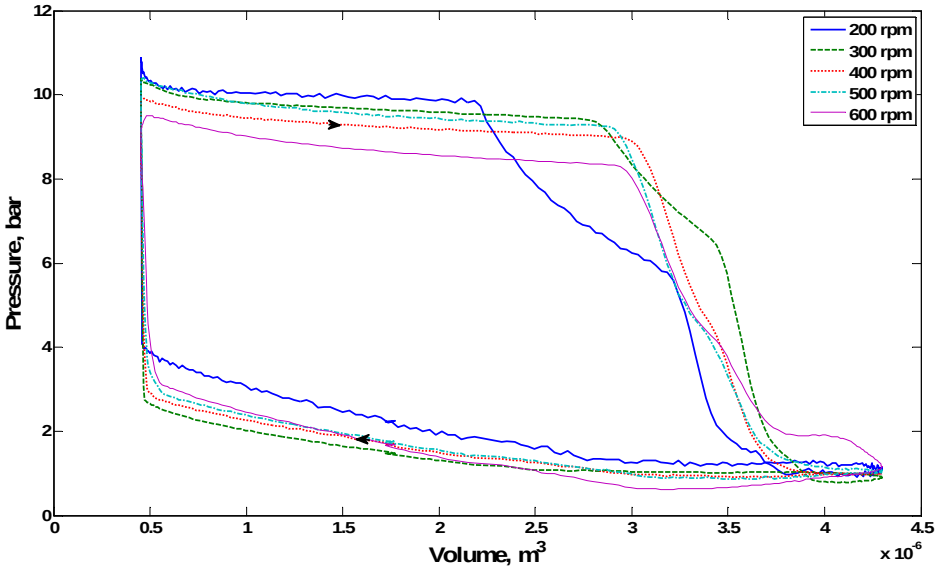

Figure 3-19 P-v diagram, uni-flow expander, 10 bar steam, with solenoid inlet valve

The comparison between calculated torque (Equation 3.1, Section 3.5.1) and measured torque is shown in Table 3-6.

Speed (rpm)	Measured Torque (N m)	Calculated Torque (N m)	Percentage Difference
200	0.4471	0.3082	-45.07
300	0.5376	0.3851	-39.60
400	0.5118	0.3536	-44.74
500	0.5530	0.3582	-54.38
600	0.5062	0.3374	-50.03

Table 3-6 Comparison of calculated and measured torque, 10 bar steam

As can be seen in Table 3-6, the difference in measured torque and calculated torque is a high percentage, this could be attributed to the limitations of the solenoid valves causing the timing of the opening and closing of the valves to be inaccurate and hence, the pressure data obtained to be unreliable.

3.5.5 Rotary expander with solenoid valves

The results contained in this section are for the rotary configuration illustrated in Figure 3-3, Section 3.2.1, in this configuration the rotary expander is equipped with valves on the inlet to make the inlet timing variable and fixed ports for the exhaust.

Speed steps (rpm) for these tests were 200, 300, 400 and 500 (maximum). Figure 3-20 shows the variation of specific power and torque over speed.

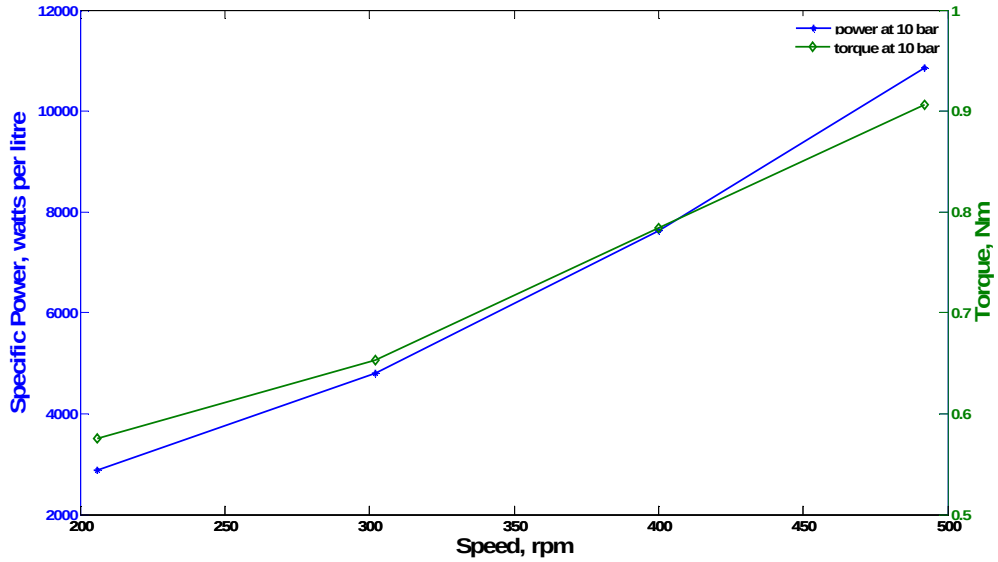

Figure 3-20 Specific power and torque, rotary expander, 10 bar steam

As can be seen from Figure 3-20, maximum torque was obtained at 500 rpm, and maximum specific power occurred at 500 rpm, maximum speed was 500 rpm for this configuration, limited by the use of the solenoid valves. Figure 3-21 shows the variation in pressure over one crank shaft rotation with 10 bar steam.

3.5 Expander test results using steam

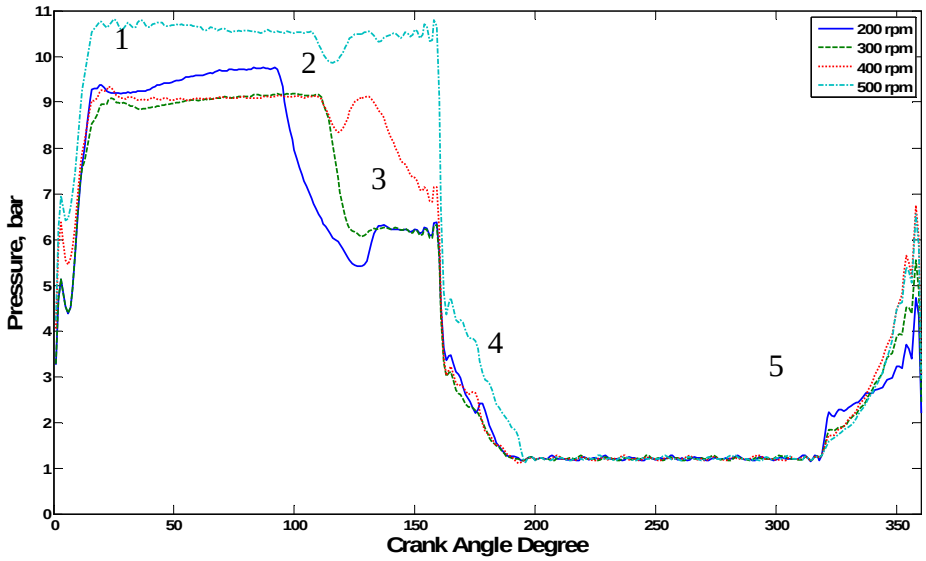

Figure 3-21 Pressure per cycle rotary expander, 10 bar steam

The pressure data is explained as follows:

1. Inlet valve opens, pressure rises to boiler pressure;
2. Inlet valve closes;
3. Some expansion seen, note no expansion seen for 500 rpm;
4. Exhaust port is opened and pressure drops to atmospheric pressure;
5. Slight rise in pressure here is due to some compression in the chamber as the volume decreases just before the inlet valve opens for the next cycle.

Figure 3-22 shows the pressure volume diagram using 10 bar steam for each speed step.

3.5 Expander test results using steam

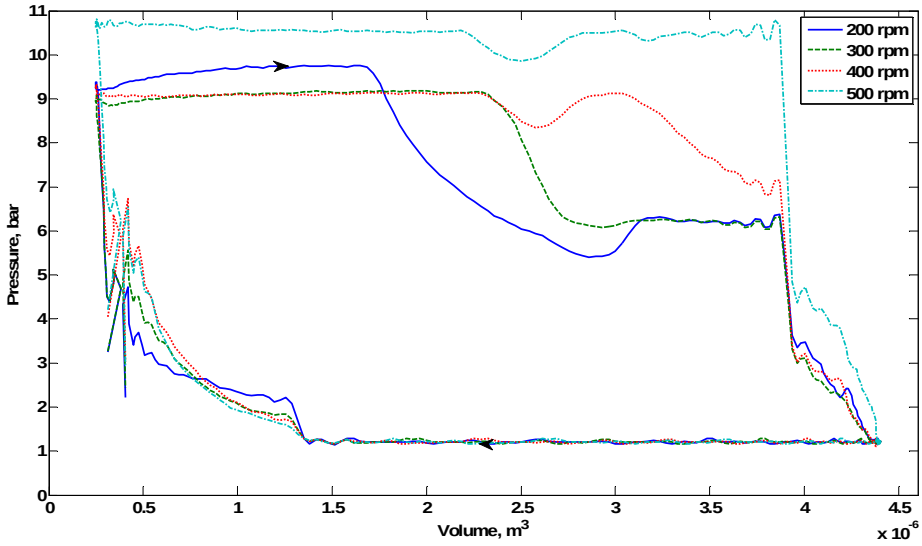

Figure 3-22 P-v diagram, rotary expander, 10 bar steam

The comparison between calculated torque (Equation 3.2, Section 3.5.1) and measured torque is shown in Table 3-7.

Speed (rpm)	Measured Torque (N m)	Calculated Torque (N m)	Percentage Difference
200	0.5757	0.6005	+4.13
300	0.6534	0.6605	+1.08
400	0.7836	0.7606	-3.02
500	0.9063	0.9889	+8.35

Table 3-7 Comparison of measured torque and calculated torque, 10 bar steam

As can be seen from Table 3-7, the measured torque and calculated torque are closer than they were for the rotary configuration used in Section 3.5.2, the percentage difference for all steps, with the exception of 500 rpm is within an acceptable ±5%. The reason for 500 rpm being slightly higher is because this was the upper working limit of the solenoid valves and hence the pressure data could be unreliable for this speed step.

3.5.6 Specific power and torque

This section presents a summary of the maximum specific power and torque measurements for each expander test. This can be seen in Table 3-8.

Expander configuration	Specific Torque N m / litre	Specific Power kW / litre
Uni-flow, 10 bar, solenoid valve	117.9	10.20
Rotary, 10 bar, port valves	124.4	21.40
Rotary, 15 bar, port valves	148.2	24.60
Rotary,10 bar, solenoid valves	210.8	10.86

Table 3-8 Maximum specific torque and power results for steam tests

The specific torque was quite high and the specific power was good, this is as expected for a small expander configuration.

3.5.7 Mass flow rates and efficiencies

This section uses recorded data and calculations to determine the mass flow rates and efficiencies obtained for each expander configuration.

3.5.7.1 Mass flow rates

Table 3-9 shows the maximum, calculated mass flow rate of steam, for each of the expander configurations where (m) indicates measured value and (c) indicates calculated value, explanatory notes follows the table.

Expander configuration	Speed (rpm)	Mass flow rate (kg/s)	Note
Uni-flow with solenoid valves, 10 bar	600	0.96e-3 (m)	-
Rotary with port valves, 10 bar	2000	5.70e-3 (c)	1
Rotary with port valves, 15 bar	2000	8.40e-3 (c)	1
Rotary with solenoid valves, 10 bar	500	1.37e-3 (m)	-

Table 3-9 Maximum mass flow rates for steam tests

Note 1 – Calculation takes the measured mass flow rate for the rotary expander with solenoid valves and re-calculates it according to speed and the density of the source at appropriate pressure. This is detailed in the following example:

Measured mass flow rate for steam 10 bar (from Table 3-9) at 500 rpm

= 0.00137 kg/s

Mass flow rate at 500 rpm = measured / density of steam at 10 bar - 5.147 kg/m^3

= 0.00137 / 5.147

= 0.00026617 kg/s

Basic mass flow rate = 0. 00026617 /(500/60) = 0.000031941 kg/s

Mass flow rate at 2000 rpm = 0. 000031941 * (2000/60) = 0.0011 kg/s

Now multiply by the density of steam at 10 bar (5.147 kg/m^3) and 15 bar (7.596 kg/m^3):

Calculated mass flow rate for steam 10 bar at 2000 rpm = 0.0057 kg/s

Calculated mass flow rate for steam 15 bar at 2000 rpm = 0.0084 kg/s

These mass flow rates are used in the next section to calculate the efficiency of each expander configuration.

3.5.7.2 Efficiencies

The isentropic efficiencies were calculated using two different procedures and the results compared. The first procedure involves Equation 3.3 through Equation 3.5.

$$T_2 = T_1\left(\frac{p_1}{p_2}\right)^{\frac{\gamma-1}{\gamma}} \qquad (3.3)$$

$$W_{is} = \dot{m}c_p\left(T_2 - T_1\right) \qquad (3.4)$$

$$\eta_{is} = \frac{W_{act}}{W_{is}} \qquad (3.5)$$

Using the recorded pressure values, and the gas temperature at entry, the exit temperature is calculated assuming an isentropic expansion. The isentropic work is calculated using this temperature drop and the mass flow rate shown in section 3.5.7.1. Finally the ratio of the actual work output, measured using a torque transducer is formed with the calculated value of isentropic work. Table 3-10 shows the maximum power and the calculated efficiency for each expander configuration using steam.

3.5 Expander test results using steam

Expander configuration	Speed (rpm)	Actual Maximum Power (W)	Isentropic Efficiency (%)
Uni-flow, 10 bar, solenoid valve	600	47.70	33.24
Rotary, 10 bar, port valves	2000	92.10	10.79
Rotary, 15 bar, port valves	2000	106.15	7.17
Rotary,10 bar, solenoid valves	500	46.70	22.76

Table 3-10 Efficiencies for steam tests

As can be seen from Table 3-10, the rotary expander with control valves on the inlet doubles the efficiency of that for when no controlled valves were utilised. The best results are for the uni-flow expander and rotary expander tests with the solenoid valves, this is expected as the steam mass flow rate is better controlled.

The second procedure for calculating the efficiency involves the results from the Steam Quality Analyser (SQA) tests found in Appendix D. The SQA was tested using the uni-flow expander and rotary expander configurations, both with solenoid valves. The SQA tests resulted in a dryness fraction. Using the enthalpy/entropy chart from steam tables [55], the ideal isentropic expansion from 10 bar to 1 bar would result in an enthalpy change from 2780 kJ/kg to 2390 kJ/kg, this relates to a change in enthalpy of 390 kJ/kg. Using the dryness fraction and the enthalpy/entropy chart the actual change in enthalpy can be determined. The isentropic efficiency is then given by the ratio of ideal change in enthalpy to actual change in enthalpy.

The calculated efficiency from the SQA results for the uni-flow expander with a solenoid valve can be seen in Table 3-11.

Speed (rpm)	Dryness fraction (x)	Enthalpy for x units (kJ/kg)	Enthalpy Difference (kJ/kg)	Isentropic Efficiency (%)
300	0.9148	2460	320	82.1
400	0.9551	2565	215	55.1
500	0.9504	2560	220	56.4
600	0.9625	2580	200	51.3

Table 3-11 Calculation of isentropic efficiency, uni-flow expander with solenoid valve

3.5 Expander test results using steam

For the uni-flow expander the efficiency results are not comparable. At 600 rpm (maximum power speed step) 33.24% efficiency was calculated whilst the SQA results gave 51.3%. This difference could be due to heat losses within the SQA setup, or flow losses within the experimental setup, additionally the plenum chamber that was attached during the SQA tests could have caused losses and also would affect the data obtained due to delays experienced when using the plenum. The calculated efficiency from the SQA results for the rotary expander with solenoid valves can be seen in Table 3-12.

Speed (rpm)	Dryness fraction (x)	Enthalpy for x units (kJ/kg)	Enthalpy Difference (kJ/kg)	Isentropic Efficiency (%)
200	0.976	2630	150	38.46
300	0.971	2610	170	43.59
400	0.977	2630	150	38.46
500	0.985	2640	140	35.90

Table 3-12 Calculation of isentropic efficiency, rotary expander with solenoid valves

Comparing the steam efficiencies calculated in Table 3-10, with the efficiencies calculated using the SQA test results it can be seen that the rotary expander efficiencies are also not comparable, 22.76% and 35.9% respectively. The differences could be attributed to the temperature losses in the SQA setup or flow losses in the experimental setup.

Even though the efficiencies for each configuration do not agree, it can be seen that both procedures result in an improvement in efficiency for the uni-flow configuration when compared to the rotary configuration, and that the improvement is of a comparable magnitude, the ratio of uni-flow to rotary efficiency is 0.68 and 0.69 for the first procedure and the second (SQA) procedure, respectively.

3.6 Conclusions for expander tests

The main aim of this part of the project was to use data, obtained from the expander testing, to determine which configuration would be best suited for steam expansion.

The uni-flow expander configuration, using a solenoid valve to control the inlet, gave the best results in terms of power and efficiency and hence would be the chosen configuration to be used as a reciprocating steam expander.

The rotary expander provided high power and torque but the efficiencies were not as good as the uni-flow. Without inlet control, the rotary was highly inefficient; the efficiency was improved with the use of solenoid valves, but would still be a second choice after the uni-flow configuration. Furthermore, the rotary expander was found to be unsuitable as a steam expander because of the expansion of the rotary tips causing the expander to seize after a short period of use.

The counter-flow expander configuration, disappointingly, gave the worst results. This is because the counter-flow arrangement is not suited to be an expander, because the counter-flow is more suited to a four-stroke combustion cycle than a two-stroke compression/expansion cycle; further, it proved difficult to get a good result using the solenoid valves. Tests were initially done using the injectors, but the results were even worse, for the same reasons as the uni-flow results were poor with the injector inlet in that the injector cross-sectional volume could not cope with the mass flow rate required and that they did not perform well with high temperatures.

When medium size expanders are tested, it is recommended that a better specification of inlet valve is used that could perform at higher speeds and also at steam temperatures and pressures.

It is worth mentioning that the steam boiler used for the expander tests did not provide a steady source of steam with respect to pressure. For example when the tests were being

run at 10 bar, the source would fluctuate between 8 and 12 bar, the fluctuations were gradual, and whilst 10 bar was held for most of the time, the pressure would begin to rise causing a vent to open which caused the pressure to drop, these fluctuations were cyclic and were a characteristic of the boiler used.

A further recommendation for the next phase of expander testing is the need to consider the issue of lubrication, especially for the rotary expander. When using steam, care had to be taken to ensure the expanders were kept lubricated using a steam lubricant which was fed into the input of each expander configuration. The lubricant needed to be monitored constantly, meaning when running for long periods of time it was necessary to halt the testing in order for the lubricant to be topped up. This will need careful consideration for the next phase of testing when larger expanders are used. Also for a closed system it needs some thought into how to separate the lubricant and water before the water is pumped back into the steam boiler.

As mentioned in Section 3.5.2, the rotary expander had separate seals attached to each rotor tip, these tended to expand when using steam and after a time would expand so much they began to bind with the surface of the rotary chambers and eventually the expander would seize. This happened twice over the period of testing, both when using steam for longer than 20 minutes, the first time when using steam at 15 bar. Even with lubrication it appears the parts did not have time to cool down as they would in a normal counter-flow combustion cycle. This will need to be considered if the next phase of testing involves a larger rotary expander.

Additionally there is a need to ensure flow meters are added to the inlet and exhaust of the test setup in order to get better efficiency results for the expanders. Finally, a further recommendation is that any injectors and solenoids need to be instrumented in such a way as to indicate the actual timing for opening and closing of the inlet and exhaust for each expander configuration.

4 Modelling and validation of the small expanders

4.1 Small expander modelling introduction

This section presents the results for the modelling of the small expanders using GT-SUITE software from Gamma Technologies. GT-SUITE is an engine/vehicle simulation toolbox and has several branches, or solvers, such as GT-POWER, GT-COOL and GT-DRIVE, each of which are specialised in different areas of a vehicle, for example, the IC engine, cooling system and powertrain, respectively. GT-POWER was the branch used to model the small expanders, referred to as GT from this point forward.

The concern with small scale expander testing was its scalability. Could the results obtained from the small expander test facility be scaled up to predict and validate the results obtainable from similar, larger expander configurations? In parallel to the small expander testing, detailed in Chapter 3, models of each expander configuration were developed and tested.

The same validation process was used for the nitrogen and steam tests. The results from the GT models were compared with the experimental results, by doing this it was intended to validate the experiment results and if the validation proved to be successful, the models would be scaled up and then used to predict and validate the results for larger expander configurations.

The small expander modelling process is described in Section 4.2 and as with the previous chapter, due to poor performance of the counter-flow expander, this chapter will focus on the rotary and uni-flow expanders. Details of the counter-flow expander and the test results can be found in Appendix G.

A presentation of results from the expander modelling, including comparisons to the measured data, is given in Section 4.3.

There will then be some discussion in Section 4.4 which will attempt to validate the data acquired during the small expander testing and modelling. In general ±5% is standard

figure for an acceptable comparison range of values when comparing and validating results hence, if the modelling results were comparable to the experimental results with a ±5% margin, then this would be deemed acceptable, any larger difference would be unacceptable and concludes that the results are not comparable.

Section 4.5 will draw conclusions for the small expander modelling.

4.2 Modelling of small expanders

This section describes how the models of the small expander configurations, used in the mini test facility, were developed and validated.

4.2.1 Uni-flow expander model

The uni-flow expander configuration was simple to model using GT-Power; Figure 4-1 shows the GT model for the uni-flow expander configuration.

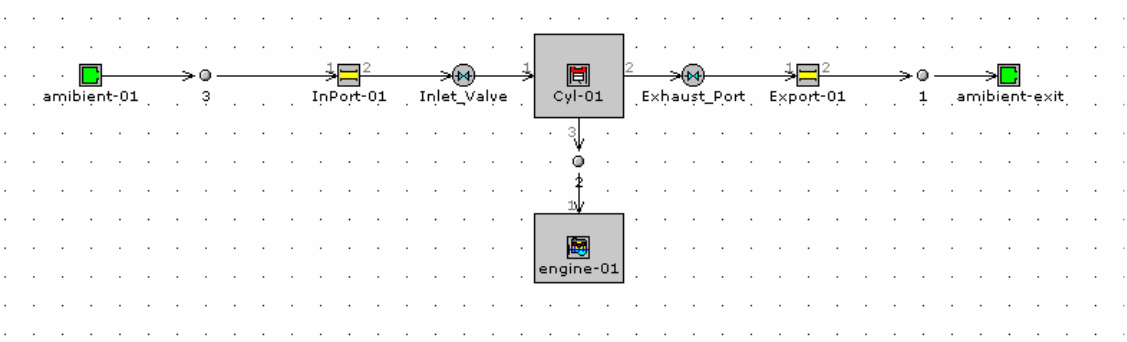

Figure 4-1 GT model of the uni-flow expander configuration

The uni-flow model used a fixed size exhaust port component. The dimensions from the mini test facility for the pipes, valves and cylinder were incorporated into the model. For the inlet variable timing; named variables were used so that when the model test cases were created, timings could easily be altered without altering the model components.

The timings used for the experiments were used when initially running the GT model; however it became apparent that there was not a direct correlation between the timings used in the experiments and the timings required by the GT model, as the results for torque were much lower than expected. For the uni-flow valve timings, the opening time used for the experiments was multiplied by a factor of three (after experimenting with different factors) when running the GT model. This correlation worked at a satisfactory level for 200, 300 and 400 rpm, but not for 500 rpm, this was because 500 rpm was at the top end of the valves' working speed range. The torque was recorded for each GT speed step and compared to the experimental results; additionally the pressure data was

compared for the closest value. Appendix H contains graphs that compare the two stroke timings used in the experiments and in the GT modelling tests.

4.2.2 Rotary expander model

The GT-SUITE model library did not include a rotary expander, so a model for the small Wankel expander was created using the volume information for the chambers of the rotary expander and by using this data to alter traditional cylinder components to behave like a rotary chamber. Three cylinders were used to represent each chamber; this can be visualized in Figure 4-2.

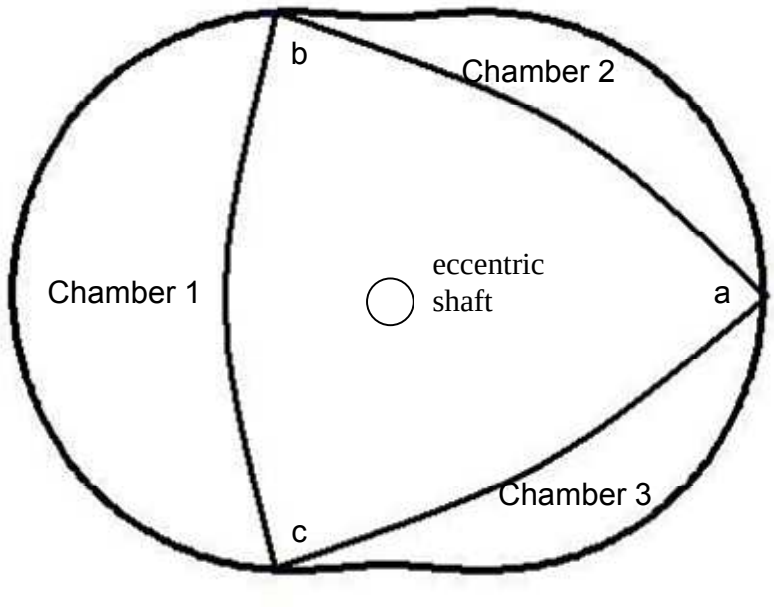

Figure 4-2 Rotary expander chambers and rotor tip labels

The rotor rotates anti-clockwise so that *Chamber 1* is followed by *Chamber 2* then *Chamber 3*. The rotor tips are labeled a, b and c. All data was calculated so that the TDC=0° referred to when the tips are at their starting point shown in Figure 4-2, tip *a* was at 0°, tip *b* was at 120° and tip *c* was at 240°. The piston positions were altered, from previous settings, so that when running the model, the volume changes represented the changes experienced by each chamber, as shown in Figure 4-3.

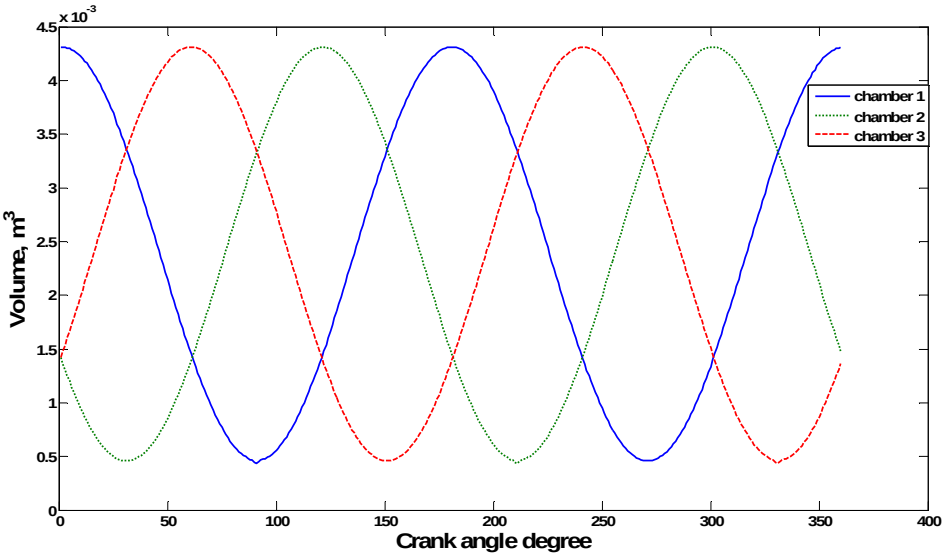

Figure 4-3 Volume for each chamber of the rotary expander

The volume was calculated using equations from [56], these are summarised as follows:

$$V_{\min} = Le^2\left\{\frac{\pi}{3} + 2\sqrt{K^2-9} + \left(\frac{2}{9}K^2+4\right)\sin^{-1}\left(\frac{3}{K}\right) - \frac{\sqrt[3]{3}}{2}K\right\} \qquad (4.1)$$

$$V = V_{\min} + \frac{\sqrt[3]{3}}{2}e^2KL\left\{1-\sin\left(\frac{2}{3}\alpha+\frac{\pi}{6}\right)\right\} \qquad (4.2)$$

Where L is the axial length of the rotor and rotor housing, e is the radius of the inner circle, K is the radius-to-eccentricity ratio (where this radius is the length from the inner circle (eccentric shaft) to the outer circle), α is the angular position of the rotor (starting point, 0° is as shown in Figure 4-2), V_{min} is the minimum volume and V is the Volume for the rotor position.

The GT rotary expander model is shown in Figure 4-4.

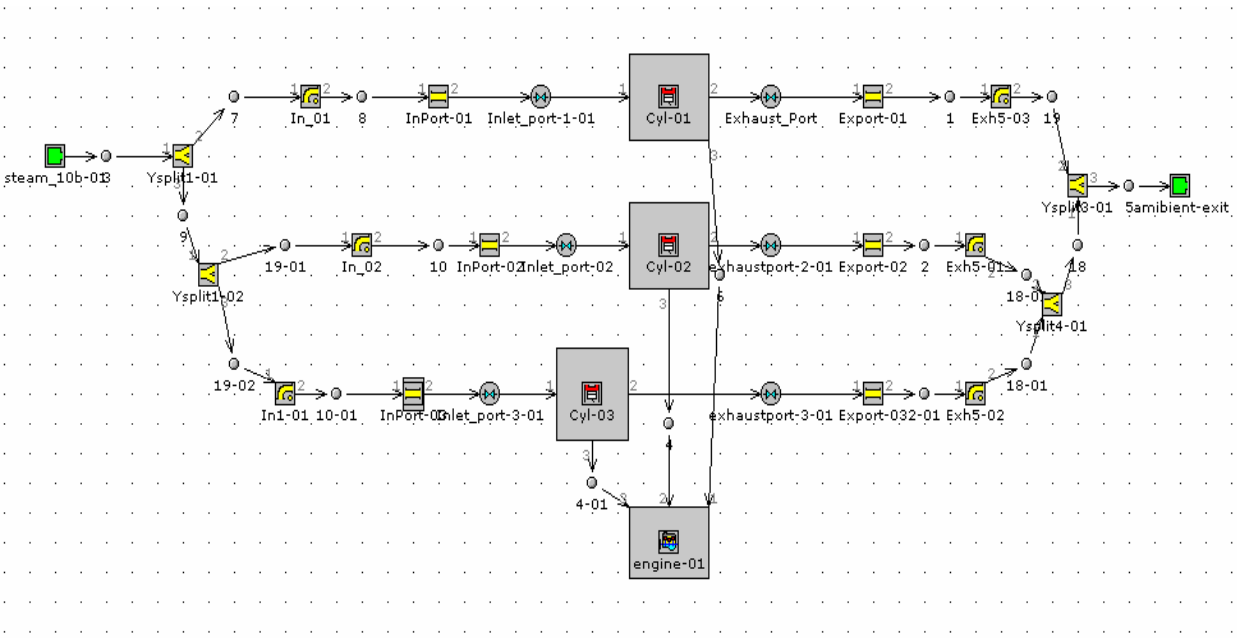

Figure 4-4 GT model of the rotary expander configuration

The torque was calculated from the pressure and volume data acquired from the GT model run results, using Equation 3.2, from Section 3.4.1.

4.3 Results from small expander modelling

This section presents the key results from the expander modelling tests and then compares them with the corresponding experimental results. The variation of torque over speed results are compared graphically and summarised in a table that includes a comparison. Choosing a speed point at which the torque is closest in comparison, the variation in pressure over one complete rotor revolution for the experimental data and GT data are compared graphically.

4.3.1 Uni-flow expander results

This section presents the results for the uni-flow expander configuration with a solenoid valve on the inlet. The results are compared with the experimental results from Section 3.4.4.

4.3.1.1 Steam results

Figure 4-5 compares the variation in torque with speed for the experimental data and GT data using 10 bar steam.

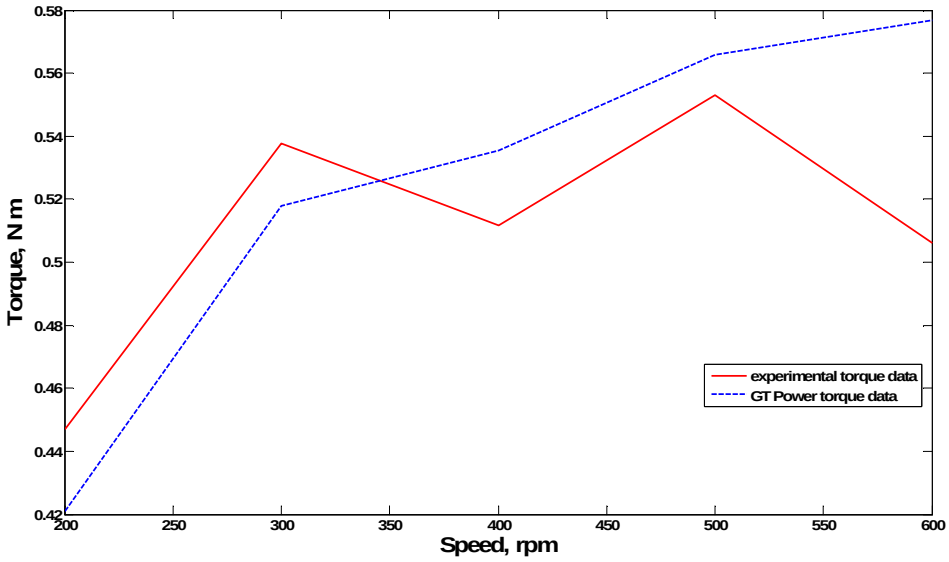

Figure 4-5 Uni-flow expander, 10 bar steam, comparison of torque

Table 4-1 compares the torque for each speed step and presents the percentage difference between the two values.

Speed (rpm)	Measured Torque (N m)	GT Model Torque (N m)	Percentage Difference
200	0.4471	0.4210	-6.19
300	0.5376	0.5179	-3.80
400	0.5118	0.5356	+4.44
500	0.5530	0.5660	+2.29
600	0.5062	0.5767	+12.22

Table 4-1 Uni-flow expander, 10 bar steam, percentage difference for torque comparison

Figure 4-6 compares the variation in pressure over one complete rotor revolution for the experimental data and GT data, 400 rpm was chosen as a midway test point.

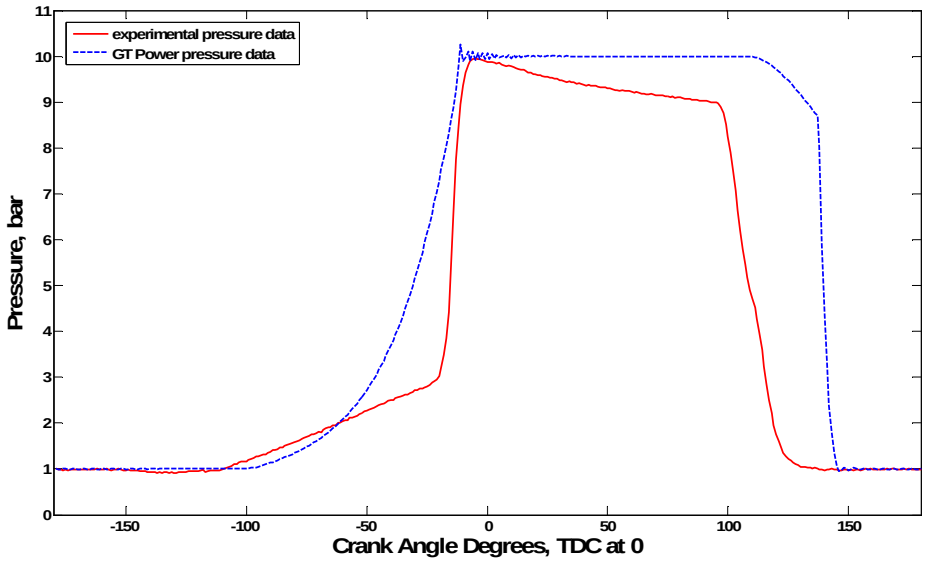

Figure 4-6 Uni-flow expander, 10 bar steam, comparison of pressure cycles, 400 rpm

Figure 4-5, Table 4-1 and Figure 4-6 show that the GT model for the uni-flow expander with 10 bar steam yielded similar results to the experimental data for the lower speed steps with the torque data being within the acceptable ±5% margin. However, for the maximum speed step the torque data was different by 12% which exceeds the acceptable

margin. This could be due to the fact that this was the maximum speed that the solenoid valves could operate at, hence the timing was not as accurate as for the lower speeds.

4.3.1.2 Nitrogen results

Figure 4-7 compares the variation in torque with speed for the experimental data and GT data using 10 bar nitrogen.

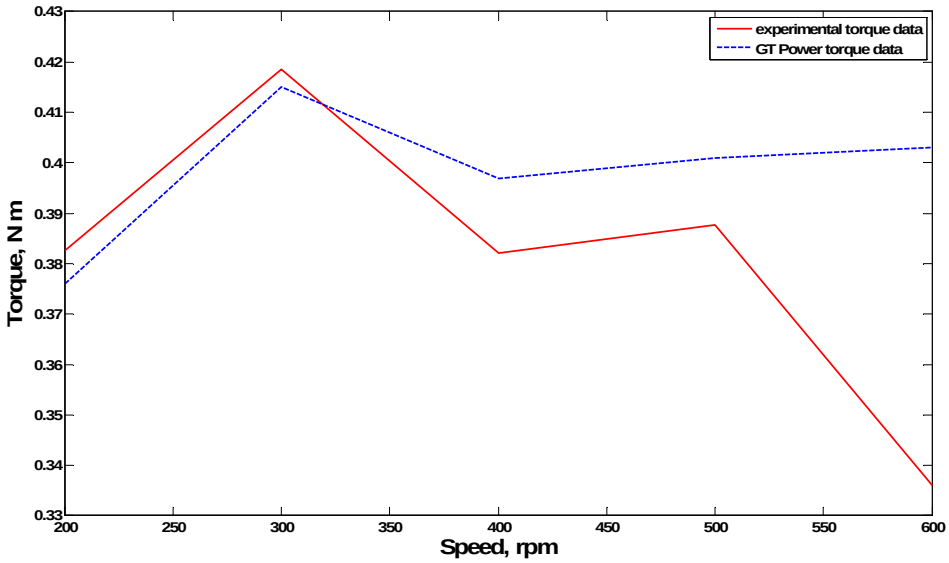

Figure 4-7 Uni-flow expander, 10 bar nitrogen, comparison of torque

Table 4-2 compares the torque for each speed step and presents the percentage difference between the two values.

Speed (rpm)	Measured Torque (N m)	GT Model Torque (N m)	Percentage Difference
200	0.3826	0.376	-1.76
300	0.4186	0.415	-0.87
400	0.3820	0.397	+3.78
500	0.3876	0.401	+3.34
600	0.3361	0.403	+16.6

Table 4-2 Uni-flow expander, 10 bar nitrogen, percentage difference for torque comparison

Figure 4-8 compares the variation in pressure over one complete rotor revolution for the experimental data and GT data, 300 rpm was chosen as this resulted in the closest torque comparison.

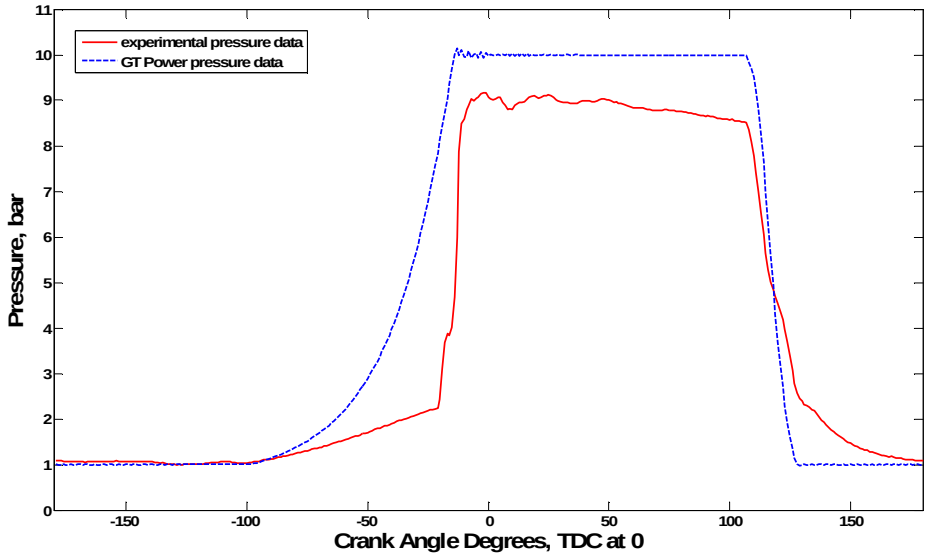

Figure 4-8 Uni-flow expander, 10 bar nitrogen, comparison of pressure cycles, 300 rpm

Figure 4-7, Table 4-2 and Figure 4-8 show that the GT model for the uni-flow expander with 10 bar nitrogen yielded similar results to the experimental data for the lower speed steps with the torque data being within the acceptable ±5% margin. However, for the maximum speed step the torque data was different by 16% which considerably exceeds the acceptable margin. Again, this could be due to the fact that this was the maximum speed that the solenoid valves could operate at, hence the timing was not as accurate as for the lower speeds.

Figure 4-9 compares the variation in torque with speed for the experimental data and GT data using 15 bar nitrogen.

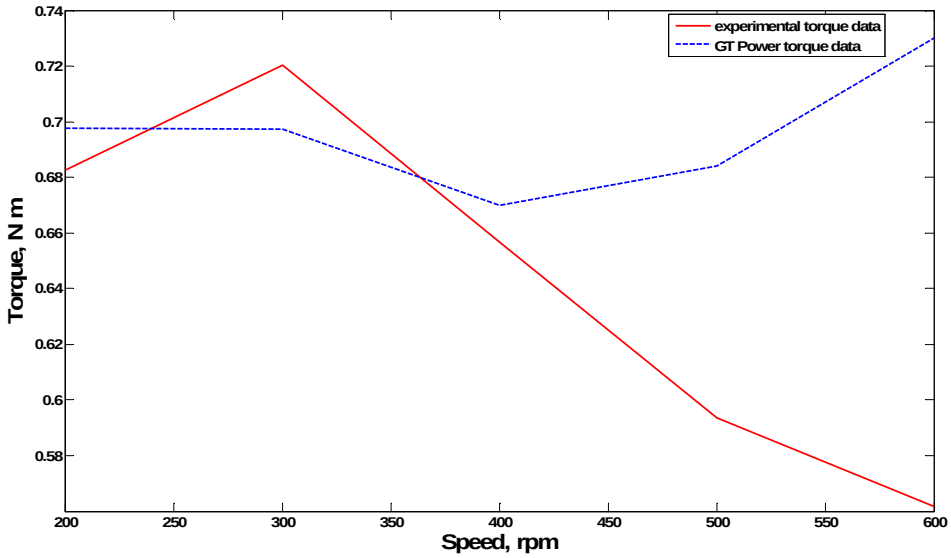

Figure 4-9 Uni-flow expander, 15 bar nitrogen, comparison of torque

Table 4-3 compares the torque for each speed step and presents the percentage difference between the two values.

Speed (rpm)	Measured Torque (N m)	GT Model Torque (N m)	Percentage Difference
200	0.6826	0.6978	+2.18
300	0.7202	0.6973	-3.28
400	0.6568	0.6700	+1.97
500	0.5935	0.6850	+13.36
600	0.5618	0.7300	+23.04

Table 4-3 Uni-flow expander, 15 bar nitrogen, percentage difference for torque comparison

Figure 4-10 compares the variation in pressure over one complete rotor revolution for the experimental data and GT data, 400 rpm was chosen as this speed step gave the closest comparison in the torque data results.

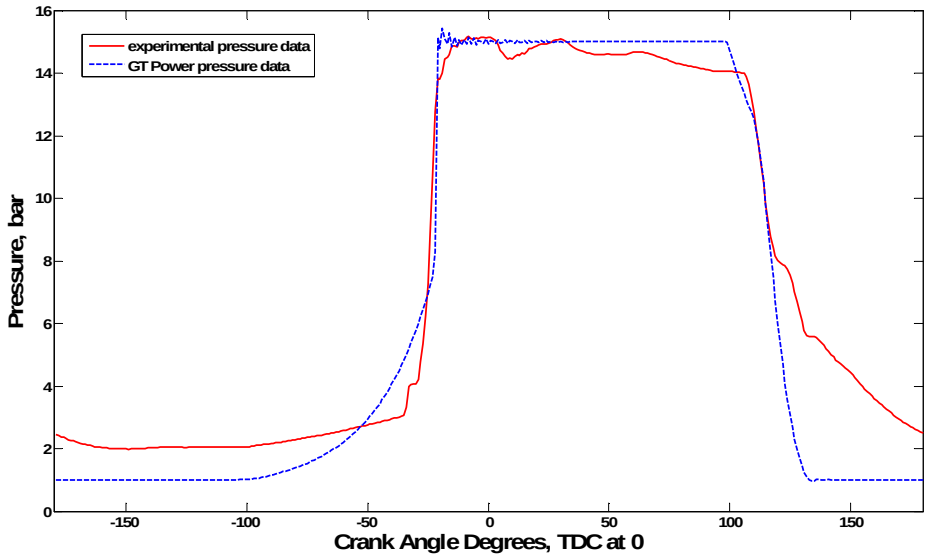

Figure 4-10 Uni-flow expander, 15 bar nitrogen, comparison of pressure cycles, 400 rpm

Figure 4-9, Table 4-3 and Figure 4-10 show that the GT model for the uni-flow expander with 15 bar nitrogen yielded similar results to the experimental data for the lower speed steps with the torque data being within the accepted ±5% margin. However, for the top two speed steps, 500 and 600 rpm, the torque data was different by 13% and 23%, respectively, which is unacceptable. Once again, this could be due to the fact this was the maximum speed that the solenoid valves could operate at, hence the timing was not as accurate as for the lower speeds, at this higher pressure.

4.3.2 Results for rotary expander with port valves

This section presents the results for the rotary expander configuration with no control valves on the inlets. The results are compared with the experimental results from Section 3.4.2.

4.3.2.1 Steam results

Figure 4-11 compares the variation in torque with speed for the experimental data and GT data using 10 bar steam.

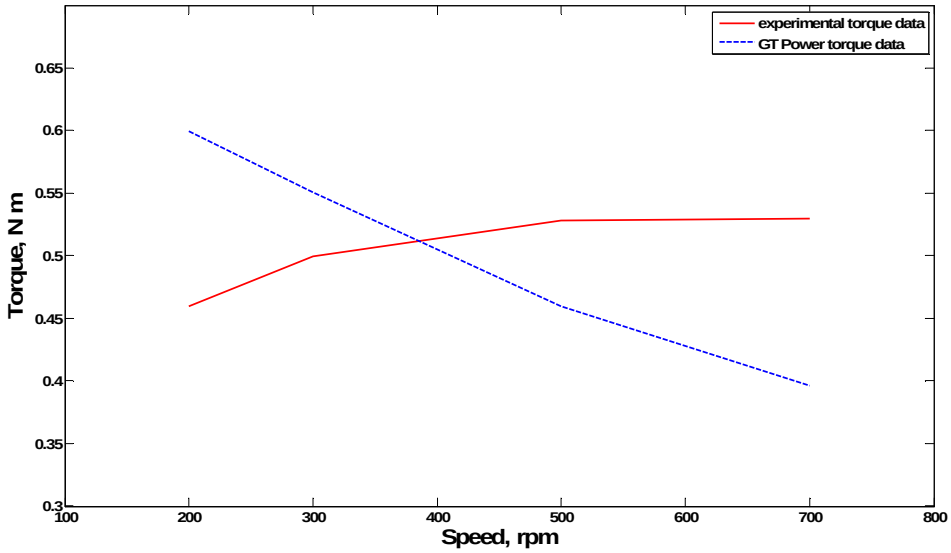

Figure 4-11 Rotary expander, 10 bar steam, comparison of torque

Table 4-4 compares the torque for each speed step and presents the percentage difference between the two values.

Speed (rpm)	Measured Torque (N m)	GT Model Torque (N m)	Percentage Difference
200	0.460	0.6000	+23.33
300	0.500	0.5508	+9.22
500	0.528	0.4596	-14.88
700	0.530	0.3900	-35.89

Table 4-4 Rotary expander, 10 bar steam, percentage difference for torque comparison

Figure 4-12 compares the variation in pressure over one complete rotor revolution for the experimental data and GT data, 300 rpm was chosen as the speed that gave the closest torque comparison.

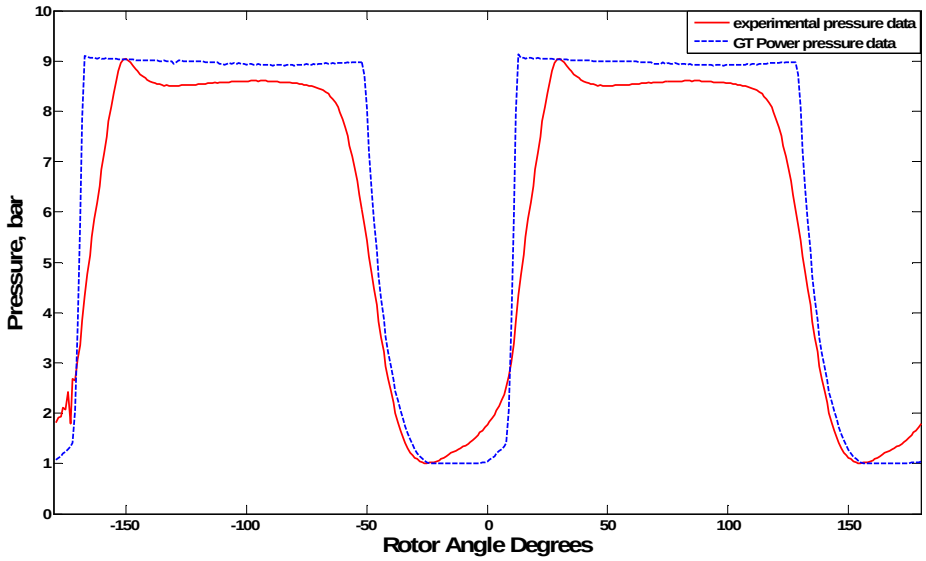

Figure 4-12 Rotary expander, 10 bar steam, comparison of pressure cycles, 300 rpm

As can be seen from Figure 4-11 and Table 4-4 the torque data obtained from the rotary model, with 10 bar steam, was not comparable with the experimental data with the difference being considerably more than the acceptable ±5% margin and the gradient of the line is also different, this could be due to the fact that steam performed differently to nitrogen (it will be shown in the next section that the nitrogen results were more comparable) and that this needed to be added to the rotary expander model in some form of heat exchange calculation; at the time of writing, due to time constraints, this could not be further investigated. However the pressure data shown in Figure 4-12 gives a comparable curve, so it can be concluded that the GT rotary expander model is performing in a similar way to the actual rotary expander.

4.3.2.2 Nitrogen results

Figure 4-13 compares the variation in torque with speed for the experimental data and GT data using 10 bar nitrogen.

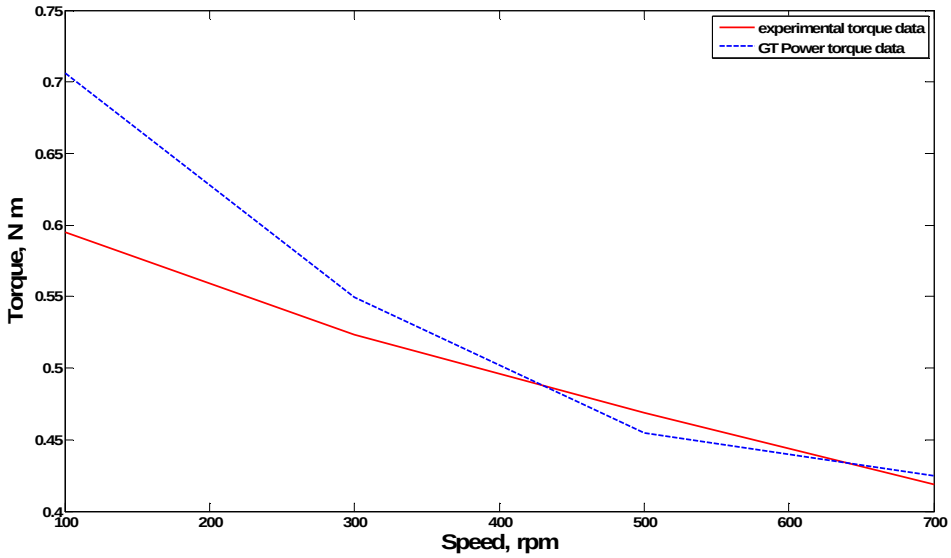

Figure 4-13 Rotary expander, 10 bar nitrogen, comparison of torque

Table 4-5 compares the torque for each speed step and presents the percentage difference between the two values.

Speed (rpm)	Measured Torque (N m)	GT Model Torque (N m)	Percentage Difference
100	0.6669	0.7062	+5.57
300	0.5449	0.5494	+0.82
500	0.4979	0.4547	-9.50
700	0. 4245	0.4529	+6.69

Table 4-5 Rotary expander, 10 bar nitrogen, percentage difference for torque comparison

Figure 4-14 compares the variation in pressure over one complete rotor revolution for the experimental data and GT data, 300 rpm was chosen as this speed step gave the best result in the torque comparison table.

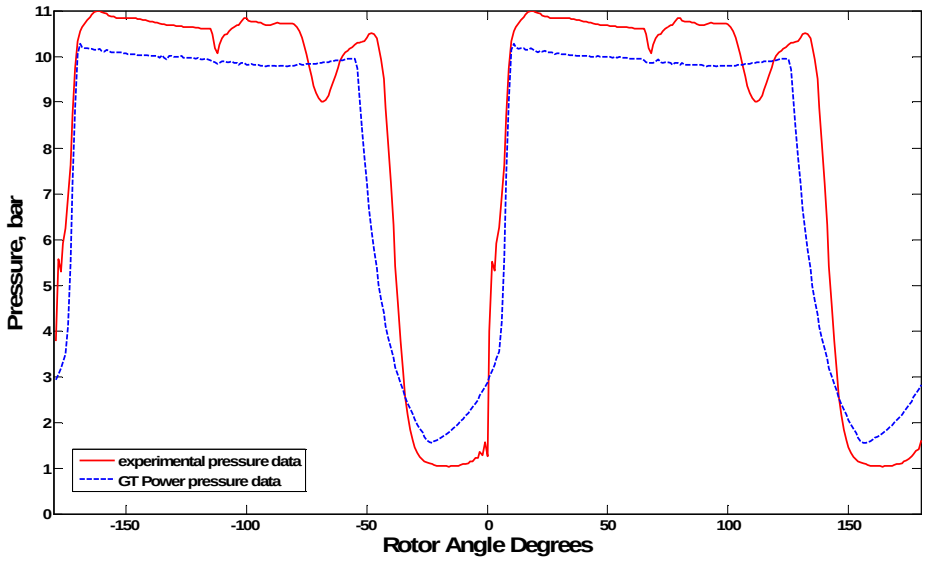

Figure 4-14 Rotary expander, 10 bar nitrogen, comparison of pressure cycles, 300 rpm

Figure 4-13, Table 4-5 and Figure 4-14 show that the GT model for the rotary expander with 10 bar nitrogen yielded similar results to the experimental data for lower speed steps with the torque data being within ±5% acceptable margin; however the higher speed steps exceed the acceptable margin so there is room for improvement. This could be due to the GT model using cylinder attributes to represent the rotary expander chambers, which could yield a different performance; the model could be improved to allow for this.

Figure 4-15 compares the variation in torque with speed for the experimental data and GT data using 15 bar nitrogen.

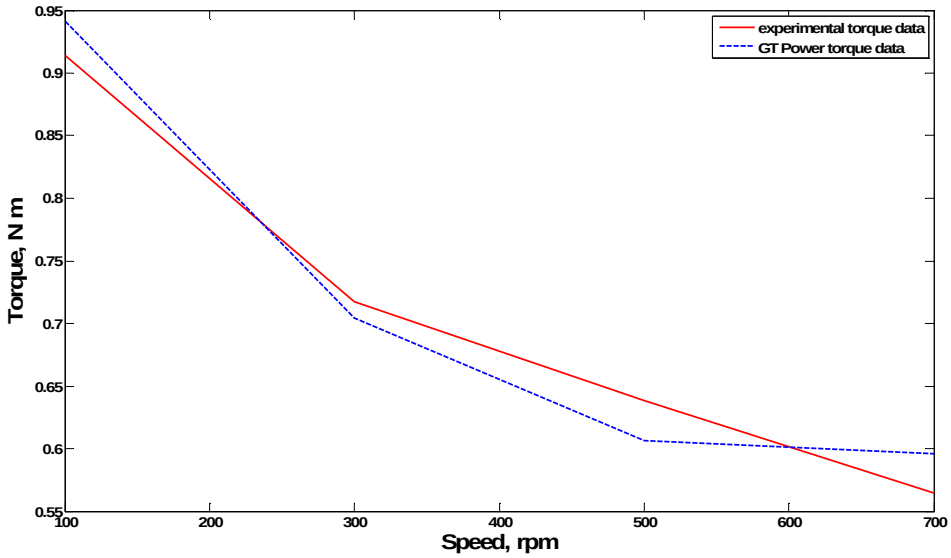

Figure 4-15 Rotary expander, 15 bar nitrogen, comparison of torque

Table 4-6 compares the torque for each speed step and presents the percentage difference between the two values.

Speed (rpm)	Measured Torque (N m)	GT Model Torque (N m)	Percentage Difference
100	0.9139	0.9415	+2.93
300	0.7172	0.7041	-1.86
500	0.6385	0.6061	-5.45
700	0.5641	0.5955	+5.27

Table 4-6 Rotary expander, 15 bar nitrogen, percentage difference for torque comparison

Figure 4-16 compares the variation in pressure over one complete rotor revolution for the experimental data and GT data, once again 300 rpm was chosen as it gave the best torque comparison.

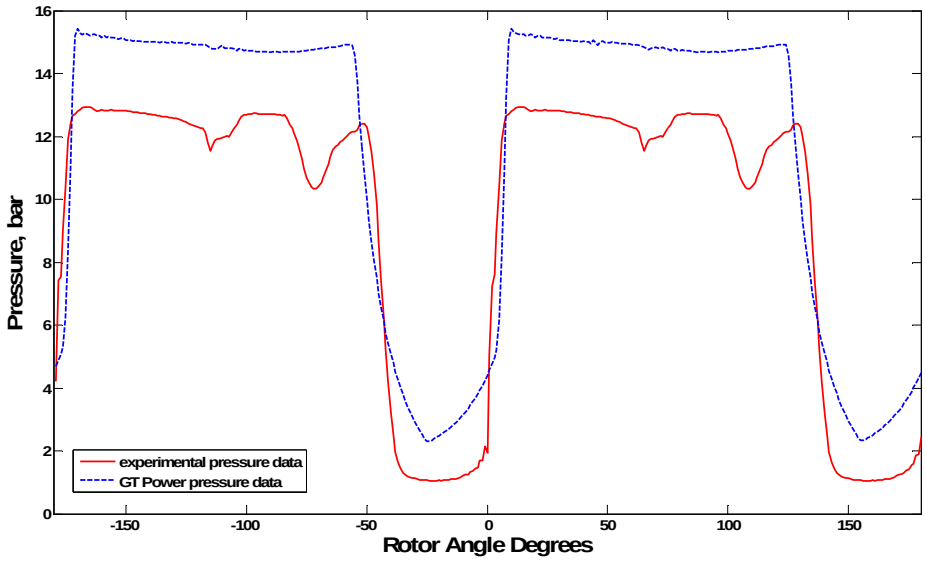

Figure 4-16 Rotary expander, 15 bar nitrogen, comparison of pressure cycles, 300 rpm

Figure 4-15, Table 4-6 and Figure 4-16 show that the GT model for the rotary expander with 15 bar nitrogen yielded similar results to the experimental data for all speed steps with the torque data being within the acceptable ±5% margin. This is a good result and is an improvement on the 10 bar nitrogen results, but could still be improved further. This could be due to the GT model using cylinder attributes to represent the rotary expander chambers, which could yield a different performance; the model could be improved to allow for this.

4.3.3 Results for rotary expander with solenoid valves

This section shows the results for the rotary expander configuration with control valves attached to the inlets. The results are compared with the experimental results from Section 3.4.5.

4.3.3.1 Steam results

Figure 4-17 compares the variation in torque with speed for the experimental data and GT data using 10 bar steam.

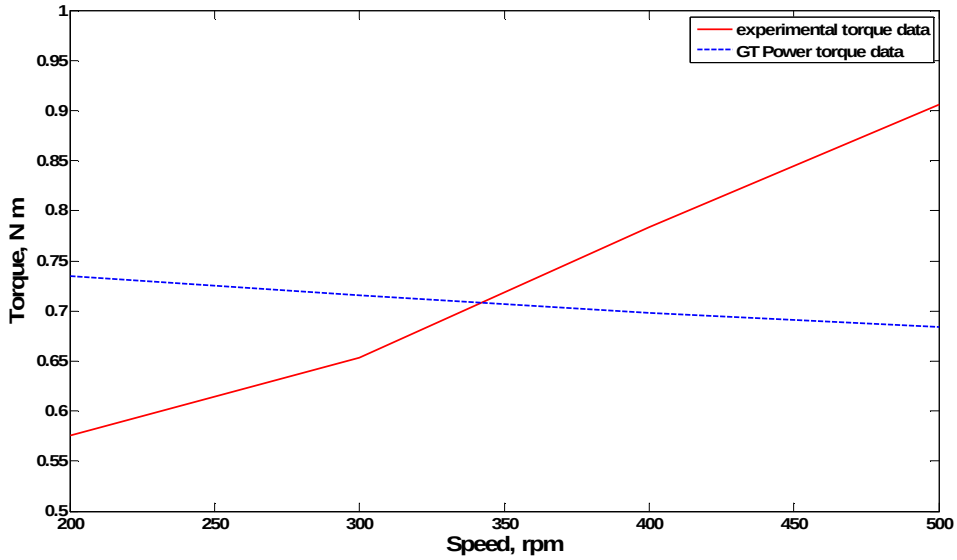

Figure 4-17 Rotary expander with solenoid valves, 10 bar steam, comparison of torque

Table 4-7 compares the torque for each speed step and presents the percentage difference between the two values.

Speed (rpm)	Measured Torque (N m)	GT Model Torque (N m)	Percentage Difference
200	0.5757	0.7345	+21.60
300	0.6534	0.7153	+8.60
400	0.7836	0.6994	-10.80
500	0.9063	0.6840	-24.52

Table 4-7 Rotary expander with solenoid valves, 10 bar steam, percentage difference for torque comparison

Figure 4-18 compares the variation in pressure over one complete rotor revolution for the experimental data and GT data, once again 300 rpm was chosen as the speed that gave the closest torque comparison.

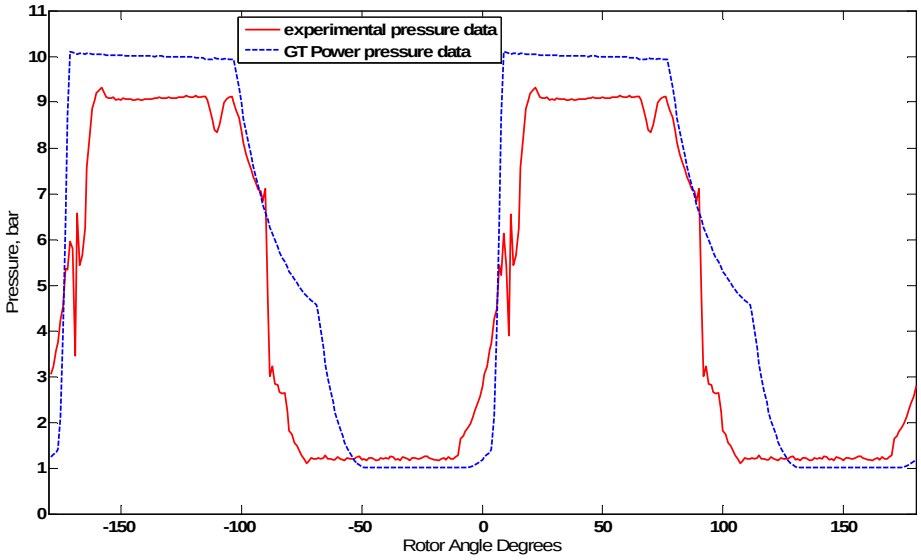

Figure 4-18 Rotary expander with solenoid valves, 10 bar steam, comparison of pressure cycles, 300 rpm

As can be seen from Figure 4-17 and Table 4-7, the torque data obtained from the rotary model, with 10 bar steam, was not comparable with the experimental data with the difference being considerably more than the accepted ±5% margin and, as with the steam results for the rotary expander with port valves, the gradient of the line is also different, this could be due to the fact that steam performed differently to nitrogen (it will be shown in the next section that the nitrogen results were more comparable) and that this needed to be added to the rotary expander model in some form of heat exchange calculation; at the time of writing, due to time constraints, this could not be further investigated. However the pressure data shown in Figure 4-18 gives a comparable curve, so it can be concluded that the GT rotary expander model is performing in a similar way to the actual rotary expander. The difference in maximum pressure is due to the fact that the GT model holds the pressure at a constant 10 bar, whereas the boiler used for the experiments tended to drift between 9 bar and 12 bar.

4.3.3.2 Nitrogen results

Figure 4-19 compares the variation in torque with speed for the experimental data and GT data using 10 bar nitrogen.

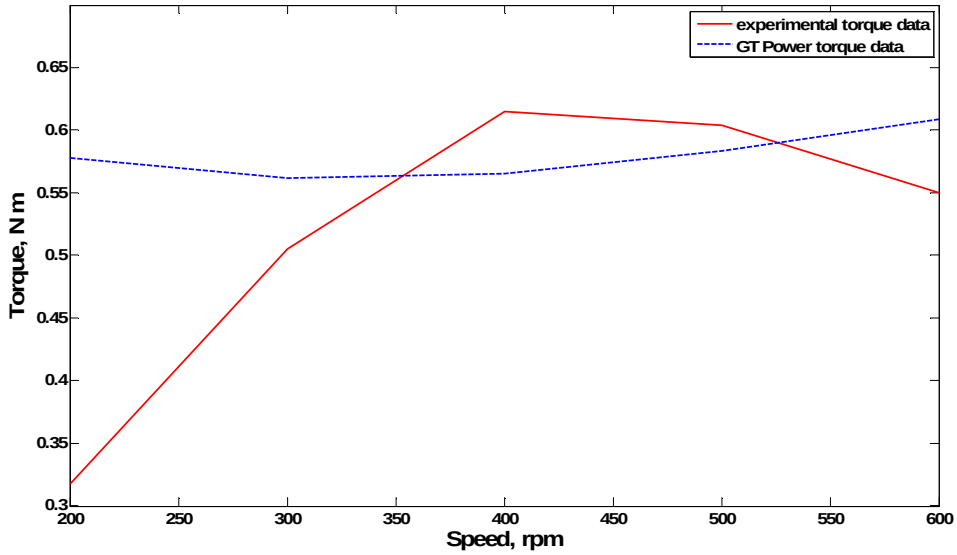

Figure 4-19 Rotary expander with solenoid valves, 10 bar nitrogen, comparison of torque

Table 4-8 compares the torques for each speed step and presents the percentage of difference between the two values.

Speed (rpm)	Measured Torque (N m)	GT Model Torque (N m)	Percentage Difference
200	0.3176	0.5782	+44.10
300	0.5055	0.5622	+10.10
400	0.6147	0.5656	-7.99
500	0.6037	0.5833	-3.38
600	0.5501	0.6086	+9.60

Table 4-8 Rotary expander with solenoid valves, 10 bar nitrogen, percentage difference for torque comparison

Figure 4-19 and Table 4-8 and show that the GT model for the rotary expander, with solenoid valves, using 10 bar nitrogen yielded similar results to the experimental data for higher speed steps with the torque data exceeding the acceptable ±5% margin for all but one speed step, moreover for the lowest speed step of 200 rpm the torque was not comparable, with the torque for the experimental data at 200 rpm being 45% less than the torque obtained from the GT model. Overall, this is a not good result; the differences are probably due to the use of the solenoid valves and the uncertainty of the actual timing for

the experiments. The differences could also be due to the GT model using cylinder attributes to represent the rotary expander chambers, which could yield a different performance; the model could be improved to allow for these issues.

Figure 4-20 compares the variation in pressure over one complete rotor revolution for the experimental data and GT data, this time 400 rpm was chosen as it was a good mid-point in the torque comparison results.

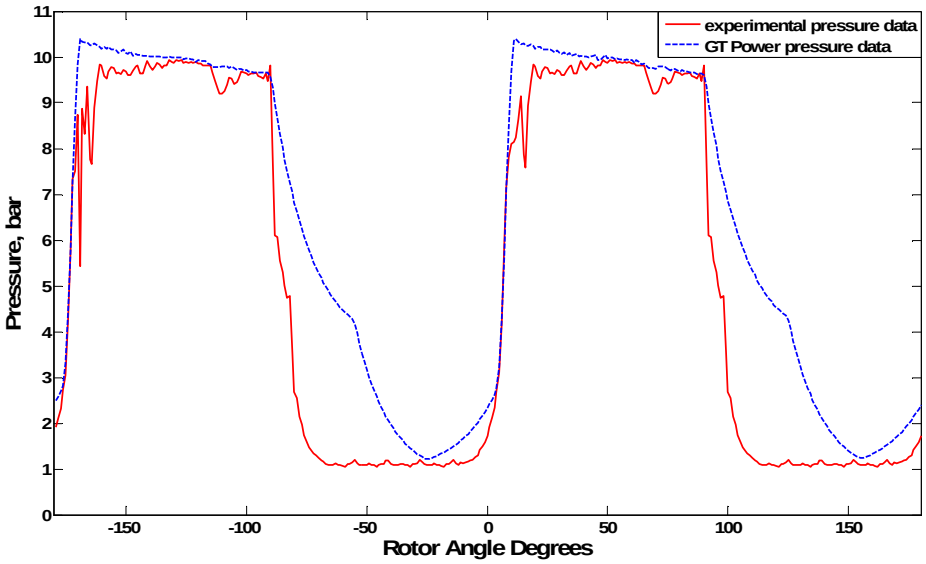

Figure 4-20 Rotary expander with solenoid valves, 10 bar nitrogen, comparison of pressure cycles, 400 rpm

Figure 4-20 shows that the pressure cycle at 400 rpm for the experimental data share some similarities with the pressure data obtained from the GT model. The opening and closing times are comparable, as is the upper and lower pressure levels, however there is more expansion observed in the GT results compared to the experimental results, this could be due to a couple of factors. Firstly, the experimental data used two sensors, so the data between the two could contain some uncertainty. Secondly, the GT model is perfect with respect to expansion, and improvement between the two could be to impress the expansion index from the experimental data onto the GT model, time constraints did not

allow for this to be explored fully, but would be a recommendation should the models be used in future projects.

Figure 4-21 compares the variation in torque with speed for the experimental data and GT data at 15 bar nitrogen.

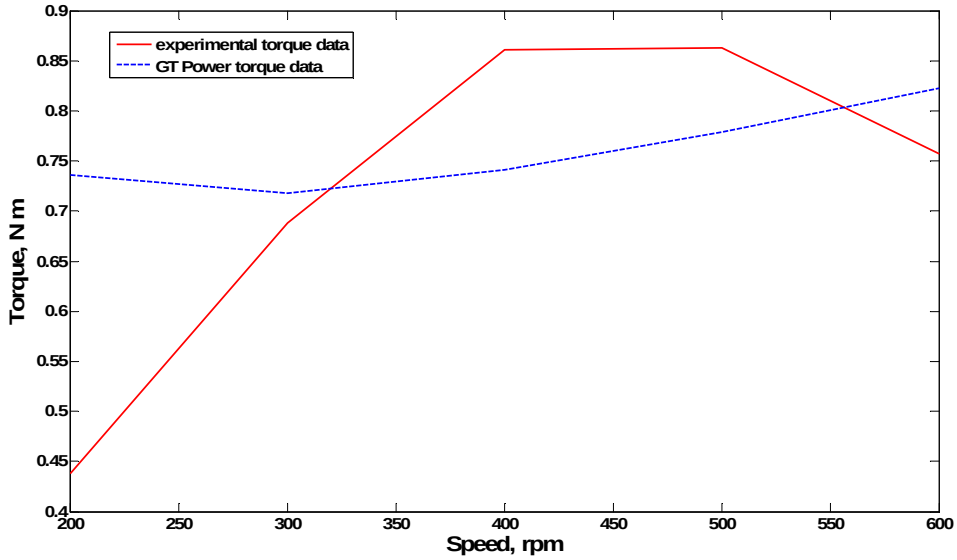

Figure 4-21 Rotary expander with solenoid valves, 15 bar nitrogen, comparison of torque

Table 4-10 compares the torque for each speed step and presents the percentage difference between the two values.

Speed (rpm)	Measured Torque (N m)	GT Model Torque (N m)	Percentage Difference
200	0.4382	0.7359	+40.5
300	0.6879	0.7175	+4.1
400	0.8608	0.7410	-13.9
500	0.8625	0.7790	-9.7
600	0.7575	0.8226	+7.9

Table 4-9 Rotary expander with solenoid valves, 15 bar nitrogen, percentage difference for torque comparison

Figure 4-21 and Table 4-9 show that the GT model for the rotary expander, with solenoid valves, using 15 bar nitrogen yielded similar results to the experimental data for higher speed steps with the torque data exceeding the acceptable ±5% margin for all but one of the speed steps, moreover for the lowest speed step of 200 rpm the torque was not comparable, with the torque for the experimental data at 200 rpm being 40% less than the torque obtained from the GT model. Overall, this is not a good result and could be improved; the differences, especially the anomaly in these results for 400rpm being above ±10% difference, are probably due to the use of the solenoid valves and the uncertainty of the actual timing for the experiments. The differences could also be due to the GT model using cylinder attributes to represent the rotary expander chambers, which could yield a different performance; the model could be improved to allow for these issues.

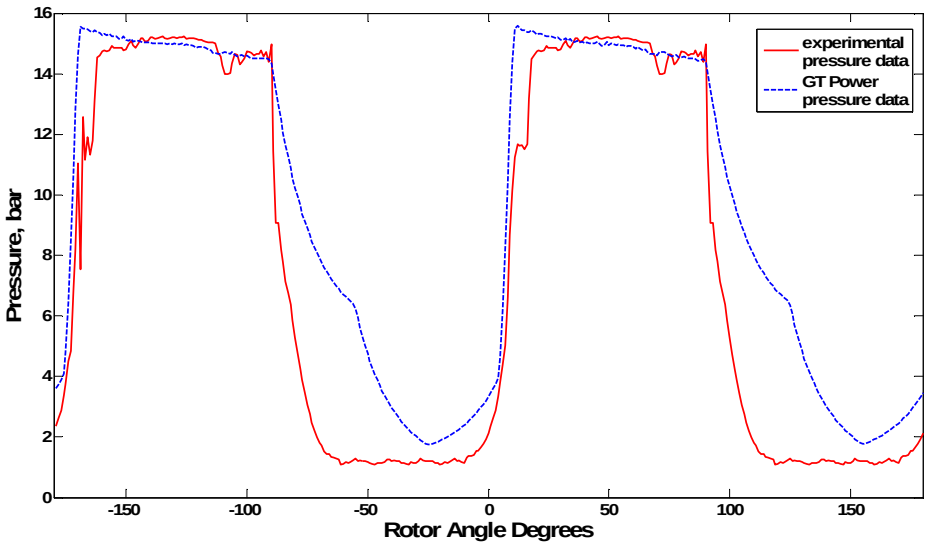

Figure 4-22 Rotary expander with solenoid valves, 15 bar nitrogen, comparison of pressure cycles, 300 rpm

As with the results for 10 bar nitrogen, Figure 4-22 shows that the pressure cycle at 300 rpm for the experimental data share some similarities with the pressure data obtained from the GT model. The opening and closing times are comparable, as is the upper and lower pressure levels, however there is some expansion in the pressure cycle for the GT

model that is not experienced in the experimental data, this could be due to the limitations of the solenoid valves used in the experiments and the GT results could be improved with investigation into how to alter the expansion index in the GT model, time constraints did not allow for this to be explored fully, but as with the 10 bar model this would be a recommendation should the models be used in future projects.

4.4 Comparison of experimental and model results

This section discusses some of the results presented in the previous section with respect to the validation issues and summarises the conclusions for this part of the project.

4.4.1 Correlation between media

This section will investigate the correlation between the nitrogen and steam results and discuss whether the nitrogen results could be used to predict the steam results for larger sized expander configurations.

The way this was investigated was to use the torque data from the GT results along with the GT (inlet) opening time, Δt, to result in a parameter that could be used as a comparison. The opening times were different for each of the tests 10 bar nitrogen, 15 bar nitrogen and 10 bar steam, so the assumption is that by dividing the torque by this variation in time, a new parameter, $T/\Delta t$, would be obtained.

These parameters were then compared by:

i. calculating the ratio of nitrogen 10 bar $T/\Delta t$ with nitrogen 15 bar $T/\Delta t$, ratio should be approximately 1.5, as for the pressure ratios;
ii. calculating the ratio of nitrogen 10 bar $T/\Delta t$ with steam 10 bar $T/\Delta t$, ratio should be close to 1.

Table 4-10 shows the collated data for the uni-flow experiments, Δt is given in crank angle degrees.

Speed (rpm)	Nitrogen 10 bar		Steam 10 bar		Nitrogen 15 bar	
	Δt	Torque (N m)	Δt	Torque (N m)	Δt	Torque (N m)
200	124	0.38	107	0.45	107	0.68
300	134	0.42	134	0.54	110	0.72
400	127	0.38	149	0.51	120	0.66
500	130	0.39	161	0.55	134	0.59
600	136	0.34	170	0.51	149	0.56

Table 4-10 Uni-flow timing and experimental torque data

Table 4-11 shows the ratios for nitrogen at 10 bar and nitrogen at 15 bar together with steam at 10 bar and nitrogen at 10 bar for each speed step.

Speed (rpm)	Nitrogen *T/Δt* ratio	10 bar *T/Δt* ratio
200	2.06	1.35
300	2.09	1.28
400	1.81	1.14
500	1.48	1.15
600	1.52	1.21

Table 4-11 Uni-flow ratios between nitrogen tests and 10 bar tests

The uni-flow tests show a close correlation for the higher three speed steps than for the lower speed steps, this could be related to the timing issues with the solenoid valves, or it could be that the *T/Δt* method is not appropriate. This would need further investigation and validation if the models are used further for the next expander size testing.

Table 4-12 shows the collated data for the experiments with the rotary expander configuration with port valves. The Δt value, in crank angle degrees, is irrelevant in this case as the same timings were used throughout.

Speed (rpm)	Nitrogen 10 bar		Steam 10 bar		Nitrogen 15 bar	
	Δt	Torque (N m)	Δt	Torque (N m)	Δt	Torque (N m)
200	120	0.6669	120	0.460	120	0.9139
300	120	0.5449	120	0.500	120	0.7172
500	120	0.4979	120	0.528	120	0.6385
700	120	0.4529	120	0.530	120	0.5641

Table 4-12 Rotary expander, port valves, timing and experimental torque data

Table 4-13 shows the ratios for nitrogen at 10 bar and nitrogen at 15 bar together with steam at 10 bar and nitrogen at 10 bar for each speed step.

Speed (rpm)	Nitrogen 10 bar/15 bar ratio	10 bar steam/nitrogen ratio
200	1.37	0.69
300	1.32	0.92
500	1.28	1.06
700	1.25	1.17

Table 4-13 Rotary expander, port valves, ratios between nitrogen tests and 10 bar tests

The correlation for the rotary expander, for the 10 bar results are acceptable for the mid-range speeds, 300 and 500 rpm, but are not acceptable for the lower or higher speed steps. Additionally the nitrogen results do not correlate at any speed steps. This means that either the *T/Δt* method is not suitable for the rotary expander, or that the results are unreliable, which could be due to fluctuations in source pressure. As explain in the previous section, the GT model holds the pressure constant, whereas the boiler used for the experiments tended to drift between ±4 bar.

Table 4-14 shows the collated data for the experiments with the rotary expander configuration with valves attached to the inlets. Again, the Δt value, in crank angle degrees, is irrelevant in this case as the same timings were used throughout.

Speed (rpm)	Nitrogen 10 bar		Steam 10 bar		Nitrogen 15 bar	
	Δt	Torque (N m)	Δt	Torque (N m)	Δt	Torque (N m)
200	80	0.3176	80	0.5757	80	0.4382
300	80	0.5055	80	0.6534	80	0.6879
400	80	0.6147	80	0.7836	80	0.8608
500	80	0.6037	80	0.9063	80	0.8625
600	80	0.5501	-	-	80	0.7575

Table 4-14 Rotary expander, with valves, timing and experimental torque data

Table 4-15 shows the ratios for nitrogen at 10 bar and nitrogen at 15 bar together with steam at 10 bar and nitrogen at 10 bar for each speed step.

Speed (rpm)	Nitrogen 10 bar/15 bar ratio	10 bar steam/nitrogen ratio
200	1.38	1.81
300	1.36	1.29
400	1.40	1.27
500	1.43	1.50
600	1.38	-

Table 4-15 Rotary expander, with valves, ratios between nitrogen tests and 10 bar tests

For this configuration the correlation results were not good, the 10 bar results were not acceptably close, although the Nitrogen ratios were slightly better than without the valve ratios, they were still not good enough to be reliable. Once again this means that either this method is not suitable for the rotary expander, or that the results are unreliable, which could be due to fluctuations in source pressure.

In summary, the correlation with the uni-flow expander looked favourable and hence could be used to predict the results; however more investigation of the results would be needed for the rotary configurations before they were used to predict results for different sources or pressures.

4.4.2 Validation of test results

This section will discuss the possibility of the GT-SUITE results being used to validate the expander test results.

Looking at the results in Section 4.3.1 for the uni-flow expander model, the valve timings used in the experiments were found to be inadequate; a factor of 3 was used to multiply the experimental opening times to get GT results that were closer to the experimental torque. The torque obtained was within ±5% of the experimental data for the lower speed steps. However for the higher speed steps the difference was greater than ±5%, ±13% for steam at 10 bar, ±16% for nitrogen at 10 bar and ±29% for nitrogen at 15 bar. The reason for this required multiplication factor could be down to the solenoid valves not operating as smoothly or quickly as expected. So for the experiments, when the LabVIEW control program sent out a pulse width of, for example, 30 crank angle degrees, because of the

delay of the solenoid valve this actually corresponded to a real width of 90 crank angle degrees. However, as some of the higher speed steps were not within the acceptable ±5%, it can be concluded that the correlation may not be a simple factor that is the same for all speed steps. For the higher speed steps, the valve delay would be increased and hence a different factor would be required.

The results for the rotary expander configuration with port valves in Section 4.3.2 did yield a good correlation especially for the nitrogen tests, with the torque comparison being below ±5% between the experimental data and the GT data. The steam results were not as good for this configuration being in between ±9% and ±35%, this could be due to the poor behaviour of the rotary expander with steam, or due to the steam boiler pressure fluctuations.

Finally, the rotary configuration with valve control results were worse for the nitrogen tests, between ±3% and ±44%, but slightly improved for the steam tests, ±8% to ±24%. This could be attributed to the fact that the solenoid valve timing was not perfect and they could only operate at slow speeds, and also due to boiler fluctuations, which were not taken into consideration for the GT models.

These issues would need to be considered when using GT to validate different expander sizes of the same configuration.

4.4.3 Scalability

This section will discuss if the GT results can be used to predict the results for larger expander configurations.

The GT models for the uni-flow and some rotary configurations yielded good results, especially at the lower speeds, so with careful re-modelling, GT could be used to predict the results for larger expanders; however a further validation step with a larger expander size would be necessary to be really confident in the scalability.

4.5 Conclusions for small expander modelling

The main aim of this part of the project was to create models of the small expanders and see if the model result data would validate the experimental data and further if the models could then be scaled up to predict the performance of larger sized expanders.

It can be concluded that the models can predict the torque output of the uni-flow and rotary configuration with no valve control, for speeds below 500 rpm to within ±5% of the experimental torque. However, when the solenoid valves were used with the rotary expander, good results were not obtained; hence that configuration would require more investigation. In order to answer the question of scalability, some further modelling and testing would need to be done with medium size expander configurations to be confident whether scalability would be possible or not.

The GT models using steam as a source would be greatly improved if more investigation were carried out into the heat transfer characteristics and expansion index. If these parameters were variable, then a closer model for each configuration and test type could be made. For example by recording the expansion index for the experimental results and inserting these into the GT model, a closer pressure shape would be obtainable.

Additionally further investigation needs to be done into the correlation between the timings used in the experiments and in the GT modelling. If further experiments were carried out, an accurate way to record inlet and exhaust timings should be employed, as using the timings from the Labview programs was not sufficient.

Finally, as stated in the conclusions for the small expander tests, a more suitable valve arrangement should be sourced that is able to handle higher speed ranges. On a similar note, a method should be developed to prevent the fluctuations from the source boiler pressure being passed onto the inlet of the expander and hence affecting the results.

5 Control strategy: development and modelling

5.1 Control strategy introduction

This chapter presents an overview of the control strategies that were investigated and modelled.

The aim of the control system is to minimise the fuel consumption whilst generating a percentage of the torque demanded on the IC engine. The two strategies that are considered are respectively a hierarchical control structure and a multi-variable control structure.

In Section 5.2, the overall HYSTOR concept will be revisited in order to present the hierarchical control structure; this will take into consideration the overall supervisory control strategy and break the system down into individual control components.

Section 5.3 proceeds to discuss the control variables and objectives which were considered when creating individual, *SISO* controllers and which are also used to in the formulation of a *MIMO* controller.

Section 5.4 presents a Simulink model for a simple *MIMO* controlled system and the results.

PID controls were used as the basis for development of an observer-controller system and this is detailed in Section 5.5. The observer-controller is designed using firstly pole-placement then an LQ method. In neither case did the performance reach the level defined by the distributed PID controllers. The conclusion drawn was that the model developed for the system was never sufficient in its representation of the dynamics to form the basis for an adequate design. There is further work needed to complete a comprehensive system identification process and to test a variety of controllers including multi-mode linear and fixed gain robust controllers.

Section 5.6 describes how the PID control was integrated into the hybrid vehicle models detailed in Chapter 2. The new PID controlled models were run using the same drive cycles used in Chapter 2. A comparison is made of fuel consumption improvement when compared to the conventional vehicle and also the accumulator model from Chapter 2. Additionally the power outputs for each drive cycle are presented.

Section 5.7 summarises and concludes the control development and modelling strategy.

5.2 Control structure

The section begins by revisiting the basic HYSTOR concept shown in Figure 5-1.

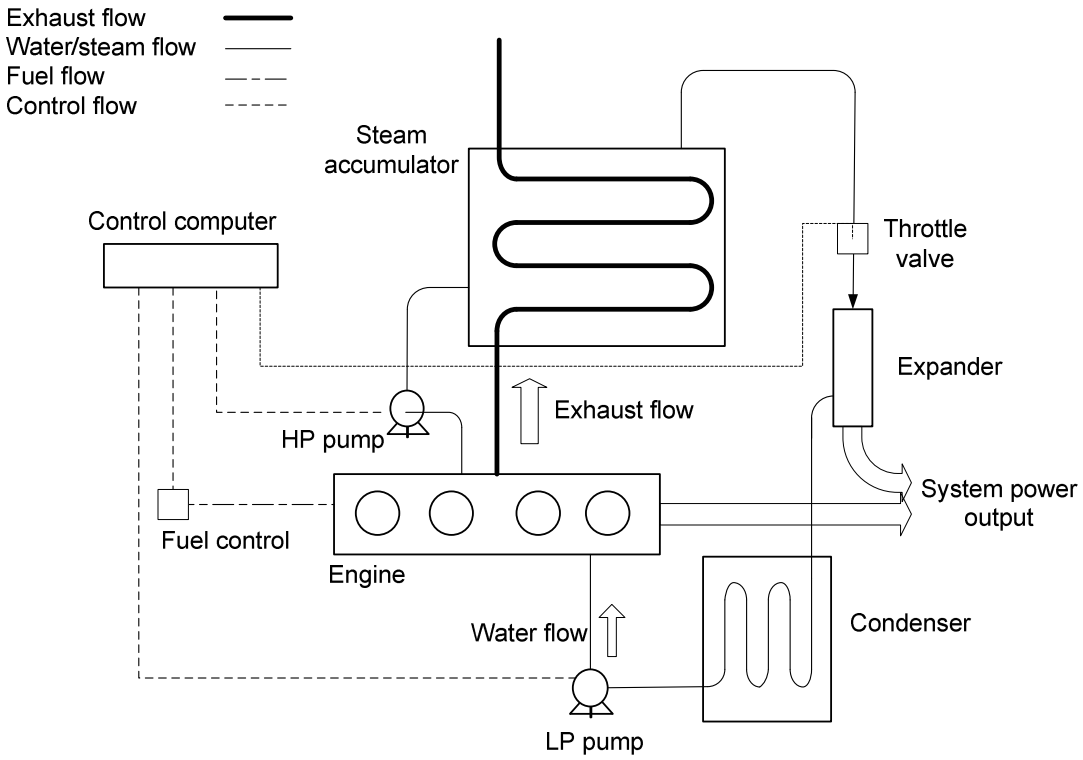

Figure 5-1 Overall HYSTOR system concept

The control of the HYSTOR system can be divided into two main areas, global, or supervisory control, and local control, the latter being individual controls for key functions within the system.

5.2.1 Control hierarchy

The supervisory control unit will monitor the local control units and the IC engine system in order to supervise local control units in a hierarchical structure. The hierarchical flow is shown in Figure 5-2.

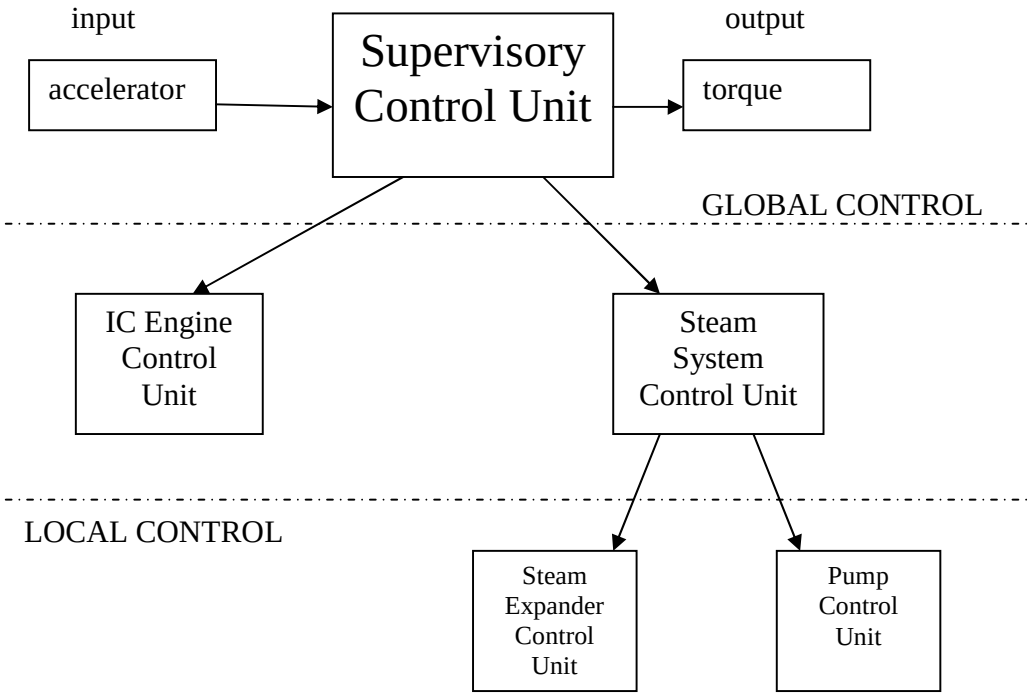

Figure 5-2 Hierarchical structure of the control system

A possible first step for dealing with a control requirement is to split the overall system up into units and treat each unit as a single loop control entity or module. The units for the steam expander and pump are described in Appendix J.1.

5.3 Control objectives and variables

The control objectives for the complete HYSTOR system are as follows:

Power/Torque – the power or torque demand from the vehicle driver needs to be met by the IC engine, the steam expander, or a combination of both IC engine and steam expander;

Fuel Economy – the fuel consumption needs to be kept to a minimum;

Steam Supply/Reserve – the supply of water to the boiler needs to be kept at an appropriate pressure/mass flow rate to ensure there is a constant steam supply or a reserve of available steam for the steam expander;

Steam Quality – the quality of the steam supply or reserve needs to reach a superheated state in order to get the best efficiency from the steam expander, and to ensure there is minimum risk of droplet damage to the expander, which would be caused if using steam that is too wet.

These objectives will be met by identifying the variables within the system that are controllable and also by monitoring and interacting with the IC engine system.

The two main control modules are the pump controller and the expander controller. The control variables that need to be considered for these control modules are as follows:

1) the cut-off timing of the throttle for the expander, this will be referred to throughout as α;
2) the water mass flow rate from the high pressure water pump, which in turn is determined by the speed of the pump. The water mass flow rate shall be referred to throughout as $\dot{m}_w$ and the speed as *n*.

These variables and their controls can be separated into three controllable units. The pump controller monitors $\dot{m}_w$ and uses the demanded pressure to control the pump speed *n*. The expander controller monitors demanded torque and the system pressure to control the expander inlet valve timing using α. Finally, the third controller is a supervisory controller that monitors the steam system and IC engine conditions and controls the

required changes in $\dot{m}_w$ and α. As the system pressure is proportional to the mass flow rate of water, by monitoring and controlling the demanded system pressure, the correct mass flow rate of water will be maintained by the system to generate good quality superheated steam using the available exhaust gas temperature and mass flow rate.

In Figure 5-1 there is a control link to the low pressure pump from the condenser, this will not be further developed at this time, but should be considered in future design developments.

PID control loops were used to develop the individually controlled units. PID control loops were chosen as a benchmark for the control system and because PID loops are widely used to develop simple, yet robust control systems. The PID control results would also help to compare any results gained when developing a more complex, optimised, controller. Each control unit is presented in more detail as individual control blocks, with their governing equations and test results in Appendix J.2. The overall control system and its connections are shown in Figure 5-3.

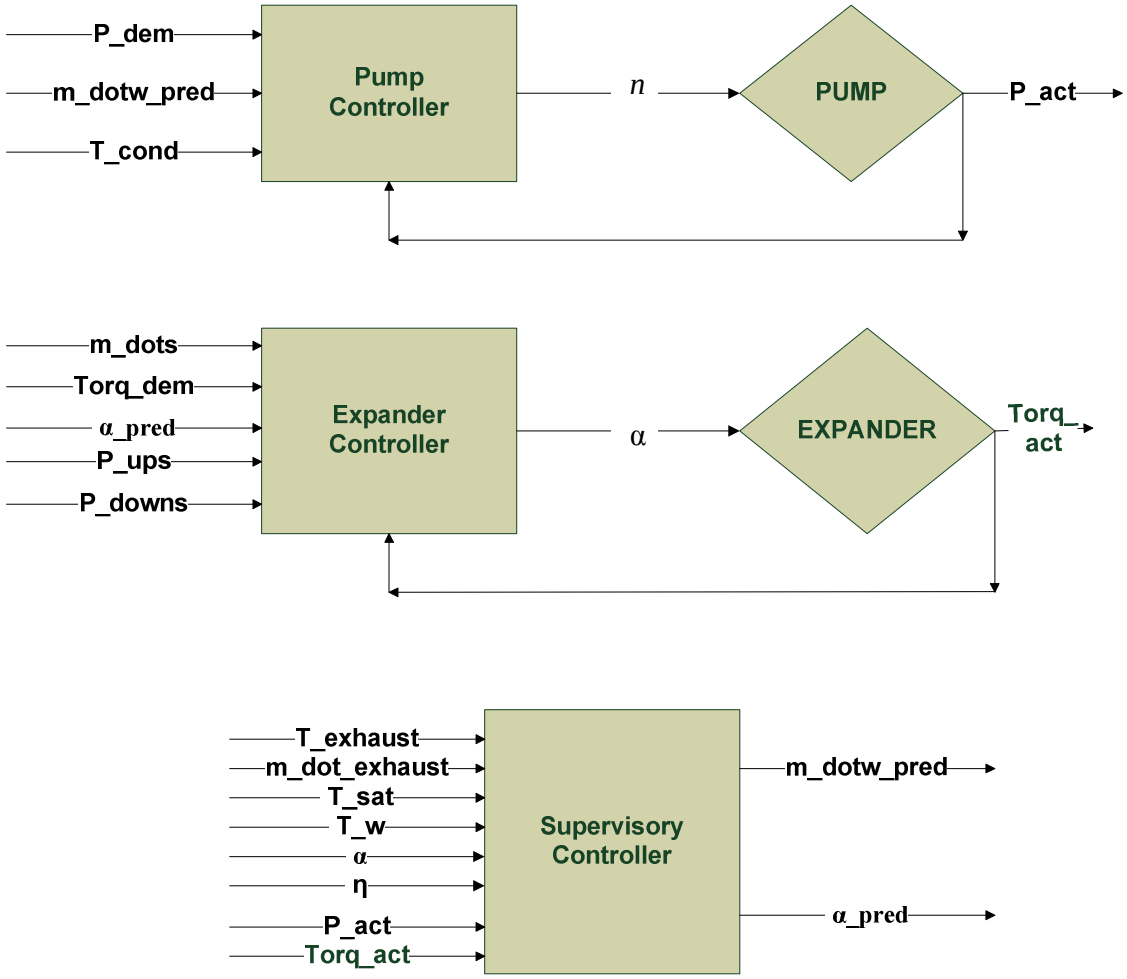

Figure 5-3 Overall control system

Figure 5-3 was used to develop and integrate the controller modules, the Simulink model and tests performed are detailed in Appendix J.2.

5.4 A simple PID controlled system

The positive displacement pump, expander and supervisory control models were integrated into one Simulink model; additionally a block representing the heat exchanger was added to the pump control loop in order that the heat exchange process was taken into consideration for the system pressure calculations. This system controlled with two PID loops is shown in Figure 5-4.

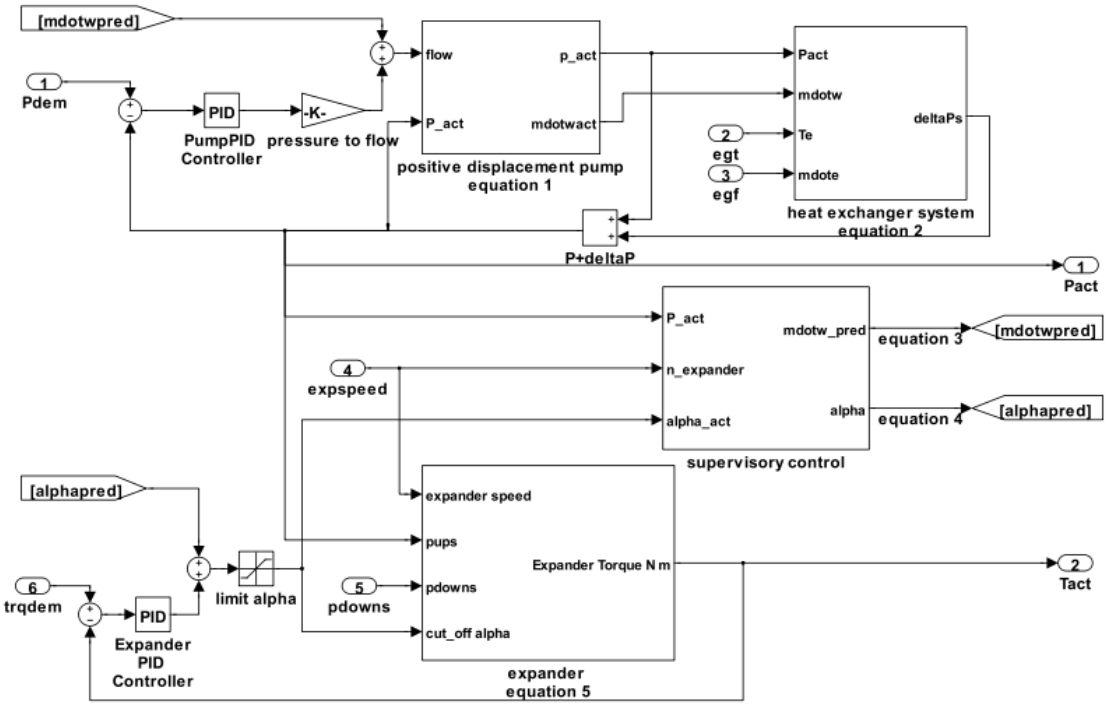

Figure 5-4 System with two PID control loops

The Simulink blocks shown in Figure 5-4 contain references to equations 1 through 6 in their names, these equations are as follows:

positive displacement pump equation 1 incorporates Equation 5.1 through Equation 5.3, as used for the positive displacement pump and developed in Appendix J.2.1;

Volumetric flow $F_n = K_s \times n$ (5.1)

Leakage flow $F_l = K_l \times p$ (5.2)

Total flow $F = F_n - F_l$ (5.3)

heat exchanger system equation 2 incorporates Equation 5.4 which is used to calculate the change in pressure with respect to time. It is proportional to the sum of the heat transferred, to the mass flow rate of water and inversely proportional to the mass flow rate of the steam used by the expander;

$$\frac{\partial P_s}{\partial t} = K_1.\dot{Q} + K_2.\dot{m}_w - K_3.\dot{m}_s \qquad (5.4)$$

where K_1, K_2 and K_3 are constants, $\dot{Q}$ is the rate of heat transfer (using Equation 2.2 from Section 2.2.1), $\dot{m}_w$ is the mass flow rate of water, and $\dot{m}_s$ is the mass flow rate of steam through the expander;

mdotwpred equation 3 is Equation 5.6, as used for the supervisory controller, developed in Appendix J.2.3;

$$\dot{m}_{pred} = n_{\exp}.\alpha.V.\rho \qquad (5.6)$$

alphapred equation 4 is Equation 5.7 as used for the supervisory controller, developed in Appendix J.2.3;

$$\alpha_{pred} = K.\frac{p_n}{p_{n-1}} \qquad (5.7)$$

expander equation 5 is Equation 5.8 as used for the expander, developed in Appendix J.2.2;

.

$$work = \left((p_b.(\alpha_v.V)) + \left(\frac{k1}{1-\eta}\right).\left[\frac{1}{V_3^{\eta-1}} - \frac{1}{V_2^{\eta-1}}\right]\right) - (p_c.V_5) \qquad (5.8)$$

A test harness for the system was created; this is shown in Figure 5-5. Additionally a limit was imposed on the demanded torque to keep the system in a stable state. This was achieved, in the initialisation file, by using the expander Equation 5.8, with the volume of the expander set to 0.2 litres, a fixed p_c value of 1 bar and then the maximum torque calculated for system working pressures of between 18 bar and 25 bar. This formed a lookup table for the Simulink block, the output of which was used to limit the torque demand.

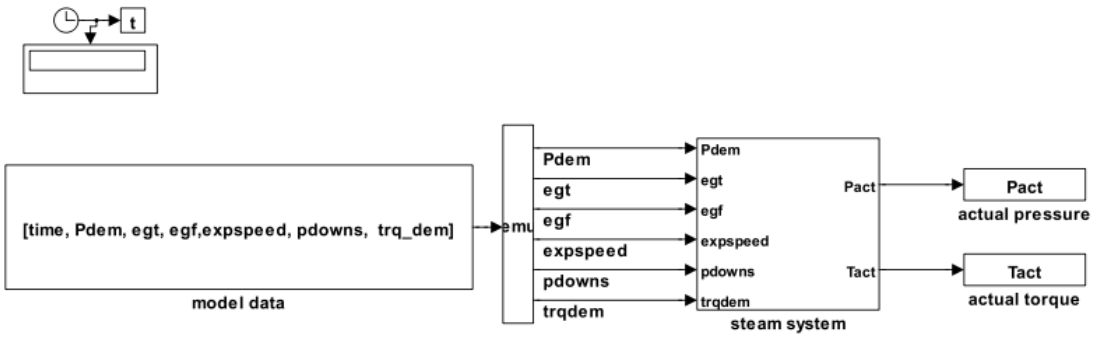

Figure 5-5 Test harness for PID controlled model

Test data were created to test the following different scenarios:

- constant system pressure demand, varying torque demand;
- constant torque demand, varying system pressure demand;
- varying system pressure and torque demand exceeds maximum torque available;
- T_{exh} (egt) too low to generate steam;
- $\dot{m}_{exh}$ (egf) too low to generate steam;
- using a drive cycle to run the model.

Figure 5-6 presents the results for the test with a constant torque demand, of 35 N m, while the pressure demand input is varied between 18 bar and 21 bar.

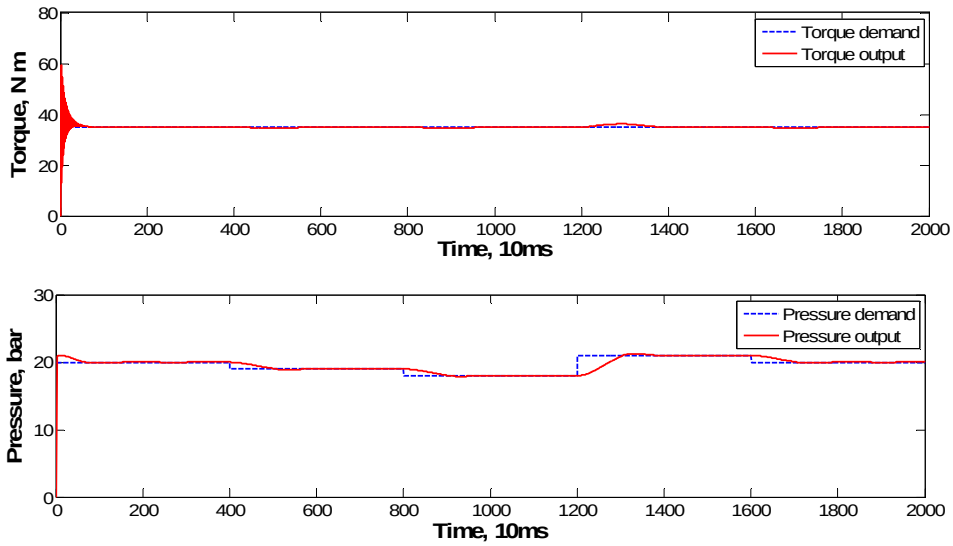

Figure 5-6 Constant torque demand with varying pressure demand

It can be seen in Figure 5-6 that the pressure output follows the demand with a slight delay and whilst the torque output is affected by the varying pressure demand, the torque output stabilises back to the torque demand. Figure 5-7 presents the results for the test with a constant pressure demand, of 20 bar, whilst the torque demand input is varied between 30 N m and 45 N m.

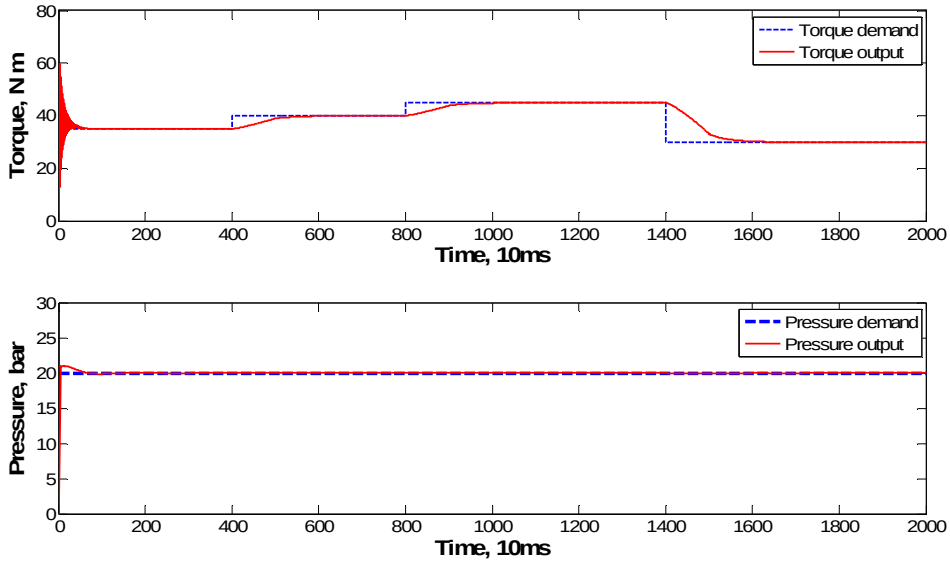

Figure 5-7 Constant pressure demand with varying torque demand

It can be seen in Figure 5-7 that the torque output follows the demand with a slight delay and whilst the pressure output is affected only slightly by the varying torque. Figure 5-8 shows the results when testing the maximum torque demand. Two system pressures are used, 20 bar and 23 bar, for an expander of volume 0.2 litres and a condenser pressure value of 1 bar. The system pressures correspond to maximum torques of 63 N m and 73 N m, respectively.

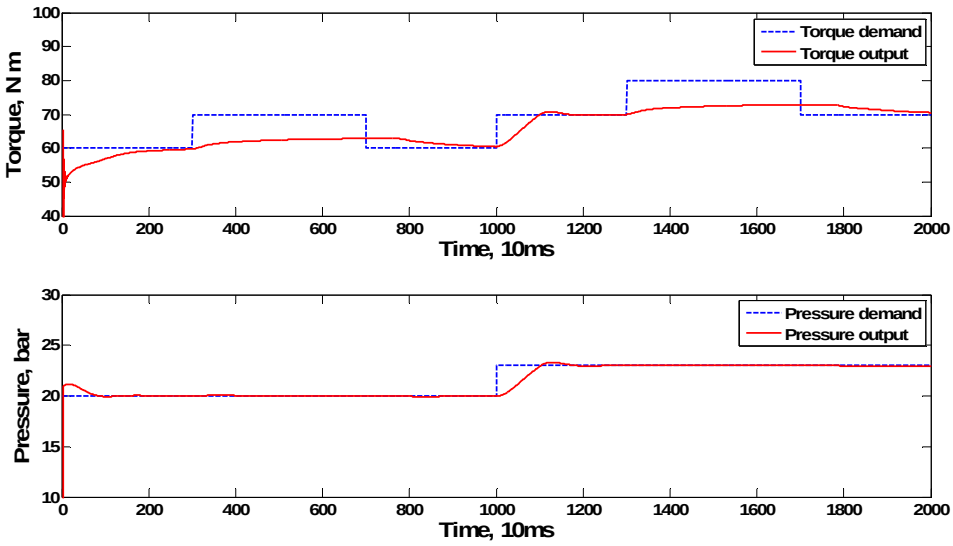

Figure 5-8 Control of maximum torque demand

It can be seen in Figure 5-8 with the pressure controlled to 20 bar and a torque demand of 70 N m, the output torque is limited to 63 N m. The second half of the graph shows that when the pressure demand is increased to 23 bar, then the torque demand of 70 N m is met, but when the torque demand increases to 80 N m, at this pressure, the output is limited to 73 N m. In each case the system is working close to a limiting torque value that corresponds to a maximum (100%) cut-off with the particular steam pressure.

Figure 5-9 presents the results for the test with a constant pressure and torque demands input (20 bar and 35 N m, respectively) whilst the exhaust gas mass flow rate input is changed to just above the threshold (0.01 kg/s) to below the threshold and back to above the threshold, over 20 seconds.

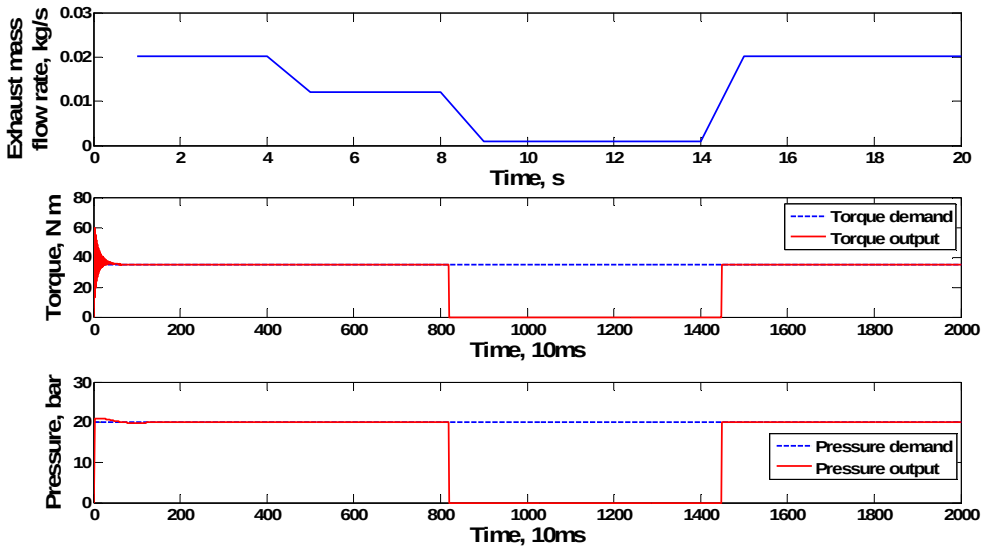

Figure 5-9 Constant pressure and torque demands with varying exhaust gas mass flow rate

It can be seen in Figure 5-9 that while the exhaust gas mass flow rate remains above the threshold for being able to produce steam, the demanded torque is met. However once the exhaust gas mass flow rate has reduced to a rate below the threshold, the steam generator system is turned off and no torque is produced.

Figure 5-10 presents the results for the test with a constant pressure and torque demands input (20 bar and 35 N m, respectively) whilst the exhaust gas temperature input is changed to just above the threshold (485 degrees Kelvin, saturation at 25 bar) to below the threshold and back to above the threshold, over 20 seconds.

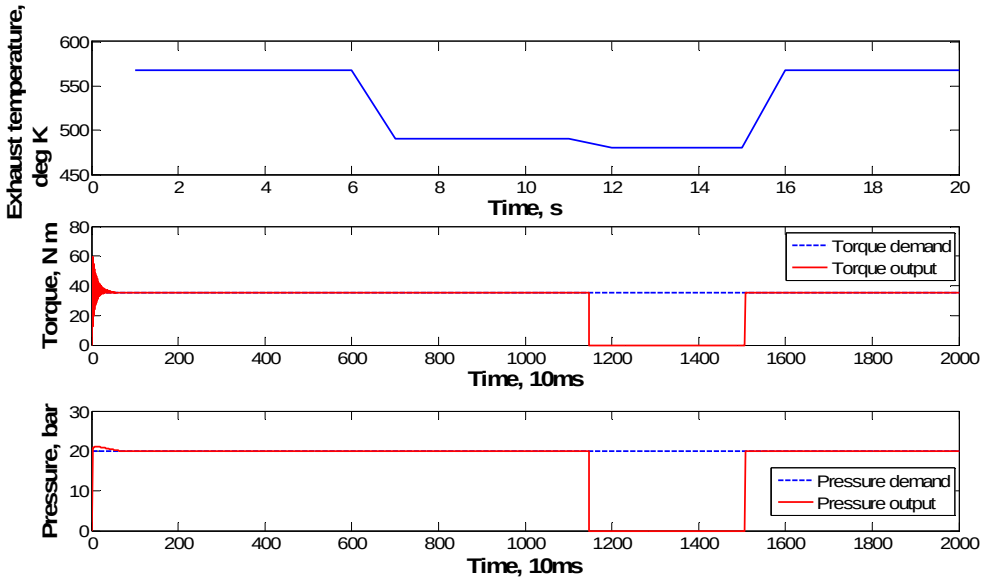

Figure 5-10 Constant pressure and torque demands with varying exhaust gas temperature

It can be seen in Figure 5-10 that while the exhaust gas temperature remains above the threshold for steam production, the demanded torque is met. However once the exhaust gas temperature has reduced to a rate below the threshold, the steam generator system is turned off and no torque is produced.

The final test for the PID controlled model was to use the drive cycle data as inputs for the model. The data was obtained from running the QSS-TB model in Chapter 2. Figure 5-11 shows the torque comparison for the NEDC data.

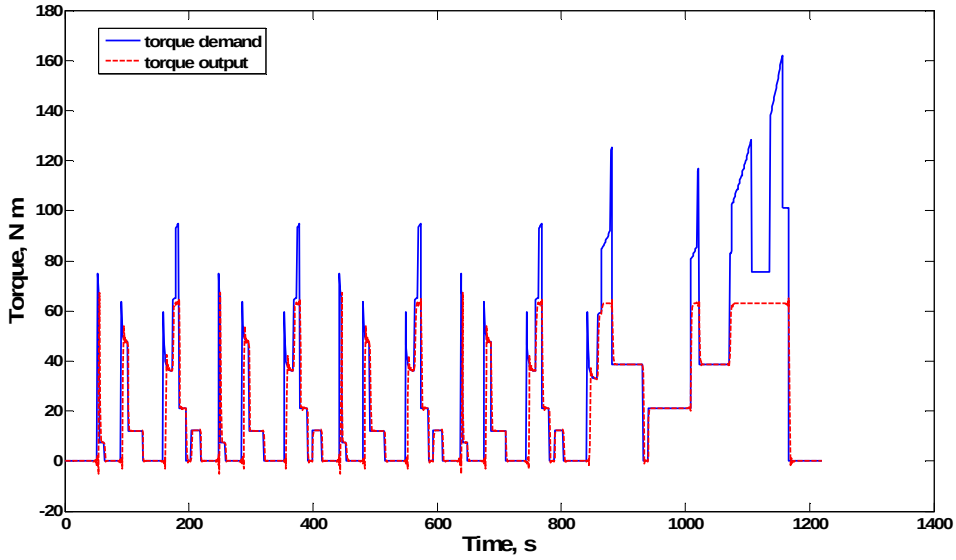

Figure 5-11 Running the PID controlled model with NEDC data

It can be seen in Figure 5-11 that the torque demand is met, within the limitations. The system pressure was a constant 20 bar, so the torque output was limited to 63 N m. The torque output closely follows the demand from the NEDC data.

Using the results from these tests, it was concluded that the simple PID controlled system was effective; the system is further used as a building block to develop the observer-controller, described in Section 5.5. Additionally the PID controlled system was integrated into the QSS-TB and PSAT models (developed in Chapter 2) so that the performance could be compared with the basic models from Chapter 2. These results are presented in Section 5.6.

5.5 Observer-controller system

This section describes the further development of the control system by creating an observer-controller with state feedback. This is achieved by performing system identification on the dynamic model, in order to obtain a linear, state-space model, which in turn was used to develop the observer-controller design; this procedure is described in the first three sub-sections. Two dynamic models were developed, initially a reduced version of the PID controlled model, but the behaviour of the resulting state-space model and observer-controller were not adequate. This is discussed in Section 5.5.3. The PID controlled model was used with input and output data sampled to generate the state-space model, and gave slightly better results, but did not reach the performance defined by the PID controls. The modelling process is discussed in Section 5.5.5.

5.5.1 PRBS creation

In order to perform system identification, pseudo random binary sequences (PRBSs) were created for the system inputs, α and *n*. The range for α was 0 to 1 in steps of 0.1 and the range for *n* was 600 rpm to 1600 rpm in varied steps between 100 rpm and 400 rpm.

The PRBS sequences were created using the Matlab command *idinput* from the *System Identification Toolbox (SIT).* An example is shown below:

```
alpha_prbs=idinput([sim_steps 1],'prbs',[0 0.1],[n1 n2]);
```

where *sim_steps* is the number of simulation steps, for example 600 seconds, *n1* is the lower PRBS value and *n2* is the upper PRBS value. An example of the PRBS generated is shown in Figure 5-12.

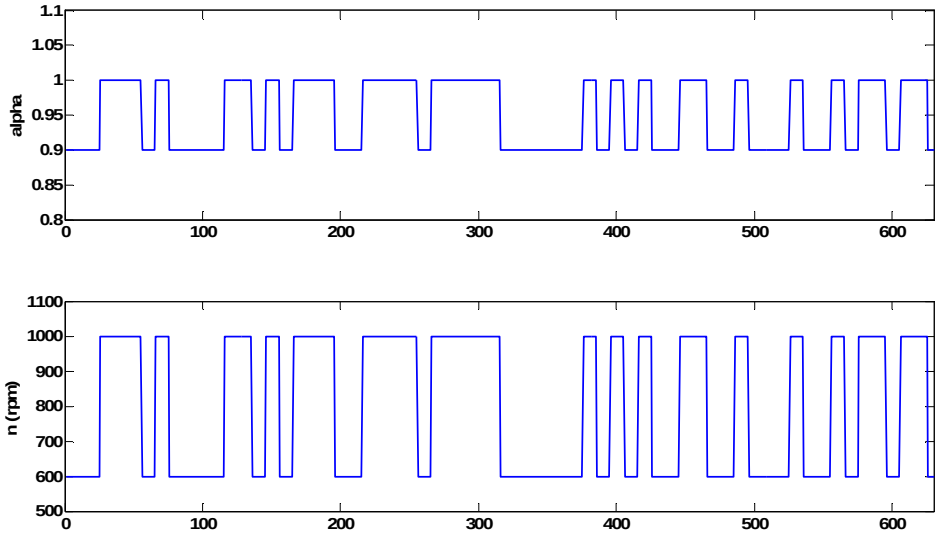

Figure 5-12 PRBS input signals for cut-off and pump speed respectively

With the PRBS inputs created, the next step was to run each set of inputs with the basic dynamic model, record the output for T_{act} (actual torque) and P_{act} (actual pressure). The output for the PRBS in Figure 5-12 is shown in Figure 5-13.

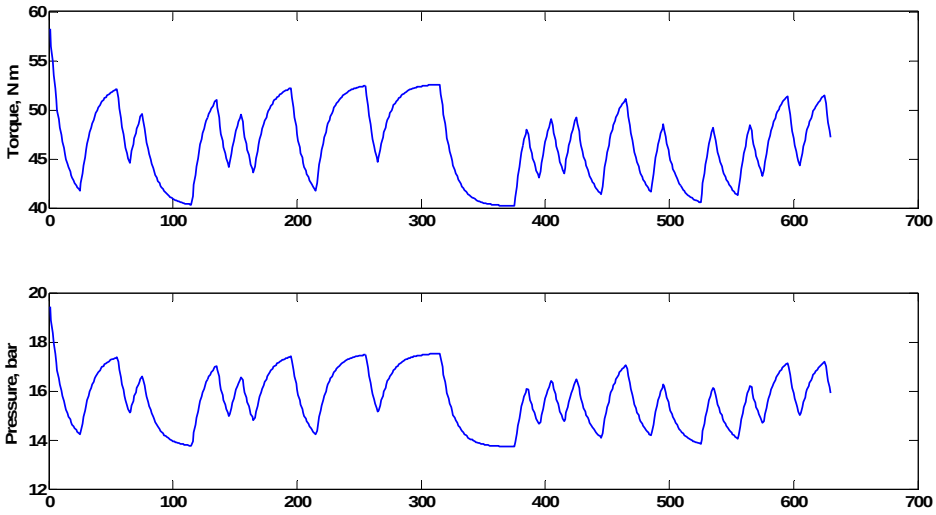

Figure 5-13 Torque and pressure output

With the inputs and outputs recorded the Matlab *SIT* was further utilized to identify possible state-space models for each of the inputs.

5.5.2 System identification

Various Matlab commands were used to perform the system identification. First the PRBS inputs and their respective outputs were used to create a Matlab class for time series data using the command *iddata*. The data was then de-trended. After allocating input and output names, a discrete state-space model was created using the Matlab command *pem* with the first half of the data. The *pem* command contains an input variable to specify the order required of the resulting model.

A validation test was conducted on the model using the compare command and the second phase of the data. The Matlab command sequence is as follows:

```
steamsys=iddata([Tact,Pact],[alpha_prbs,npump_prbs],1);
steamsys=detrend(steamsys);
steamsys.inputname={'alpha','npump'};
steamsys.outputname={'Torque','Pressure'};
assignin('base', [idd_str index_str],steamsys);
mp=pem(steamsys(1:300),order);
[y, f, x]=compare(steamsys(301:600),mp)
```

The variable *f* obtained from the *compare* command denotes the best fit and is recorded as a percentage. The fit was recorded for each set of inputs and was plotted for each case. An example of best fit data is shown in Figure 5-14.

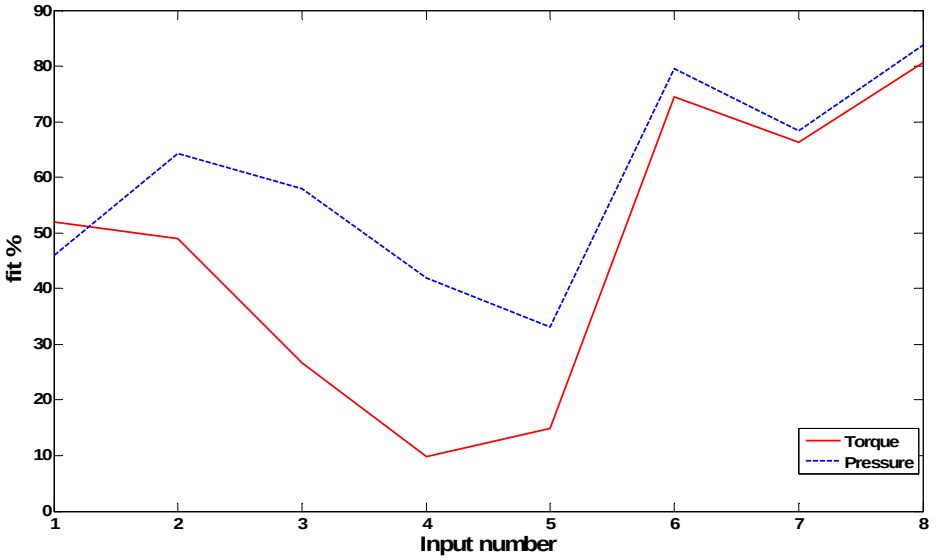

Figure 5-14 Best fit data generated state-space models

By executing the *pem* and *compare* commands for different orders, the best order for the model was determined. A lower order model is always preferred, as it is simpler, and hence the development of the control is less complex than for higher order models. The *pem* command was executed for all input/output data using orders from 2nd to 9th; the results for two of the data sets are shown in Table 5-1.

Order	Data set 1			Data set 2		
	Best index	Torque fit	Pressure fit	Best index	Torque fit	Pressure fit
2nd	8	78	77	9	92	86
3rd	7	82	79	8	95	83
4th	6	83	79	1	87	72
5th	8	87	83	6	93	88
6th	6	86	84	2	33	48
7th	8	88	87	8	94	89
8th	8	86	88	9	93	91
9th	8	90	87	7	94	88

Table 5-1 Best fit data for different orders

A 5th order model was selected for both pressure and torque.

As well as the best fit data, the *pem* command resulted in a discrete state-space model, stored as an *idss* class within the Matlab workspace. Along with the state-space matrices, the *idss* class also contains two useful parameters which are *Loss Function* and *Formal Prediction Error*.

The *Loss Function* parameter is also know as the quadratic loss function and is a function of the residual error. The parameter can be calculated various ways, according to the Matlab *SIT* literature [57], the loss function, V, is defined in Equation 5.9:

$$V = \det\left(\frac{1}{N}\sum_{1}^{N} E(t,\theta_N) * \left(E(t,\theta_N)\right)^T\right) \qquad (5.9)$$

where:

E = residual error;

N = number of samples.

According to Norton [58], the error worsens as the *Loss Function* increases, hence when deciding the best model to use, a low value for the loss function is desirable.

The *Formal Prediction Error* (*FPE*) parameter is calculated using the loss function, again from the Matlab *SIT* literature [57], the formula is given in Equation 5.10:

$$FPE = V * \left\{\frac{\left(1+\frac{d}{N}\right)}{\left(1-\frac{d}{N}\right)}\right\} \qquad (5.10)$$

As with the *Loss Function*, the smallest value *FPE* corresponds to the lowest value. *Loss Function* and *FPE* that values are shown in Table 5-2.

Input index	Loss Function	FPE
1	7.449e-7	9.417e-7
2	5.800e-6	7.333e-6
3	9.677e-5	1.223e-4
4	6.092e-2	7.446e-2
5	9.637e-2	1.178e-1
6	3.136e-7	3.964e-7
7	2.326e-6	2.941e-6
8	2.960e-6	3.742e-6

Table 5-2 Loss function and FPE for state-space models

The calculated models were converted to continuous time state-space models using the Matlab command *d2c* (discrete to continuous). This system identification process resulted in state-space models containing the *ABCD* matrices such that:

$$\begin{aligned} \dot{x}(t) &= Ax(t) + Bu(t) \\ y(t) &= Cx(t) + Du(t) \end{aligned} \qquad (5.11)$$

where x is the state, u is the input and y is the output.

As well as converting the models, the poles for each model were obtained using the Matlab command *eig* which finds the eigenvalues and eigenvectors for the model, with the eigenvalues corresponding to the system poles. This information was then used with pole placement techniques to create an observer for the model.

5.5.3 Observer-controller modelling

The process of development for the observer-controller model was obtained from different sources in order to make best use of the Matlab commands, Ledin [59] was a good source of information regarding the use of pole placement techniques to generate the required K and L gain matrices for an observer-controller and for creating feedback models. To determine if a model is suitable for pole placement and hence observer design, it must be checked for controllability and observability. Once these checks have been performed, and the system is controllable and observable, the state-space matrices can be used along with pole placement to generate the observer-controller model and its

associated gain matrices for *K*, *L* and *N*. The resulting observer-controller, with referenced input, is shown in Figure 5-15.

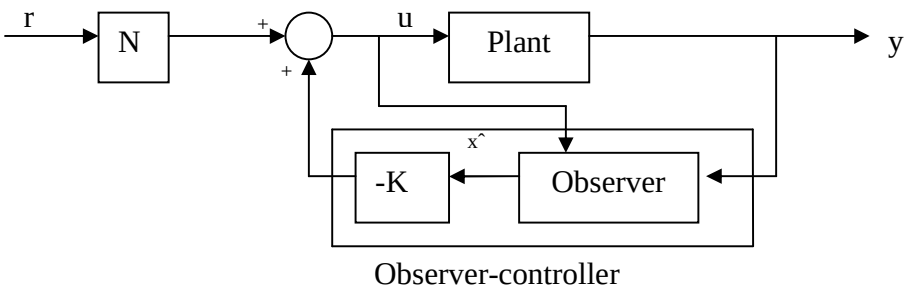

Figure 5-15 Observer-controller model

The observer is constructed from the state-space matrices and a gain *L*, the observer configuration is shown in Figure 5-16.

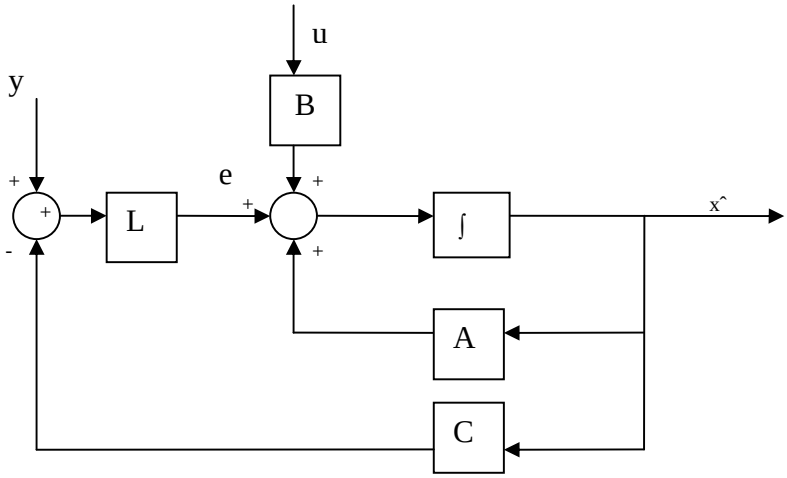

Figure 5-16 Observer configuration

The input *u* is calculated as follows:

$$u = Nr - K\hat{x}(t) \qquad (5.12)$$

The process suggested by Ledin is to use the Matlab *place* command to determine the *K* and *L* matrices. The poles used in this case were generated from a trial and error process whereby the system poles and their step response were observed. These poles were used to generate the *L* matrix and then divided by 4 to give the *K* matrix. This resulted in an

observer with a faster response time, when compared to the gain response time, which are the required conditions for an observer-controller. When the observer was constructed, the step response was observed and compared to the original system response. Using this method gave stable models which responded quickly, but the amplitude of the signals were too large. So a different approach was required.

This approach follows the development of feedback control detailed in the course notes from the MIT graduate module, Feedback Control Systems [60]. These course notes contained good examples and information for creating different feedback models. The gain on the reference input, *N*, was calculated from the state-space matrices, as follows, from part 13 of the MIT course notes:

$$N = -(C(A - BK)^{-1}B)^{-1} \qquad (5.13)$$

5.5.4 Initial state-space model and observer-controller

The PID controlled model shown in Figure 5-4 was stripped down to its simplest form with a slight change to some of the system dynamics, this is shown in Figure 5-17

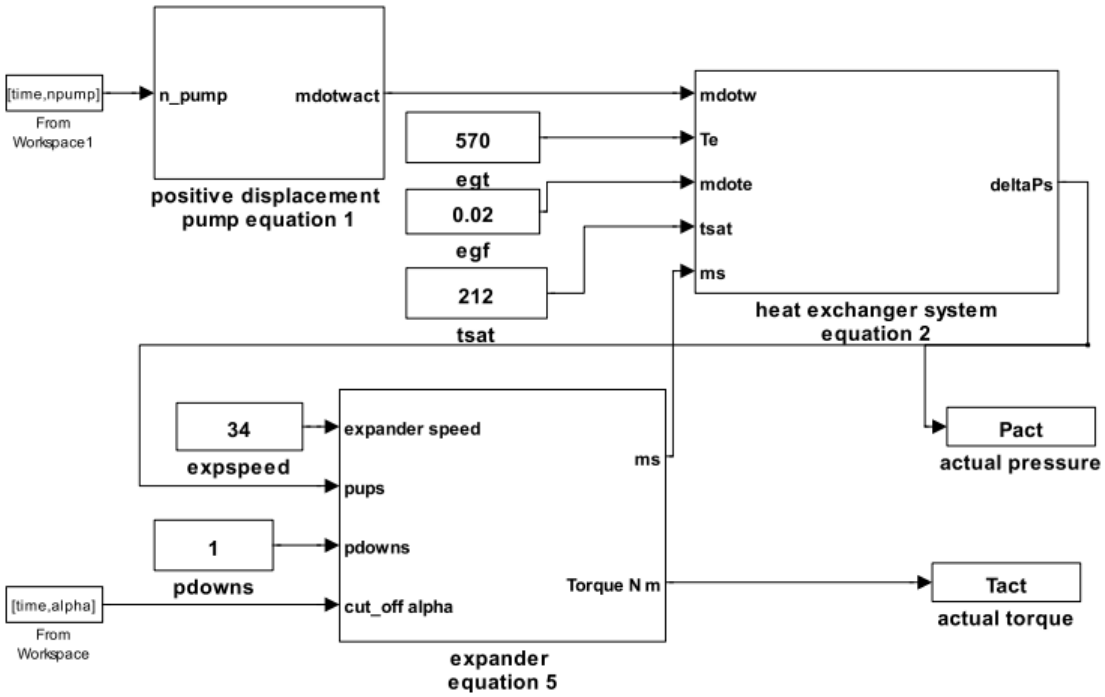

Figure 5-17 Basic dynamic system model

The Simulink blocks in Figure 5-17 refer to numbered equations these relate to the equations from Section 5.4 and are related as follows:

positive displacement pump equation 1 is Equation 5.1, note the leakage used in the PID controlled was removed for simplicity;

heat exchanger system equation 2 is Equation 5.4;

expander equation 5 is Equation 5.8.

Note that the cross-coupling equations were also removed for simplicity. The parameters for exhaust gas temperature (*egt*), exhaust gas mass flow rate (*egf*), expander speed (*expspeed*) and the lower system pressure (*pdowns*) were constants. The values for constants *egt*, *egf* and *expspeed* were chosen as the average values obtained from the initial modelling results of running the NEDC cycle with the QSS-TB/VW Golf model from Chapter 2.

The state-space models created were controllable and observable and the system was stable. However the resulting observer-controller did not behave as expected to different inputs. Using the same inputs as for the PID controller, the test results were disappointing. An investigation showed that in spite of an excellent model fit, the identified model was not able to reproduce the system dynamics.

In a different approach, the PID controlled model was used to acquire data for the system identification while the PID loops were operating.

5.5.5 Second state-space model and observer-controller

The PID controller shown in Figure 5-4 was used to generate new data. Real PRBS data was created for the pressure demand and torque demand signal inputs. The torque demand had a range of 30 N m to 70 N m in steps of 5 N m, and the pressure demand had a range of 15 bar to 25 bar in 1 bar steps. The PID model was then run with the different PRBS inputs. With eight different torque PRBS signals and ten for pressure PRBS signals, this gave 80 sets of data recorded.

All the data was then used to create new state-space models, with orders from 2nd to 9th, as specified in Section 5.5.2. For each data set, the result from executing the *pem* command was checked and if the fit was more than 85% for each of the outputs, then a continuous model was created, the system poles (eigenvalues) were obtained and if these were negative, then the model was saved. This resulted in 9 state-space models; detailed in Table 5-3.

Order	**Torque range (N m)**	**Pressure range (bar)**	**Fit % (torque/pressure)**
2	60-65	16-17	93/90
3	40-45	22-23	88/85
4	30-35	17-18	94/85
4	40-45	19-20	90/86
4	40-45	21-22	89/88
4	45-50	18-19	92/90
4	50-55	16-17	94/88
9	50-55	18-19	91/90
9	50-55	18-19	93/87

Table 5-3 System identification results for different input data sets

In turn, each of the models were used to create observer-controllers. The best was the 4th order model with torque input range of 40 N m to 45 N m and pressure input range of 19 bar to 20 bar. The overall effect was a slight improvement in the control performance when compared with the performance of the initial observer-controller developed in Chapter 5.5.4.

5.6 Integrating the PID control model into QSS and PSAT

This section details how the model with two PID control loops was integrated and tested using the QSS and PSAT toolboxes. The Simulink hybrid vehicle models developed in Chapter 2 were used as base models to add the new PID control loops and then run using the three drive cycles detailed in Chapter 2. The drive cycle fuel consumption results are shown in tabular form. Engine power outputs are compared graphically.

5.6.1 PID controlled system with QSS-TB

The PID controlled system detailed in Section 5.4 was integrated into the hybrid vehicle model using the QSS toolbox. The updated model is shown in Figure 5-18.

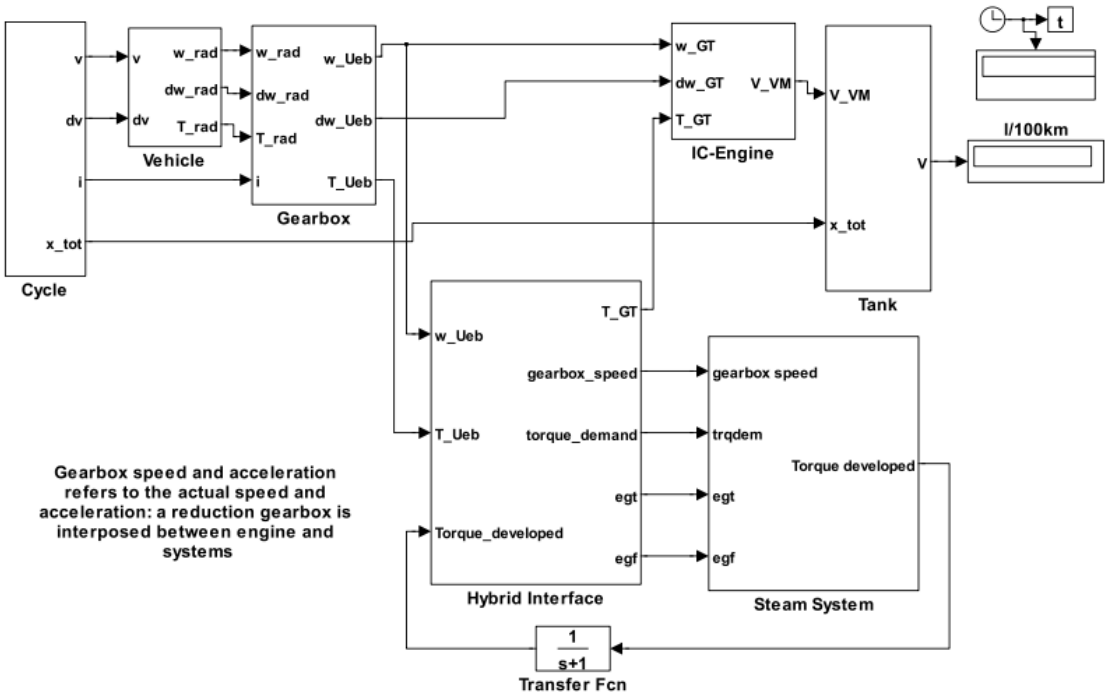

Figure 5-18 The PID controlled HYSTOR hybrid vehicle model using QSS-TB

As can be seen in Figure 5-18, the *Steam System* and *Hybrid Interface* blocks have been updated from the model used in Chapter 2. *Steam System* is a complete new block containing the PID controlled system which now includes a check on the exhaust

parameters to ensure that they are at values that where steam generation is reasonable. Figure 5-19 shows the updated *Hybrid Interface* block.

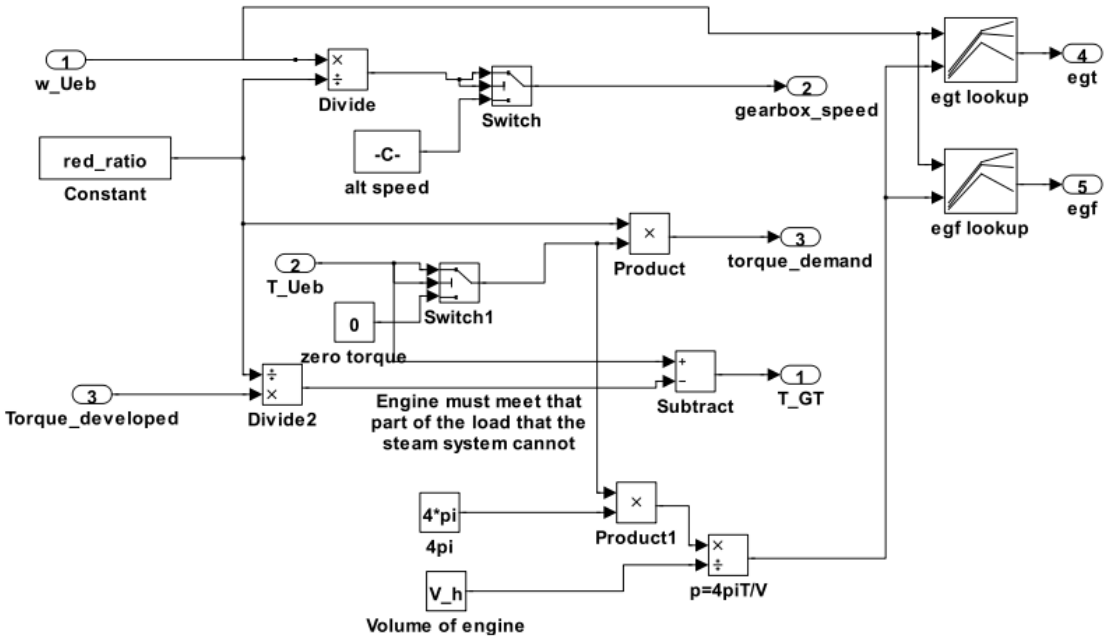

Figure 5-19 Updated *Hybrid Interface* block

The *Hybrid Interface* block was updated to include the lookup tables that match the IC engine speed and load conditions to the exhaust gas mass flow rate and temperature. This feature was originally included in the *Steam Generator* block of the basic QSS-TB model. Additionally a limit was enforced on the torque demand input to the expander PID controller; this was calculated in the initialisation file and was a function of the system pressure, using Equation 5.8 from Section 5.4.

The complete Simulink files for the PID controlled steam system can be found in Appendix J.

The PID controlled QSS-TB model was run using the NEDC, FTP-75 and US-06 drive cycles, details of which can be found in Appendix A. Table 5-4 shows the fuel consumption results for each of the drive cycles and compares them to the conventional vehicle and also to the results for the accumulator hybrid model from Section 2.5.2.

Drive Cycle	Fuel used with conventional vehicle (litres/100 km)	Fuel used with accumulator model (litres/100 km)	Fuel used with PID controlled model (litres/100 km)	Percentage improvement conventional /accumulator
NEDC (European)	6.507	5.248	4.202	35.4 / 19.9
FTP-75 (Urban)	6.557	5.075	3.811	41.9 / 24.9
US-06 (Highway)	6.694	6.161	4.319	35.5 / 29.9

Table 5-4 QSS-TB fuel consumption results, accumulator model, VW Golf data

Table 5-4 shows a considerable reduction in fuel consumption with the PID controlled model compared with the conventional vehicle and also a good improvement over the performance of the accumulator model reported in Chapter 2, which contained a very simple control mechanism. The percentage improvement resulting from the US-06 drive cycle is closer to the results for the other two drive cycles. This is because the model for the steam system is now taking into consideration the changing exhaust gas conditions and altering the mass flow rate of water accordingly. This observation is consistent with the conclusion made for Chapter 2.

Figure 5-20 shows the power data recorded for the FTP-75 drive cycle, using the VW Golf data. Only this drive cycle is shown as it is the most difficult to control. The others can be found in Appendix J. This data consists of three variables:

1) *power_demanded* on the vehicle (T_ueb * w_ueb from the *Gearbox* block);
2) *power_developed* by the steam system (Torque developed * expander speed from *Steam System* block);
3) *power_developed* by the IC engine (T_GT * w_ueb from *Hybrid Interface* block).

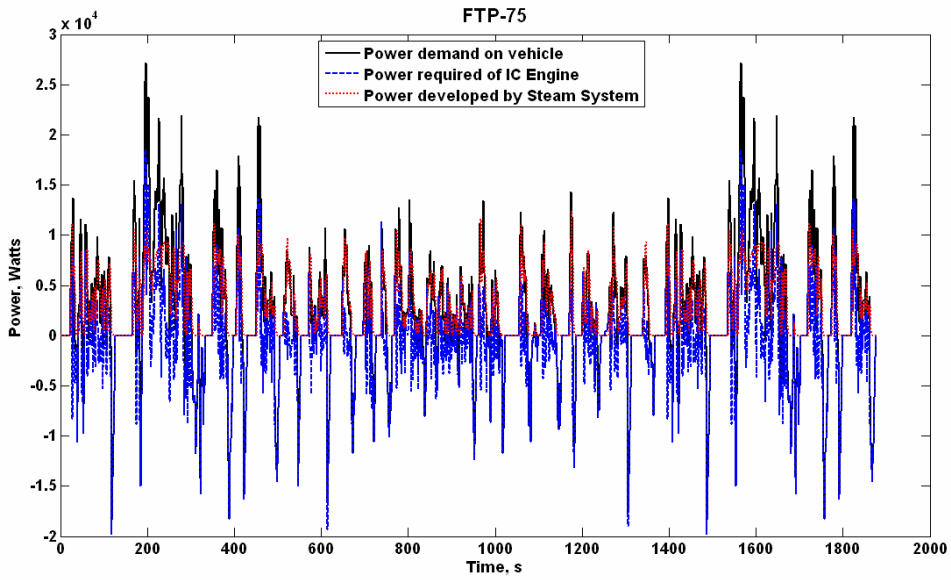

Figure 5-20 Power comparison for QSS-TB PID controlled model, FTP-75

As can be seen in Figure 5-20, the power output has increased when compared with the accumulator model in Chapter 2.

5.6.2 PID controlled system modelled with PSAT

The PSAT model was updated to accommodate the new PID controlled steam system; the new steam system component is shown in Figure 5-21. The complete Simulink files for the PID controlled steam system can be found in Appendix J, these are the same Simulink blocks as for the QSS-TB model from *Level 3 – PID controlled system* downwards.

5.6 Integrating the PID control model into QSS and PSAT

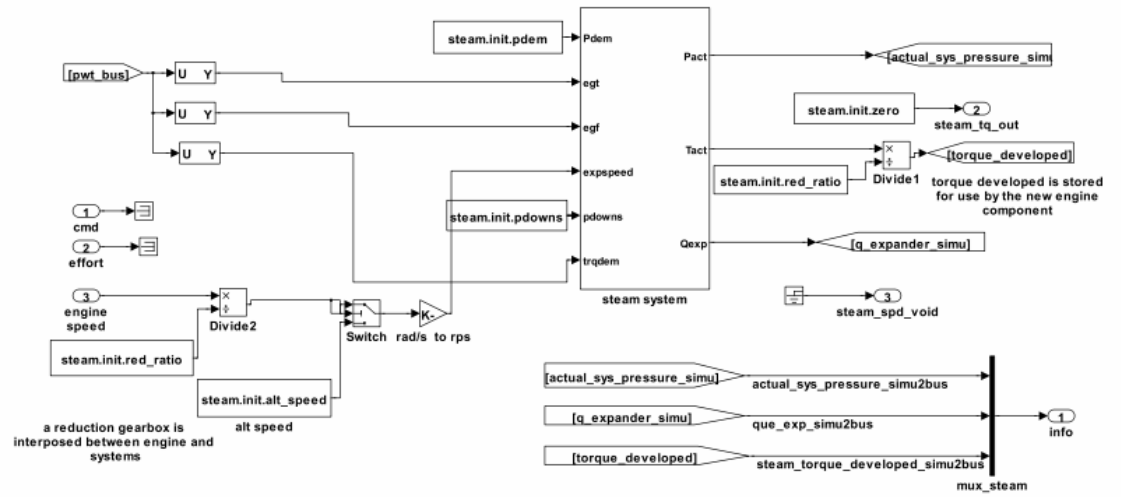

Figure 5-21 PSAT steam system component with PID control

The *steam system* block replaces the *Steam Generator* and *Control* blocks from the previous model. Additionally, the *steam_torque_developed* is stored in the PSAT bus structure for use within the accumulator engine block, as described in Section 2.3.1.

The PID controlled PSAT model was run using the NEDC, FTP-75 and US-06 drive cycles, details of which can be found in Appendix A. Table 5-5 shows the fuel consumption results for each of the drive cycles and compares them to the conventional vehicle and also to the results for the accumulator hybrid model from Section 2.5.2.

Drive Cycle	Fuel used with conventional vehicle (litres/100 km)	Fuel used with accumulator model (litres/100 km)	Fuel used with PID controlled model (litres/100 km)	Percentage improvement conventional /accumulator
NEDC (European)	6.70	4.93	4.32	35.45/ 12.3
FTP-75 (Urban)	6.69	4.24	4.07	39.20 / 4.0
US-06 (Highway)	7.28	6.60	5.37	26.20 / 18.6

Table 5-5 PSAT fuel consumption results, accumulator model, Honda Civic data

Table 5-5 shows a considerable reduction in fuel consumption with the PID controlled model compared with the conventional vehicle, with the percentage improvements being

similar to those obtained for the QSS-TB model. As with the results for the QSS-TB PID controlled model, the percentage improvement for the US-06 drive cycle is more in line with the results for the other two drive cycles. Once again, this is because the model for the steam system is now taking into consideration the changing exhaust gas conditions and altering the mass flow rate of water accordingly, agreeing with the conclusion from Chapter 2.

The percentage improvement between the accumulator and PID control are not as large as they were for the QSS-TB results, shown in Table 5-4. This could be due to the fact that the PSAT model is a more faithful representation of the system dynamics than the QSS-TB model and already demonstrated a substantial improvement with the accumulator model, which is placed differently to the QSS-TB model accumulator.

Figure 5-22 shows the power data recorded for the FTP-75 drive cycle. For NEDC and US-06 see Appendix J. This data consists of three variables:

1) *power_demanded* on the vehicle (*accmech_pwr_out* from the *Mechanical Accessory* block);
2) *power_developed* by the steam system (*steam_torque_developed* multiplied by *eng_spd_out_simu* from *Steam System* and *Engine* blocks, respectively);
3) *power_developed* by the IC engine (*cpl_pwr_in* from *Clutch* block).

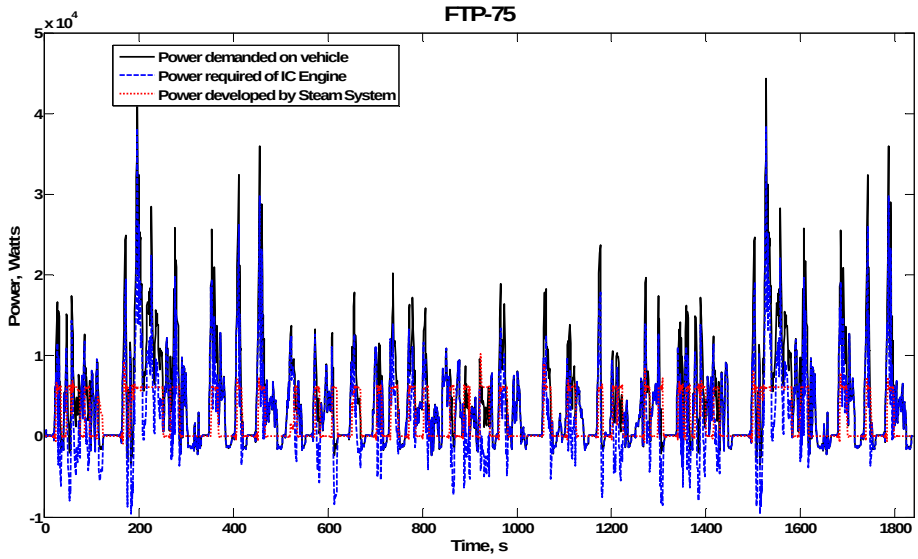

Figure 5-22 Power comparison for PSAT PID controlled model, FTP-75

As with the QSS-TB model, it can be seen in Figure 5-22 that the steam system power output has increased when compared with the graphs obtained for the accumulator model in Chapter 2.

5.7 Conclusions for control strategy development and modelling

Using a simple PID controlled model improved the fuel consumption, compared with the fuel consumption of the conventional vehicle, by between 26% and 41%, when comparing with the simple accumulator algorithm, the improvement was between 4% and 29%.

The largest improvement was seen for the US-06 drive cycle where the new models more faithfully represent the varying exhaust conditions and consequently the resulting steam flows are better represented, this confirms the conclusions made in Chapter 2 with respect the low fuel consumption improvements of the US-06 results. The mass flow rate of water into the heat exchanger was varied in proportion to the change in exhaust conditions, and hence more heat was exchanged and more work generated.

Reiterating the comments made in the conclusions for Chapter 2, the question of whether the results are realistic must be considered. The model components were less simplistic at this stage, for example the expander model was no longer a simple representation of ideal isentropic expansion, and the heat exchange process had some simple dynamics added, additionally a pump model had been added to the system. However, some issues remain such as the weight of the added system components, the friction losses due to mechanically coupling the steam expander and IC engine work outputs. Finally, the models again assumed that heat was available instantaneously, and did not consider the dynamics of the system over time. These issues will be considered for further work.

The system identification and modelling of the observer-controller model failed to capture the full system dynamics. The most likely cause was the non-linear nature of the system that called for a full non-linear or multi-model approach.

5.7 Conclusions for control strategy development and modelling

The PID controlled models performed well and these results indicate that a linear multivariable controller using low order representations would be very likely to work if based on a capable underlying system model.

Proving the controller remains a task to be completed. The heat exchanger results that include the heat transfer dynamics were not available as this thesis was being drafted. The low order model assumed in this chapter is still considered to be the most likely result even though the parameters could only be finally evaluated from the experimental data.

6 Optimisation strategies

6.1 Optimisation introduction

This chapter presents a brief overview of the optimisation strategy for the system. The overall optimisation requirement is to minimise the fuel consumption whilst generating a percentage of the torque demanded on the IC engine and maximising the use of the steam available.

Due to time constraints, the actual modelling and execution of the optimisation strategies was not possible, hence there are no results for this chapter. However each optimisation requirement will be presented so that the implementation of the algorithms, for any future work that may occur on the system concept, is assisted.

Section 6.2 will discuss the optimisation requirements and possible solutions for the minimisation of fuel consumption. Section 6.3 will discuss the requirements to maximise the use of the steam generated by the system. Section 6.4 presents some additional considerations for optimising the control and behaviour of the HYSTOR system which were investigated using the QSS-TB model. Section 6.5 will summarise and conclude the optimisation strategies.

6.2 Optimisation of fuel consumption

The overall project goal is to improve the fuel efficiency of the IC engine. With the addition of the steam hybrid system, it has been shown in Chapter 5 how the fuel consumption is reduced with a simple, PID controller. However, by optimising the control with respect to the IC engine's efficiency, it is anticipated that the fuel consumption could be further reduced. This section will present possible solutions towards developing optimisation algorithms to minimise the fuel consumption.

The following is true of the HYSTOR steam system:

1) If the torque demand is negative, then the torque is the sum of the IC engine torque, T_{ice}, plus the braking torque, T_{brake}, as given in Equation 6.1;

$$-veT_{demand}; T_{out} = T_{ice} + T_{brake} \qquad (6.1)$$

2) If the torque demand in positive, then the torque output is the sum of the IC engine torque, $T_{ice,}$ plus the steam system torque, T_{ss}, as given in Equation 6.2.

$$+veT_{demand}; T_{out} = T_{ice} + T_{ss} \qquad (6.2)$$

An IC engine has an efficiency diagram associated with it that details the ideal load conditions on the IC engine to get maximum efficiency for each speed step; this is usually referred as the *e-line*. If the IC engine torque output is close to the *e-line* for the engine, then this will provide the optimal fuel consumption. Thus it is required to minimise the fuel mass flow rate, $\dot{m}_f$ with respect to the torque supply, this is shown in Equation 6.3.

$$\underset{(T_{ice}(t),T_{ss}(t),t\in\{1toN\}}{Minimise} \sum_{t=1}^{N} \dot{m}_f(t) \qquad (6.3)$$

Where *N* is the duration of the drive cycle or trip taken.

The first step is to determine the e-line for the IC engine. The PSAT toolbox contained data and maps for the fuel consumption; the map used for the Honda Civic is shown in Figure 6-1.

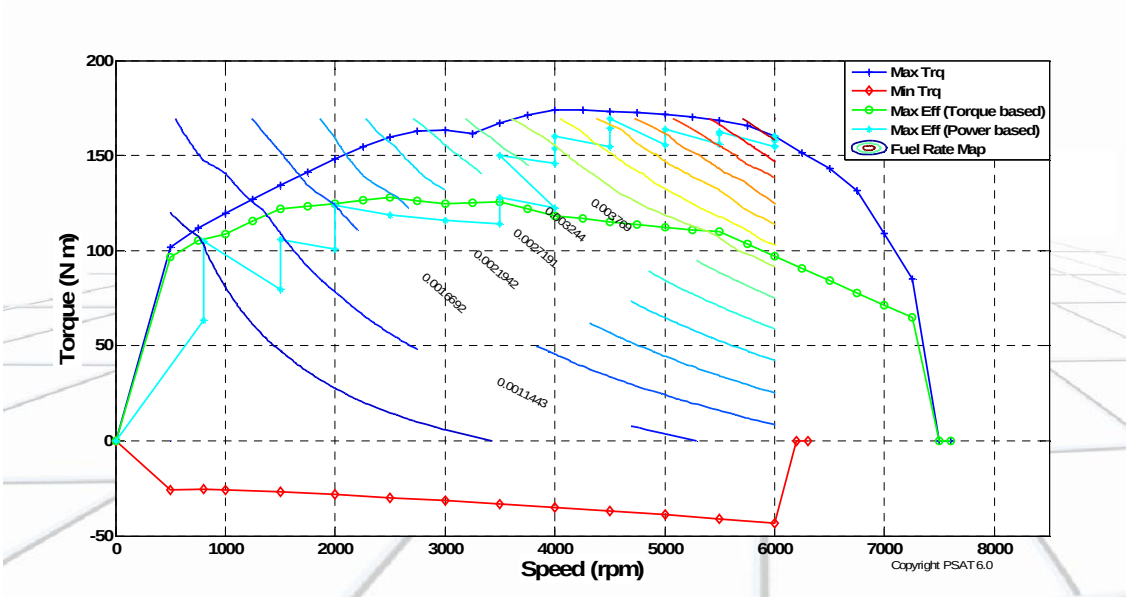

Figure 6-1 Fuel consumption map for Honda Civic, using PSAT data

With the acquired speed/load data for the e-line, an optimisation algorithm can be developed so that in ideal conditions, the torque demand is met by the most efficient output for that speed by the IC engine, and if there is any torque demand not met by this, then the steam expander will supply the rest of the demand. Using the Honda Civic data as an example, if the speed of the IC engine is 2000 rpm, and the torque demand in 150 N m, it can be seen from Figure 6-1 that the most efficient torque output is 130 N m from the IC engine. Therefore the optimum output from the steam expander is 20 N m, this is the torque demand that should be fed to the steam system.

There are three scenarios when the torque demand is positive:

1) Torque demanded, T_{dem}, is less than the IC engine efficiency line, $T_{ice\varepsilon}$;
2) T_{dem}, is equal to the IC engine efficiency line, $T_{ice\varepsilon}$;
3) T_{dem}, is more than the IC engine efficiency line, $T_{ice\varepsilon}$.

For scenario 1 a decision needs to be made as to how to split the torque between the steam system and the IC engine. For scenarios 1 and 2, the decision is whether to run on steam only (if there is sufficient steam) or IC engine only (if there is not sufficient steam), this will be further investigated in the next section on optimising the steam usage.

For scenario 3, T_{dem}, is greater than $T_{ice\varepsilon}$, hence the IC engine is able to run at its optimum load, but only if there is sufficient torque available form the steam system to make up the remaining torque demand. The optimisation algorithm is developed in Equations 6.4 and 6.5:

$$T_{dss} = T_{dem} - T_{ice\varepsilon} \tag{6.4}$$

$$J_{\min} = \lambda_1 (T_{ice\varepsilon} - T_{ice})^2 + \lambda_2 (T_{dss} - T_{actss})^2 \tag{6.5}$$

Where:

T_{dss} is the torque demand on the steam system;

T_{actss} is the actual torque available from the steam system.

Equation 6.4 calculates the difference in demanded IC engine torque and the optimal IC engine torque that results in the torque demanded on the steam system, T_{dss}. From Equation 6.5, it can be seen that the values for constants λ_1 and λ_2 can be chosen to prioritise the IC engine torque or the steam system torque with respect to the cost function *J*. This cost function represents the balance, or trade-off, between the IC engine efficiency and the availability of torque from the steam system. The cost function constants would have different settings for different drive modes, depending on the priority of, for example, fuel consumption or IC engine emissions.

6.3 Optimisation of steam usage

This section will discuss maximising the steam usage. Two configurations are considered, a system with a steam accumulator and a system without a steam accumulator.

For the system with a steam accumulator, the system should control the storage of unused steam in order to meet other optimisation requirements, e.g. keeping the IC engine near to its e-line, and also to reserve the steam for use within an emissions free zone. This system would need to consider some of the issues related to battery charging/electrical storage, like the SOC parameter. There will be no problem with overcharging the steam accumulator, although obviously the steam would need to be diverted if the accumulator was full, but what is the life expectancy of stored steam? Discharge rates etc? The answers to these questions would hopefully be answered from analysing the results of the heat exchanger tests, when they are available. A new variable could be used to represent the life expectancy of the stored steam *Length of Charge* or *LOC* could be used for this variable.

For the system without the accumulator, a battery could be charged with any excess steam if steam is being generated but not required at that time, for example when the car is going down a hill, the alternative is to waste the steam or somehow cease to generate steam, for example, divert the exhaust gases or implement a cooling system.

Additionally the efficient use of the steam needs careful consideration. The mass flow rate of steam needs to be optimised to either create steady torque, or sharp bursts of high torque, depending on the driving demands.

6.4 Further considerations for the optimisation of the HYSTOR system

The section briefly details some variables for consideration in relation to the optimisation of the HYSTOR system. Some of these variables have been run through a simple optimisation exercise using the PID controlled model.

6.4.1 Expander size and reduction gearbox ratio

The size of the steam expander in the models was fixed at 0.2 litres and the reduction gearbox ratio (gearing of mechanical coupling for steam expander to drivetrain) was fixed at 2. These two variables were given ranges, the expander size from 0.1 litres to 1 litre and the gear ratio 2 to 16, and the resulting fuel consumption from running the NEDC with the PID controlled model. The results of this task are shown in Figure 6-2.

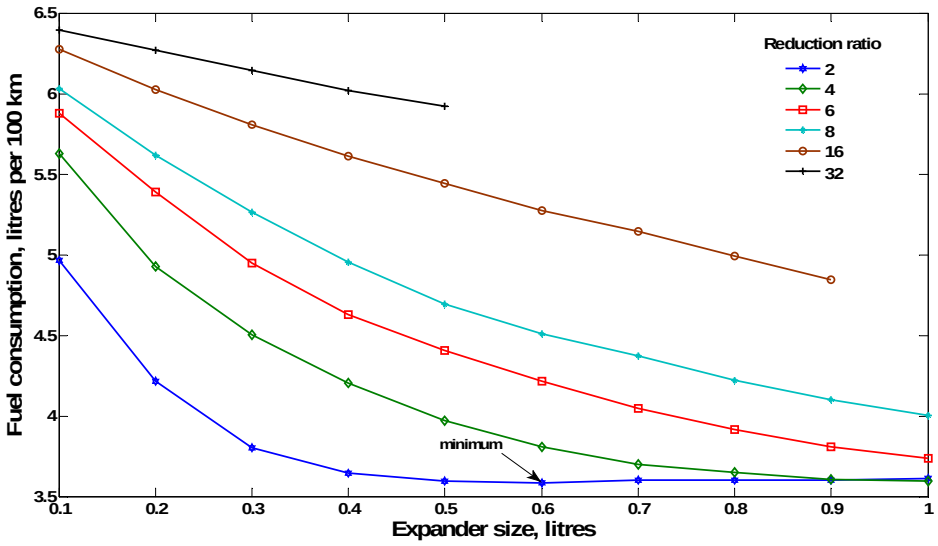

Figure 6-2 Optimisation of fuel consumption for different expander sizes and gearbox ratios

It can seen from this simple optimisation task, that the optimised fuel consumption can be found with an expander of 0.6 litres and a gearbox reduction ratio of 2:1. This task was executed with large steps between values, a further optimisation could be performed

using the Matlab *fminsearch* command, from the optimisation toolbox, which would run with much smaller steps and focuses around start points. Note for reduction ratios of 16 and 32, the model did not complete its run; hence the results were not available.

6.4.2 Volume of water and accumulator size

The volume of water available in the system could be optimised along with the size of the accumulator vessel. The volume of the water includes the water in the supply reservoir and the accumulator/heat exchanger. These variables should be optimised together as they are related. The optimisation would need to be done over a long period of time, with respect to running the model, especially with larger volumes and accumulator sizes, to allow for the steam to build up and use the accumulator size fully. Also a new driving cycle would need to be created to create conditions whereby steam is being generated for a long period, but not used, followed by a period of heavy steam usage; this would give a result when optimising the volume and size.

6.4.3 Condenser size

Currently the model lacks a condenser block. If a condenser is modelled in the future, then the size could also be optimised; possibly coupled with the optimisation of the water volume and accumulator size. Additionally, when modelling the condenser, consideration should be given to including the condenser as part of the IC engine cooling system, as this would reduce the overall vehicle weight, and hence should give lower fuel consumption than if the condenser was added as a new component.

6.5 Conclusions for optimisation development and modelling

The development of the algorithms and optimised variables presented in this chapter give a good overview of the optimisation possible with the HYSTOR system. The simple optimisation routine from Section 6.4.1 shows that further fuel consumption reduction is possible using different variables for the system components.

Once the control models have been fully developed, using the heat exchanger test data, then the optimisation algorithms can be modelled, tested and then implemented into an embedded control system.

7 Conclusions and recommendations for further work

This chapter begins by summarising the conclusions made for each of the chapters in this thesis. Overall conclusions are then made including a review of the objectives for the thesis as stated in Chapter 1. Finally some improvements and recommendations for further work on the HYSTOR system are presented and discussed.

7.1 Conclusions for software modelling and simulation of the HYSTOR concept

The initial software modelling and simulation in Chapter 2 show that there are significant fuel economy advantages to be made (up to 36% improvement from the PSAT simulation results) and that these are achievable at practical operating pressures (18 bar was used for the initial models).

The results improved at a similar rate as the thermal models were improved from the boiler model to the accumulator model. Both the NEDC and FTP-75 cycle results showed fuel consumption improvements within 13.1% to 36%. However for the US-06 results, the improvements were less, between 6.89% and 9.4%. Although it was initially thought that this drive cycle would give better results than the other two drive cycles, due to high, constant speeds representative of highway driving, this result agrees with the findings made by Bayley [6] who reported that the FUDS drive cycle gave a better performance than the FHDS drive cycle with respect to fuel consumption reduction; FUDS and FHDS being earlier versions of FTP-75 and US-06, respectively. It is concluded that this is due to the US-06 cycle operating at higher temperatures during the high speed section of the cycle whilst the mass flow rate of water through the steam system remains constant. If the water mass flow rate were increased with the exhaust gas temperatures, then more heat would be transferred, more steam generated and hence more work available to assist the IC engine. It was anticipated that this would be taken into account when developing the control further and hence a more significant improvement would be experienced.

Chapter 2 also presented comparisons of the speed/load for each of the drive cycle results. For the boiler model results, the loads are reduced for both positive and negative

points, whereas for the accumulator model the loads are only reduced for the positive points. This is because the accumulator algorithm introduces a simple control to only generate torque when positive torque is demanded and to accumulate the torque (steam) when negative torque is demanded on the IC engine.

As expected, the PSAT models yielded better results than QSS-TB, for the NEDC and FTP-75 cycles, due to its dynamic properties which are better suited for HYSTOR dynamics due to the heat transfer calculations.

7.2 Conclusions for small expander testing

Chapter 3 concludes that the two stroke expander in a uni-flow configuration, using a solenoid valve to control the inlet, gave the best results in terms of power and efficiency for use as a reciprocating steam expander.

The rotary expander was inefficient compared to the uni-flow expander and, when used with steam, had problems with the rotor tips which would increase in size, due to the high temperature, and caused the expander to cease. The counter-flow expander proved un-stable with the control valves used. These issues may only be relevant to the size of the expanders, and a further recommendation would be to experiment with slightly larger sized expanders, where such limitations may not exist.

The specific torque and power recorded for the small expanders were good, going some way to proving that the HYSTOR system concept in that there is a good power source in steam, and if the generated steam, from the heat exchanger is of good quality, then a worthwhile amount of torque and hence power is available.

7.3 Conclusions for modelling and validation of small expanders

Chapter 4 began by stating that if the models could produce results that were within ±5%, then this would be an acceptable limit and the models could be used to validate the

experimental results. It was concluded that the small expander models developed can predict the torque output of the uni-flow and rotary configuration with no valve control, for speeds below 500 rpm to within the accepted ±5% of the experimental torque. However, when the solenoid valves were used with the rotary expander, satisfactory results were not obtained, hence that configuration, and components, requires more investigation.

There was also a question of scalability; could the results be scaled up to predict the behaviour of larger expanders? Chapter 4 concludes that some further modelling and validation would need to be done with medium size expander configurations to determine whether scalability would be possible or not. Additionally, further exploration of GT-Power's ability to create different heat transfer simulations needs to be carried out when improving the models.

7.4 Conclusions for control development and modelling

With an improved model of the system dynamics and some control development, the fuel consumption for the QSS and PSAT models was further reduced, with improvements of up to 41%, corresponding to an improvement of up to 29% over the accumulator model. As anticipated in Chapter 2, taking into consideration the dynamics of the system pressure and mass flow rate of water meant that the US06 cycle gave much improved results of up to 35% when compared to the conventional vehicle fuel consumption.

The strategy for developing an observer controller was good, but was not successful. It was concluded that this strategy would have had more success if the results from the heat exchanger experiments had been available in time. Obtaining these results would have given an insight into the dynamics of the HYSTOR system and hence improved the dynamic modelling of the system. This in turn, would have resulted in state-space models that could produce a robust observer controller.

7.5 Conclusions for optimisation development and modelling

Although there was insufficient time to be able to model the optimisation algorithms and hence acquire results to compare with the control modelling results, from the discussion presented in this chapter the following can be concluded: There is plenty of scope for developing various optimisation algorithms, both complex, in relation to the minimisation of fuel consumption with respect to the efficiency of the IC engine, and simple, in relation to optimising the size of the components used in the HYSTOR system.

7.6 Overall conclusions

The small expander testing was useful to determine which expander configurations were best suited to use as a steam expander within the HYSTOR system. The uni-flow expander was considered most suitable under the test environment conditions and limitations described in Chapter 3.

The expander modelling also gave favourable results for the uni-flow expander, whilst the rotary expander and counter-flow expander models require more development before they can be used for validation. Moreover, some validation and modelling for medium size expanders needs to be carried out before the results can be used to predict results for expanders of varying sizes.

The initial software modelling resulted in satisfactory improvements in fuel consumption and the models were a good building block for the control and optimisation development. Further improvements were seen with the PID controlled model and further improvements should be obtainable with the development of both a robust LQR control model and the optimisation algorithms.

Revisiting the main objectives of the thesis, as specified in Chapter 1, has the thesis met the objectives?

Objective 1: Give a review of the expander testing completed, including discussions of the results. This objective has been fulfilled by detailing the expander test setup and presenting the results in Chapter 3, which included some discussion on the results and how they related to the observed efficiencies of the small expanders.

Objective 2: Present an overview of the software modelling performed for the project. This objective is part fulfilled by Chapter 2 for the overall system modelling where the basic HYSTOR concept was modelled, using two different toolboxes, and run with some simple hybrid configurations using standard drive cycle data. This was useful groundwork for proving the basic system concept and providing an indication of the fuel economy to be expected for the system.

Chapter 4 also fulfils this objective by detailing the small expander modelling using the GT-Power toolbox. Discussions are presented on the issues of scalability and validation using such models.

Objective 3: Discuss, in detail, how the control architecture was developed, designed and tested. This objective has been met by Chapter 5 where the development of the control architecture is presented, detailing how the project progressed from the very simple control employed in the Chapter 2 models towards developing a benchmark PID controlled system, which in turn was used to develop some more robust control models.

Objective 4: Discuss possible optimisation strategies and how they could be applied to the system concept. This objective has been satisfied by Chapter 6, which discusses both simple and complex optimisation algorithms that could be used to optimise the HYSTOR system.

Objective 5: Summarise the project progress, draw conclusions and discuss future work in this area. This objective is fulfilled by this chapter.

Thus it can be concluded that the thesis objectives have been successfully achieved. The overall objective to prove system concept has been partly met. The main reason for not completing this objective is due to time and budget constraints of the project. It is anticipated that with a follow on project providing some more time and resources, the system concept will be proven successful. As the thesis is being concluded, the heat exchanger experiments are beginning to be successful. The results will be presented in a separate document.

The work detailed in this thesis has proven to be good groundwork towards proving the HYSTOR concept, but there is still work to be done, this will be discussed in the next sub-section.

7.7 Improvements and recommendations for further work

The first area to be considered is the modelling of the hybrid vehicle configurations. The model components in the initial stage were basic, for example the expander model was a representation of ideal isentropic expansion and the modelling of an accumulator was a simple set of integrators carrying the overall net steam used and generated, this did not take into consideration the quality of the accumulated steam, which may deteriorate over time. Additionally, the weight of the added components were not taken into consideration, neither was the possible friction losses due to mechanically coupling the steam expander and IC engine work outputs. Finally, the models assumed heat was available instantaneously, and did not consider the dynamics of the system over time. These issues should be considered for further work on the modelling of the overall hybrid vehicle application.

Another area to be considered is the expander experiments; there are a number of recommendations presented in Chapter 3 relating to improvements to this task. Before beginning to test medium sized expanders some issues need careful consideration, lubrication and valve control for example. The HYSTOR project spent some time in

developing a small controllable valve that could withstand high speeds, pressures and temperatures, but in the end, due to time constraints it was deemed to be outside the scope of the project, but should be considered for future projects, or even be worthy of a project by itself.

The components to be sourced for medium sized expander tests, should themselves be larger than the small expander components were, and hence should have a less limiting set of specifications with respect to speeds, high pressures and temperatures for example. Although the conclusion is that a uni-flow configuration is the most suitable out of the configurations tested in Chapter 3, a further recommendation is to consider other types of expander, for example a steam turbine. It is interesting to note that BMW are reported to have experienced problems with their choice of expander and have opted for an axial piston configuration rather than the originally planned turbine configuration [61].

Considering the development of expander models, an improvement is needed to ensure the timing for inlet and exhaust are correctly recorded during experiments and then implemented into the models. Additionally, investigation into how to model the different heat transfer characteristics for the source is recommended. In the original project plan it was envisaged that the validated GT models would interface with the Simulink model to improve the system model, this should be considered for any future HYSTOR project.

In the original HYSTOR system concept diagram (Figure 1-6) a low pressure pump system is detailed, but not further developed in this project, this system needs consideration and development in any future project.

Another item in the original project plan was to develop an embedded control system to control a system setup similar to the heat exchanger system and form a *Hardware-in-loop* (*HIL*) system to enable the development and test of the controller. This should form part of the project plan for any future work.

An obvious consideration for the development of the control strategy is to obtain the results from the heat exchanger tests and utilise these to create a good representation of the system dynamics. Additionally if some PRBS data is used to run the heat exchanger experimental setup, then the data acquired could be used to perform system identification and hence the results from that to be used to develop a robust LQR controller. This model in turn could be used to develop an optimal controller, possibly an LQG or even investigating a model predictive controller (MPC). Additionally, careful attention is required to integrate the supervisory control requirements into the optimised controllers.

Finally, some of the control strategies listed in the literature review of Chapter 1 could be considered for further development of an optimal control system, for example the ECMS technique. This would improve the control of the HYSTOR system and also work towards an energy management control system for a HYSTOR hybrid vehicle configuration.

References

[1] DieselNet, "Cars: Greenhouse Gas Emissions" Ecopoint Inc. http://www.dieselnet.com/standards/eu/ghg.html, Access date: 20/06/2008.

[2] "Understanding Air Pollution" Californian Air Resources Board http://www.arb.ca.gov/ch/educational/understanding_air_pollution.htm, Access date: 20/06/2008.

[3] "BP Statistical Review of World Energy 2006" BP p.l.c.www.bp.com, Access date: 20/06/2008.

[4] "Building the Case for New Energy Technology" The Energy Foundation http://www.ef.org/documents/AR2002FrontEnd.pdf, Access date: 20/06/2008.

[5] R. G. El Chammas and D. Clodic, "Combined Cycle for Hybrid Vehicles" *SAE 2005 World Congress & Exhibition*, vol. SP-1973, 2005.

[6] F. J. Bayley, "The Saturated Liquid Resevoir for Energy Storage in Hybrid Vehicles" *Proceedings of the IMechE Conference on Total Vehicle Technology*, pp. 45-54, 2001.

[7] DieselNet, "FTP-75" Ecopoint Inc. Access date: 20/06/2008 http://www.dieselnet.com/standards/cycles/ftp75.html

[8] DieselNet, "US-06" Ecopoint Inc. Access date: 20/06/2008 http://www.dieselnet.com/standards/cycles/ftp_us06.html

[9] R. Stobart and R. Weerasinghe, "Heat Recovery and Bottoming Cycles for SI and CI Engines - A perspective" *SAE paper*, vol. 2006-01-0662, 2006.

[10] Y. A. C¸engel and R. H. Turner, *Fundametals of Thermal-Fluid Sciences* 1st ed: New York N.Y. ; London McGraw - Hill 2001. ISBN: 0-07-239054-9

[11] R. Stobart, S. Hounsham, and R. Weerasinghe, "The Controllability of Vapour Based Thermal Recovery Systems in Vehicles" *SAE paper*, vol. 2007-01-0207

[12] R. Stobart, "An availability approach to thermal energy recovery in vehicles" *Proc. IMechE, Part D: J.Automobile Engineering*, vol. 221, pp. 1107-1124, 2007.

[13] R. Rump, "BMW Efficient Dynamics - Managing Energy for Future Vehicles" *IMechE VTMS 8 Keynote Address Presentation*, 2007.

[14] T. Endo, S. Kawajiri, Y. Kojima, T. Takahashi, T. Baba, S. Ibaraki, T. Takahashi, and M. Shinohara, "Study on Maximizing Exergy in Automotive Engines" *SAE paper*, vol. 2007-01-0257, 2007.

[15] K. T. Chau and Y. S. Wong, "Overview of power management in hybrid vehicles" *Energy Conservation & Management*, vol. 43, pp. 1953-1968, 2001.

[16] J. Walters, H. Husted, and K. Rajashekara, "Comparative Study of Hybrid Powertrain Strategies" *SAE TRANSACTIONS*, vol. 110, pp. 1944-1953, 2001.

[17] C. G. Hochgraf, M. J. Ryan, and H. L. Wiegman, "Engine Control Strategy for a Series Hybrid Electric Vehicle Incorporating Load Leveling and Computer Controlled Energy Management" *Strategies in Electric and Hybrid Vehicle Design*, vol. SP-1156, pp. 11-24, 1996.

[18] P. Waltermann, "Adaptive Energy Management for a Series Hybrid Vehicle" *Proc. 2nd IFAC Workshop on Advances in Automotive Control*, 1998.

[19] C. Wittmer, P. Dietrich, and L. Guzzella, "Control Strategies for the ETH Hybrid Vehicle" *Proc. 1st IFAC Workshop on Advances in Automotive Control*, 1995.

[20] Y. Zhang, H. Lin, and B. Zhang, "Performance Modeling and Optimization of a Novel Multi-mode Hybrid Powertrain" *Journal of Mechanical Design*, vol. 128, pp. 79-89, 2006.

[21] N. J. Schouten, M. A. Salman, and N. K. Kheir, "Energy Management strategies for parallel hybrid vehicles using fuzzy logic" *Control Engineering Practice*, vol. 11, pp. 171-177, 2002.

[22] V. H. Johnson, K. B. Wipke, and D. J. Rausen, "HEV Control Strategy for Real-Time Optimization of Fuel Economy and Emissions" *Proceedings of the Future Car Congress*, vol. SAE Papers, 2000.

[23] M. Montazeri-Ghi, A. Poursamad, and B. Ghalichi, "Application of genetic algorithm for optimization of control strategy in parallel hybrid electric vehicles" *Journal of the Franklin Institute*, 2006.

[24] G. Paganelli, T. M. Guerra, S. Delprat, J.-J. Santin, M. Delhom, and E. Combes, "Simulation and Assessment of Power Control Strategies for a Parallel Hybrid Car" *Proceedings of the I MECH E Part D Journal of Automobile Engineering,*, vol. 214, pp. 705-717, 2000.

[25] G. Paganelli, G. Ercole, A. Brahma, Y. Guezennec, and G. Rizzoni, "General supervisory control policy for the energy optimization of charge-sustaining hybrid electric vehicles" *JSAE Review*, vol. 22, pp. 511-518, 2001.

[26] P. Rodatz, A. Paganelli, A. Sciarretta, and L. Guzzella, "Optimal power management of an experimental fuel cell/supercapacitor-powered hybrid vehicle" *Control Engineering Practice*, vol. 13, pp. 41-53, 2003.

[27] G. Pagenelli, Y. Guezennec, and G. Rizzoni, "Optimizing Control Strategy for Hybrid Fuel Cell Vehicles" *SAE Papers*, vol. PT-96, 2002.

[28] A. Sciarretta, M. Back, and L. Guzzella, "Optimal Control of Parallel Hybrid Electric Vehicles" *IEEE Transactions on Control Systems Technology*, vol. 12, pp. 352-363, 2004.

[29] Y. Guezennec, T. Choi, G. Paganelli, and G. Rizzoni, "Supervisory Control of Fuel Cell Vehicles and it's Link to Overall System Efficiency and Low-Level Control Requirements" *IGERT Student Conference*, 2003.

[30] A. Sciarretta and L. Guzzella, "Control of Hybrid Electric Vehicles" *IEEE Control Systems Magazine*, vol. 27, pp. 60-70, 2007.

[31] N. A. Khier, M. A. Salman, and N. J. Schouten, "Emissions and fuel economy trade-off for hybrid vehicles using fuzzy logic" *Mathematics and Computers in Simulation*, vol. 66, pp. 155-172, 2004.

[32] S.-C. Tzeng, K. D. Huang, and C.-C. Chen, "Optimization of the dual energy-intergration mechanism in a parallel-type hybrid vehicle" *Applied Energy*, vol. 80, pp. 225-245, 2004.

[33] K. D. Huang, S.-C. Tzeng, T.-M. Jeng, and C.-C. Chen, "Integration mechanism for a parallel hybrid vehicle system" *Applied Energy*, vol. 82, pp. 133-147, 2004.

[34] C.-C. Lin, Z. Filipi, Y. Wang, L. Louca, H. Peng, D. Assanis, and J. Stein, "Integrated, Feed-Forward Hybrid Electric Vehicle Simulation in SIMULINK and its Use for Power Management Studies" 2001.

[35] C. Musardo, S. Benedetto, S. Bittanti, Y. Guezennec, L. Guzzelle, and G. Rizzoni, "An Adaptive Algorithm for Hybrid Electric Vehicles Energy Management" *FISITA World Automotive Congress*, 2004.

[36] Z. Jiang, L. Gao, M. J. Blackwelder, and R. A. Dougal, "Design and experimental tests of control strategies for active hybrid fuel cell/battery power sources" *Journal of Power Sources*, vol. 130, pp. 165-171, 2003.

[37] A. Vahidi, A. G. Stefanopoulou, and H. Peng, "Model Predictive Control for Starvation prevention in a Hybrid Fuel Cell System" *IEEE Proceedings of 2004 American Control Conference*, 2004.

[38] S. Delprat, J. Lauber, T. M. Guerra, and J. Rimaux, "Control of a parallel hybrid powertrain: optimal control" *Vehicular Technology, IEEE Transactions on*, vol. 53, pp. 872- 881, 2004.

[39] K. Suh and A. G. Stefanopoulou, "Coordination of Converter and Fuel Cell Controllers" *International Journal of Energy Research*, vol. 29, 2005.

[40] J. Scordia, M. Desbois-Renaudin, R. Trigui, B. Jeaneret, and F. Badin, "Global optimisation of energy management laws in hybrid vehicles using dynamic

programming" *International Journal of Vehicle Design*, vol. 39, pp. 349-367, 2005.

[41] L. Guzzella, A. Amstutz, and F. Grob, "Optimal Operation Strategies for Hybrid Power-Trains" *Proc. 2nd IFAC Workshop on Advances in Automotive Control*, 1998.

[42] G. Rizzoni, L. Guzzelle, and B. Baumann, "Unified Modeling of Hybrid Electric Vehicle Drivetrains" *IEEE/ASME Transactions on Mechatronics*, vol. 4, pp. 246-257, 1999.

[43] "QSS-toolbox" Measurement and Control Laboratory, ETH, Zurich http://www.imrt.ethz.ch/research/qss, Access date: 20/06/2008.

[44] "PSAT" Argonne National Laboratory, Chicago Access date: 29/09/2008 http://www.transportation.anl.gov/modeling_simulation/PSAT/index.html

[45] AVL ADVISOR, AVL http://www.avl.com, Access date: 20/06/2008.

[46] S. Hounsham, R. Weerasinghe, and R. Stobart, "Modelling heat recovery systems for hybrid vehicle applications" *IMechE, VTMS8 paper*, vol. 2007.

[47] DieselNet, "NEDC" Ecopoint Inc. Access date: 20/06/2008 http://www.dieselnet.com/standards/cycles/ece_eudc.html

[48] Gamma-Technologies, "GTI-SOFT" Gamma-Technologies http://www.gtisoft.com/, Access date: 20/06/2008.

[49] J. Heywood, *Internal Combustion Engine Fundamentals*: McGraw-Hill, 1988. ISBN: 0471276308

[50] S. Vulli, "Engine Cylinder Pressure Reconstruction using Neural Networks and Knock Sensor Measurements" in *Engineering and Design*. University of Sussex, 2006, pp. 354.

[51] "INCA" ETAS GmbH http://en.etasgroup.com/products/inca/, Access date: 20/06/2008.

[52] V. C. Agency, "VCA Car Fuel Data" Vehicle Certification Agency, UK http://www.vcacarfueldata.org.uk/index.asp, Access date: 20/06/2008.

[53] "Warco Ltd" Warren Machine Tools, Guilford, UK http://www.warco.co.uk/, Access date: 20/06/2008.

[54] R. F. Ansdale, *The Wankel R.C. Engine : Design and Performance*, Iliffe 1968. ISBN: M0076920US

[55] W. T. Parry, *ASME international steam tables for industrial use / prepared by William T.Parry [et al.] on behalf of ASME Research and Technology Committee on Water and Steam in Thermal Systems, Subcommittee on Properties of Steam*: New York N.Y. ASME Press 2000. ISBN: 0791801543

[56] O. Badr, S. Naik, P. O'Callghan, and S. Probert, "Rotary Wankel engine as expansion devices in steam rankine cycle engine" *Applied Energy*, vol. 39, pp. 59-76, 1991.

[57] L. Ljung, *System Identification Toolbox Users Guide*, 7th ed: MATLAB, 2005.

[58] J. P. Norton, *An introduction to identification*: London Academic P. 1986. ISBN: 0125217307

[59] J. Ledin, *Embedded Control Systems in C/C++*: CMP Books, 2004. ISBN: 1-57820-127-6

[60] J. How, "Course material for 16.31 Feedback Control Systems" vol. 2008: MIT OpenCourseWare http://ocw.mit.edu, Access date: 14/07/2008

[61] BMW, "The Turbosteamer - A system introducing the principle of cogeneration in automotive applications" *MTZ Worldwide*, vol. May 2008, pp. 20-27, 2008.

[62] O.S.Engines, "O.S.Engines" vol. 2007: O.S. Engines http://www.osengines.com/index.html, Access date: 20/06/2008

[63] G. Rogers and Y. Mayhew, *Thermodynamic and transport properties of fluids : S.I. units / (by) Gordon Frederick Crichton Rogers and Yon Richard Mayhew*, 5th ed: Oxford Blackwell 1995. ISBN: 0631197036

[64] Caterpillar, "Caterpillar On-Highway Engines: C7 7.2L Diesel Engine" vol. 2008: Caterpillar http://ohe.cat.com/cda/layout?m=85520&x=7, Access date: 10/07/2008.

[65] DieselNet, "FTP Transient" vol. 2008: Ecopoint Inc. Access date: 10/07/2008 http://www.dieselnet.com/standards/cycles/ftp_trans.html

[66] DieselNet, "NTRC" vol. 2008: Ecopoint Inc. http://www.dieselnet.com/standards/cycles/nrtc.html, Access date: 10/07/2008.

[67] J. Wilkie, M. Johnson, and R. Katebi, *Control engineering : an introductory course*. Basingstoke: Palgrave, 2002. ISBN: 033377129

[68] J. F. Duncan, A. S. Thom, and A. D. Young, *Fluid Mechanics, 3rd Ed*: Prentice Hall, 1979. ISBN: 0713132418

Bibliography

Abbas, T., S. Devotta, et al. (1981). "Derived Thermodynamic Design Data for heat pump system operation of water (R718)." "Heat Recovery Systems, 1981" Vol1 No.3: 181-203.

Aguilar, F. (1982). "A Mathematically and Physically consistent library of steam properties." Nuclear Science & Engineering Vol 81(3): 467-471.

Arias, D. A., T. A. Shedd, et al. (2006). "Theoretical Analysis of Waste Heat Recovery from an Internal Combustion Engine in a Hybrid Vehicle." SAE 2006-01-1605.

Astrom, K. J. (1995). P.I.D. controllers, Research Triangle Park N.C. Instrument Society of America 1995. ISBN: 1556175167

Astrom, K. J. (1997). Computer controlled systems: theory and design, Upper Saddle River Prentice Hall 1997. ISBN: 0133148998

Badr, O., S. Naik, et al. (1991). "Expansion Machine for a Low Power Output Steam Rankine Cycle Engine." Applied Energy 39: 93-116.

Badr, O., S. Naik, et al. (1991). "Wankel Engines as Steam Expanders: Design Considerations." Applied Energy 40: 157-170.

Bauer, H. D. I. (2004). Automotive electrics. Plochingen, Robert Bosch ; Bury St. Edmunds: Professional Engineering. ISBN: 1860584365

Bonnick, A. W. M. (2001). Automotive computer controlled systems: diagnostic tools and techniques. Oxford, Butterworth-Heinemann. ISBN: 0750650893

Bosch (2004). Automotive handbook, Bury St Edmunds Professional Engineering 2004. ISBN: 1860584748

Brogan, W. L. (1991). Modern control theory, London Prentice Hall 1991. ISBN: 0135904153

Brown, G. A. and D. A. Bowlus (1976). "Rotary piston expander engine." Proceedings of the 11th ICECEC: 1187-1191.

Butler, K., M. Ehsani, et al. (1999). "A Matlab-Based Modeling and Simulation Package for Electric and Hybrid Electric Vehicle Design." IEEE Transactions on Vehicular Technology 48(6): 1770-1778.

Çengel, Y. A. (2002). Thermodynamics: an engineering approach, New York N.Y.; London McGraw - Hill 2002. 4th Ed. ISBN: 007121688X

Chapman, S. J. (2004). MATLAB programming for engineers, London ; Toronto Ont. Thomson 2004. ISBN: 0534424171

Childs, P. R. N. (2001). Practical temperature measurement, Oxford Butterworth-Heinemann 2001. ISBN: 075065080x

Childs, P. R. N. (2001). Total vehicle technology: challenging current thinking, Bury St. Edmunds Professional Engineering Publ. for The Institution of Mechanical Engineers c2001. ISBN: 1860583245

Crane, D., G. Jackson, et al. (2001). "Towards Optimization of Automotive Waste Heat Recovery Using Thermoelectrics." SAE 2001 World Congress, March 2001 SAE PAPERS (2001-01-1021).

Cunningham, J., R. Moore, et al. (2003). "A Comparison of Energy Use for a Direct-Hydrogen Hybrid Versus a Direct Hydrogen Load Following Fuel Cell Vehicle." SAE 2003-01-0416.

Cunningham, J. M. M., R.; Ramaswamy, S.; Hauer, K. (2003). "A comparison of energy use for a direct-hydrogen hybrid versus a direct-hydrogen load-following fuel cell vehicle." SAE Papers SP-1741(2003-01-0416).

Dabney, J. (2003). Mastering SIMULINK, Upper Saddle River N.J. Prentice-Hall 2003. ISBN: 0131424777

Delchamps, D. F. (1988). State space and input-output linear systems, New York Springer 1988. ISBN: 3540966595

Delprat, S. G., T.M. Rimaux, J. (2003). "Control strategies for hybrid vehicles: synthesis and evaluation." Vehicular Technology Conference, 2003. VTC 2003-Fall. 2003 IEEE 58th 5: 3246- 3250.

Denbigh, P. (1998). System analysis and signal processing: with emphasis on the use of MATLAB, Harlow Addison-Wesley 1998. ISBN: 0201178605

Devotta, S. and F. Holland (1985). "Comparison of Theoretical Rankine Power Cycle, performance data for 24 working fluids." Heat Recovery Systems "Vol 5, No.6": 503-510.

Diehl, P., F. Haubner, et al. (2001). "Exhaust Heat Recovery System for Modern Cars." SAE 2001-01-1020.

Ehsani, M. (2005). Modern electric, hybrid electric, and fuel cell vehicles: fundamentals, theory, and design, Boca Raton Fla. CRC Press c2005. ISBN: 0849331544

Engstle, A., R. Egglhuber, et al. (2005). "Energy Management for Controlling Hybrid Systems." Future Transportation Technology Conference, September 2005 SAE Papers(2005-01-3454).

Figliola, R. S. (2000). Theory and design for mechanical measurements, New York; Chichester John Wiley [2000]. ISBN: 0471350834

Franklin, G. F. P., J.D. Emami-Naeini, A. (2006). Feedback control of dynamic systems, London; Upper Saddle River N.J. Prentice Hall 2006. ISBN: 0131499300

Ganesan, V. (1994). Internal Combustion Engine, McGraw-Hill. ISBN: 007462122X

Gokdere, L. U., K. Benlyazid, et al. (2000). "A virtual prototype for a hybrid electric vehicle." Mechatronics 12: 575-593.

Goodsell, D. (1995). Dictionary of automotive engineering. Oxford, Butterworth-Heinemann. ISBN: 1560916834

Gorman, W. (1970). "Expressing steam properties as a function of pressure." "Chemical Engineering, Nov 30, 1970" "Vol 77, Issue 26"

Gu, D.-W. (2005). Robust control design with MATLAB, London Springer c2005. ISBN: 1852339837

Hafner, M., O. Jost, et al. (2002). "Mechatronic design approach for engine management systems." Mechatronics 12: 1035-1046.

Hahn, B. D. (2002). Essential MATLAB for scientists and engineers, Oxford Butterworth-Heinemann 2002. ISBN: 0750652403

Hanselman, D. C. (2001). Mastering MATLAB 6: a comprehensive tutorial and reference, Upper Saddle River N.J. Prentice Hall c2001. ISBN: 0130194689

Hard, M. and A. Jamison (1997). "Alternative Cars: The contrasting Stories of steam and diesel automotive engines." Technology in Society "Vol 19, No.2": 145-160.

Haywood, R. W. (1980). Equilibrium Thermodynamics for Engineers and Scientists, Wiley 1980. ISBN: 0471276308

Heath, S. (2003). Embedded Systems Design - 2nd ed, Newnes. ISBN: 0750655461

Hellerstein, J. (2004). Feedback control of computing systems, John Wiley, 2004. ISBN: 047126637

Heywood, J. (1981). "Automotive engines and fuels, a review of future options." Prog. Energy Combustion Science Vol 7: 155-184.

Hill, P., J. Denton, et al. (2000). "Fast & accurate inclusion of Steam properties in 2 & 3 dimensional steam turbine flow." "Proc. Inst. Mech. Engineers, 2000" "Vol 214, Part C": 903-919.

Hill, P. and K. Miyagawa (1997). "A Tabular Taylor series expansion method for fast calculation of steam properties." "Journal of Engineering for Gas Turbines, April 1997, Tr of the ASME" Vol 119: 485-491.

Hill, P. and K. Miyagawa (2001). "Rapid & accurate calculation of water and steam properties using Tabular Taylor series." "Journal of Engineering For Gas Turbines & Power, Tr of the ASME" Vol 123 July: 707-712.

Hodkinson, R. (2001). Lightweight electric/hybrid vehicle design, Warrendale Pa. SAE International c2001. ISBN: 0768008247

Hopman, U. (2004). "Diesel Engine Waste Heat Recovery Utilizing Electric Turbocompound Technology." Diesel Engine Emissions Reduction (DEER) Workshop 2004, San Diego, CA (US).

Huang, B. (1994). "Winsteam 1.0a : Steam properties for Microsft windows applications." Drying Technology 12(5): 1239-1240.

Huang, K. D., S.-C. Tzeng, et al. (2004). "Integration mechanism for a parallel hybrid vehicle system." Applied Energy 82: 133-147.

Huangfu, Y., J. Y. Wu, et al. (2007). "Development of an experimental prototype of an integrated thermal management controller for an internal-combustion-engine-based cogeneration systems." Applied Energy 84(84): 1356-1373.

Husain, I. (2003). Electric and hybrid vehicles: design fundamentals, London ; Boca Raton Fla. CRC c2003. ISBN: 0849314666

Imai, M. (2006). "Development of Intelligent Power Module for Hybrid Electric Vehicle." SP-2008(2006-01-1342).

Jefferson, C. (2002). Hybrid vehicle propulsion / C.M. Jefferson, R.H. Barnard, Boston; Southampton UK WIT Press c2002. ISBN: 1853128872

Johansson, R. and A. Rantzer (2003). Nonlinear and hybrid systems in automotive control. London, Springer. ISBN: 1852336528

Juang, J.-N. (1994). Applied system identification / (by) Jer-Nan Juang, Englewood Cliffs Prentice-Hall 1994. ISBN: 013079211X

Kiencke, U. and L. Nielsen (2000). Automotive control systems. Berlin; London, Springer. ISBN: ISBN: 3540669221

Kiencke, U. G., G.L (2001). Advances in automotive control 2001 : a proceedings volume from the 3rd IFAC Workshop, Karlsruhe, Germany, 28-30 March 2001, Oxford Published for the International Federation of Automatic Control by Pergamon 2001. ISBN: 0080436781

Lee, H. S., K. S. Jeong, et al. (2002). "An experimental study of controlling strategies and drive forces for hydrogen fuel cell hybrid vehicles." International Journal of Hydrogen Energy 28: 215-222.

Lutsey, N., J. Wallace, et al. (2004). "Modelling stationary power for heavy duty trucks: engine idling Vs. fuel cell APUs." - SAE 2004-01-1479.

Lyle, O. (1947). The Efficient Use of Steam, H.M.S.O. 1947.M0080689US

Lynn, P. and W. Fuerst (2000). Introductory Digital Signal Processing - 2nd Ed, John Wiley & Sons. ISBN: 0471976318

Mackenroth, U. (2004). Robust control systems: theory and case studies, Berlin; London Springer 2004. ISBN: 3540209298

Maeda, N. (2006). "Construction of Hybrid Vehicle Motor Generator ECU." SAE 2006 World Congress & Exhibition, April 2006, SP-2008(2006-01-1341).

Malhotra, A. and D. Panda (2001). "Thermodynamic properties of superheated & supercritical steam." Applied Energy 68: 387-393.

Mathur, G. D. (2004). Vehicle thermal management: PT-97 : heat exchangers and climate control, Warrendale Pa. SAE International 2004. ISBN: 076801445x

Miller, J. M. (2004). Propulsion systems for hybrid vehicles, London Institution of Electrical Engineers 2004. ISBN: 0863413366

Morris, K. A. (2001). Introduction to feedback control, San Diego Calif.; London Harcourt Academic 2001. ISBN: 0125076606

Muller, W. (1994). "Fast & accurate water and steam properties programs for two-phase flow calculations." Nuclear Engineering and Design 149: 449-458.

Naidu, D. S. (2002). Optimal control systems, Boca Raton Fla. CRC Press 2002. ISBN: 0849308925

Ogata, K. (2008). MATLAB for control engineers, Prentice Hall, 2008. ISBN: 0136150772

Ohkubo, M., S. Tashima, et al. (2004). "Developed Technologies of the New Rotary Engine (RENESIS)." Advanced Power Trains SAE 2004-01-1790.

Paganelli, G., S. Delprat, et al. (2002). "Equivalent Consumption Minimization Strategy for Parallel Hybrid Powertrains." Vehicular Technology Conference, 2002. VTC Spring 2002. IEEE 55th 4: 2076-2081.

Pavkovic, D., J. Deur, et al. (2005). "Adaptive control of automotive electronic throttle." Control Engineering Practice 14: 121-136.

Plint, M. A. (1999). Engine testing: theory and practice, Oxford Butterworth-Heinemann 1999. ISBN: 0750640219

Porter, D. (2003). "Turbocompunding Revisited." SAE Off Highway Engineering February 2003(11-11-1-43).

Prakash-Balan, G., A. Harnarbaskaran, et al. (1991). "Empirical Formulas calculate Steam Properties Quickly." Chemical Engineering Jan: 139-140.

Prasad, S. (1993). "Steam Engine Characteristics & Theoretical performance." Energy Conservation & Management "Vol 34, No.12": 1323-1333.

Pratap, R. (2001). Getting started with MATLAB 6: a quick introduction for scientists and engineers. New York; Oxford, Oxford University Press. ISBN: 0195150147

Pukrushpan, J. T., A. G. Stefanopoulou, et al. (2004). "Control-Oriented model of an integrated Fuel Cell stack and Fuel processor system." IFAC Symposium on Advances in Automotive Control paper no. 86.

Ribbens, W. B. and N. P. Mansour (2003). Understanding automotive electronics. Amsterdam ; London, Newnes. ISBN: 0750675993

Richards, R. J. (1979). An introduction to dynamics and control, Longman 1979. ISBN: 058244182X

Rogers, G. and Y. Mayhew (1992). Engineering Thermodynamics - Work & Heat Transfer - 4th Ed, Addison Wesley.81-7808-263-2

Schell, A., H. Peng, et al. (2005). "Modelling and control strategy development for fuel cell electric vehicles." Annual reviews in Control 29: 159-168.

Schoner, H.-P. (2003). "Automotive Mechatronics." Control Engineering Practice 12: 1343-1351.

Schouten, N. J., M. A. Salman, et al. (2002). "Energy Management strategies for parallel hybrid vehicles using fuzzy logic." Control Engineering Practice 11: 171-177.

Semmens, D. and A. Goldfinch (2003). How Steam Locomotives Really Work, Oxford University Press. ISBN: 13:9780198607823

Sepe, R. B., C. Morrison, et al. (2003). "High Efficiency of a Hybrid Electric Vehicle Starter/Generator over road profiles." IEEE Industry Applications 9(3).

Singh, K. K. (2001). System design through MATLAB Control Toolbox and SIMULINK, Springer, 2001. ISBN: 1852333375

Skogestad, S. (2005). Multivariable feedback control: analysis and design, Hoboken N.J. John Wiley 2005. ISBN: 047001167X

Soderstrom, T. (1988). System identification, New York Prentice Hall 1988. ISBN: 0138812365

Stence, R. (2005). "Hybrid Vehicle Control Systems Fast Forward with Advances in Silicon Technology." SAE Powertrain & Fluid Systems Conference 2005(2005-01-3832).

Stone, R. (1999). Introduction to internal combustion engines. Basingstoke, Macmillan. ISBN: 0333740130

Stroud, K. (2001). Engineering Mathematics - 5th Ed, Palgrave. ISBN: 0333919394

Stroud, K. (2003). Advanced Engineering Mathematics - 4th Ed, Palgrave. ISBN: 1403903123

Terrier, P. S., P.; Champliaud, H. (2005). "Comparison of Emissions and Fuel Consumption between Gasoline and E85 in a Simulated Hybrid Electric Vehicle." SAE Powertrain & Fluid Systems Conference & Exhibition, October 2005(2005-01-3829).

Tewari, A. O. t. b. (2002). Modern control design with MATLAB and SIMULINK, Chichester Wiley 2002. ISBN: 0471496790

Varrasi, J. (2005). "The True Harnessing of steam." Mechanical Engineering Jan: 46-48.

Vasic, A., S. Cheng, et al. (1992). "Comparison of predictions of high temperature steam properties." Nuclear Engineering and Design 132: 367-379.

Venkataraman, P. (2002). Applied optimization with MATLAB programming, [Chichester]; New York N.Y. Wiley c2002. ISBN: 0471349585

Verma, M. (2003). "Steam tables for pure water as an ActiveX component in VB 6.0." Computers & Geosciences 29: 1155-1163.

Wade, J. D., R. M. Tompkins, et al. (1983). "Rotary expander engine testing and analysis." Proceeding of 18th IECEC: 636-641.

Wagner, W. e. a. (1997). "IAPWS Industrial Formulation 1997 for the thermodynamic properties of water & steam." "Transacions of the ASME, Journal of Engineering" "Y-200, V-122": 150-182.

Weeks, R. W. and J. J. Moskwa (1995). "Automotive Engine Modeling for Real-Time Control Using Matlab/Simulink." SAE 950417.

Westbrook, M. H. (2001). Electric car: development and future of battery, hybrid and fuel-cell cars, London Institution of Electrical Engineers 2001. ISBN: 0852960131

Woodward, J. (1987). "Part-Load Optima in Bottoming-cycles." Energy "Vol 12, No.7": 523-530.

Yamada, K. H., H.; Sasaki, S. (2006). "Countermeasures for Mitigating Power Fluctuations in High-Power Hybrid System." SAE 2006 World Congress & Exhibition, April 2006 SP-2008(2006-01-1340).

Yusaku, N. and H. Kpsaka (2005). "Development of the Intelligent Power Unit for the V6 Hybrid Midsize Sedan." SP-1973(2005-01-0275).

Appendices

Appendix A: Drive cycle data

This appendix presents the drive cycle data used to run the software models in Chapter 2 and Chapter 5.

A.1 NEDC

The New European Drive Cycle simulates urban and highway driving conditions. The drive cycle is made up of two earlier drive cycles. The first is the ECE (Economic Commission for Europe test cycle) which is an urban drive cycle, also known as UDC, and was created to simulate inner-city driving conditions; this drive cycle is repeated four times at the start of the NEDC. The second cycle that creates the NEDC is the Extra Urban Drive Cycle (EUDC); this cycle is added to the end of the four ECE cycles to complete the NEDC. A summary of the NEDC characteristics is as follows:

Distance: 11 km;
Time: 1180 seconds;
Average speed: 32.26 km/h;
Maximum speed: 120 km/h.

The graphs in Appendix figure 1 show the speed, acceleration and gear number data used for the NEDC drive cycle.

Appendix A: Drive cycle data

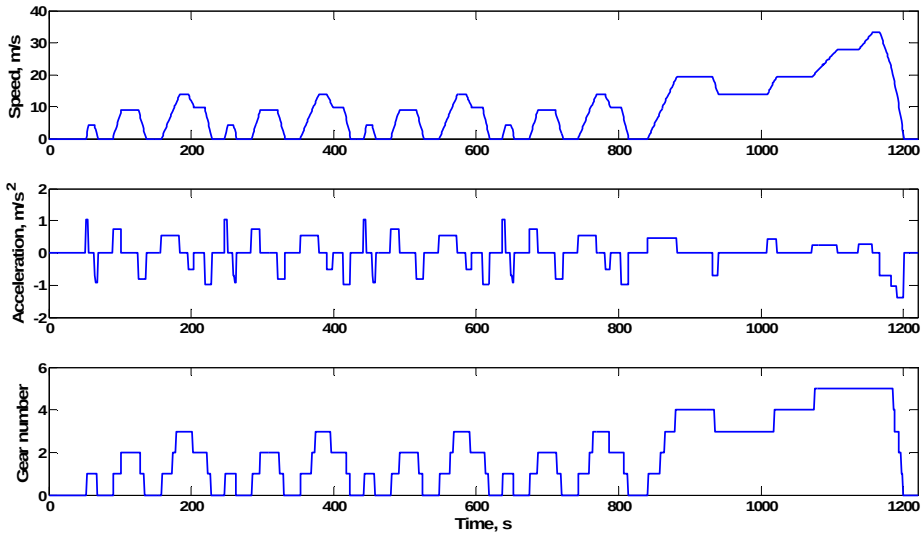

Appendix figure 1 NEDC drive cycle data used in the QSS-TB models

As can be seen, the NEDC cycle for the first two thirds consists of low speeds, frequent gear changes, which are characteristics of inner-city driving. However, the final third is made up of higher speeds and less frequent gear changes which would simulate highway driving. The fuel consumption for a conventional vehicle is as follows:

VW Golf data: 6.507 litres per 100km;
Ford I3 data: 5.538 litres per km.

Appendix figure 2 shows the speed load points for each of the data sets running the NEDC drive cycle using the QSS-TB model.

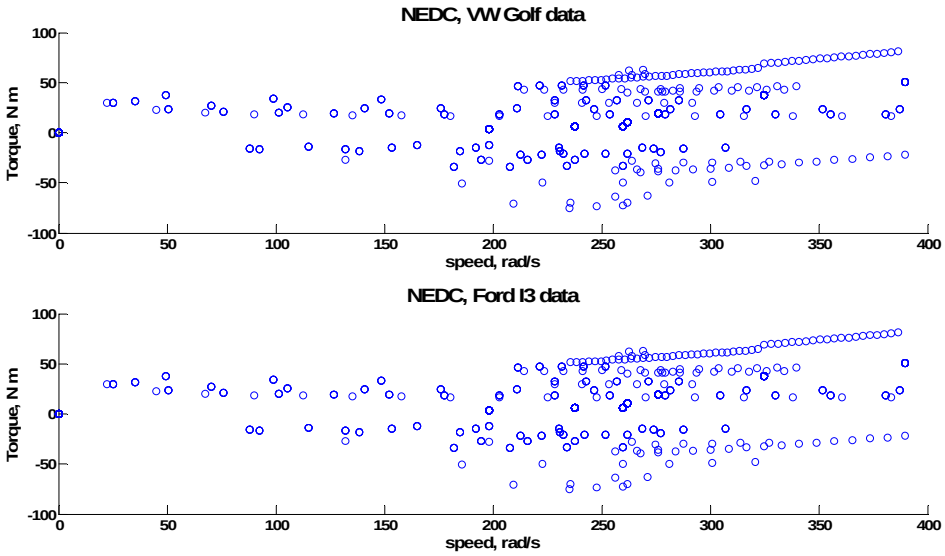

Appendix figure 2 Engine speed and load points for the NEDC drive cycle

The load points are almost equally spread about the zero axis, it is expected that adding the heat recovery system will cause the spread to be less equal as the positive load points will be lowered towards the zero axis due to the steam system generating some of the positive torque, this will in turn cause the fuel consumption to be reduced.

A.2 FTP-75

The Federal Test Procedure No.75 cycle is an American standard that simulates urban driving conditions. The drive cycle created from an earlier drive cycles called FTP-72, also known as Urban Dynamometer Driving Schedule (UDDS) which simulates a cold start phase followed by urban driving conditions with frequent stops. The difference between the FTP-72 and FTP-75 being that the first half of the FTP-72 is added onto the end creating FTP-75, a cycle of three phases:

1) Cold start;
2) Transient;
3) Hot start.

A summary of the FTP-75 characteristics is as follows:

Distance: 17.77 km;

Time: 1877 seconds;

Average speed: 34.1 km/h;

Maximum speed: 91.1 km/h.

The graphs in Appendix figure 3 show the speed, acceleration and gear number data used for the FTP-75 drive cycle.

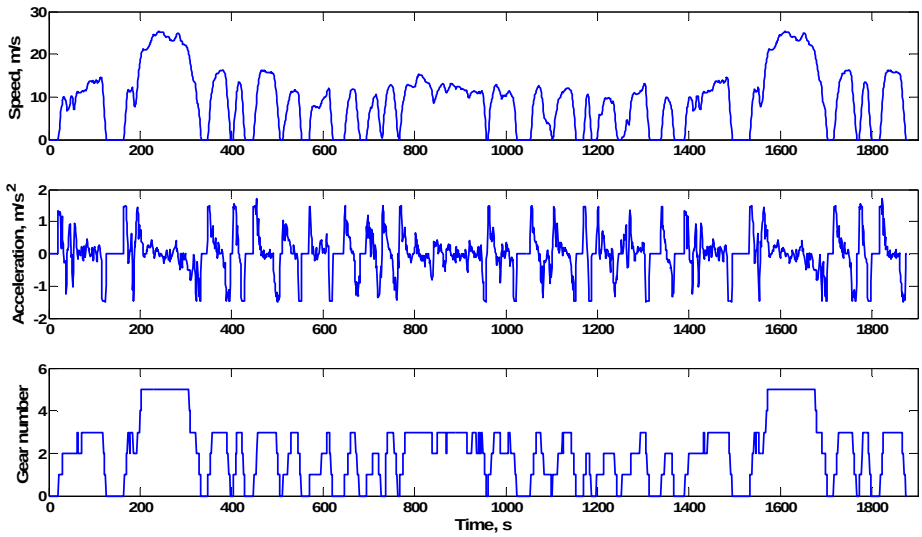

Appendix figure 3 FTP-75 drive cycle data used in the QSS-TB models

As can be seen, the FTP-75 cycle consists mainly of low speeds, frequent gear changes, which are characteristics of inner-city, or urban, driving. However, there are a couple of sections which are made up of higher speeds and less frequent gear changes which would simulate outer-city, but not highway, driving. The fuel consumption for a conventional vehicle is as follows:

VW Golf data: 6.557 litres per 100km;

Ford I3 data: 5.588 litres per km.

Appendix figure 4 shows the speed load points for each of the data sets running the FTP-75 drive cycle using the QSS-TB model.

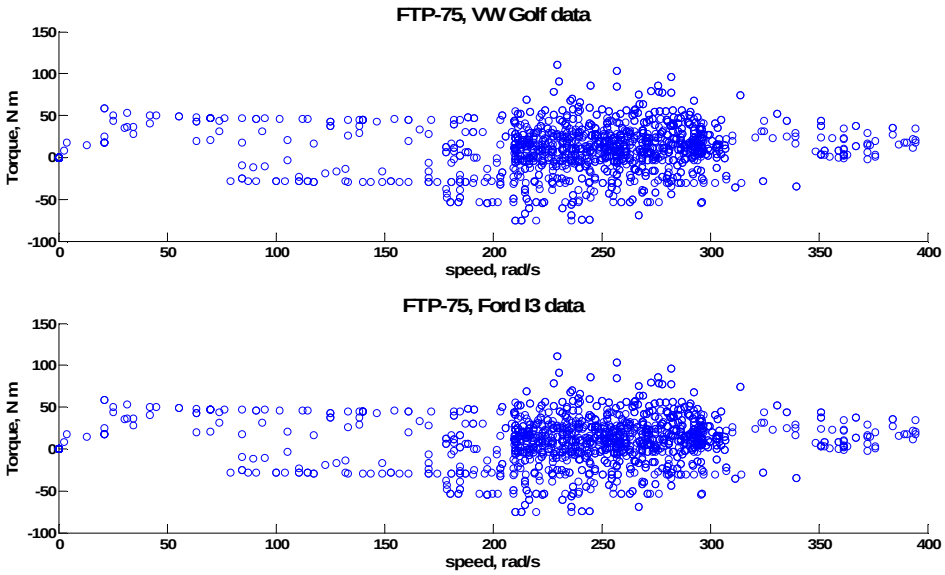

Appendix figure 4 Engine speed and load points for the FTP-75 drive cycle

The load points are almost equally spread about the zero axis with some points slightly higher on the positive side It is expected that adding the heat recovery system will cause the spread to be less equal as the positive load points will be lowered towards the zero axis due to the steam system generating some of the positive torque, this will in turn cause the fuel consumption to be reduced.

A.3 US-06

The United States 06 (US-06) also known as US-06 Supplemental Federal Test Procedure (SFTP) is another American standard that was developed to create the short-comings of the FTP-75 cycle and hence this cycle simulates aggressive driving conditions with high speeds and high accelerations.

A summary of the US-06 characteristics is as follows:

Distance: 12.8 km;

Time: 596 seconds;

Average speed: 48.4 km/h;

Maximum speed: 129.2 km/h.

The graphs in Appendix figure 5 show the speed, acceleration and gear number data used for the US-06 drive cycle.

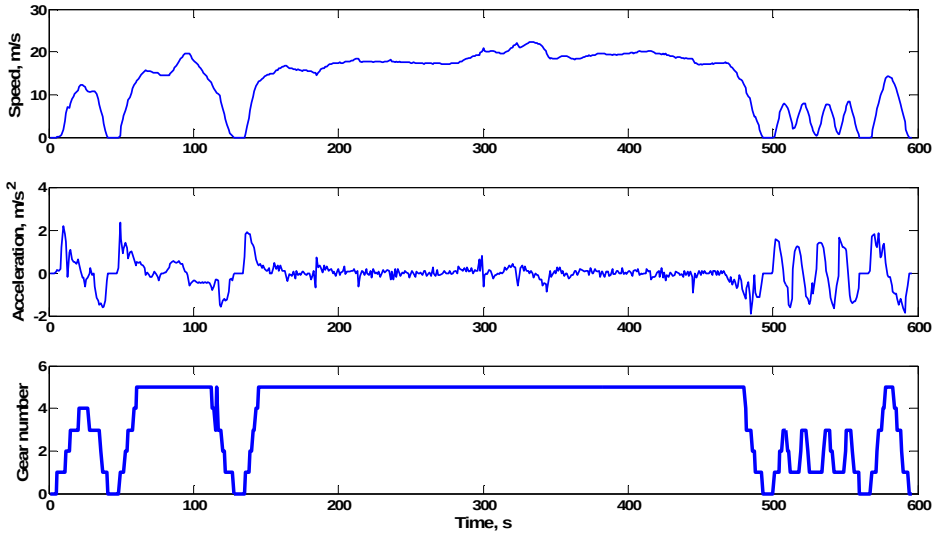

Appendix figure 5 US-06 drive cycle data used in the QSS-TB models

As can be seen, the US-06 cycle consists mainly of high speeds and few gear changes, which are characteristics of a highway driving schedule. However, there are a couple of sections which are made up of lower speeds and frequent gear changes which would simulate inner-city driving. The fuel consumption for a conventional vehicle is as follows:

VW Golf data: 6.694 litres per 100km;
Ford I3 data: 6.023 litres per km.

Appendix figure 6 shows the speed load points for each of the data sets running the US-06 drive cycle using the QSS-TB model.

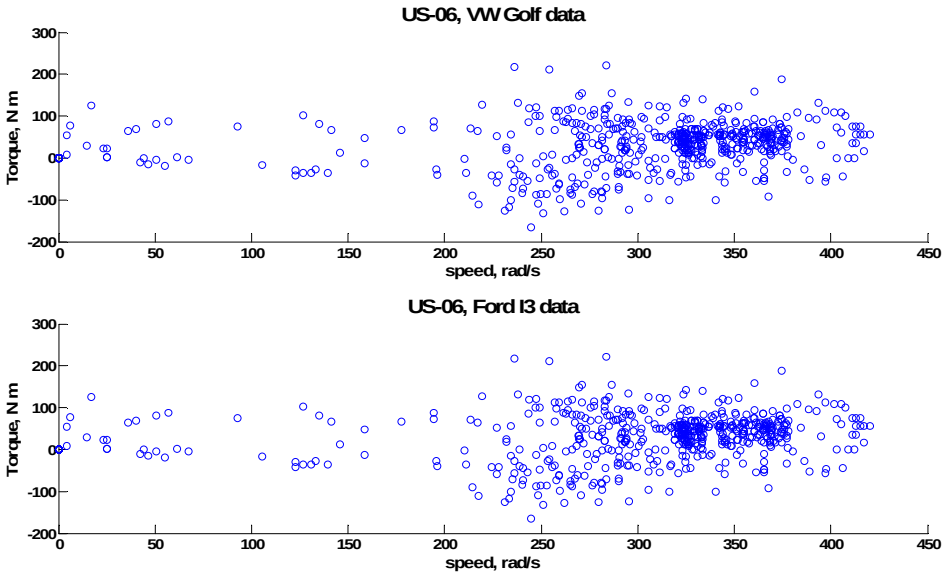

Appendix figure 6 Engine speed and load points for the US-06 drive cycle

The load points are almost equally spread about the zero axis with some points slightly higher on the positive side. It is expected that adding the heat recovery system will cause the spread to be less equal as the positive load points will be lowered towards the zero axis due to the steam system generating some of the positive torque, this will in turn cause the fuel consumption to be reduced.

Appendix B: Matlab and Simulink data for the software modelling and simulation

This appendix contains the Matlab files and Simulink blocks used for the initial software modelling of the HYSTOR concept.

Section B.1 contains the Simulink blocks for the basic steam hybrid model that is described to in Section 2.2.1. The model is divided into levels with level 1 representing the top level of the model and levels 2 through 4 representing the lower levels.

Section B.2 contains the Simulink blocks for the accumulator steam hybrid model that is described to in Section 2.2.1. The model is divided into levels with level 1 representing the top level of the model and levels 2 through 4 representing the lower levels.

Section B.3 contains the Matlab files that are required to initialise the QSS-TB steam hybrid models. These files are referenced in Section 2.2.2. A description for each file is given before the actual file contents.

Section B.4 contains the Matlab files that are required to initialise the PSAT steam hybrid models. The file and its use is described in Section 2.3.2.

B.1 Simulink blocks for the basic model

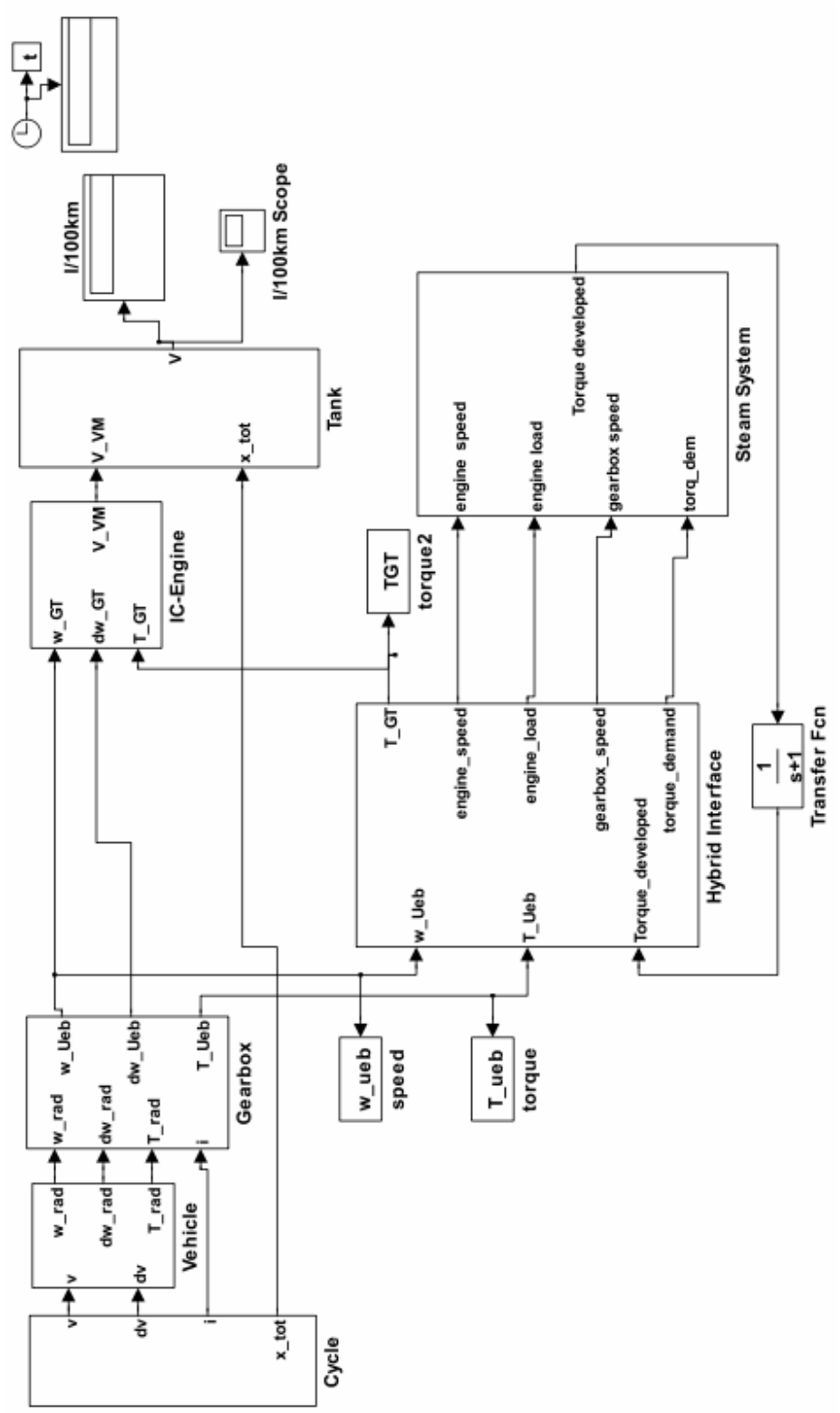

Appendix figure 7 Level 1 – QSS-TB basic steam hybrid

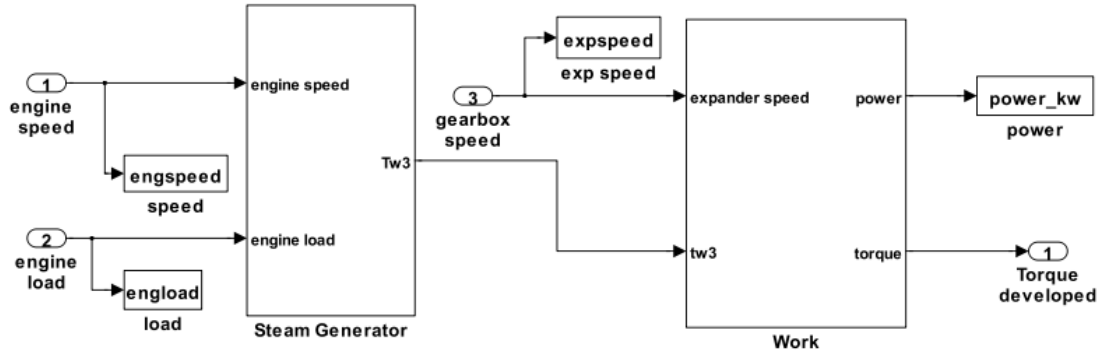

Appendix figure 8 Level 2 – Steam system

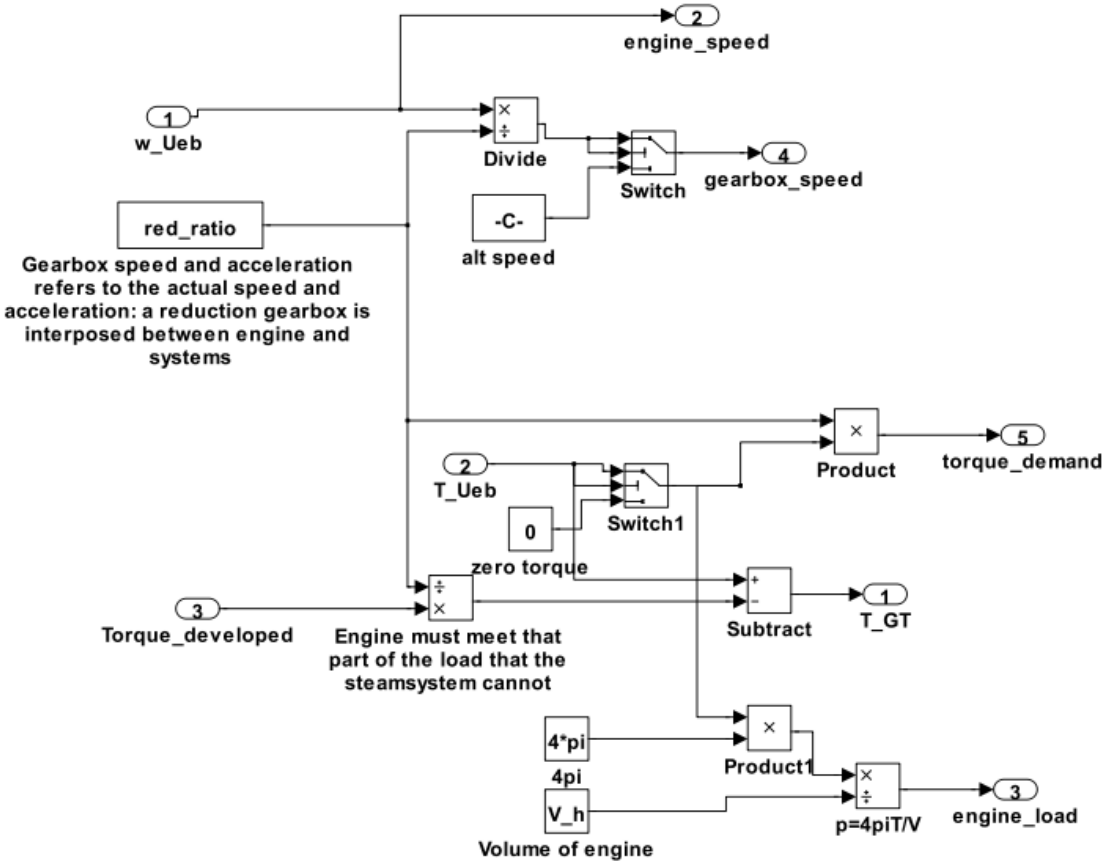

Appendix figure 9 Level 2 – Hybrid interface

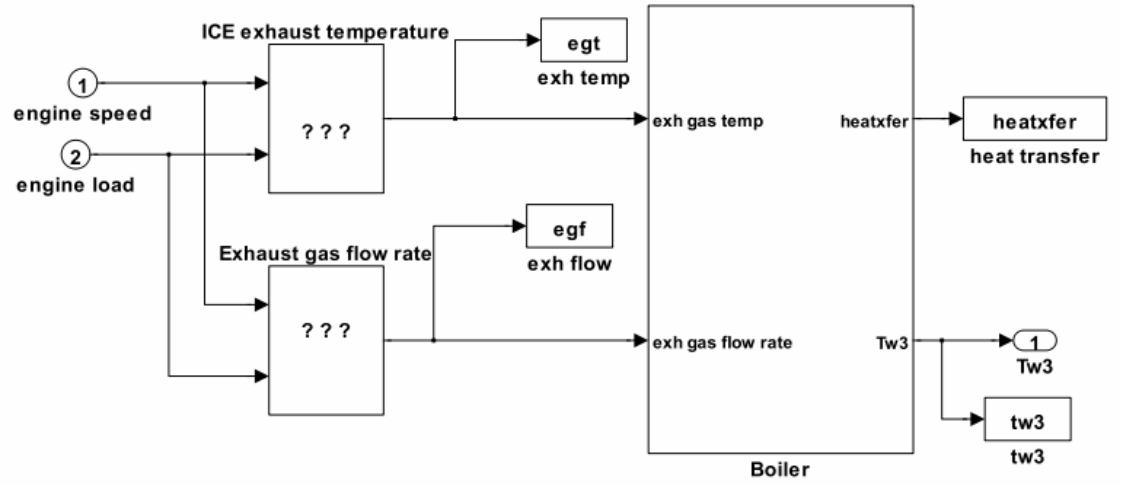

Appendix figure 10 Level 3 – Steam generator

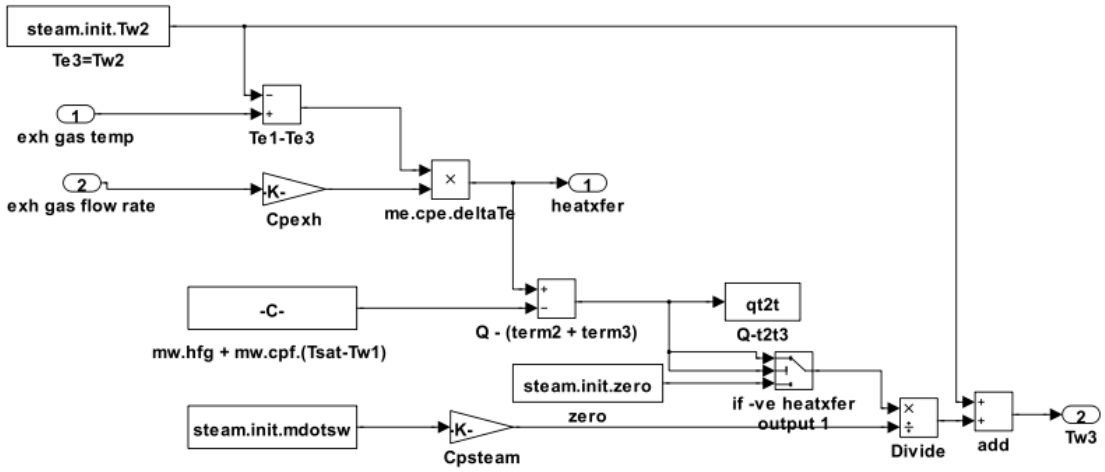

Appendix figure 11 Level 4 – Boiler

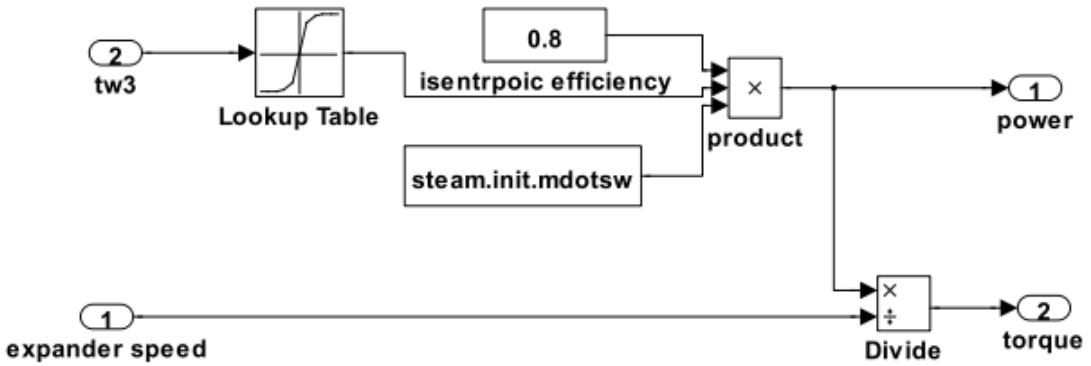

Appendix figure 12 Level 3 – Work

B.2 Simulink files for the accumulator steam system

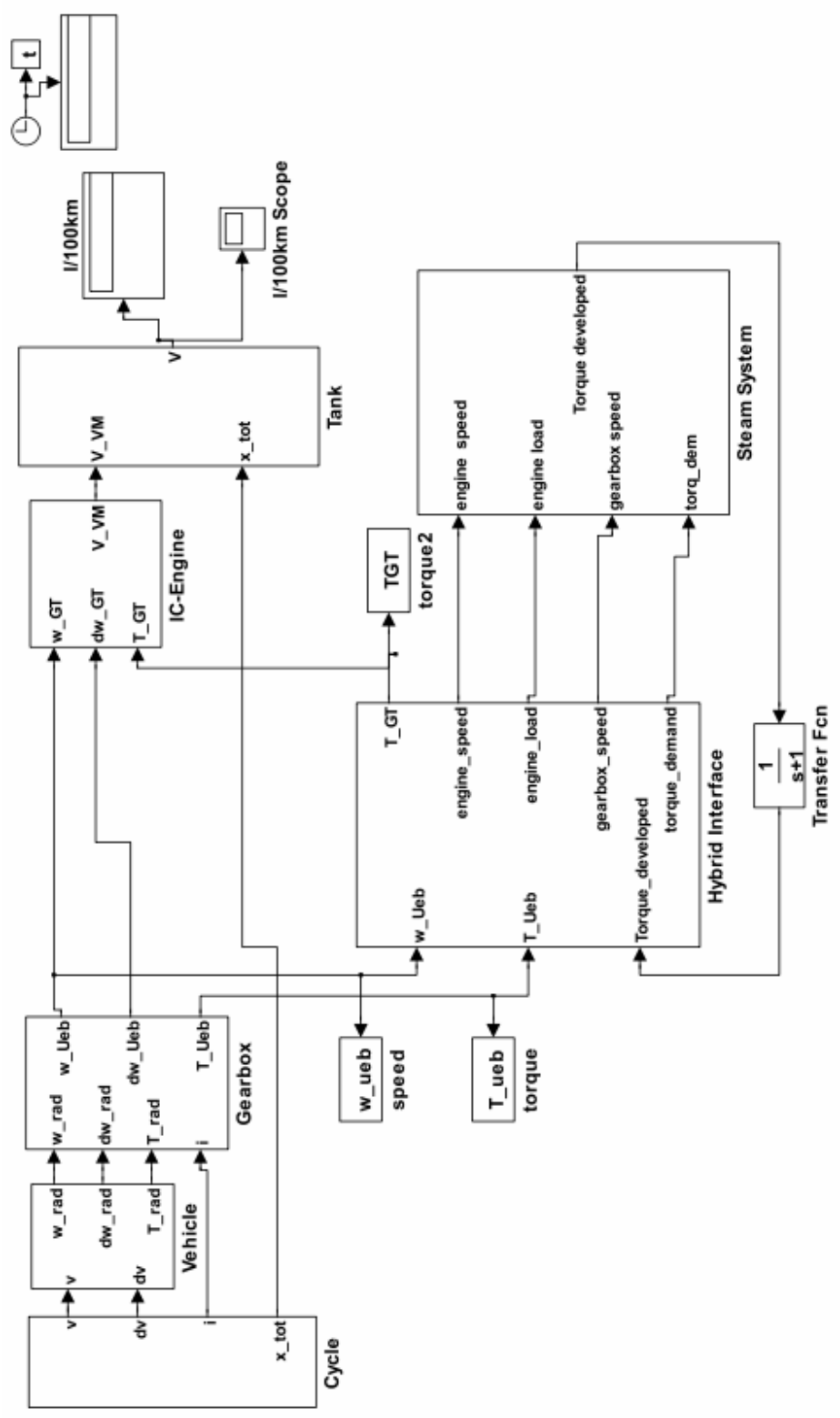

Appendix figure 13 Level 1 – QSS-TB accumulator steam hybrid

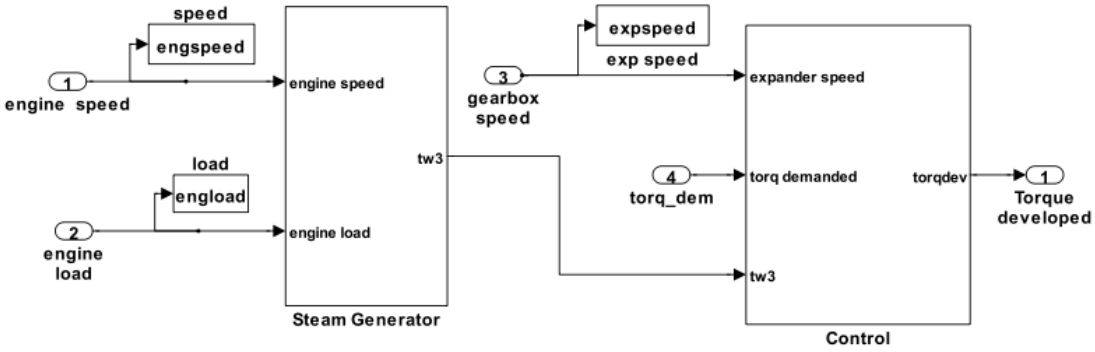

Appendix figure 14 Level 2 – Steam system

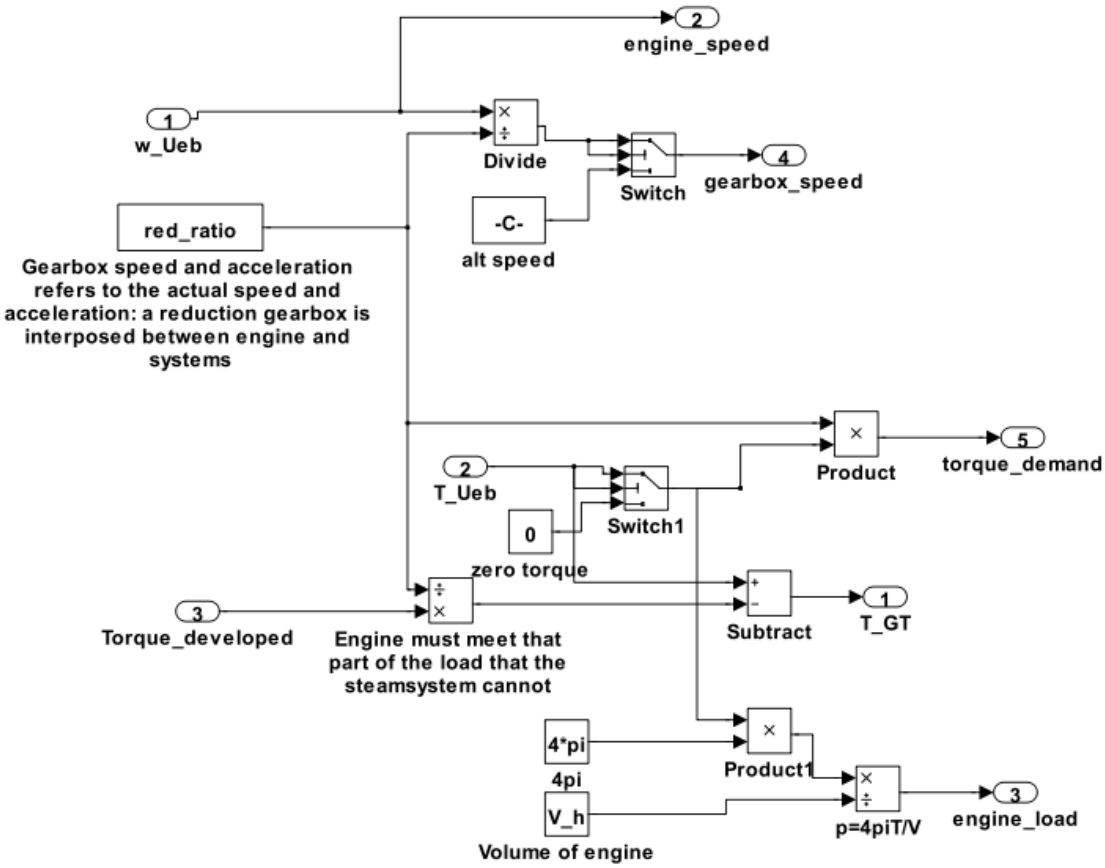

Appendix figure 15 Level 2 – Hybrid interface

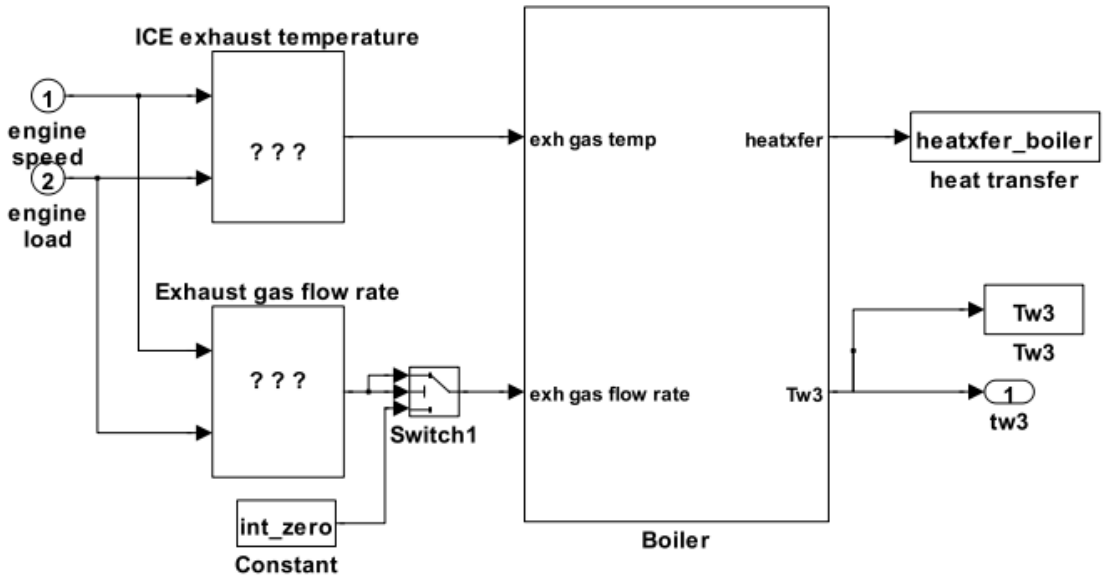

Appendix figure 16 Level 3 – Steam generator

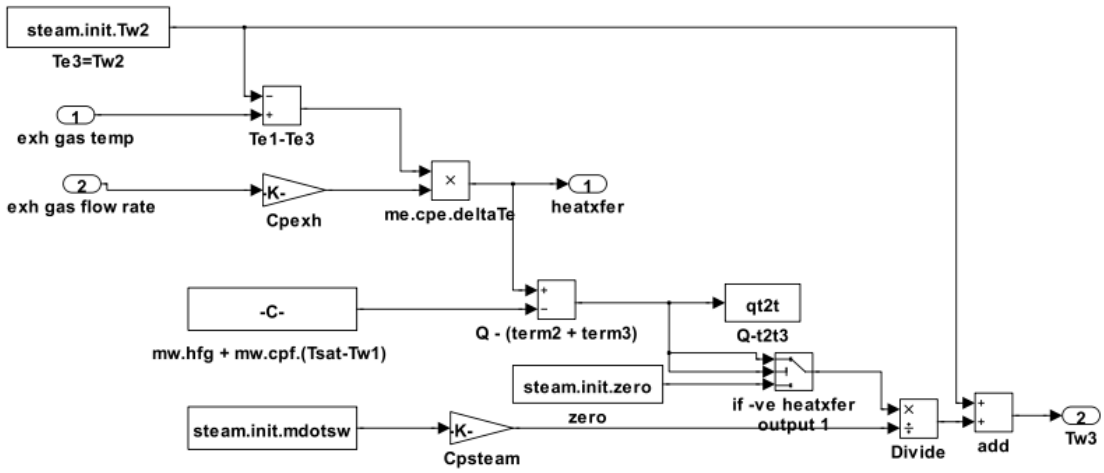

Appendix figure 17 Level 4 – Boiler

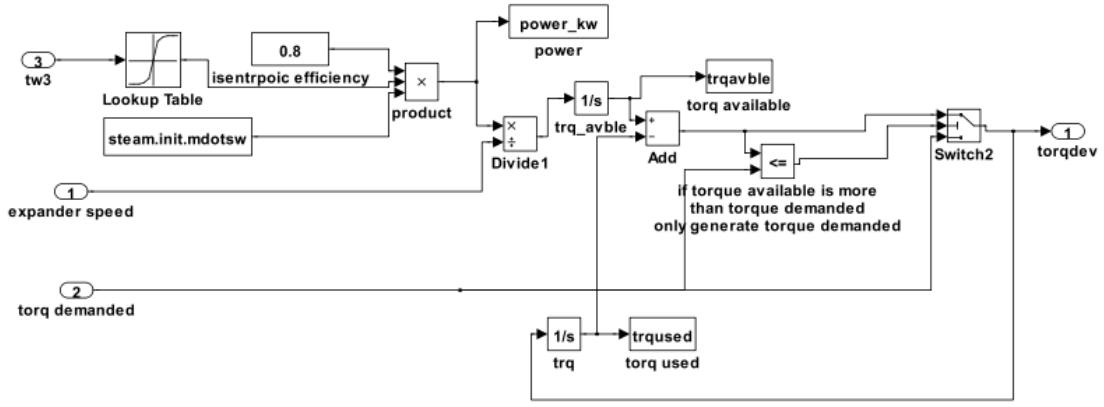

Appendix figure 18 Level 3 – Control

B.3 Initialisation files for QSS-TB

initdataG.m – For VW Golf Vehicle

This Matlab file loads all the necessary parameters for the function blocks for the QSS-TB model. Drive cycle files are loaded which contain a time constant, speed and gear number for the drive cycle; from this data acceleration is calculated. The parameters for the gearbox, fuel, vehicle and engine function blocks are also specified in this file. VW Golf data is used throughout.

```
% Parameters, run first
% ********************

% Simulation parameter
global h;
h     =    1;           % Step size (s)

% Load drive cycle
% load NEDC_TVG;        % Load time, speed and gear from NEDC drive
% load FTP_75;          % Load time, speed and gear from FTP drive
load FTPUS06;           % Load time, speed and gear for US06

nnn=max(size(V_z));
D_z=[V_z(2:nnn)-V_z(1:nnn-1);0]/h; % Compute acceleration (m/s^2)
t_sim = (nnn-1)*h;                     % Cycle length (s)

% Gear ratios (incl. differential) - Vehicle specific (VW Golf 1.6)
i_1 = 14.68375;
i_2 =  8.262;
i_3 =  5.8225;
i_4 =  4.386;
i_5 =  3.6125;

P_GT0   = 300;                  % Gearbox efficiency
e_GT      = 0.90;               % Gearbox efficiency (-)(VW Golf 1.6)
Ueb_min   = 0.1;                % Min. gear ratio (-)
w_rad_min = 1.00;               % Min. wheel speed (rad/s)

% Create schedule of gear change
I_z =  0*ones(size(G_z));
for i=1:nnn;
    if     G_z(i)==0;
        I_z(i)=0;
    elseif G_z(i)==1;
        I_z(i)=i_1;
    elseif G_z(i)==2;
        I_z(i)=i_2;
    elseif G_z(i)==3;
        I_z(i)=i_3;
```

```
    elseif G_z(i)==4;
        I_z(i)=i_4;
    elseif G_z(i)==5;
        I_z(i)=i_5;
    end;
end;

% Parameter fuel
H_u      = 43.5e6;                      % Heat in value (J/kg)
rho_B    =  0.75;                       % Density (kg/m^3)
k_ks     =  1.15;                       % Cold start factor (-)

% Parameters for vehicle
r_rad =    0.309;                       % Wheel radius (m)(VW Golf 1.6)
m_f   =    1181.0;                      % Mass (kg)(VW Golf 1.6)
mu    =    0.007;                       % Friction coefficient (-)
g     =    9.81;                        % Erdbeschleunigung (m/s^2)
rho   =    1.18;                        % Density air (kg/m^3)
cw    =    0.321;                       % Drag coefficient (-)(VW Golf
1.6)
A_f   =    2.1;                         % Frontal area (m^2)(VW Golf
1.6)

% Parameter engine
V_h        = 1.60e-3;             % Displaced volume (m^3)(VW Golf 1.6)
theta_VM   = 0.125;                     % Inertia (m^2 kg)(VW Golf 1.6)
T_VM_SchaB = -5;                        % Decel torque (Nm)
V_VM_SchaB =  0;                        % Decel consumption (kg/s)
w_VM_idle  = 105.0;                     % Idle speed (rad/s)
V_VM_idle  = 2.6e3*h/H_u;               % Idle consumption (kg/s)
T_VM_idle  = 0;                         % Idle torque (Nm)

% Fuel  Consumption map(kg/s)
load w_VM_row;
load p_me_col;
load p_me_max;
load w_VM_max;

T_VM_col   = p_me_col'*V_h/(4*pi);      % Compute torque

mapallvars_Golf;                        % call map function call to
                                        % plot fuel consumption
w_VM_upper = max(w_VM_max);             % Max. speed (rad/s)
T_VM_max   = p_me_max'*V_h/(4*pi);      % Max. torque (Nm)

% Now initialise the steam sub-system
initialise_system;                      % Initialise steam system
```

initdataI – for Ford I3 Vehicle

This Matlab file loads all the necessary parameters for the function blocks for the QSS-TB model. Drive cycle files are loaded which contain a time constant, speed and gear

number for the drive cycle; from this data acceleration is calculated. The parameters for the gearbox, fuel, vehicle and engine function blocks are also specified in this file. For the Ford I3 model, only the engine data was available hence for the other parameters the VW Golf data is used.

```
% Parameters, run first
% *********************

% Simulation parameter
global h;
h     =    1;           % Step size (s)

% Load speed cycle
load NEDC_TVG;          % Load time, speed and gear from NEDC drive
%load FTP_75;           % Load time, speed and gear from FTP drive
%load FTPUS06b;         % Load time, speed and gear for US06

nnn=max(size(V_z));
D_z=[V_z(2:nnn)-V_z(1:nnn-1);0]/h;      % Compute acceleration (m/s^2)

%plot(T_z,V_z,D_z,G_z)
t_sim = (nnn-1)*h;                      % Cycle length (s)

% Gear ratios (incl. differential) - Vehicle specific (VW Golf 1.6)
i_1 = 14.68375;
i_2 =  8.262;
i_3 =  5.8225;
i_4 =  4.386;
i_5 =  3.6125;

P_GT0   = 300;                          % Gearbox efficiency
e_GT      = 0.90;                       % Gearbox efficiency (-)(VW Golf
1.6)
Ueb_min   = 0.1;                        % Min. gear ratio (-)
w_rad_min = 1.00;                       % Min. wheel speed (rad/s)

% Create schedule of gear change
I_z =  0*ones(size(G_z));
for i=1:nnn;
    if     G_z(i)==0;
        I_z(i)=0;
    elseif G_z(i)==1;
        I_z(i)=i_1;
    elseif G_z(i)==2;
        I_z(i)=i_2;
    elseif G_z(i)==3;
        I_z(i)=i_3;
    elseif G_z(i)==4;
        I_z(i)=i_4;
    elseif G_z(i)==5;
        I_z(i)=i_5;
    end;
```

```
end;

% Parameter fuel
H_u      = 43.5e6;                    % Heatin value (J/kg)
rho_B    =  0.75;                     % Density (kg/m^3)
k_ks     =  1.15;                     % Coldstart factor (-)

% Parameters for vehicle
r_rad =    0.309;                     % Wheel radius (m)(VW Golf 1.6)
m_f   =    1181.0;                    % Mass (kg)(VW Golf 1.6)
mu    =    0.007;                     % Friction coefficient (-)
g     =    9.81;                      % Erdbeschleunigung (m/s^2)
rho   =    1.18;                      % Density air (kg/m^3)
cw    =    0.321;                   % Drag coefficient (-)(VW Golf 1.6)
A_f   =    2.1;                     % Frontal area (m^2)(VW Golf 1.6)

% Parameter engine
V_h        = 1.1e-3;                  % Displaced volume (m^3)(I3 1.1)
theta_VM   = 0.125;                     % Inertia (m^2 kg)(VW Golf 1.6)
T_VM_SchaB = -5;                        % Decel torque (Nm)
V_VM_SchaB =  0;                        % Decel consumption (kg/s)
w_VM_idle  = 105.0;                     % Idle speed (rad/s)
V_VM_idle  = 2.5e3*h/H_u;               % Idle consumption (kg/s)
T_VM_idle  = 0;                         % Idle torque (Nm)

% Fuel Consumption
load w_VM_row;
load p_me_col;
load p_me_max;
load w_VM_max;
T_VM_col   = p_me_col'*V_h/(4*pi);  % Compute torque

mapallvars_I3;                      % call map function call
                                    % to calculate fuel consumption
w_VM_upper = max(w_VM_max);         % Max. speed (rad/s)
T_VM_max   = p_me_max'*V_h/(4*pi);  % Max. torque (Nm)

% Now initialise the steam sub-system
initialise_system;                      % Initialise steam system
```

mapallvars_Golf.m

This Matlab data file uses speed and load information along with exhaust temperature data (calculated for the VW Golf) to calculate the various maps and lookup tables that are used in the QSS-TB models. V_VM_map is the fuel consumption lookup table used by the *Tank* function block. E_map is the exhaust temperature lookup table and F_map is the exhaust mass flow rate lookup table. These are used by the HYSTOR steam system in the heat exchange calculations.

```
% Computes efficiency map
% Willans-Parameter
ww= [   116,    302,   458,   653,  780];     % speed support (rad/s)
% Index of top element
ee= [  0.38, 0.4025,0.4150,0.4150,0.410];     % indicated efficiency
pp= [ 1.484,  1.880, 2.378, 3.032, 3.85]*1e5; % friction mean pressure

% Exhaust temperature parameters in degC
% At higher speeds - same load then temperature is slightly higher
exhaust_temp = [600, 575, 550, 525, 500, 475, 450, 425, 400, 375, 360,
345, 330, 315, 305, 300];

temperature_rise = 100;
exhaust_density = 0.8;  % kg/cubic meter

% Compute map
i=0;
j=0;
eta_VM=zeros(16,15);
E_map = zeros (16,15);
F_map = zeros (16,15);
p_me_vec=[11,10,9,8,7,6,5,4,3,2,1.5,1,0.5,0.25,0.1,0]*1e5;
p_me_vec_r = reversr(p_me_vec);
w_VM_vec=[50:800/14:850];
for i=1:16;
    for j=1:15;
        e=spline(ww,ee,w_VM_vec(j));
        p_me0=spline(ww,pp,w_VM_vec(j));
        p_mB=(p_me_vec(i)+p_me0)/e;
        eta_VM(i,j)=p_me_vec(i)/p_mB;
    end;
end;

max_speed = length (w_VM_vec);
speed_correction = temperature_rise /(w_VM_vec(max_speed) -
w_VM_vec(1));
eta_vec=[0.33,0.31,0.32,0.3,0.275,0.2,0.1,0.05];

% Prepare for QSS-TB
nnn=max(size(p_me_vec));
mmm=max(size(w_VM_vec));

P_VM_idle  = 2.6e3;                    % Idle power (W)
E_VM_idle  = P_VM_idle*h;              % Idle energy

% Compute consumption map (kg/s)
V_map=ones(size(eta_VM));
for i=1:nnn;

    for j=1:mmm;
        if eta_VM(i,j)>0.00;
            V_map(i,j)=w_VM_vec(j)*p_me_vec(i)*V_h/(4*pi)*h/eta_VM(i,j);
        else
```

```
            V_map(i,j)=w_VM_vec(j)*p_me_vec(i-1)*V_h/(4*pi)*h/eta_VM(i-
1,j);
        end;
    end;
end;
V_VM_map=V_map/H_u;

% Compute exhaust temperature map
w_VM_SC_r = w_VM_vec;   % speed, row vector in Steam Generator
p_me_SC_c = p_me_vec_r; % temp, column vector in Steam Capacity

for i=1:nnn;  % take load steps
    for j=1:mmm;  % take speed steps
            E_map(i,j)= ((w_VM_vec(j) - w_VM_vec(1)) * speed_correction)
+ exhaust_temp(i);
    end;
end;
E_map = E_map + 273.15; % convert from Celsius to Kelvin

% Compute exhaust mass flow map rate and assume that it is load
% independent
for i=1:nnn;  % take load steps
    for j=1:mmm;  % take speed steps
            F_map(i,j)= w_VM_vec(j) * (V_h / (4 * pi)) *
exhaust_density;
    end;
end;

% Save for QSS-TB - fuel consumption first
V_VM_map=reversi(V_VM_map);
V_VM_map=V_VM_map';
save V_VM_map V_VM_map

% Repeat for exhaust mass flow rate and temperature
E_map=reversi(E_map);
E_map=E_map';
save E_map E_map

F_map=reversi(F_map);
F_map = F_map';
save F_map F_map

% and reverse mep vector
p_me_vec_rev = reversi (p_me_vec);

eta_VM=reversi(eta_VM);
save eta_VM eta_VM
```

mapallvars_I3.m

This Matlab data file uses speed and load information along with exhaust temperature data (actual engine data from the Ford I3 test runs) to calculate the various maps and

lookup tables that are used in the QSS-TB models. V_VM_map is the fuel consumption lookup table used by the *Tank* function block. E_map is the exhaust temperature lookup table and F_map is the exhaust mass flow rate lookup table. These are used by the HYSTOR steam system in the heat exchange calculations.

```
% Computes efficiency map
% Willans-Parameter
ww= [   116,    302,   458,   653,  780];   % speed support (rad/s)
% Index of top element
ee= [  0.38, 0.4025,0.4150,0.4150,0.410];   % indicated efficiency
pp= [ 1.484,  1.880, 2.378, 3.032, 3.85]*1e5; % friction mean pressure

% Compute map
p_me_vec_r = p_me_col;
p_me_vec = reversr(p_me_col);

nnn=max(size(p_me_vec));
mmm=max(size(w_VM_row));

eta_VM=zeros(nnn,mmm);
E_map = zeros (nnn,mmm);
F_map = zeros (nnn,mmm);

w_VM_vec=[50:800/14:850];
for i=1:nnn;
    for j=1:mmm;
        e=spline(ww,ee,w_VM_row(j));
        p_me0=spline(ww,pp,w_VM_row(j));
        p_mB=(p_me_vec(i)+p_me0)/e;
        eta_VM(i,j)=p_me_vec(i)/p_mB;
    end;
end;

eta_vec=[0.33,0.31,0.32,0.3,0.275,0.2,0.1,0.05];

P_VM_idle  = 2.6e3;                     % Idle power (W)
E_VM_idle  = P_VM_idle*h;               % Idle energy
magic=1.0;

% Compute consumption map (kg/s)
V_map=ones(size(eta_VM));
for i=1:nnn;

    for j=1:mmm;
        if eta_VM(i,j)>0.00;
            V_map(i,j)=w_VM_vec(j)*p_me_vec(i)*V_h/(4*pi)*h/eta_VM(i,j);
        else
            V_map(i,j)=w_VM_vec(j)*p_me_vec(i-1)*V_h/(4*pi)*h/eta_VM(i-
1,j);
        end;
    end;
end;
```

```
V_VM_map=V_map/H_u;

% Compute exhaust temperature map
% Speed(rad/s) Row vector in Steam Generator
w_VM_SC_r =[104.719, 209.438, 314.157, 417.2355, 628.314];
%p_me (Pa) Column vector in Steam Generator
p_me_SC_c =[0; 1.5; 4; 7.3; 7.5; 8; 8.3; 9.6; 10.2]*1e5;

%exhaust temps at 1000 rpm
e_1000=[225, 229.7, 403.4, 596.1, 601,606,611,616,6211];
%exhaust temps at 2000 rpm
e_2000=[307, 311.8, 550, 737, 742, 747, 811, 816,816];
%exhaust temps at 3000 rpm
e_3000=[392, 397, 621.7, 790, 795, 800, 879, 884, 889];
%exhaust temps at 4500 rpm
e_4500=[747, 752.4, 822.2, 862, 867, 875.1, 873, 878, 883.8];
%exhaust temps at 6000 rpm
e_6000=[828, 833.8, 883.3, 883.55, 883.8, 888.9, 888.9, 888.9, 888.9];
%Exhaust Temp map for I3 engine
E_map=[e_1000;e_2000;e_3000;e_4500;e_6000];

E_map = E_map + 273.15; % convert from Celsius to Kelvin

%exhaust mass flow rate at 1000 rpm
f_1000=[0.006, 0.006, 0.0053, 0.0098, 0.01, 0.011, 0.012, 0.013, 0.014];
%exhaust mass flow rate at 2000 rpm
f_2000=[0.0121, 0.0121, 0.0138, 0.0167, 0.0172, 0.0177, 0.0192, 0.0197,
0.0197];
%exhaust mass flow rate at 3000 rpm
f_3000=[0.0214, 0.0214, 0.016, 0.0205, 0.025, 0.0272, 0.0294, 0.0316,
0.0316];
%exhaust mass flow rate at 4500 rpm
f_4500=[0.0162, 0.0162, 0.0258, 0.0350, 0.0442, 0.0454, 0.0465, 0.0476,
0.0488];
%exhaust mass flow rate at 6000 rpm
f_6000=[0.0224, 0.0224, 0.036, 0.0460, 0.056, 0.061, 0.061, 0.061,
0.061];
%Exhaust mass flow rate map for I3 engine
F_map=[f_1000;f_2000;f_3000;f_4500;f_6000];

% Save for QSS-TB - fuel consumption first
V_VM_map=reversi(V_VM_map);
V_VM_map=V_VM_map';
save V_VM_map V_VM_map

eta_VM=reversi(eta_VM);
save eta_VM eta_VM
```

initialise_system.m

This Matlab file is used to set the parameters and variables used by the HYSTOR *Steam System* function blocks. Thermodynamic properties are set for the working pressures of

the system along with the variable that sets the reduction gearbox variable and an alternative speed for when the engine speed goes below a nominal value. Additionally the volumes and masses are set for the HYSTOR steam system. The same file is used for both the VW Golf and the Ford I3 models.

```
%
%  Initialise HYSTOR variables
%

zero =0;

% Thermodynamic properties
load degk_deltah.mat;
h_work_steam = 2796000;         % Saturation enthalpy for steam at
working pressure (18bar) J/kg
h_work_water = 884000;         % Saturation enthalpy for water at
saturation conditions (18bar) J/kg
Hfg_work = h_work_steam - h_work_water;    % enthalpy change at 18 bar


%%%%%%%%%%%%%%%% Hybrid Interface %%%%%%%%%%%%%%%%%%%%%%%%%%
red_ratio = 2.0;   % Reduction ration of gearbox connecting expander
with engine drive shaft
alt_speed = 215;    % Alternative speed for gearbox when actual speed
goes below 10 (rad/s)

%%%%%%%%%%%%%%%% Steam Generator %%%%%%%%%%%%%%%%%%%%%%%%%%%%
ambient_temp = 298;           % degK use 25 degC as the normal ambient
temperature for the car
steam.init.Tw2 = 480;         % Saturation temperature degK
steam.init.Tw1=ambient_temp;  % Tw1 is ambient

steam.init.mdotsw = 0.004;    % mass flow rate of water kg/s
steam.init.cpsteam = 3097;    % heat capacity of steam at 18 bar J/kgK

% Gain blocks
cpexhaust = 1041;             % heat capacity of exhaust gas J/kgK
steam.init.Kegfr = cpexhaust; % Gain on Exhaust Gas mass flow rate

steam.init.cpwater = 4500;    % heat capacity of water J/kgK

steam.init.term2 = steam.init.mdotsw*Hfg_work;
steam.init.term3 = steam.init.mdotsw*steam.init.cpwater*(steam.init.Tw2-
ambient_temp);
steam.init.term2plus3=steam.init.term2+steam.init.term3;
```

B.4 Initialisation file for PSAT

```
%% File description
% Name : steam_system_Sussex_University
% Author : V. Freyermuth 12/06/06
% Description : Initialize the steam system
% Data from Sandra Hounsham
% Proprietary: Sussex
% Model :  lib_steam_generator_Sussex_University,
lib_steam_generator_SU_bph_trqneg, lib_steam_generator_SU_acc_trqneg
% Vehicle Type : Light, Heavy

%% File content
steam.list.init =
{'h_work_steam';'h_work_water';'h_cond_steam';'h_cond_water';'Hfg_work';
    'red_ratio';'alt_speed';'T_work';'ambient_temp';'cpexhaust';
    'zero'; };

load degk_deltah.mat;

% Thermodynamic properties at 18 and 1 bar
steam.init.h_work_steam = 2796000;        % Saturation enthalpy for
steam at working pressure (18bar) kJ/kg
steam.init.h_work_water = 884000;        % Saturation enthalpy for water
at saturation conditions (18bar) kJ/kg

steam.init.h_cond_steam = 2674000;        % Saturation enthalpy for
steam at condenser pressure (1bar) kJ/kg
steam.init.h_cond_water = 417000;         % Saturation enthalpy at water
at condenser pressure (1bar) kJ/kg

steam.init.Hfg_work = steam.init.h_work_steam - steam.init.h_work_water;
% Latent heat of vapourisation at working pressure

%%%%%%%%%%%%%%%%%%%%%%%%%%%% Steam System %%%%%%%%%%%%%%%%%%%%%%%%%%%%
 steam.init.red_ratio = 2.0;   % Reduction ration of gearbox connecting
expander with engine drive shaft
steam.init.alt_speed = 215;    % Alternative speed for gearbox when
actual speed goes below 10 (rad/s)
steam.init.zero =0; % generic integrator initlial value
% steam.init.n_expander=1.3;         % polytropic index, from PV diagram
for water/steam
steam.init.n_expander=1;         % polytropic index, from PV diagram for
water/steam
steam.init.Kms = 1/steam.init.n_expander;     % On mass steam available,
turn into max rate
 steam.init.T_work=480;         % Normal working temperature
degK(corresponding to saturation at 18 bar)
 steam.init.ambient_temp = 298;  % degK use 25 degC as the normal
ambient temperature for the car

% Gain blocks
steam.init.Kw = 1/(2*pi);     % Gain on work output, correct to Nm
                    % also used to change rad/s to rps
```

Appendix B: Matlab and Simulink data for the software modelling and simulation

```
%%%%%%%%%%%%%%%%%%%%%%%%%% Steam Generator %%%%%%%%%%%%%%%%%%%%%%%%%%
steam.init.mdotsw =0.004; % mass flow rate of water/steam kg/s
steam.init.Tw2=480;   % saturation temp at 18bar = 207 degC, or 480 degK
steam.init.cpsteam = 3097;     % heat capacity of steam at 18 bar

steam.init.cpexhaust = 1041;     % heat capacity of exhaust gas
steam.init.Kegfr = steam.init.cpexhaust; % Gain on Exhaust Gas mass flow
rate
steam.init.Tw1=steam.init.ambient_temp;   % Normal working temperature
degK is slightly above ambient
steam.init.cpwater = 4500; % heat capacity of water

steam.init.neghx=-480;
steam.init.term2 = steam.init.mdotsw*steam.init.Hfg_work;
steam.init.term3 = steam.init.mdotsw*steam.init.cpwater*(steam.init.Tw2-
steam.init.ambient_temp);
steam.init.term2plus3=steam.init.term2+steam.init.term3;
```

Appendix C: Expander technical data

This appendix contains data for the expanders used in the experiments, as detailed in Section 3.2. This is technical data from the O.S. Engines website [62].

Rotary expander

This is the O.S. Max 49-PI Type II .30 Wankel Rotary Engine.

SPECS:
Displacement: .30 cu in (4.97cc)
Carburetor: #21G
Power Output: 1.27 bhp at 17,000 RPM
Weight: 335g (11.8oz)
Practical RPM: 2,500 - 18,000 RPM
Crankshaft thread: 1/4-28
Length (back of engine mount to front of drive washer): 60mm (2.36")
Height (not including carb or muffler): 61mm (2.4")
Width (not including carb or muffler): 69mm (2.7")
Propeller: 9x6-7, 10x4-6 or 11x4-5

Uni-flow expander

This .32 SX is a Sport RC Airplane Engine.

SPECS: Displacement: 5.23cc (0.319 cu in)
Bore: 19.5mm (.77")
Stroke: 17.5mm (.69")
Output: 1.2 BHP at 18,000 RPM
Weight: 270g (9.5oz) 12.32oz w/muffler
Practical RPM Range: 2,000 - 22,000 RPM
Crankshaft Thread Size: 1/4-28
Recommended Props: 10x6, 10.5x6, 11x6
Height: 73mm (2.87")
Width: 30mm (1.18") Width neglecting the engine mounting flanges
38mm (1.50") Width between the centers of the mounting holes
Length: 75mm (2.95") From back plate to the front of the drive washer.

Counter-flow expander

This is a FS-30 Surpass Four-Stroke Model Aircraft Glow Engine.

SPECS: Displacement: 4.89cc (.299 cu in)
Bore: 19.5mm (.767") Stroke: 16.4mm (.648")
Power Output: .5 HP at 10,000 RPM

Appendix C: Expander technical data

Weight with muffler: 10.4oz (295g)
Weight without muffler: 9.8oz (278g)
Practical RPM Range: 2,500 - 13,000 RPM
Crankshaft Thread Size: 1/4-28
Valve Clearance: Between .04mm and .1mm (.0015" and .004"),
Measured between the valve tip and rocker arm.
Length: 84mm (3.31") from back plate to front of Drive Washer.
Width: 29mm (1.14") width of engine neglecting the mounting flanges
36mm (1.42") mounting holes side-to-side on-center
Height: 86.5mm (3.41")
Suggested Prop(s): 9x6, 9x7, 10x4, or 10x6
Construction: Aluminum and aluminum alloys

Appendix D: Steam quality analyser (SQA)

The project team developed a device, a Steam Quality Analyser (SQA), to measure the quality of wet steam based on the steam property tables and electrical heating. This appendix further describes the concept and calibration for the SQA device.

D.1 Steam quality measurement of wet steam

To enable the project to calculate the efficiency of the steam expanders, the quality of the exhausted wet steam, sometimes referred to as the dryness fraction, needed to be determined. The dryness fraction represents the amount of the steam which is dry, for example if the steam is 5% water, then the steam is said to be 95% dry, with a dryness fraction of 0.95. Physical measurement of the quality of steam in the wet region is associated with inaccuracies and involves very expensive and sophisticated measuring equipment. An alternative way of obtaining the steam quality is to heat the exhausted wet steam with a known quantity of energy so that the steam becomes superheated and then measure the state of that steam by recording the temperatures and pressures. The dryness fraction can then be determined by performing an energy balance calculation, with the use of steam property tables [63].

D.2 Concept for the SQA device

The SQA consisted of an insulated pipe with an electrical heating element which was supplied with an input power in the form of a voltage and current. The SQA was supplied with wet steam which was converted into superheated steam as a result of the heating element and applied power. Pressure and temperature readings were taken at the inlet and outlet of the SQA together with temperature readings of the SQA casing and ambient temperature. Appendix figure 19 shows a schematic of the SQA and a simple temperature vs. entropy graph for the process.

Appendix D: Steam quality analyser (SQA)

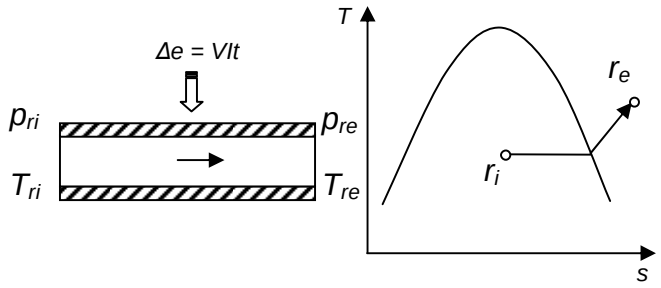

Appendix figure 19 SQA concept

The quality of the steam at the inlet is given by Equation D.1:

$$x = \frac{h_1 - h_f}{h_g - h_f} \qquad \text{(D.1)}$$

Equation D.1 requires knowledge of h_f and h_g which can be obtained from steam tables at the inlet pressure. The value of h_1 can be obtained by performing an enthalpy-energy balance for the SQA such that:

$$h_1 = h_2 + \text{losses} - \frac{VIt}{M} \qquad \text{(D.2)}$$

Where: h_1 = inlet enthalpy (kJ/kg);

h_2 = outlet enthalpy (kJ/kg);

V = input voltage (v);

I = input current (amps);

t = time (seconds);

M = mass of water collected in time t (kg/s);

losses = convective heat loss from the SQA (per unit mass flow rate).

Since the outlet state is superheated steam, a value of enthalpy (h_2) can be obtained from standard steam tables at the measured pressure and temperature. The value of input VIt is known as is measured output M. This leaves "losses" to be defined. A value for losses was obtained by performing a calibration on the SQA.

D.3 Calibration of the SQA device

Calibration of the SQA was performed by supplying it with superheated steam. If the SQA could be considered ideal then when supplied with superheated steam there would be no losses and the steam properties at the exit would be the same as at the inlet. However, the SQA will not be ideal as there will be a convective heat loss from the SQA to its surroundings. This convective heat loss will be equal to the required supplied power to make $Q_1 = Q_2$ and hence:

$$Q_{VI} = Q_{SQA} + Q_{loss}$$

Therefore:

$$Q_{loss} = Q_{SQA} - Q_{VI} \qquad (D.3)$$

Where: Q_{loss} = the convective heat loss from the SQA to its surroundings (W) i.e. the losses term in Equation D.2;

Q_{SQA} = the SQA enthalpy power (W) = $\dot{m}(h_2 - h_1)$;

Q_{VI} = the supplied power (W).

From Equation D.3 it can be seen that the value of Q_{loss} is a function of the mass flow rate through the SQA, the inlet and outlet temperatures (used to define/find h_1 and h_2) and the applied power. However, the value of h_1 will be unknown when the SQA is under normal operation (with wet steam) and so a different method of calculating Q_{loss} is required. Recalling that Q_{loss} will be in the form of a convective heat loss from the SQA to its surroundings it can be expressed by Equation D.4:

$$Q_{loss} = \lambda A \Delta T \qquad (D.4)$$

Where: λ = the heat transfer coefficient of the surrounding air (W/m^2K);

A = the total surface area of the SQA (m^2);

$\Delta T = T_{SQA} - T_{amb}$ (K).

The SQA area, A, is constant and so the value of Q_{loss} becomes a function of H and $T_{SQA} - T_{amb}$. The value of these variables obviously depends on the applied VI and so by operating the SQA over a range of VI it was possible to plot the variation of Q_{loss} against $T_{SQA} - T_{amb}$ which could then be used in Equation D.2 for when the SQA is under normal operation.

D.4 SQA calibration procedure

The procedure used to calibrate the SQA device was as follows:

1. Set the mass flow rate $\dot{m}$, entering the SQA and set an input power (VI);
2. Use the pressure and temperature readings, P_1, P_2, T_1 and T_2, at the inlet and outlet to obtain values of inlet and outlet enthalpy, h_1 and h_2 respectively, from steam tables;
3. Ensure the mass flow rate through the SQA is in the units of kg/s;
4. Calculate Q_{SQA} as follows:

$$Q_{SQA} = \dot{m}(h_2 - h_1)$$

5. Calculate Q_{loss} as follows:

$$Q_{loss} = Q_{VI} - Q_{SQA}$$ (where Q_{VI} is the applied VI);

6. Q_{loss} can also be expressed as:

$$Q_{loss} = \lambda A(T_{SQA} - T_{amb}) \qquad (D.5)$$

7. Equation D.5 requires a value of λ (the heat transfer coefficient of the air surrounding the SQA). This will vary very little over the range of case temperatures expected under normal use but since all remaining variables in Equation D.5 are known, it can be calculated by a simple re-arrangement as follows:

$$\lambda = \frac{Q_{VI} - Q_{SQA}}{A(T_{SQA} - T_{amb})}$$

8. Repeat steps 2 to 6 at six[1] set time intervals and calculate a mean value of Q_{loss};
9. Plot the mean value of Q_{loss} against $T_{SQA} - T_{amb}$;
10. Repeat steps 1 to 7 at different values of input power.

D.5 Normal operation of the SQA device

Under normal operating conditions, where the SQA is supplied with wet steam, the value of losses in Equation D.2 can be obtained from the plot produced in the calibration procedure described in Section B.3. The calibration results are shown in Appendix figure 20 and Appendix Table 1.

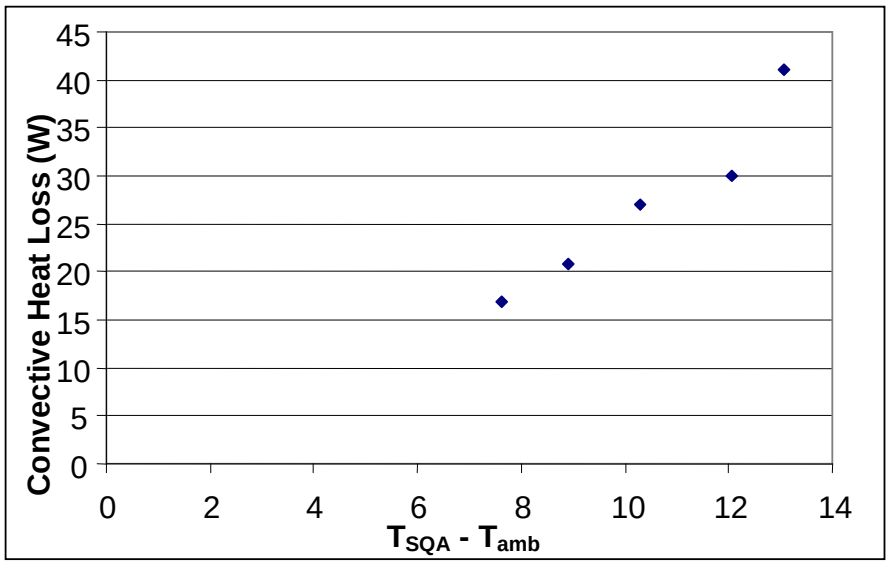

Appendix figure 20 Convective heat loss from the SQA for a range of T_{SQA} - T_{amb}

[1] The process is repeated six times to ensure repeatability (six being the accepted good practice number of repeats).

$\Delta T = T_{SQA} - T_{amb}$ (K)	Mean Q_{loss} (W)
13.08	41.01
12.05	29.94
10.29	27.07
8.91	20.76
7.64	16.83

Appendix Table 1 Values of convective heat losses from the SQA for a range of $T_{SQA} - T_{amb}$

Simple interpolation can be used to calculate the losses for different values of $T_{SQA} - T_{amb}$ which are not shown in Appendix figure 20 and Appendix Table 1.

Having now obtained a value of losses, Equation D.2 can be solved to obtain a value of inlet enthalpy. Finally this value of inlet enthalpy can then be used in Equation D.1 in order to establish the quality of the inlet wet steam.

D.6 SQA results

In addition to the torque, power and pressure results presented in Section 3.4, the expander configurations were also used to acquire data using the SQA device. For each speed step, the expander ran for 10 minutes and data collected at 2 minute intervals, data recorded was:

input pressure;
input temperature;
output pressure;
output temperature;
ambient pressure;
ambient temperature;
SQA case temperature;
mass flow rate from the condenser.

Using this data along with Equation D.1 and Equation D.2 the dryness fraction (x) for each speed step was calculated.

D.6.1 Uni-flow expander with a solenoid valve

Additionally, for the uni-flow SQA tests a plenum chamber had to be inserted between the expander exhaust and the SQA inlet. This was because the pulsing observed by the pressure wave, from the expander exhaust, seemed to affect the SQA in such a way that it was difficult to get a good temperature difference across the SQA device. Once the plenum chamber had been attached, the pulsing was still observed, but a good temperature difference was obtained.

The measured and calculated enthalpies are shown in Appendix Table 2. The work, Q, input to the SQA was 96.8 watts.

Speed (rpm)	**Mass flow rate (g/s)**	**ΔT (deg C)**	**Q_{loss} (watts)**	**h_2 (kJ/kg)**	**h_1 (kJ/kg)**	**T_2 (deg C)**	**P_2 (bar)**
300	0.435	22.70	35.73	2710.9	2524.1	123.43	2.18
400	0.847	6.75	14.08	2690.2	2589.9	109.39	1.38
500	0.771	7.08	15.10	2692.1	2581.6	110.68	1.43
600	0.958	7.91	17.67	2694.2	2610.9	112.07	1.53

Appendix Table 2 Calculation of inlet enthalpy, h_1, using Equation D.1

Appendix Table 3 shows the resulting dryness fraction *x*.

Speed (rpm)	**h_1 (kJ/kg)**	**h_f (kJ/kg)**	**h_g (kJ/kg)**	**x**
300	2524.1	518.38	2710.9	0.9148
400	2589.9	458.81	2690.2	0.9551
500	2581.6	464.23	2692.1	0.9504
600	2610.9	470.15	2694.2	0.9625

Appendix Table 3 Calculation of dryness fraction, *x*, using Equation D.2

The dryness fraction shows the amount of vapor contained in the steam; the values in the table are all above 91% so the steam was of good quality. The dryness factor was used in Section 3.4.7.2 to calculate the isentropic efficiency.

D.6.2 Rotary expander with a solenoid valve

The measured and calculated enthalpies are shown in Appendix Table 4. The work, Q, input to the SQA was 72 watts.

Speed (rpm)	Mass flow rate (g/s)	ΔT (deg C)	Q_{loss} (watts)	h_2 (kJ/kg)	h_1 (kJ/kg)	T_2 (deg C)	P_2 (bar)
200	0.810	3.9126	5.30	2686.0	2633.0	106.69	1.25
300	0.900	2.8811	2.10	2682.9	2616.7	104.71	1.16
400	1.092	1.6887	1.58	2680.6	2629.8	103.21	1.12
500	1.370	1.0888	1.20	2680.2	2645.4	102.94	1.10

Appendix Table 4 Calculation of inlet enthalpy, h_1, using Equation D.1

Appendix Table 5 shows the resulting dryness fraction *x*.

Speed (rpm)	h_1 (kJ/kg)	h_f (kJ/kg)	h_g (kJ/kg)	x
200	2633.0	447.4	2686.0	0.976
300	2616.7	438.9	2682.9	0.971
400	2629.8	432.6	2680.6	0.977
500	2645.4	431.5	2680.2	0.985

Appendix Table 5 Calculation of dryness fraction, *x*, using Equation D.2

The dryness fraction shows the amount of vapor contained in the steam; the values in the table are all above 96% so the steam was of good quality.

Appendix E: Expander test results using nitrogen

This appendix contains the results for testing the expander configurations with 10 and 15 bar nitrogen, as referred to in Section 3.4.

E.1 Rotary expander with port valves

The results contained in this section are for the rotary configuration illustrated in Figure 3-2, Section 3.2.1. For this configuration the rotary expander was equipped with ports that create fixed inlet and exhaust timings.

Speed steps (rpm) for these tests were 100, 200, 300, 500, 700, 900, 1100, 1300, 1700, 2000 and 2300 (maximum). Appendix figure 21 shows the variation of specific power and torque over speed.

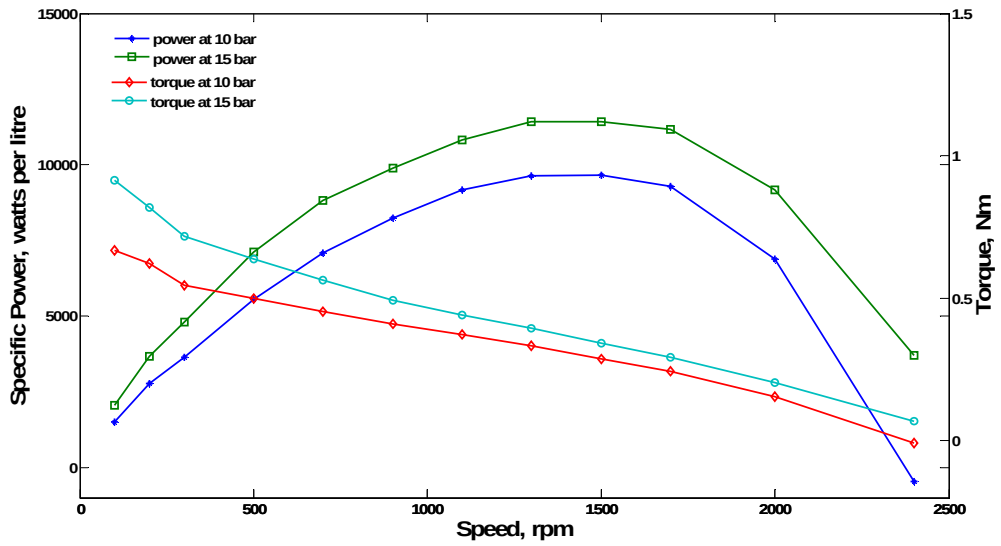

Appendix figure 21 Specific power and torque, rotary expander, 10 bar and 15 bar compressed nitrogen

As can be seen from Appendix figure 21, higher torques and specific power were recorded at the higher pressure setting, maximum torque for both pressures was obtained at 100 rpm, and maximum specific power occurred at 1500 rpm, maximum speed was

2300 rpm for this configuration. Appendix figure 22 shows the variation in pressure over two crank shaft rotations with 10 bar nitrogen.

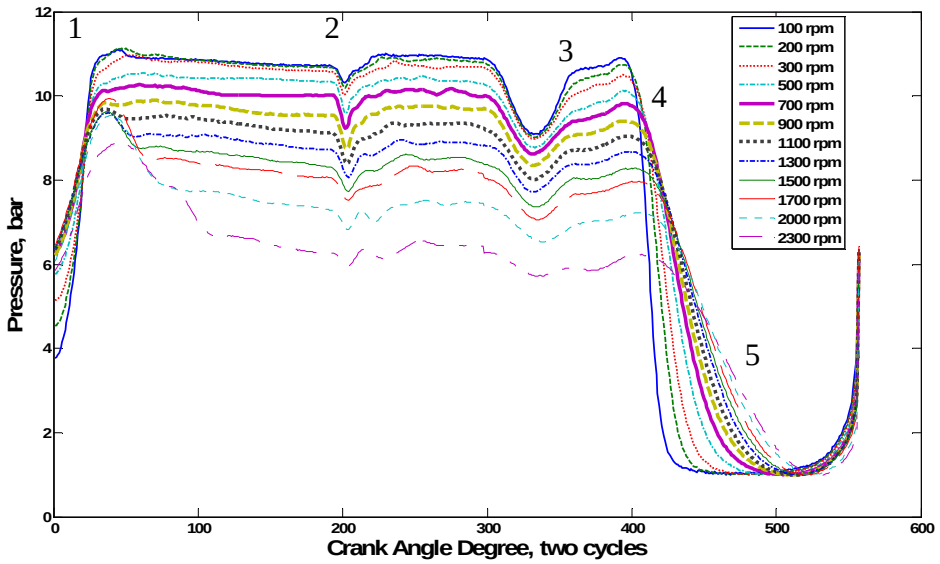

Appendix figure 22 Pressure over two cycles, rotary expander, 10 bar nitrogen, with two pressure sensors

The pressure data is explained as follows:

1. Inlet port opened, pressure rises to maximum pressure;
2. Pressure held at maximum pressure whilst inlet is closed, dip represents rotor tip going past sensor;
3. Some expansion seen before the volume starts to decrease causing compression;
4. Inlet port is closed at the same time the exhaust port is opened and pressure drops to atmospheric pressure;
5. Slight rise in pressure here is due to some compression in the chamber as the volume decreases just before the inlet is opened in the next cycle.

Appendix figure 23 shows the variation in pressure over two crank shaft rotations with 15 bar steam.

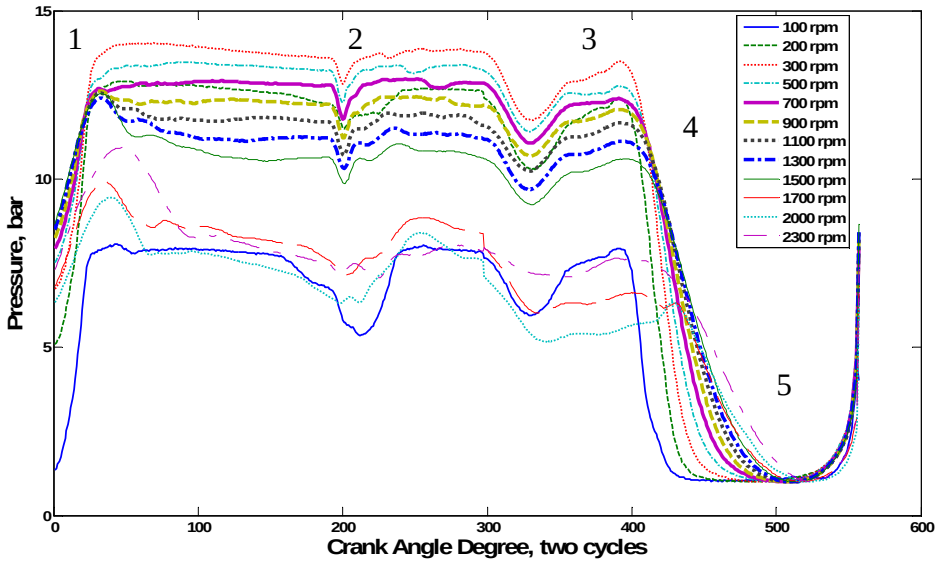

Appendix figure 23 Pressure over two cycles, rotary expander, 15 bar nitrogen, with two pressure sensors

At this high pressure, the expander did not cope well with the minimum speed of 100 rpm, this was due to the pressure forcing the expander to go faster than the dynamometer motor speed, and this caused the shaft rotation to be irregular as the dynamometer motor competed with the expander. This meant that the data acquired, which was driven by the optical shaft encoder was also irregular and could not be used. With the higher speeds, above 1500 rpm, the expander struggles to perform; this explains why the specific power decreased at higher speeds.

The pressure data is explained as follows:

1. Inlet port opened, pressure rises to maximum pressure;
2. Pressure held at maximum pressure whilst inlet is closed, dip represents rotor tip going past sensor;
3. Some expansion seen before the volume starts to decrease causing compression;
4. Inlet port is closed at the same time the exhaust port is opened and pressure drops to atmospheric pressure;

5. Slight rise in pressure here is due to some compression in the chamber as the volume decreases just before the inlet is opened in the next cycle.

Appendix figure 24 shows the pressure volume diagram using 10 bar nitrogen for each speed step.

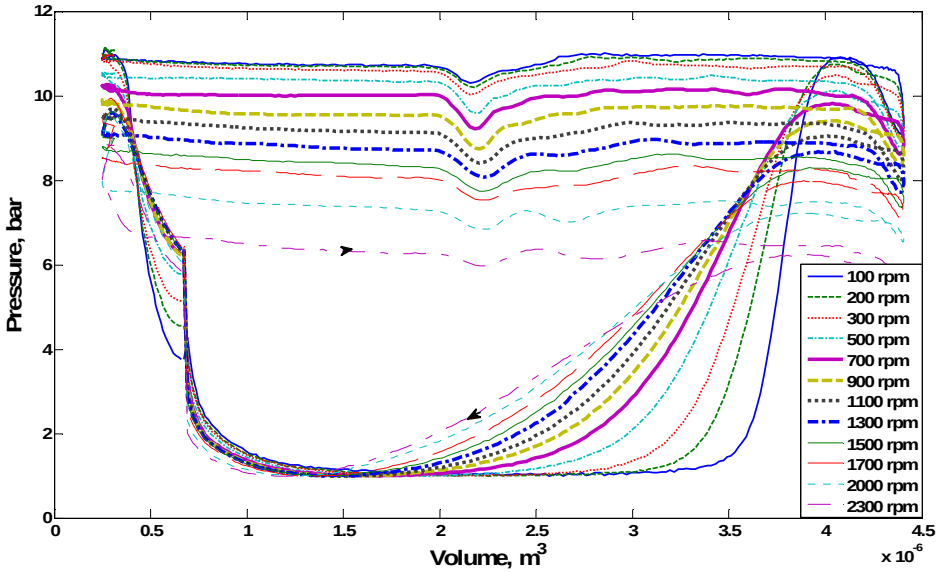

Appendix figure 24 P-v diagram, rotary expander, 10 bar nitrogen, with two pressure sensors

Appendix figure 25 shows the pressure volume diagram using 15 bar nitrogen for each speed step.

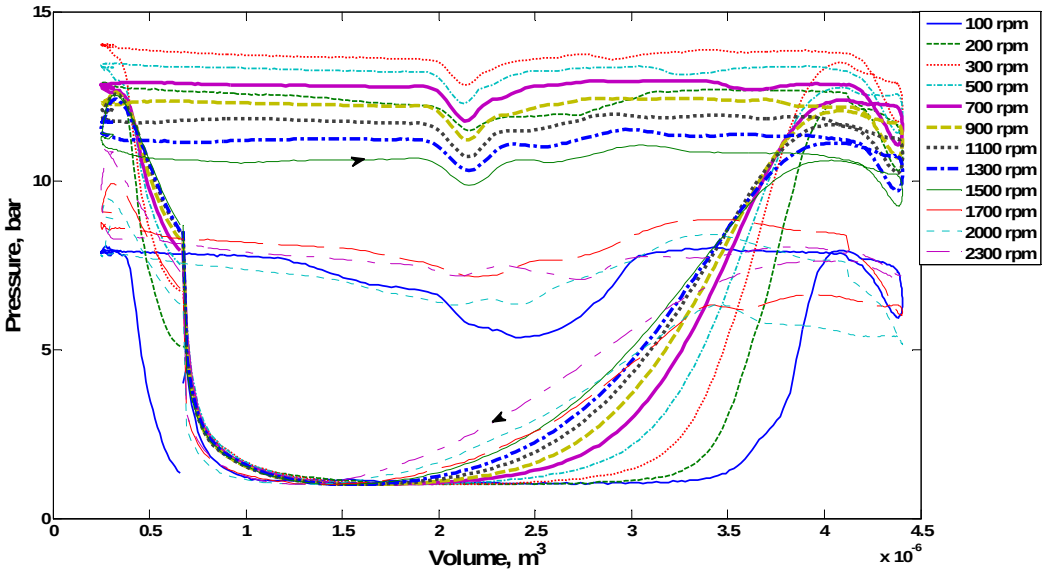

Appendix figure 25 P-v diagram, rotary expander, 15 bar nitrogen, with two pressure sensors

The comparisons between calculated torque (using Equation 3.2, Section 3.4.1) and measured torque are shown in Appendix Table 6 and Appendix Table 7.

Speed (rpm)	Measured Torque (N m)	Calculated Torque (N m)	Percentage Difference
100	0.6669	0.5449	-22.39
300	0.5449	0.5234	-4.11
500	0.4979	0.4686	-6.25
700	0.4529	0.4181	-8.32

Appendix Table 6 Comparison of measured torque and calculated torque, 10 bar nitrogen

Speed (rpm)	Measured Torque (N m)	Calculated Torque (N m)	Percentage Difference
100	0.9139	0.9115	-0.26
300	0.7172	0.7125	-0.66
500	0.6385	0.7247	+11.89
700	0.5641	0.6569	+14.13

Appendix Table 7 Comparison of measured torque and calculated torque, 15 bar nitrogen

The comparison of calculated and measured torque gives reasonable results (within ±5%) for some speed steps, but not others, this could be due to the fact that the pressure data is made up of data from two separate sensors and hence is not always reliable.

E.2 Uni-flow expander with an injector valve

The results contained in this section are for the uni-flow expander in uni-flow configuration using injector valves to control the inlet.

Speed steps (rpm) for these tests were 200, 300, 500, 700, 900, 1100, 1300, 1700, 2000 and 2300 (maximum). Appendix figure 26 shows the variation of specific power and torque over speed.

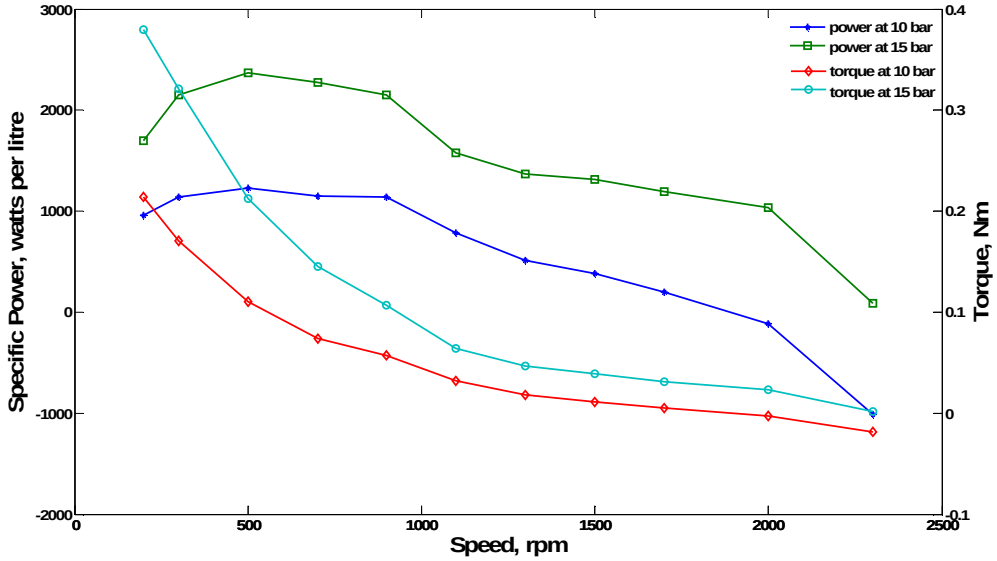

Appendix figure 26 Specific power and torque, uni-flow expander, 10 bar and 15 bar compressed nitrogen

As can be seen from Appendix figure 26, higher torques and specific power were recorded at the higher pressure setting, maximum torque for both pressures was obtained at 200 rpm, and maximum specific power occurred at 500 rpm, maximum speed was 2300 rpm for this configuration. Appendix figure 27 shows the variation in pressure over one crank shaft rotation with 10 bar nitrogen.

Appendix E: Expander test results using nitrogen

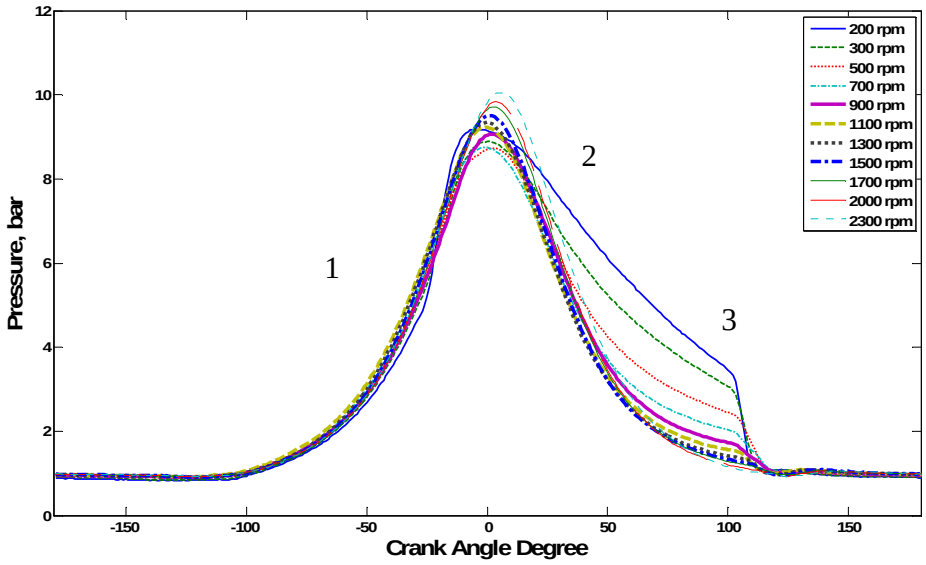

Appendix figure 27 Pressure per cycle, uni-flow expander, 10 bar compressed nitrogen, with injector inlet valve

The pressure data is explained as follows:

1. Inlet injector opens, pressure rises to maximum pressure;
2. Injector closes and expansion occurs;
3. Exhaust port is opened, pressure falls to atmospheric.

Appendix figure 28 shows the variation in pressure over one crank shaft rotation with 15 bar nitrogen.

Appendix E: Expander test results using nitrogen

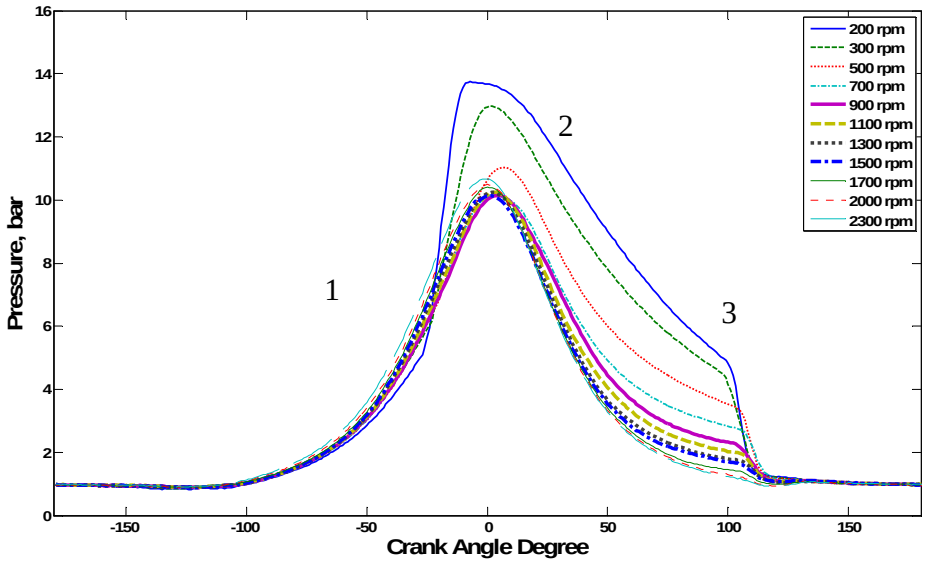

Appendix figure 28 Pressure per cycle, uni-flow expander, 15 bar compressed nitrogen, with injector inlet valve

The pressure data is explained as follows:

1. Inlet injector opens, pressure rises to maximum pressure;
2. Injector closes and expansion occurs;
3. Exhaust port is opened, pressure falls to atmospheric.

Appendix figure 29 shows the pressure volume diagram using 10 bar nitrogen for each speed step.

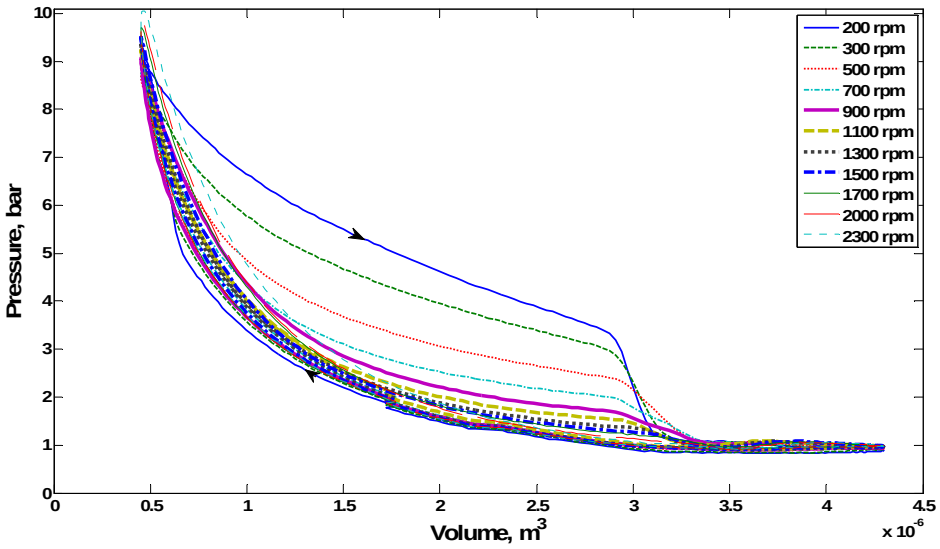

Appendix figure 29 P-v diagram, uni-flow Expander, 10 bar compressed nitrogen, with injector inlet valve

Appendix figure 30 shows the pressure volume diagram using 15 bar nitrogen for each speed step.

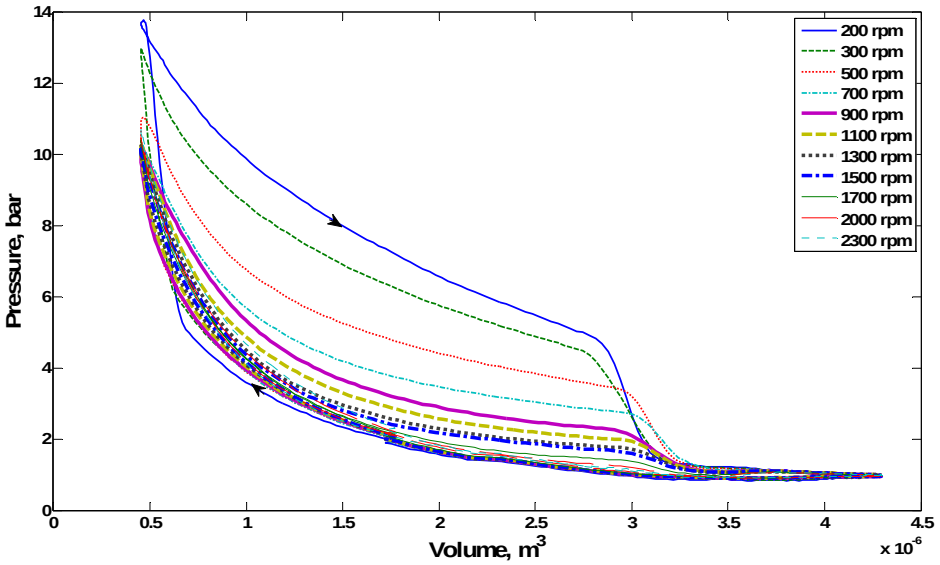

Appendix figure 30 P-v diagram, uni-flow expander, 15 bar compressed nitrogen, with injector inlet valve

The injectors did not perform well; the cross sectional area of the injector holes limited the flow of compressed air resulting in a low power output, as seen in Appendix figure 26.

E.3 Uni-flow expander with a solenoid valve

The results contained in this section are for the uni-flow expander in uni-flow configuration using solenoid valves to control the inlet. Speed steps (rpm) for these tests were 200, 300, 400, 500 and 600 (maximum).

Appendix figure 31 shows the variation of specific power and torque over speed.

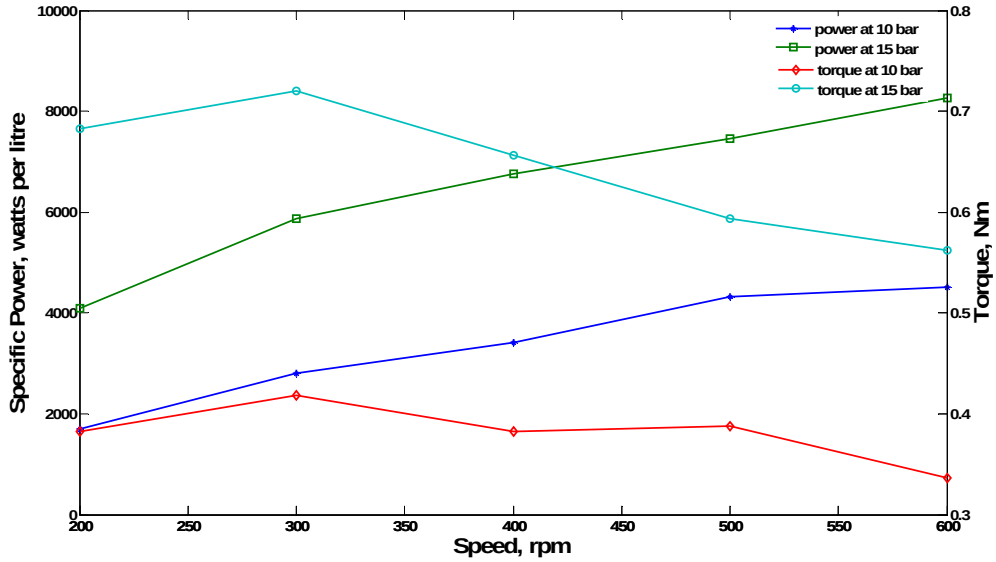

Appendix figure 31 Specific power and torque, uni-flow expander, 10 bar and 15 bar compressed nitrogen

As can be seen from Appendix figure 31, higher torques and specific power were recorded at the higher pressure setting, maximum torque for both pressures was obtained at 300 rpm, and maximum specific power occurred at 600 rpm, maximum speed was 600 rpm for this configuration, again the speed was limited by the use of the solenoid valves. Appendix figure 32 shows the variation in pressure over one crank shaft rotation with 10 bar nitrogen.

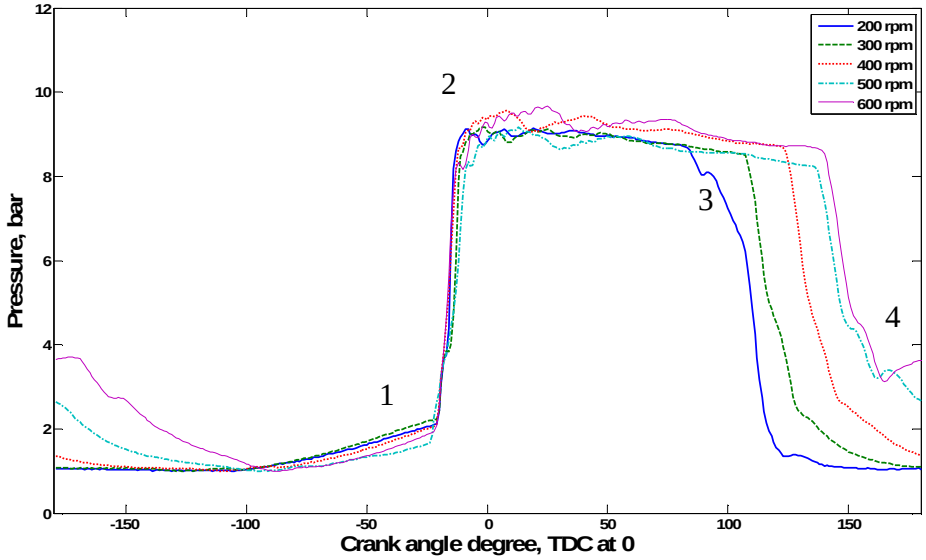

Appendix figure 32 Pressure per cycle, uni-flow expander, 10 bar compressed nitrogen, with solenoid inlet valve

The pressure data is explained as follows:

1. Small compression witnessed as piston rises and volume decreases;
2. Inlet valve opens, pressure rises to maximum pressure;
3. Inlet valve closes, some expansion occurs;
4. Exhaust port is opened, pressure falls to atmospheric.

Appendix figure 33 shows the variation in pressure over one crank shaft rotation with 15 bar nitrogen.

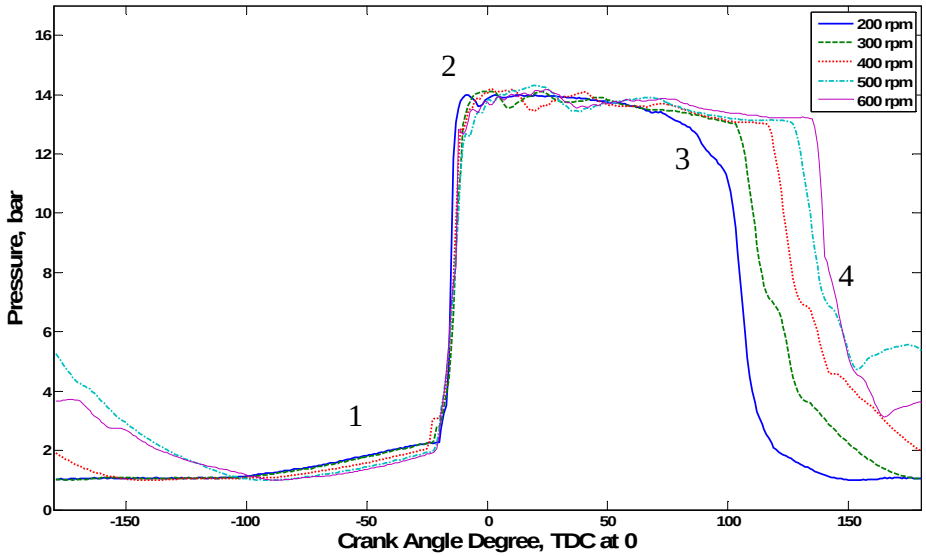

Appendix figure 33 Pressure per cycle, uni-flow expander, 15 bar compressed nitrogen, with solenoid inlet valve

The pressure data is explained as follows:

1. Small compression witnessed as piston rises and volume decreases;
2. Inlet valve opens, pressure rises to maximum pressure;
3. Inlet valve closes, some expansion occurs;
4. Exhaust port is opened, pressure falls to atmospheric.

Appendix figure 34 shows the pressure volume diagram using 10 bar nitrogen for each speed step.

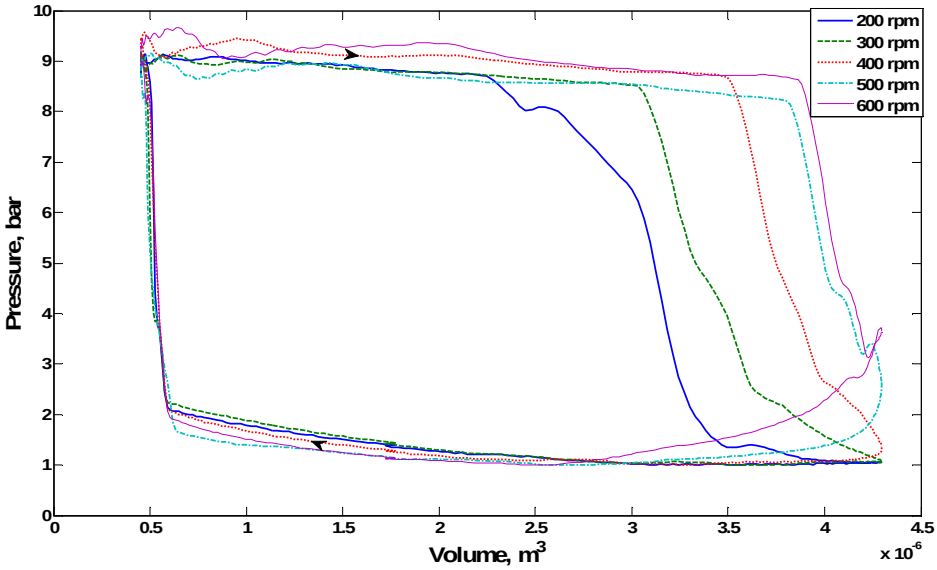

Appendix figure 34 P-v diagram, uni-flow expander, 10 bar compressed nitrogen, with solenoid inlet valve

Appendix figure 35 shows the pressure volume diagram using 15 bar nitrogen for each speed step.

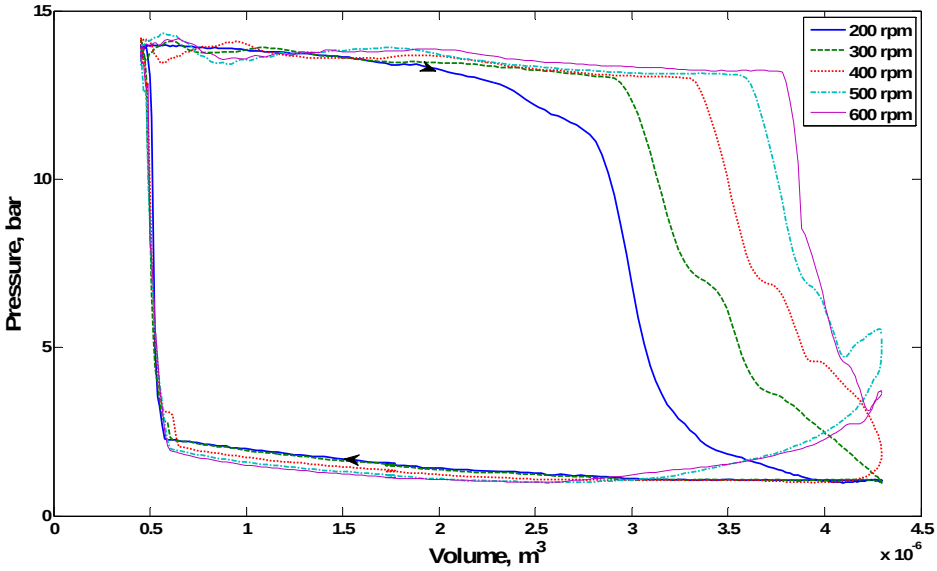

Appendix figure 35 P-v diagram, uni-flow expander, 15 bar compressed nitrogen, with solenoid inlet valve

The comparisons between calculated torque (Equation 3.1, Section 3.4.1) and measured torque are shown in Appendix Table 8 and Appendix Table 9.

Speed (rpm)	Measured Torque (N m)	Calculated Torque (N m)	Percentage Difference
200	0.3826	0.3633	-5.30
300	0.4186	0.4008	-4.45
400	0.3820	0.4559	+16.21
500	0.3876	0.4391	+11.72
600	0.3361	0.4415	+23.87

Appendix Table 8 Comparison of calculated and measured torque, 10 bar nitrogen

Speed (rpm)	Measured Torque (N m)	Calculated Torque (N m)	Percentage Difference
200	0.6826	0.5657	-20.68
300	0.7202	0.6441	-11.82
400	0.6568	0.6969	+5.76
500	0.5935	0.6795	+12.67
600	0.5618	0.7054	+20.35

Appendix Table 9 Comparison of calculated and measured torque, 15 bar nitrogen

As can be seen, the torque comparison is not always within a reasonable ±5%, this could be attributed to the solenoid valves causing the pressure data to be unreliable.

E.4 Counter-flow expander with solenoid valves

The results contained in this section are for the counter-flow expander using solenoid valves to control the inlet and exhaust.

Speed steps (rpm) for these tests were 200, 300, 400 and 500 (maximum). Appendix figure 36 shows the variation of specific power and torque over speed.

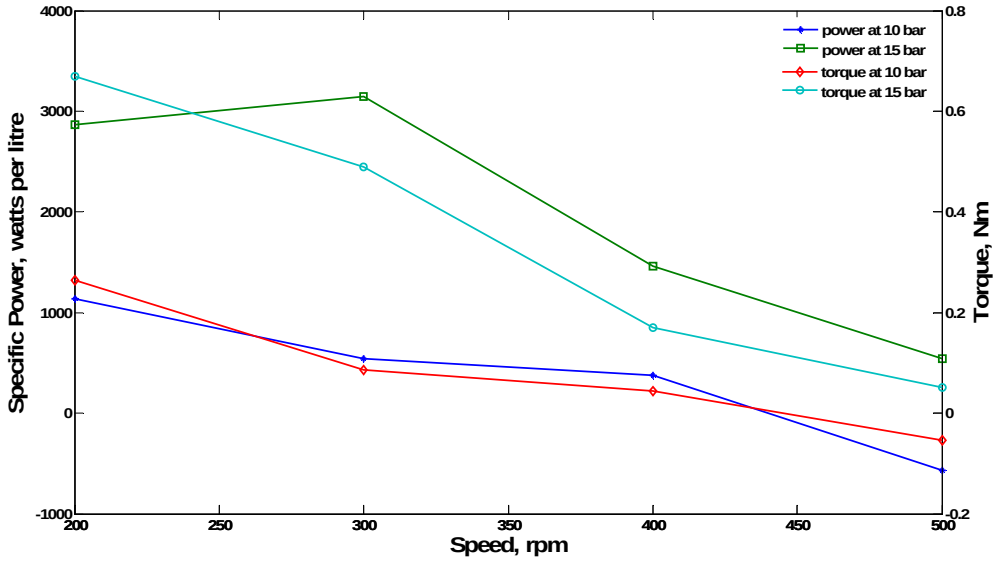

Appendix figure 36 Specific power and torque, counter-flow expander, 10 and 15 bar compressed nitrogen

As can be seen from Appendix figure 36, higher torques and specific power were recorded at the higher pressure setting, maximum torque for both pressures was obtained at 200 rpm, and maximum specific power occurred at 200 rpm for 10 bar and 300 rpm for 15 bar. Maximum speed was 500 rpm for this configuration; again the speed was limited by the use of the solenoid valves. Appendix figure 37 shows the variation in pressure over one crank shaft rotation with 10 bar nitrogen.

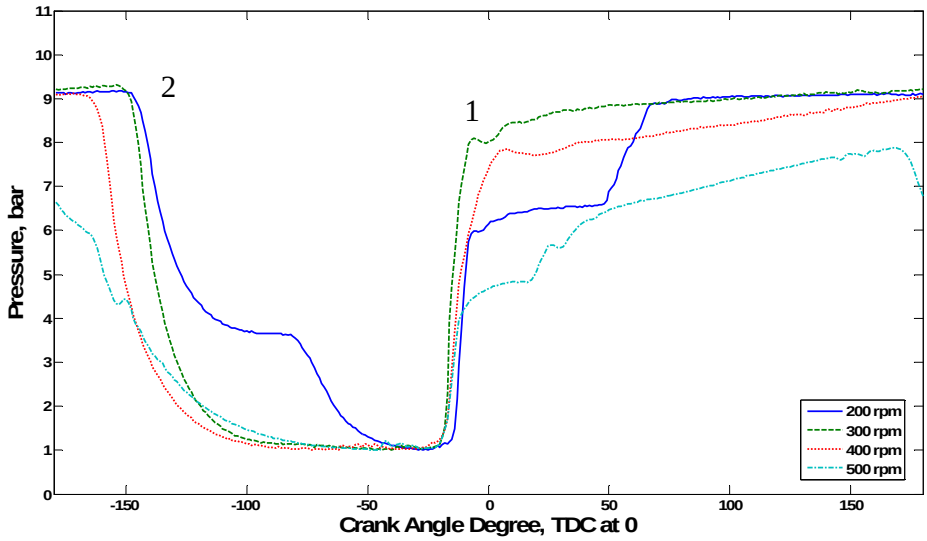

Appendix figure 37 Pressure per cycle, counter-flow expander, 10 bar compressed nitrogen

The pressure data is explained as follows:

1. Inlet valve opens, pressure rises to maximum pressure;
2. Exhaust port is opened, pressure falls to atmospheric, and no expansion is experienced.

Appendix figure 38 shows the variation in pressure over one crank shaft rotation with 15 bar nitrogen.

Appendix E: Expander test results using nitrogen

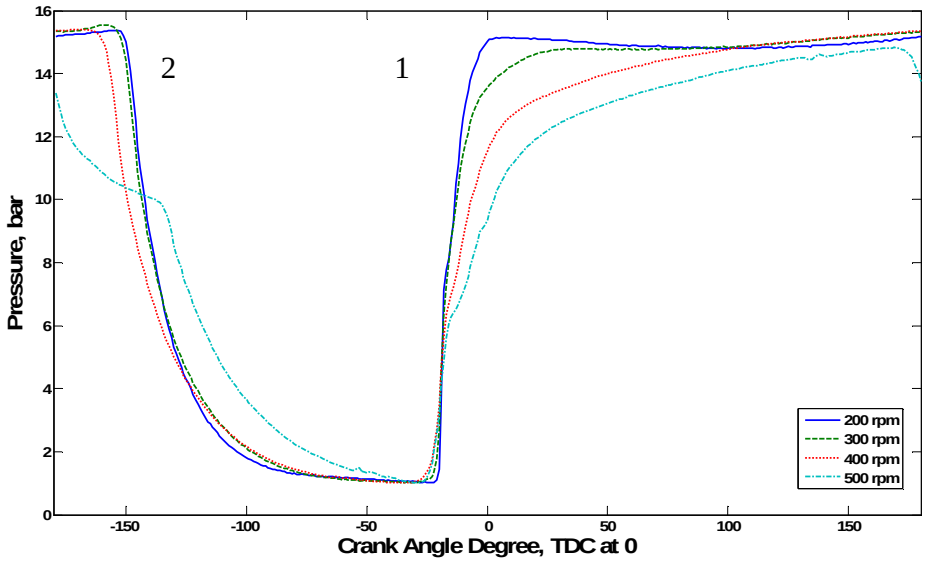

Appendix figure 38 Pressure per cycle, counter-flow expander, 15 bar compressed nitrogen

The pressure data is explained as follows:

1. Inlet valve opens, pressure rises to maximum pressure;
2. Exhaust port is opened, pressure falls to atmospheric, and no expansion is experienced.

Appendix figure 39 shows the pressure volume diagram using 10 bar nitrogen for each speed step.

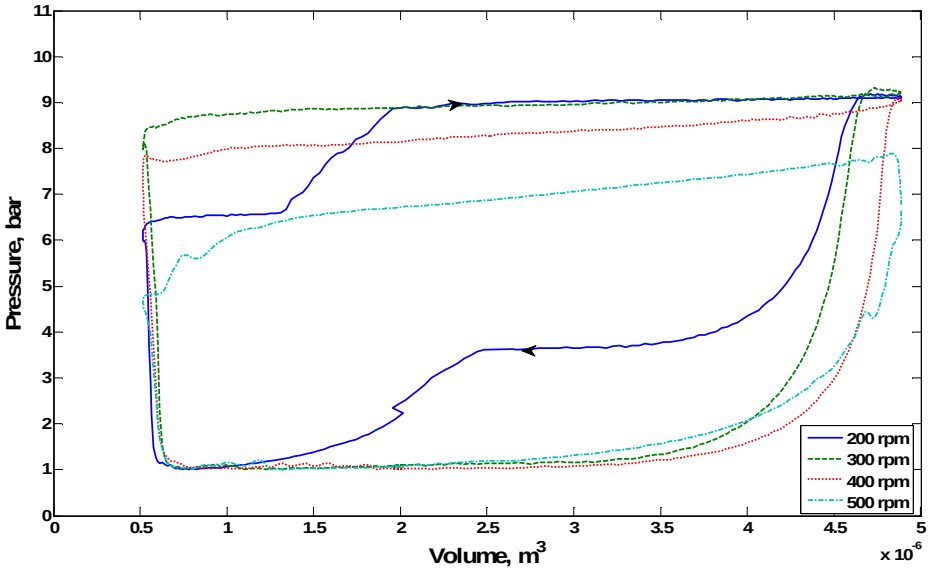

Appendix figure 39 P-v diagram, counter-flow expander, 10 bar compressed nitrogen

Appendix figure 40 shows the pressure volume diagram using 15 bar nitrogen for each speed step.

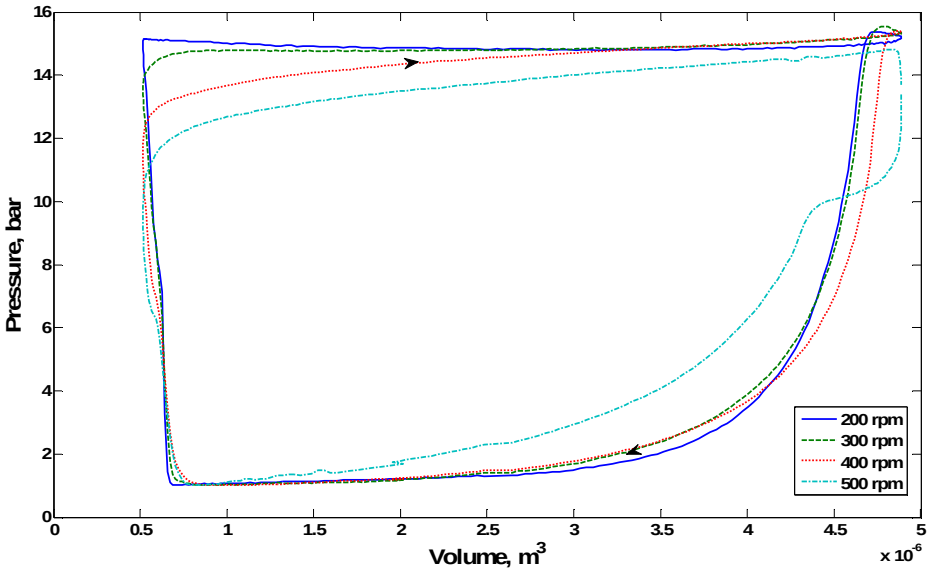

Appendix figure 40 P-v diagram, counter-flow expander, 15 bar compressed nitrogen

The comparisons between calculated torque (Equation 3.1, Section 3.4.1) and measured torque are shown in Appendix Table 10 and Appendix Table 11.

Speed (rpm)	Measured Torque (N m)	Calculated Torque (N m)	Percentage Difference
150	0.3227	0.2146	-50.36
200	0.2648	0.3638	+27.20
300	0.0851	0.3724	+77.15
400	0.0438	0.2814	+84.42
500	-0.0533	0.3061	+117.43

Appendix Table 10 Comparison of calculated and measured torque, 10 bar nitrogen

Speed (rpm)	Measured Torque (N m)	Calculated Torque (N m)	Percentage Difference
300	0.6705	0.6368	-5.29
400	0.4903	0.6225	+21.23
500	0.1702	0.6182	+72.47
600	0.0509	0.5039	+89.89

Appendix Table 11 Comparison of calculated and measured torque, 15 bar nitrogen

As can be seen, the torque comparison is not always within a reasonable ±5%, this could be attributed to the solenoid valves causing the pressure data to be unreliable. As the counter-flow configuration uses the solenoid valves on both inlet and outlet, this doubles the possible problems when compared to the uni-flow; this could explain why the values are so different for some speed steps.

E.5 Rotary expander with solenoid valves

The results contained in this section are for the rotary configuration illustrated in Figure 3-3; Section 3.2.1, in this configuration the rotary expander is equipped with solenoid valves on the inlet to make the inlet timing variable and fixed ports for the exhaust.

Speed steps (rpm) for these tests were 150, 200, 300, 400, 500 and 600 (maximum). Appendix figure 41 shows the variation of specific power and torque over speed.

Appendix E: Expander test results using nitrogen

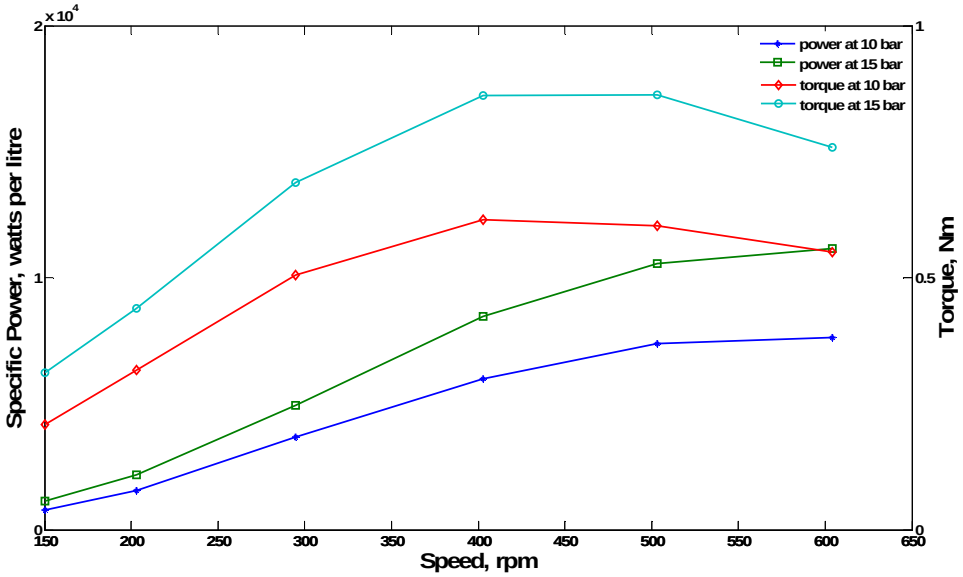

Appendix figure 41 Specific power and torque, rotary expander, 10 and 15 bar compressed nitrogen

As can be seen from Appendix figure 41, higher torques and specific power were recorded at the higher pressure setting, maximum torque for both pressures was obtained at 400 rpm, and maximum specific power occurred at 600 rpm. Maximum speed was 600 rpm for this configuration; again the speed is limited by the use of the solenoid valves. Appendix figure 42 shows the variation in pressure over one crank shaft rotation with 10 bar nitrogen.

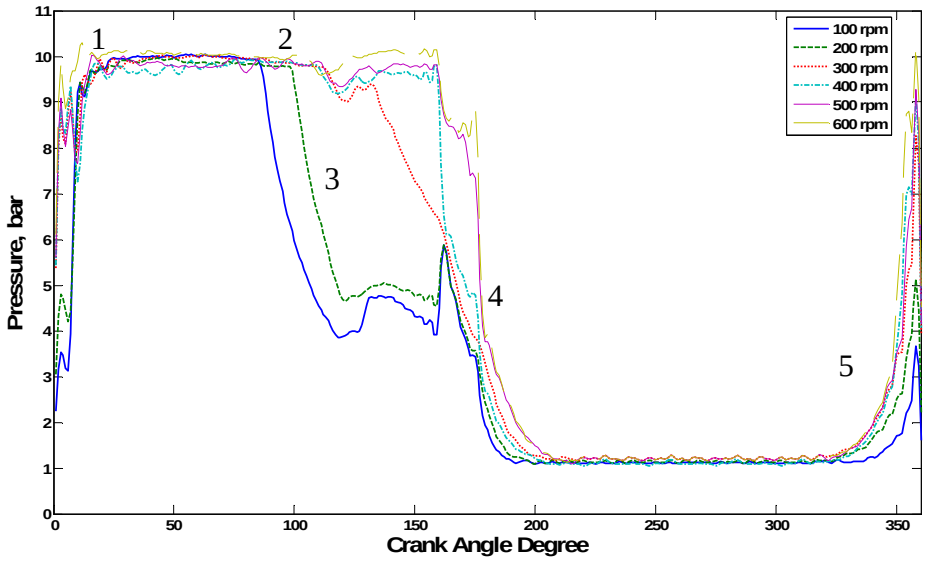

Appendix figure 42 Pressure per cycle, rotary expander, 10 bar compressed nitrogen

The pressure data is explained as follows:

1. Inlet valve opens, pressure rises to maximum pressure;
2. Inlet valve closes;
3. Some expansion seen, note no expansion seen for 500 rpm or 600 rpm;
4. Exhaust port is opened and pressure drops to atmospheric pressure;
5. Slight rise in pressure here is due to some compression in the chamber as the volume decreases just before the inlet valve opens for the next cycle.

Appendix figure 43 shows the variation in pressure over one crank shaft rotation with 15 bar nitrogen.

Appendix E: Expander test results using nitrogen

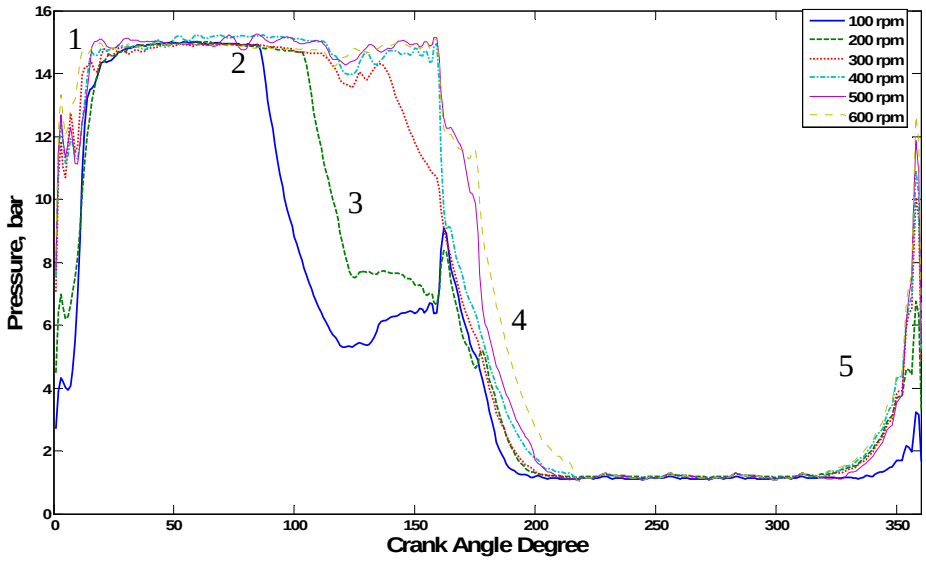

Appendix figure 43 Pressure per cycle, rotary expander, 15 bar compressed nitrogen

The pressure data is explained as follows:

1. Inlet valve opens, pressure rises to maximum pressure;
2. Inlet valve closes;
3. Some expansion seen, note no expansion seen for 500 rpm or 600 rpm;
4. Exhaust port is opened and pressure drops to atmospheric pressure;
5. Slight rise in pressure here is due to some compression in the chamber as the volume decreases just before the inlet valve opens for the next cycle.

Appendix figure 44 shows the pressure volume diagram using 10 bar nitrogen for each speed step.

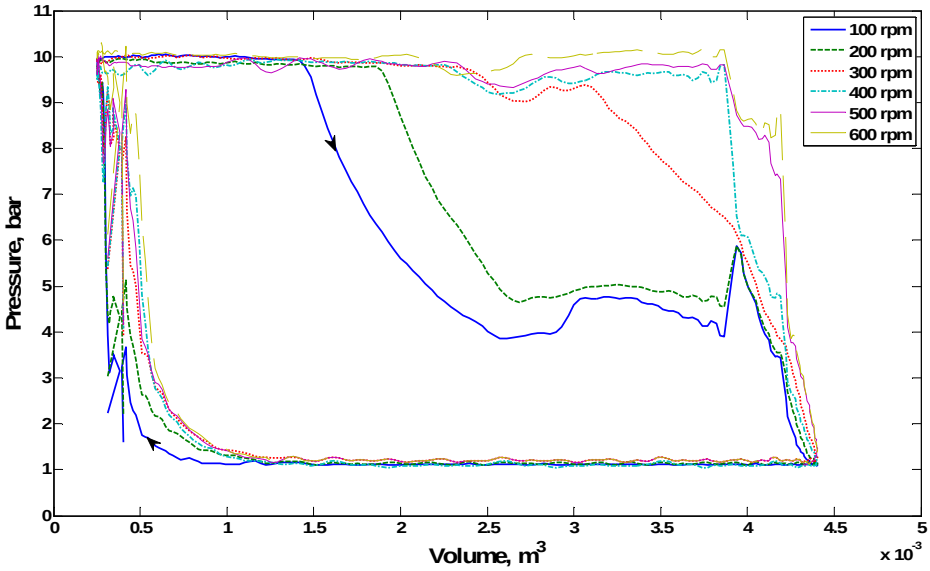

Appendix figure 44 P-v diagram, rotary expander, 10 bar compressed nitrogen

Appendix figure 45 shows the pressure volume diagram using 15 bar nitrogen for each speed step.

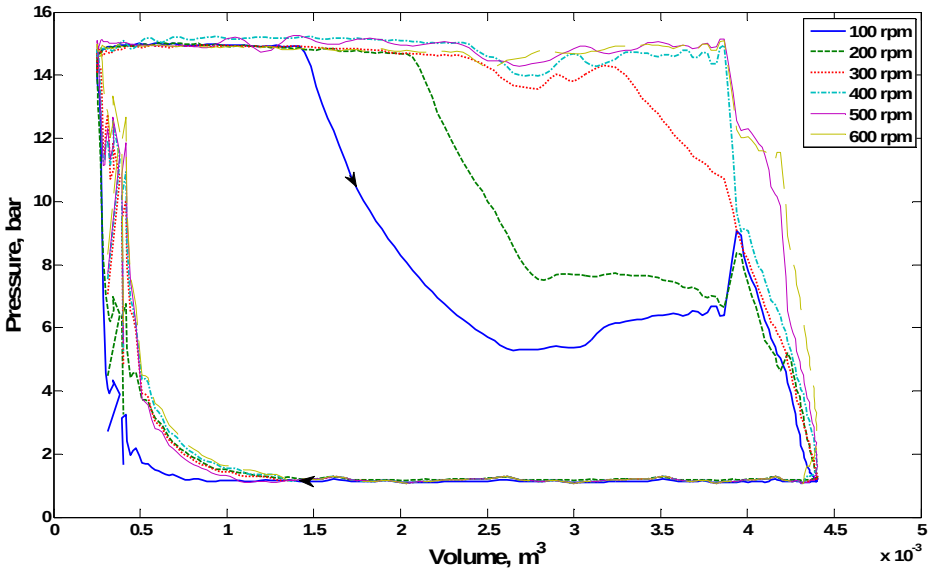

Appendix figure 45 P-v diagram, rotary expander, 15 bar compressed nitrogen

The comparisons between calculated torque (Equation 3.2, Section 3.4.1) and measured torque are shown in Appendix Table 12 and Appendix Table 13.

Speed (rpm)	Measured Torque (N m)	Calculated Torque (N m)	Percentage Difference
100	0.2080	0.2565	+18.91
200	0.3176	0.3205	+0.91
300	0.5055	0.5156	+1.96
400	0.6147	0.5912	-3.98
500	0.6034	0.6591	+8.45
600	0.5501	0.6513	+15.54

Appendix Table 12 Comparison of measured torque and calculated torque, 10 bar nitrogen

Speed (rpm)	Measured Torque (N m)	Calculated Torque (N m)	Percentage Difference
100	0.3113	0.3112	-0.03
200	0.4382	0.4500	+2.62
300	0.6879	0.7106	+3.19
400	0.8608	0.8162	-5.46
500	0.8625	0.9251	+6.77
600	0.7575	0.8991	+15.75

Appendix Table 13 Comparison of measured torque and calculated torque, 15 bar nitrogen

The torque comparisons shown in these tables are nearly all within a reasonable ±5%, the steps that do not fall within the ±5% value could be due to the solenoid valves operating near there tolerated limit for speed.

E.6 Specific power and torque

This section presents a summary of the maximum specific power and torque measurements for each expander test. This can be seen in Appendix Table 14.

Expander configuration	Specific Torque (N m / litre)	Specific Power (kW / litre)
Uni-flow, 10 bar, injector	45.7	1.48
Uni-flow, 15 bar, injector	80.9	2.80
Uni-flow, 10 bar, solenoid valve	89.3	4.50
Uni-flow, 15 bar, solenoid valve	153.6	8.30
Rotary, 10 bar, port valves	138.6	10.54
Rotary, 15 bar, port valves	185.1	12.47
Rotary,10 bar, solenoid valves	142.9	7.64
Rotary,15 bar, solenoid valves	200.6	11.14
Counter-flow, 10 bar, solenoid valves	65.9	1.13
Counter-flow, 15 bar, solenoid valves	156.2	3.15

Appendix Table 14 Maximum specific torque and power results for nitrogen tests

The specific torque was quite high and the specific power is good, this is as expected for an expander configuration.

E.7 Mass flow rates and efficiencies

Appendix Table 15 shows the maximum calculated mass flow rate of nitrogen, for each of the expander configurations, with explanatory notes where necessary.

Expander configuration	Speed (rpm)	Mass flow rate (kg/s)	Note
Uni-flow with injector valves, 10 bar	600	0.24e-3	2
Uni-flow with injector valves, 15 bar	600	0.36e-3	2
Uni-flow with solenoid valves, 10 bar	600	0.48e-3	1
Uni-flow with solenoid valves, 15 bar	600	0.72e-3	1
Rotary with port valves, 10 bar	2000	3.48e-3	1 and 3
Rotary with port valves, 15 bar	2000	5.22e-3	1 and 3
Rotary with solenoid valves, 10 bar	500	0.29e-3	4
Rotary with solenoid valves, 15 bar	500	0.44e-3	4

Appendix Table 15 Maximum mass flow rates for nitrogen tests

Note 1 – Calculation takes the theoretical mass flow rate (meters cubed x revs per second) and multiplies it by the density of the source at appropriate pressure. This is sometimes referred to as the speed density method and is detailed in the following example:

Meters cubed for uni-flow = 4.3 x 10e-6

Theoretical mass flow rate at 600 rpm = 600/60 x 0.000043

= 0.00043 kg/s

Nitrogen density at 10 bar = pressure/ (gas constant x temperature in)

= 1000000 / (296.8 x 303)

= 11.1197 (kg/m^3)

Mass flow rate = 11.1197 x 0.00043 = 0.004781 kg/s

Note 2 – Mass flow rate with injectors is approximately half of mass flow rate with solenoid valves.

Note 3 –The rotary mass flow rate is multiplied by 2 to account for the configuration of two inlets and two exhausts.

Note 4 – Rotary with solenoids cuts down the opening time by approximately a third, hence this value is the without solenoids value divided by 3.

Appendix Table 16 shows the maximum power and the calculated efficiency for each expander configuration using compressed nitrogen.

Expander configuration	**Actual Maximum Power (W)**	**Isentropic efficiency (%)**
Uni-flow, 10 bar, injector	6.96	25.30
Uni-flow, 15 bar, injector	13.16	27.52
Uni-flow, 10 bar, solenoid valve	21.12	36.70
Uni-flow, 15 bar, solenoid valve	38.76	40.53
Rotary, 10 bar, port valves	45.30	11.86
Rotary, 15 bar, port valves	53.62	10.30
Rotary,10 bar, solenoid valves	32.83	21.49
Rotary,15 bar, solenoid valves	47.91	23.03

Appendix Table 16 Efficiencies for nitrogen tests

As can be seen, the rotary expander with control valves on the inlet doubles the efficiency than when no control valves were utilised. The best results are for the uni-flow expander and rotary expander tests with the solenoid valves, this is expected as the nitrogen mass flow is better controlled.

Appendix F: Counter-flow expander description and test results using steam

Due to the counter-flow expander not performing as well as the uni-flow and rotary expanders, the configuration is described and the test results are presented in this appendix, as referenced in Section 3.2.

F.1 Counter-flow configuration

The expander used for the counter-flow tests was a 4.89 cc four-stroke reciprocating expander in a counter-flow configuration. Initially the inlet and exhaust were controlled by injector valves; these were later replaced by a solenoid valves to improve the mass flow rate. The configuration and flow is shown in Appendix figure 46.

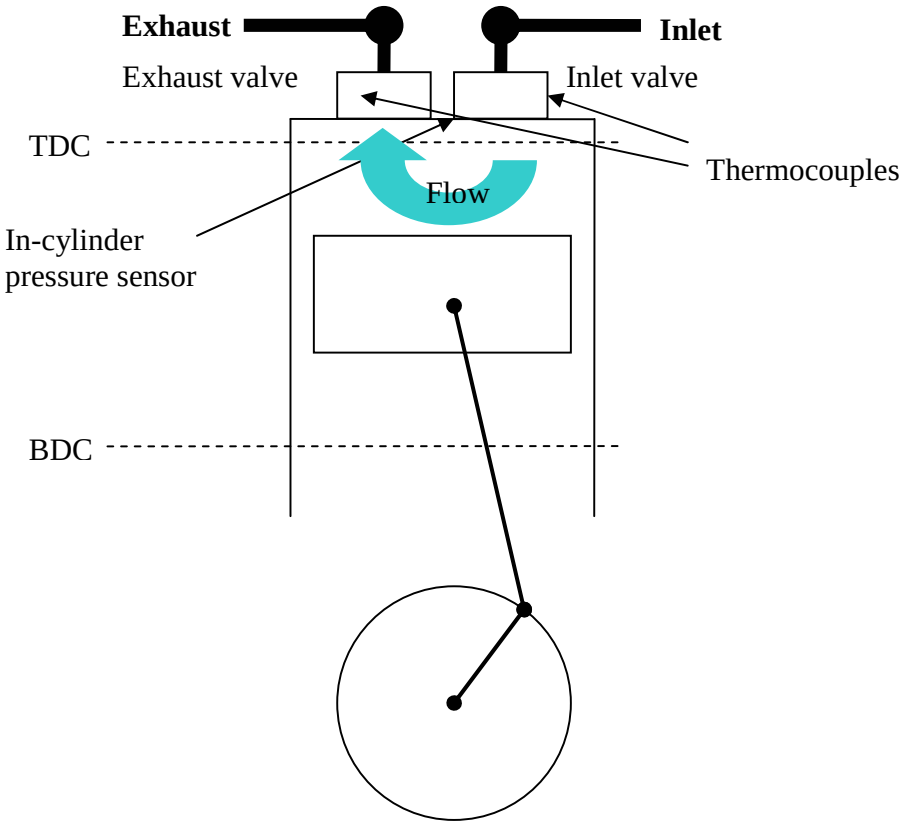

Appendix figure 46 Outline of the counter-flow expander and sensors

For the counter-flow configuration, both the inlet and exhaust opening times were controlled using the counters on the DAQ cards. The inlet and exhaust valve opening times were optimized for each speed step as previously described for the uni-flow expander. The inlet and exhaust results are shown in Appendix Table 17 and Appendix Table 18, respectively, Top Dead Centre (TDC) is assumed at 0°.

Speed (rpm)	**10 bar Steam**		**10 bar Nitrogen**		**15 bar Nitrogen**	
	Open before TDC	**Closed after TDC**	**Open before TDC**	**Closed after TDC**	**Open before TDC**	**Closed after TDC**
150	9	119	29	91	-	-
200	1	79	15	65	14	71
300	1	51	10	50	9	56
400	3	41	8	42	7	48
500	4	36	7	38	4	46

Appendix Table 17 Timings for the counter-flow expander inlet, in crank angle degrees

Speed (rpm)	**10 bar Steam**		**10 bar Nitrogen**		**15 bar Nitrogen**	
	Open before TDC	**Closed after TDC**	**Open before TDC**	**Closed after TDC**	**Open before TDC**	**Closed after TDC**
150	150	240	150	240	-	-
200	90	250	90	250	85	170
300	60	140	60	140	70	200
400	51	116	50	115	55	165
500	45	85	45	85	50	150

Appendix Table 18 Timings for the counter-flow expander exhaust, in crank angle degrees

The data shown in Appendix Table 17 and Appendix Table 18 can be visualised by in the example timing diagram as shown in Appendix figure 47.

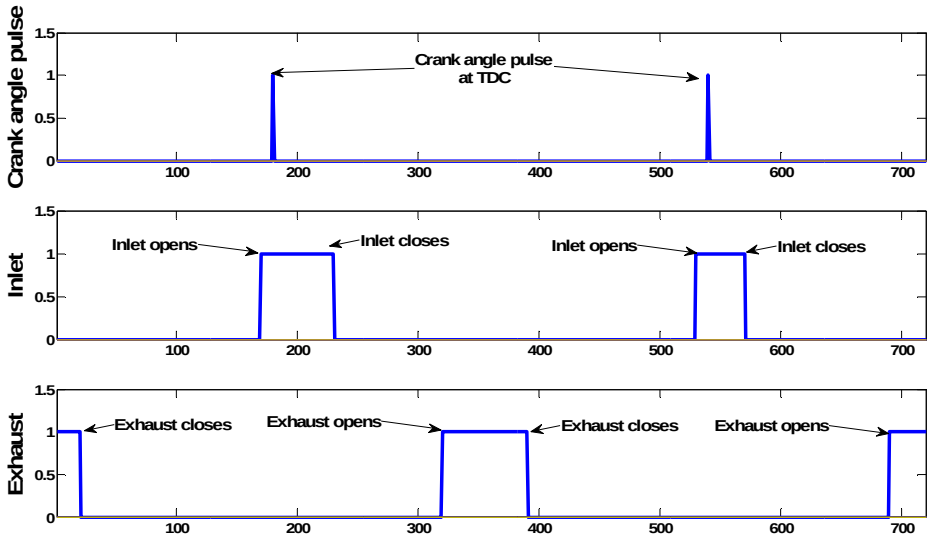

Appendix figure 47 TDC, inlet valve and outlet valve pulse shown over two revolutions

The top graph shows the one pulse per crank shaft revolution, the second graph shows the inlet pulse, the rising edge indicates the opening of the inlet and the pulse width indicates the opening time. The third graph represents the exhaust valve pulse, again the rising edge indicates the opening of the exhaust and the pulse width indicates the exhaust opening time.

F.2 Counter-flow expander test results

The results contained in this section are for the counter-flow expander using solenoid valves to control the inlet and exhaust.

Speed steps (rpm) for these tests were 200, 300, 400, 500 and 600 (maximum). Appendix figure 48 shows the variation of specific power and torque over speed.

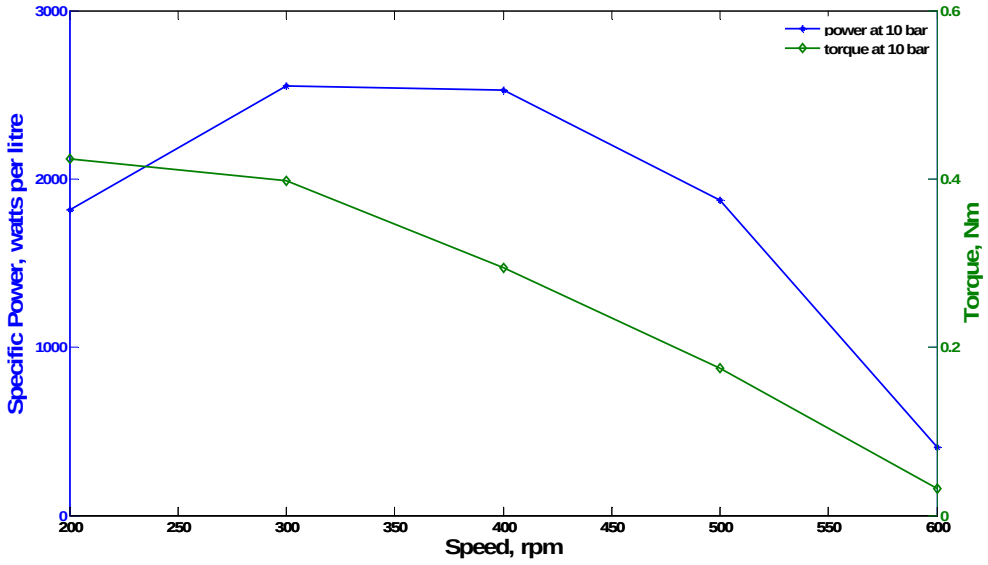

Appendix figure 48 Specific power and torque, counter-flow expander, 10 bar steam

As can be seen from Appendix figure 48, maximum torque was obtained at 200 rpm, and maximum specific power occurred at 300 rpm, maximum speed was 600 rpm for this configuration, limited by the use of the solenoid valves. Appendix figure 49 shows the variation in pressure over one crank shaft rotation with 10 bar steam.

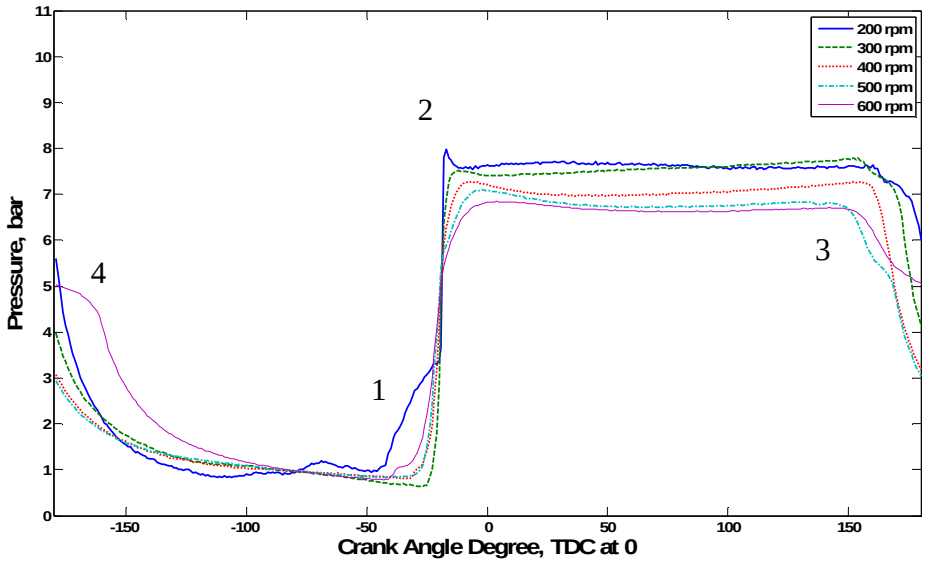

Appendix figure 49 Pressure per cycle, counter-flow expander, 10 bar steam

The pressure data is explained as follows:

1. Small compression witnessed as piston rises and volume decreases;
2. Inlet valve opens, pressure rises to boiler pressure;
3. Inlet valve closes, some expansion occurs;
4. Exhaust port is opened, pressure falls to atmospheric.

Appendix figure 50 shows the pressure volume diagram using 10 bar steam for each speed step.

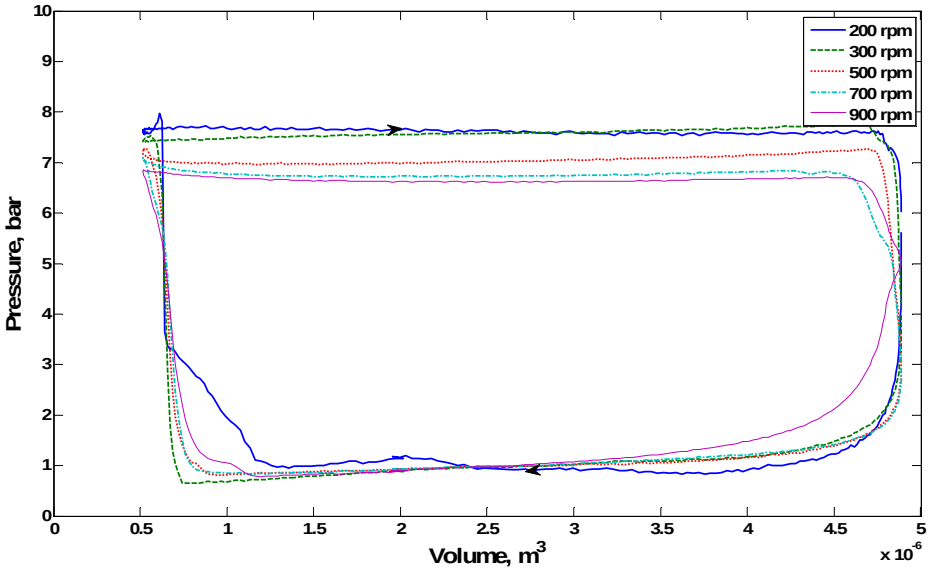

Appendix figure 50 P-v diagram, counter-flow expander, 10 bar steam

The comparison between calculated torque (Equation 3.1, Section 3.4.1) and measured torque is shown in Appendix Table 19.

Speed (rpm)	Measured Torque (N m)	Calculated Torque (N m)	Percentage Difference
200	0.4242	0.4253	+0.24
300	0.3977	0.4244	+6.29
400	0.2948	0.3958	+25.53
500	0.1750	0.3753	+53.50
600	0.0314	0.3291	+90.46

Appendix Table 19 Comparison of calculated and measured torque, 10 bar steam

Appendix G: Counter-flow expander model and test results

Due to the counter-flow expander not performing as well as the uni-flow and rotary expanders, the model is described and the test results are presented in this appendix, as referenced in Section 4.3.

G.1 Counter-flow expander model

The counter-flow expander configuration was a simple GT model; Appendix figure 51 shows the GT model for the counter-flow expander configuration.

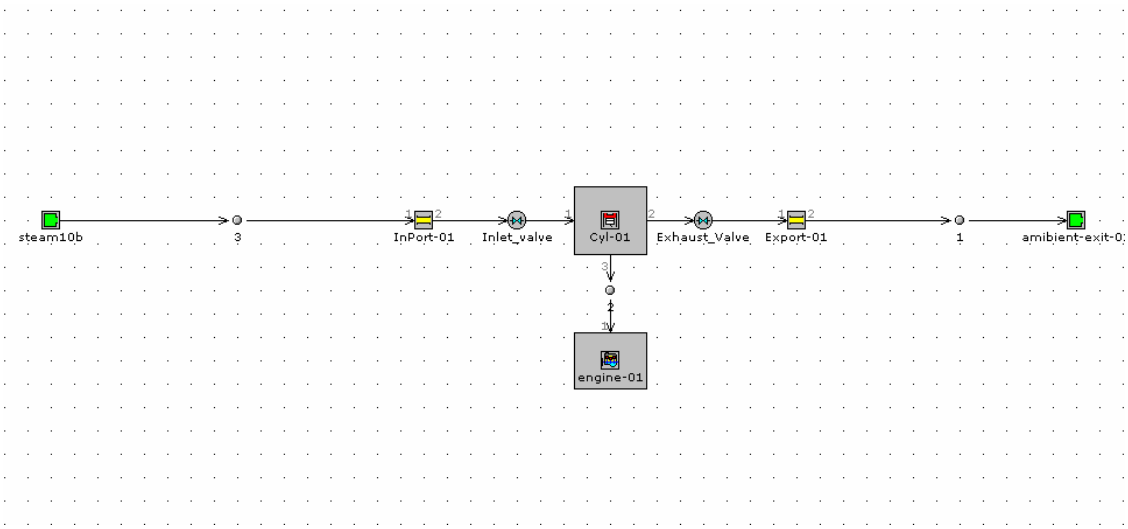

Appendix figure 51 GT model of the counter-flow expander configuration

The main difference between the uni-flow in and the counter-flow model was that the uni-flow model used a fixed size exhaust port component and the counter-flow used a variable exhaust valve component. The dimensions for the pipes, valves and cylinder were incorporated into the models, where the inlet or outlet had variable timing; named variables were used so that when the model case setup was created, timings could easily be altered without altering the model components.

The timing used for the actual tests were used when initially executing the models, however it was soon obvious that the timings did not have a direct correlation with the timings required by the model. The four stroke timings did not seem to have the simple correlation, as for the uni-flow model, the timings used in the actual tests gave completely different results in the GT executions. One reason for this is because the solenoid valves were used to control the inlet and outlet, so there was more room for error, also the response time of the valves opening and closing need careful attention, the response time was believed to be a fixed 6 ms, but it looked like this was not the case. For the four stroke GT results, the timings were altered to give as close a result for torque as possible, and then pressure diagrams were compared for 300 rpm.

Appendix H contains graphs that compare the four stroke timings used in the actual tests and in the GT modelling tests as can be seen in these graphs, the values are quite different.

G.2 Counter-flow expander results

This section shows the results for the uni-flow expander configuration with a solenoid valve on the inlet. The results are compared with the experimental results from Appendix E (nitrogen) and Appendix F (steam).

G.2.1 Steam results

Appendix figure 52 compares the variation in torque over speed for the experimental data and GT data using steam at 10 bar.

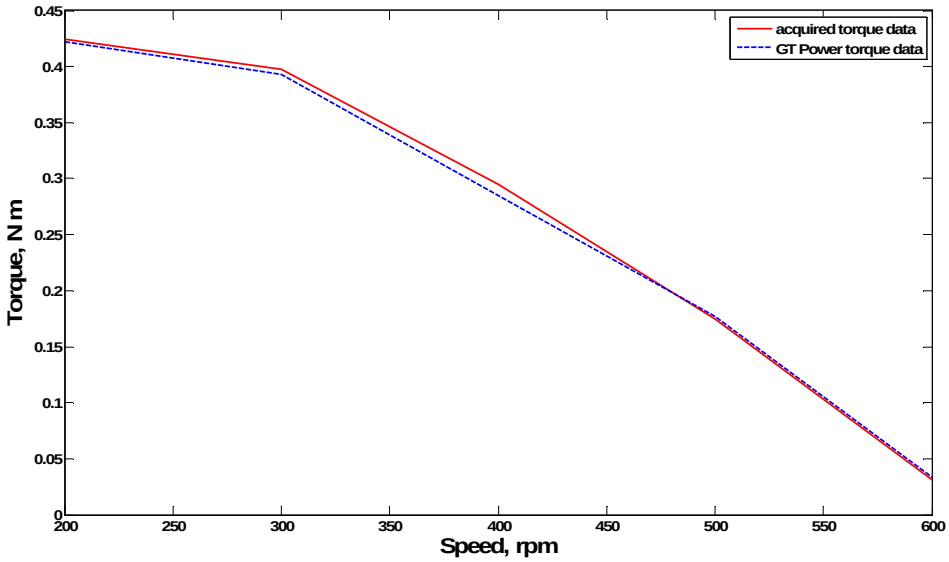

Appendix figure 52 Counter-flow, 10 bar steam, comparison of torque

Appendix Table 20 compares the torques for each speed step and presents the percentage of difference between the two values.

Speed (rpm)	Measured Torque (N m)	GT model Torque (N m)	Percentage Difference
200	0.4242	0.4220	-0.52
300	0.3977	0.3930	-1.19
400	0.2948	0.2850	-3.44
500	0.1750	0.1770	+1.13
600	0.0314	0.0336	+6.55

Appendix Table 20 Comparison of measured torque and torque obtained from GT tests, 10 bar steam

Appendix figure 52 and Appendix Table 20 show that the GT model for the counter-flow expander with 10 bar steam yielded similar results to the experimental data for the lower speed steps with the torque data being within ±4%. However, for the maximum speed steps, 600 rpm, the torque data was different by ±6.5%, which is unacceptable. Also it is worth pointing out that the timings had been altered to gain a close torque result. Appendix figure 53 compares the variation in pressure over one complete rotor revolution for the experimental data and GT data.

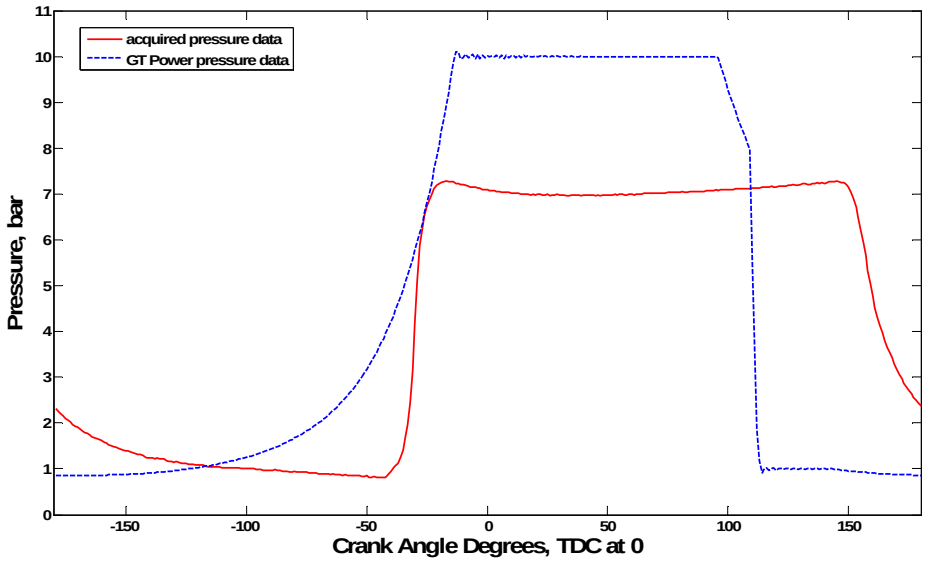

Appendix figure 53 Counter-flow, 10 bar steam, comparison of pressure cycles, 300 rpm

As can be seen in Appendix figure 53, the pressure wave was not at all similar. The difference in maximum pressure and width of the pressure wave could be due to the fact that the GT model was a perfect representation and that the solenoid valves which operated the inlet and outlet were affecting the performance of the expander, especially with the higher temperatures for 10 bar steam (180°C). A small quantity of steam expansion can be seen in the GT data; however, no expansion was experienced in the experimental data.

G.2.2 Nitrogen results

Appendix figure 54 compares the variation in torque over speed for the experimental data and GT data using nitrogen at 10 bar.

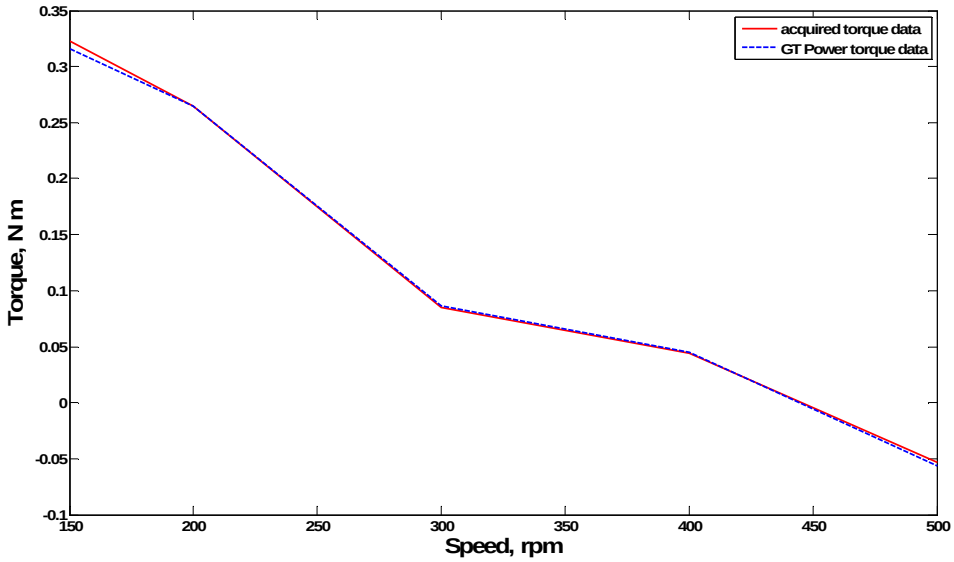

Appendix figure 54 Counter-flow, 10 bar nitrogen, comparison of torque

Appendix Table 21 compares the torques for each speed step and presents the percentage of difference between the two values.

Speed (rpm)	Measured Torque (N m)	GT model Torque (N m)	Percentage Difference
150	0.3227	0.3160	-2.12
200	0.2648	0.2650	-0.08
300	0.0851	0.0862	+1.28
400	0.0438	0.0450	+2.67
500	-0.0533	-0.0566	-5.83

Appendix Table 21 Comparison of measured torque and torque obtained from GT tests, 10 bar nitrogen

Appendix figure 54 and Appendix Table 21 show that the GT model for the counter-flow expander with 10 bar nitrogen yielded similar results to the experimental data for the lower speed steps with the torque data being within ±6%. However, it is worth pointing out that the timings had been altered to gain a close torque result. Appendix figure 55 compares the variation in pressure over one complete rotor revolution for the experimental data and GT data.

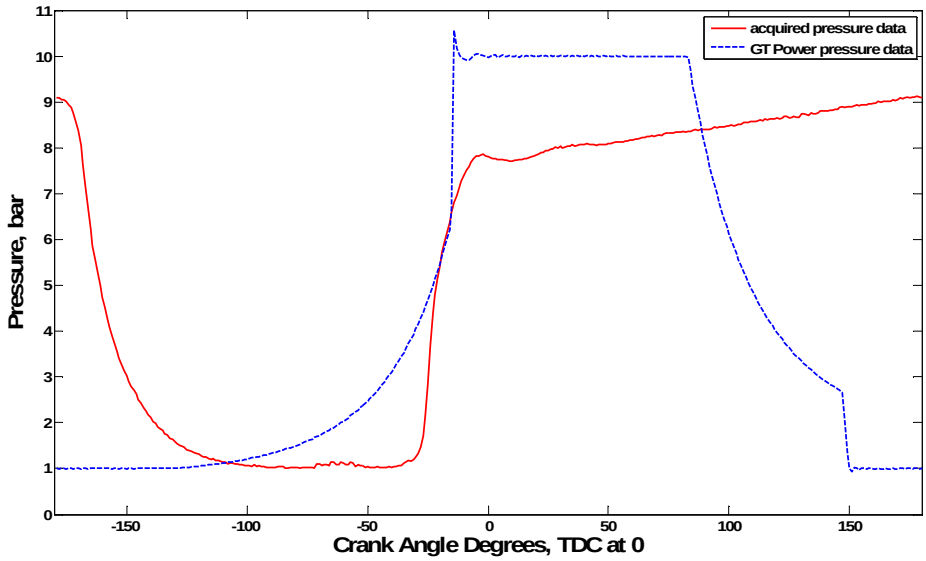

Appendix figure 55 Counter-flow, 10 bar nitrogen, comparison of pressure cycles, 300 rpm

As can be seen in Appendix figure 55, the pressure wave was not at all similar. The difference in maximum pressure and width of the pressure wave could be due to the fact that the GT model was a perfect representation and that the solenoid valves which operated the inlet and outlet were affecting the performance of the expander. A good expansion curve can be seen in the GT data; however, no expansion was experienced in the experimental data.

Appendix figure 56 compares the variation in torque over speed for the experimental data and GT data using nitrogen at 15 bar.

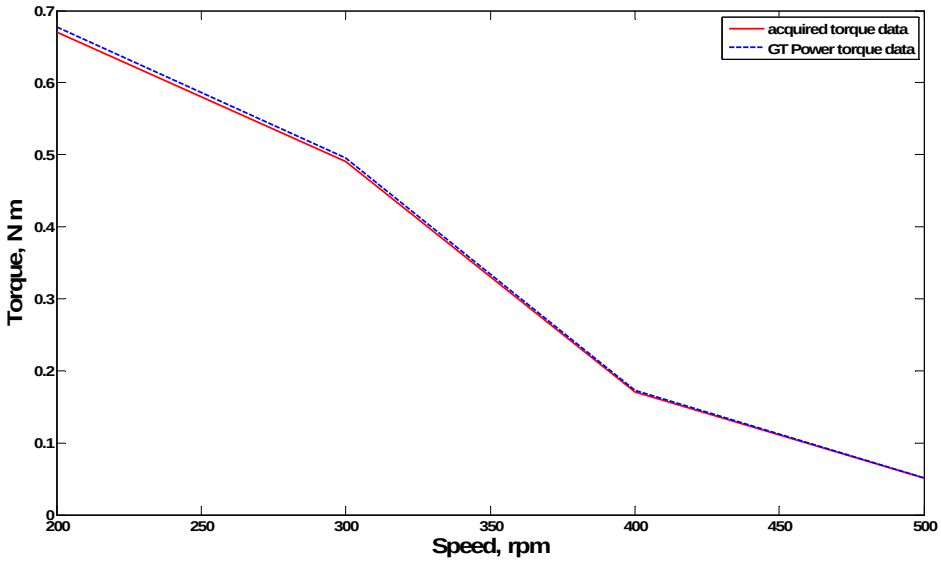

Appendix figure 56 Counter-flow, 15 bar nitrogen, comparison of torque

Appendix Table 22 compares the torques for each speed step and presents the percentage of difference between the two values.

Speed (rpm)	Measured Torque (N m)	GT model Torque (N m)	Percentage Difference
300	0.6705	0.6775	+1.03
400	0.4903	0.4954	+1.03
500	0.1702	0.1732	+1.73
600	0.0509	0.0508	-0.19

Appendix Table 22 Comparison of measured torque and torque obtained from GT tests, 15 bar nitrogen

Appendix Table 22 and Appendix figure 56 show that the GT model for the counter-flow expander with 15 bar nitrogen yielded similar results to the experimental data for the lower speed steps with the torque data being within ±2%. However, it is worth pointing out that the timings had been altered to gain a close torque result. Appendix figure 57 compares the variation in pressure over one complete rotor revolution for the experimental data and GT data.

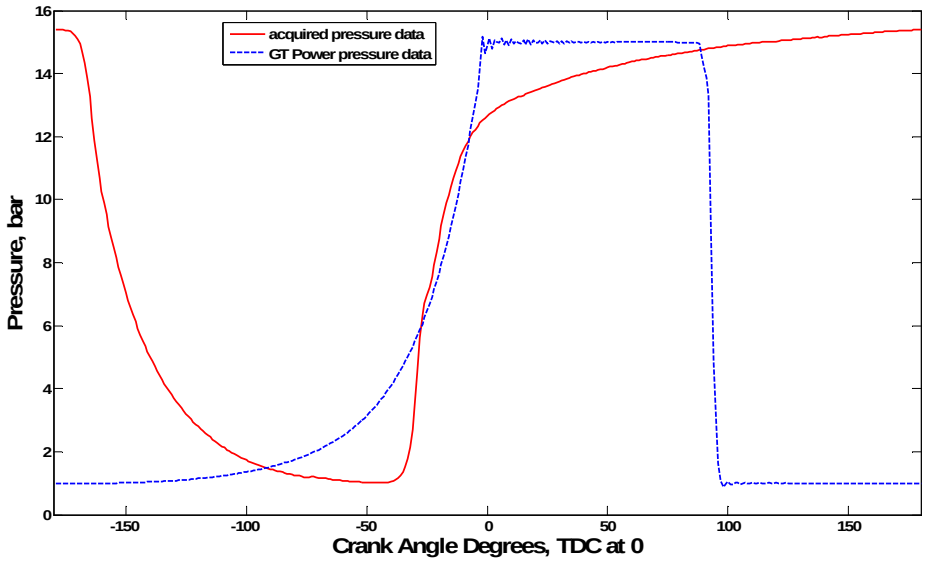

Appendix figure 57 Counter-flow, 15 bar nitrogen, comparison of pressure cycles, 300 rpm

As can be seen in Appendix figure 57, the pressure wave was not at all similar. The maximum pressure is similar, but there is still a difference in the width of the pressure wave. This could be due to the fact that the GT model was a perfect representation and that the solenoid valves which operated the inlet and outlet were affecting the performance of the expander. No expansion was experienced in the experimental or the GT data, this is probably due to the timing used in the GT model not allowing for expansion to take place before the exhaust valve is opened.

The counter-flow results could not be used for validation as the timings are off to get a close torque, when the experimental timings were used, even using the uni-flow correlation of multiplying by a factor of three did not yield the correct torque, this is why the timings were altered in such a way.

G.2.3 Correlation between media and GT validation

This section presents the results for the counter-flow expander, as detailed for the uni-flow expander in Section 4.4.1. Appendix Table 23 shows the collated data for the counter-flow experiments.

Speed (rpm)	Nitrogen 10 bar		Steam 10 bar		Nitrogen 15 bar	
	Δt	Torque	Δt	Torque	Δt	Torque
150	116	0.3227	125	0.4242	123	0.7639
300	127	0.2648	135	0.3977	133	0.6705
400	97	0.0851	130	0.2948	125	0.4903
500	87	0.0438	108	0.1750	93	0.1702
600	77	-0.0533	93	0.0314	70	0.0509

Appendix Table 23 Counter-flow tests timing and experimental torque data

Appendix Table 24 shows the ratios first for nitrogen at 10 and 15 bar and second for 10 bar steam and nitrogen at each speed step.

Speed (rpm)	Nitrogen 10 bar/15 bar ratio	10 bar steam/nitrogen ratio
150	2.23	1.22
300	2.42	1.41
400	4.47	2.58
500	3.63	3.22
600	1.05	0.48

Appendix Table 24 Counter-flow tests, ratios between nitrogen tests and 10 bar tests

The counter-flow tests there was a no close correlation for the any of the speed steps, this could be related to the timing issues, because for the counter-flow GT models the timing values were altered to obtain good torque data and so the values bore no relation to the actual timing used in the experiments. This would need further investigation and validation if the models are used further for the next expander size testing.

Considering the results for the counter-flow model, the execution of this model was approached in a different way to the uni-flow configuration, as the timings did not seem to be as easy to solve as for the uni-flow. The timings were adjusted until the torque was within ±5% of the measure torque, but this resulted in the GT data curves looking very

different to the experimental pressure data. This is attributed to having the solenoid valves on both the inlet and exhaust causing the timings to be incorrect and also the counter-flow loop-flow configuration was not suitable to act as an expander as no expansion was experienced.

Appendix H: Timing comparisons

This appendix contains graphs that compare the timings used for the actual expander tests with the timings used in GT tests to get the same results. Section H.1 contains the uni-flow comparisons, as described in Section 4.3.1. Section H.2 contains the counter-flow comparisons, as described in Appendix G.

For all the figures contained in this appendix section, the x-axis corresponds to the crank angle degree, with 0 representing top dead centre (TDC) and the y-axis represents the state of the valve with 0 representing closed and 1 representing open.

H.1 Uni-flow comparisons

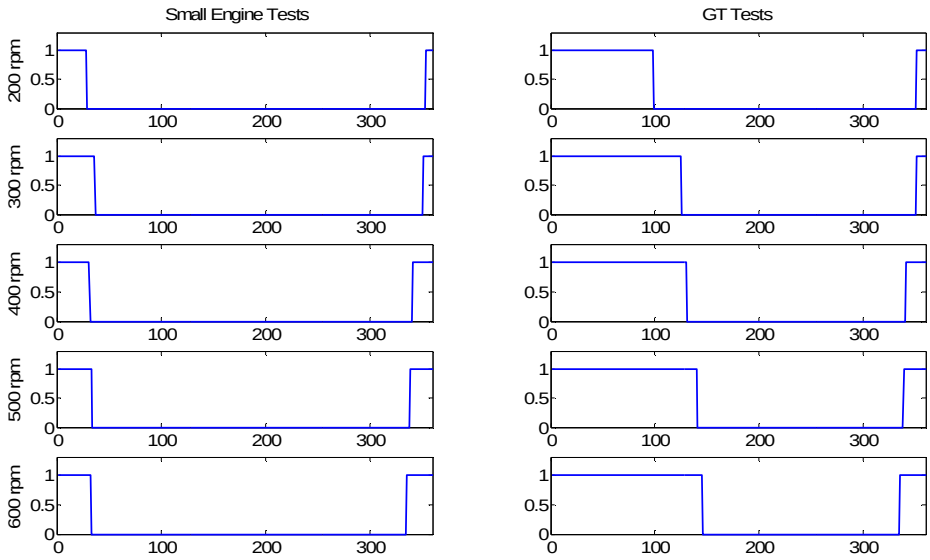

Appendix figure 58 Two-stoke timing comparisons, 10 bar steam

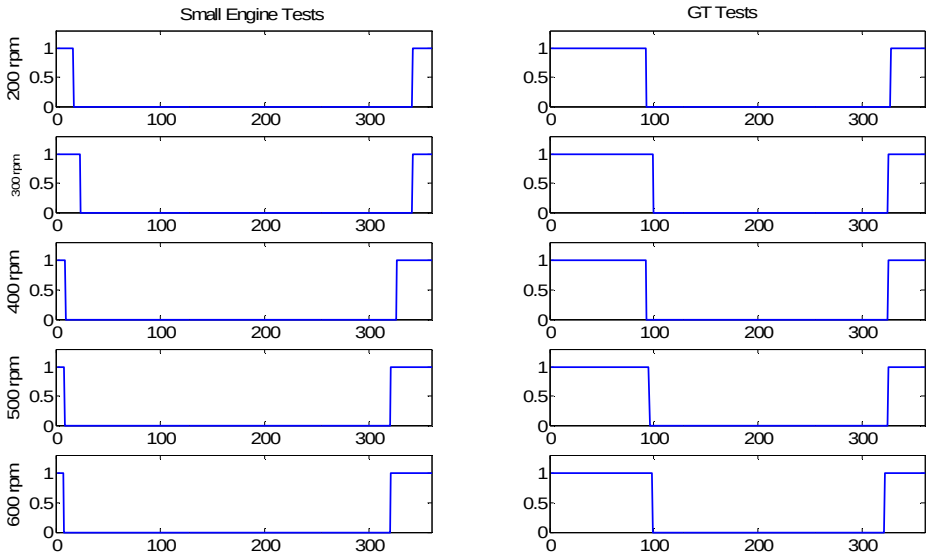

Appendix figure 59 Two-stoke timing comparisons, 10 bar nitrogen

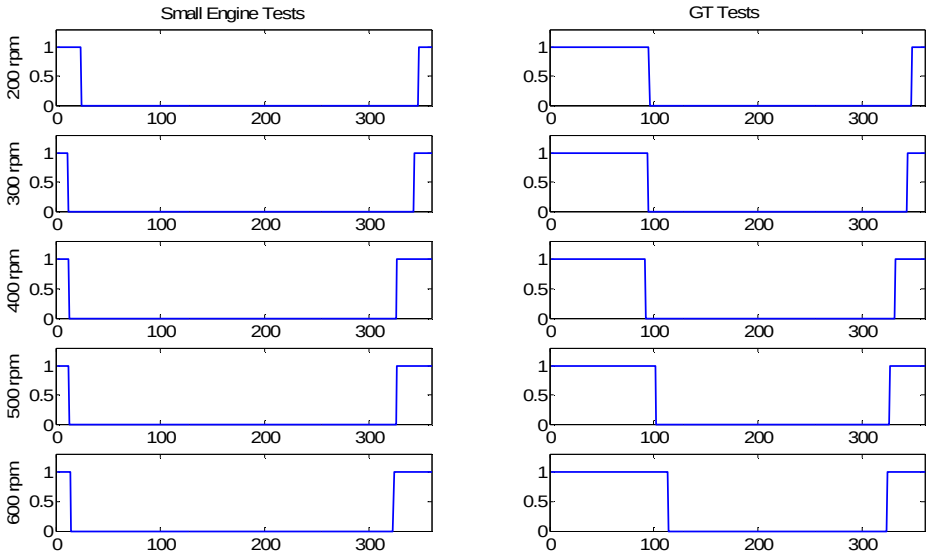

Appendix figure 60 Two-stoke timing comparisons, 15 bar nitrogen

H.2 Counter-flow timing comparisons

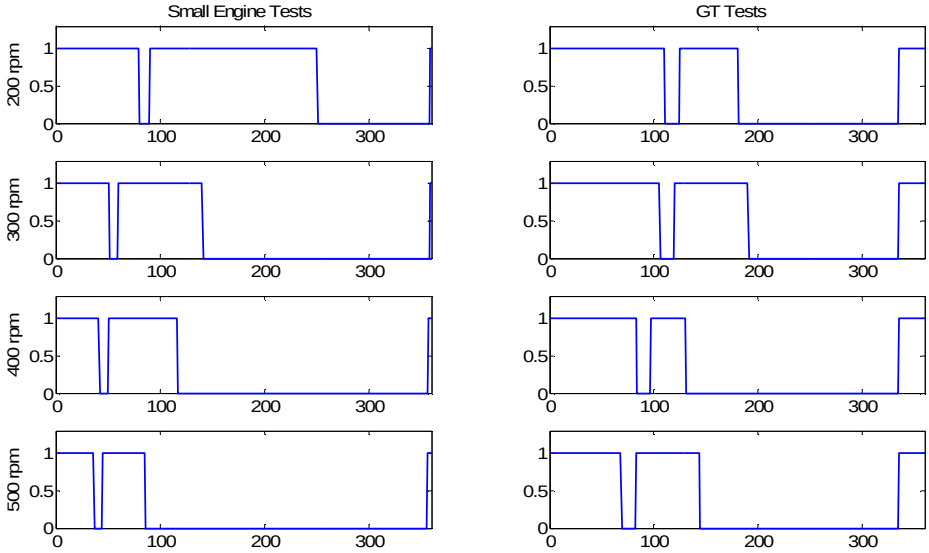

Appendix figure 61 Four-stoke timing comparisons, 10 bar steam

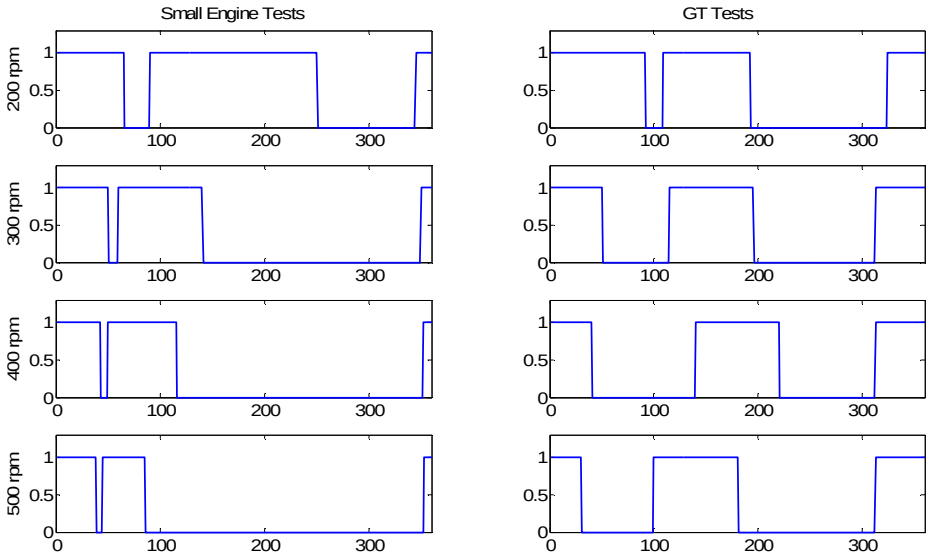

Appendix figure 62 Four-stoke timing comparisons, 10 bar nitrogen

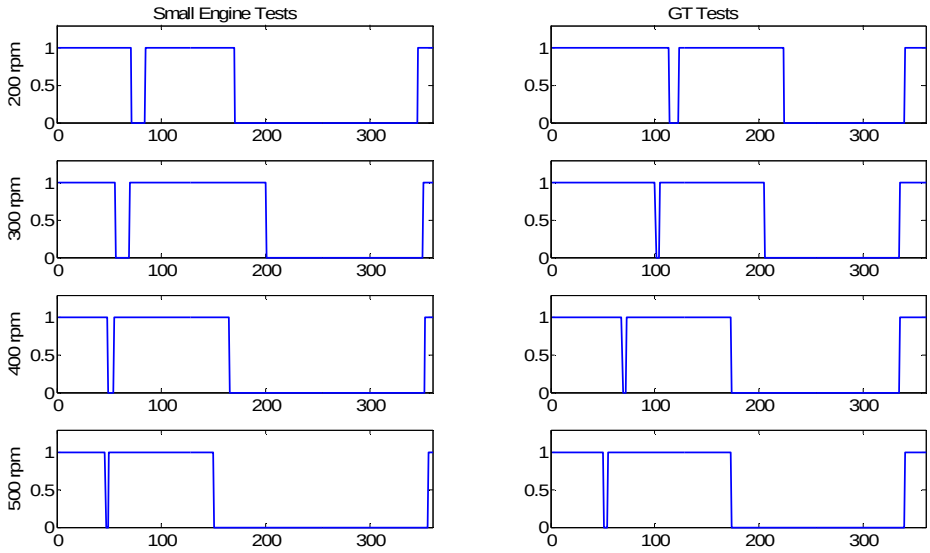

Appendix figure 63 Four-stoke timing comparisons, 15 bar nitrogen

Appendix I: Design, setup and testing of the heat exchanger

I.1 Heat exchanger test introduction

This appendix presents a brief overview of the setup for the heat exchanger test facility, the data acquisition requirements and a summary of the results from the heat exchanger testing.

The main objective of this part of the project was to setup and demonstrate the basic HYSTOR concept, the most appropriate and available test facility at the University of Sussex contained a Caterpillar 7.2 litre engine [64]. Even though this engine was initially considered to be on the large side because, up until that point in the project, the modelling and testing had only considered passenger sized vehicles. However the engine was deemed suitable as it allows a range of test parameter to be varied which would be applicable to different sized vehicles. One such parameter was the angle setting for a variable geometry turbocharger (VGT), the use of which allowed different exhaust conditions to be simulated; in this way exhaust conditions for a smaller engine could be emulated.

As the exhaust duct for the Caterpillar engine was of specific dimensions, an off-the-shelf heat exchanger was not available; therefore the heat exchanger was designed in-house so that it would fit the dimension and engine specifications exactly. Section I.2 gives a description of the heat exchanger design including diagrams and design parameters.

A description of the heat exchanger test facility and test instrumentation specifications are given in Section I.3, followed by details of the test plan in Section I.4.

At the time of writing the thesis, the heat exchanger test results were not available, hence no conclusions can be made as yet, however, Section I.5 will give an overview of what

was expected from the test results and how the test data would have been used to improve the dynamic modelling and control techniques described in Chapter 5.

I.2 Heat exchanger design

As stated in the introduction to this chapter, a suitable heat exchanger could not be sourced off-the-shelf; hence, the heat exchanger was designed in-house by the HYSTOR project team. There were certain limitations and design parameters that were taken into consideration. These limitations and parameters are detailed in this section. The main objective for the heat exchanger within the HYSTOR system is to generate steam from water using a heat transfer process from the exhaust gas, with the generated steam feeding an expander that will provide the work for the powertrain of the hybrid vehicle.

The design points for the hot side of the heat exchanger were taken from existing test data for the Caterpillar engine. The temperature of the exhaust, T_{hi} was chosen to be 750 K with the exhaust mass flow rate, $\dot{m}_h$, set at 0.239 kg/s and with a pressure, P_h, of 1.3 bar. The design points for the cold side were chosen to be ambient temperature, T_{ci}, 293 K, with the mass flow rate of water, $\dot{m}_w$, to be 0.5 L/min (equivalent to 0.5 kg/min or 0.0083 kg/s) at a pressure, P_c, of 25 bar. The parameters and their thermodynamic properties are summarised in Appendix Table 25.

Parameter	Value	Unit	Details
T_{hi}	750	K	Exhaust gas entry temperature
T_{ho}	696	K	Exhaust gas exit temperature
T_{ci}	293	K	Steam exit temperature
T_{co}	527	K	Water entry temperature
T_{sat}	470	K	Saturation temperature, at 25 bar
h_{fg}	1840	kJ/kg	Latent heat of vaporisation at 25 bar
c_{pg}	3250	kJ/kg K	Specific heat capacity for steam at 25 bar
c_{pf}	4630	kJ/kg K	Specific heat capacity for water at 25 bar

Appendix Table 25 Design parameters for the heat exchanger

The limitation on the physical dimensions for the heat exchanger arose from the availability of places where it could possibly be placed within the existing test facility with minimum alterations. The Caterpillar engine configuration included two legs from

the exhaust outlet, each of which had a catalytic converter attached, the horizontal length of these converters was 0.89 metres, hence it was decided to remove the catalytic converters and blank off one of the exhaust legs and attach the heat exchanger to the other.

A number of heat exchanger geometries were considered: vertical tubes, horizontal tubes, coiled tube(s) and fins and plates. In addition all three standard heat exchanger flow configurations were considered: parallel flow, cross flow and counter flow. The chosen design was a double coil geometry with a counter flow configuration. The reason for choosing a double coil geometry was because of the simplicity of the design. Also one could be designed to fulfill both thermal and physical requirements of the project. The reason for choosing a counter flow configuration was because it is this configuration which gives the highest heat exchanger effectiveness. The final designs for the heat exchanger can be seen in the following diagrams. Appendix figure 64 shows the inner coils.

Appendix figure 64 The final design for the heat exchanger showing the coils

Appendix figure 65 shows the detail of the piping for the inner and outer coils

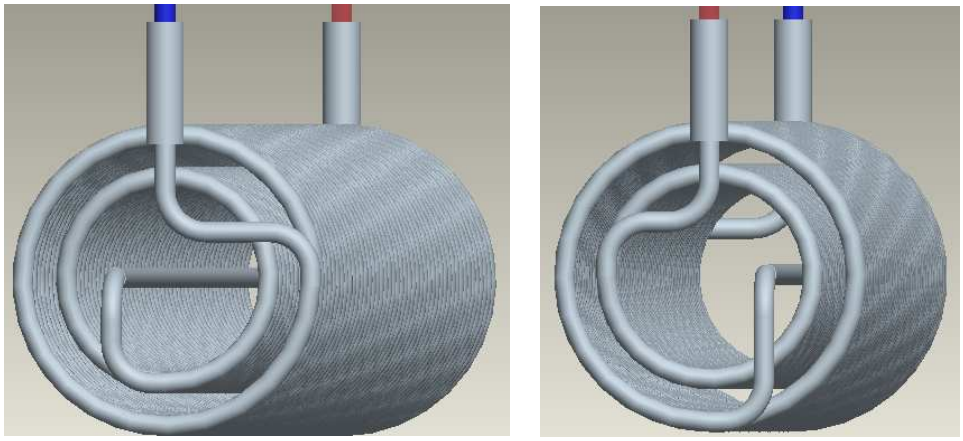

Appendix figure 65 Heat exchanger inlet coil detail (left) and outlet coil details (right)

Finally Appendix figure 66 shows the two coils inside the outer tubing along with the design parameters for heat transfer.

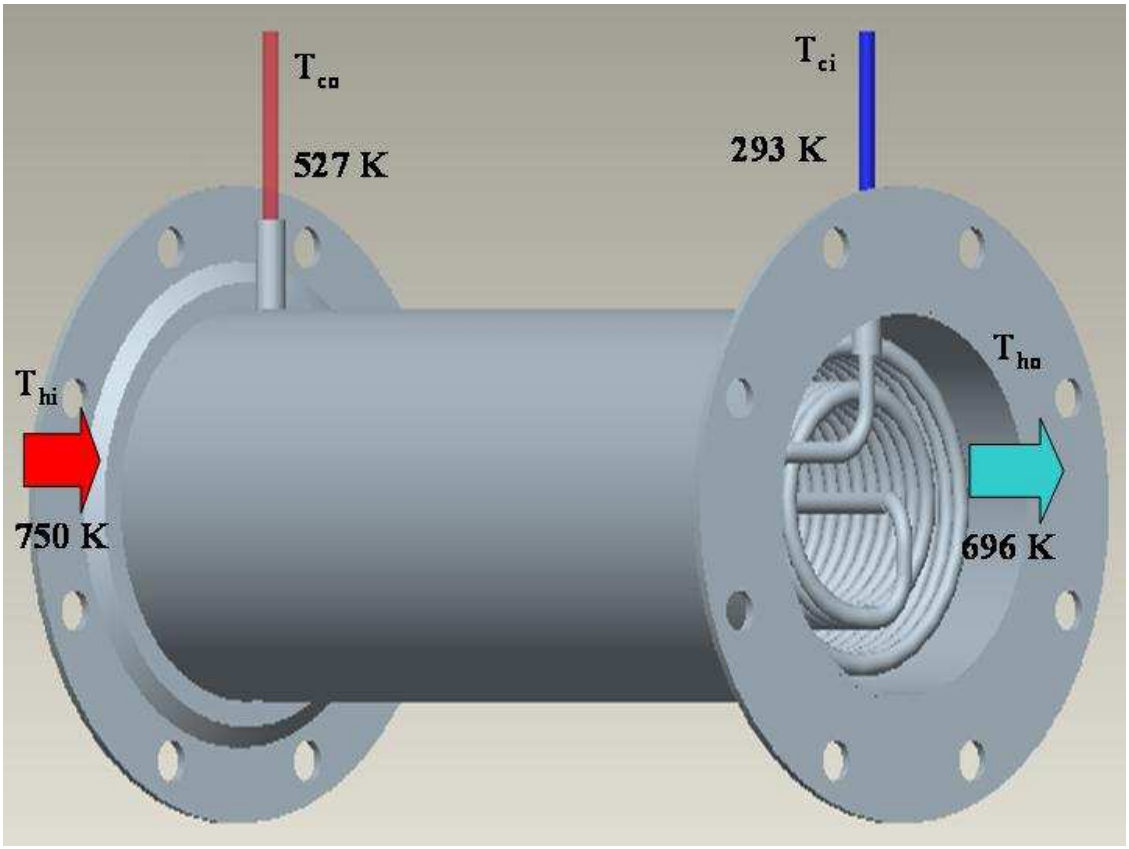

Appendix figure 66 Coil-in-tube, counter-flow heat exchanger design

The cold side coils were made from 316 stainless steel. Initial designs used copper for the coil, but it became apparent that cooper would not be suitable for the temperatures and pressures required for the heat exchanger, hence stainless steel was chosen as this material was more suitable for the requirements. The cold fluid enters the heat exchanger tube and travels round the outer coil first, and then returns to the cold fluid entrance via a central straight pipe (right hand side in Appendix figure 66) then travels back along the inner coil. When the fluid exits the heat exchanger, with the conditions matching the design points, the steam will be just beyond saturation temperature, which would be greater than 470 K at 25 bar. This is to ensure that only superheated steam is fed to the expander in order to avoid water droplet damage to the expander.

I.3 Heat exchanger test setup and specification

The experimental set-up for the heat exchanger is shown in Appendix figure 67 and consisted of a water reservoir (for source and sink), a water pump (with safety relief valve), a flow meter, the heat exchanger, a control valve and an expander with bypass valve. Additionally, thermocouples and pressure transducers were employed for temperature and pressure measurements. The data acquisition from the pressure transducers, thermocouples and flow meter was controlled by National Instruments LabVIEW software.

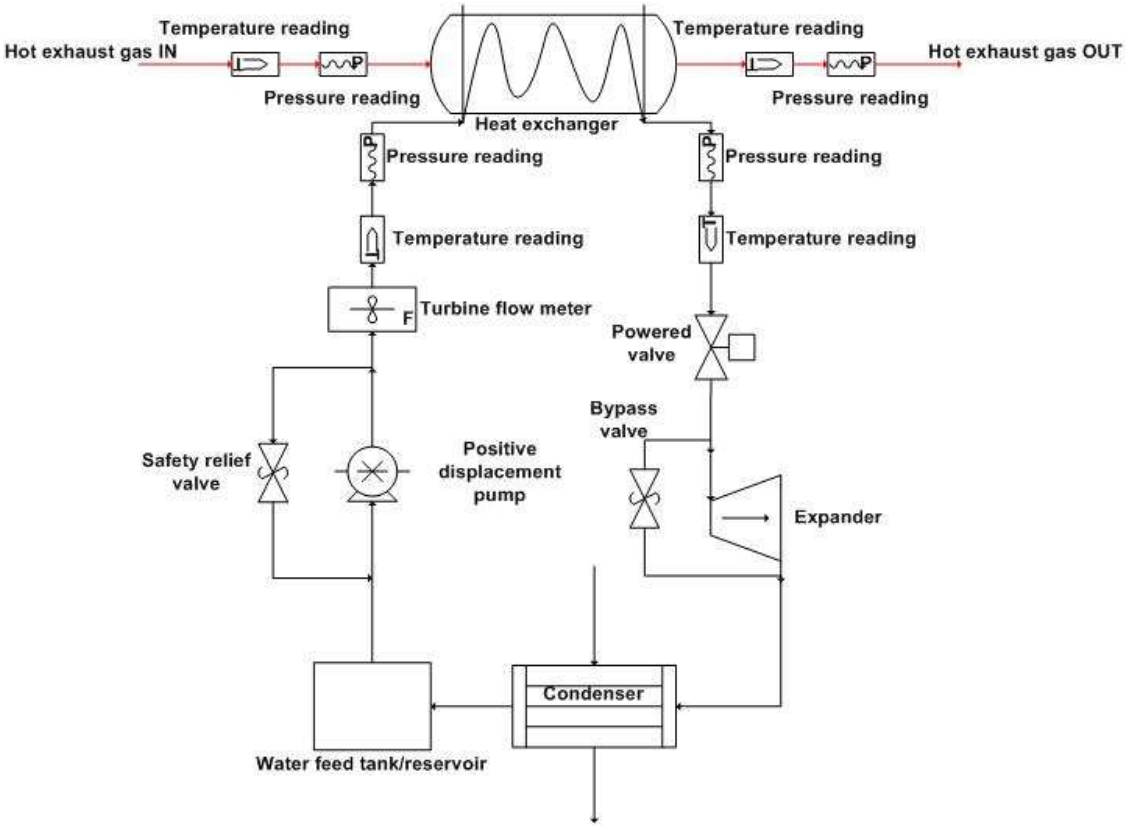

Appendix figure 67 Experimental setup

The sensor inputs were fed to a PC using a National Instruments data acquisition system. The pressure sensors were sourced from RS, part number 249-3836, the thermocouples were all type K and the flow meter was a turbine flow meter supplied by Kobold Instruments, part number DF 05GR08MAG34S. The water pump was a positive displacement water pump sourced from Michael Smith Engineers Ltd. The make and model is Hydra-Cell G-22.

I.3.1 Data acquisition

The data acquisition system consisted of a cDAQ-9172 chassis and 9211 input module. The input module was suitable for thermocouple input signals and the voltage inputs from the pressure transducers and flow meter. The connection between the cDAQ and the PC was a USB cable. The input module had the following specifications.

Resolution: 24 bits;

Sampling rates: 3.2 (MS/s) (multiple channel);
Gain error: 0.1% max at -40°C to 70°C;
Input voltage range: ±80 mV.

I.3.2 Inputs to LabVIEW

Appendix Table 26 lists the various inputs to the PC and LabVIEW, what unit the inputs were measuring and how they were connected.

Quantity (Unit)	Connection to system	Connection to PC	Range
Exhaust inlet temperature (°C)	K type thermocouple	NI-DAQ system	Temp: 0°C to 300°C Voltage: ±80 mV
Exhaust outlet temperature (°C)	K-type thermocouple	NI-DAQ system	Temp: 0°C to 300°C Voltage: ±80 mV
Water inlet temperature (°C)	K type thermocouple	NI-DAQ system	Temp: 0°C to 300°C Voltage: ±80 mV
Water/vapour outlet temperature (°C)	K-type thermocouple	NI-DAQ system	Temp: 0°C to 300°C Voltage: ±80 mV
Exhaust inlet pressure (Pa)	Pressure transducer	NI-DAQ system	Pressure:0 bar to 25 bar Voltage: ±10 V
Exhaust outlet pressure (Pa)	Pressure transducer	NI-DAQ system	Pressure:0 bar to 25 bar Voltage: ±10 V
Water inlet pressure (Pa)	Pressure transducer	NI-DAQ system	Pressure:0 bar to 25 bar Voltage: ±10 V
Steam outlet pressure (Pa)	Pressure transducer	NI-DAQ system	Pressure:0 bar to 25 bar Voltage: ±10 V
Mass flow rate (L/min)	Turbine flow meter	NI-DAQ system	Flow: 0.08 L/min to 0.5 L/min Voltage: 0-10 V

Appendix Table 26 Inputs to data acquisition software, LabVIEW

I.4 Heat exchanger tests planned

This section details the tests that were planned for the heat exchanger. The aim of these tests was to observe the heat exchanger and record the results for various different test points and execute drive cycles.

Where the tests require constants values for certain parameters whilst others are varying, these were as follows:

Constant speed point: 1200 rpm;

Constant load point: 1400 N m;

Constant exhaust mass flow rate: 0.2 kg/s;

Constant water mass flow rate: 0.008333 kg/s (0.5 L/min).

I.4.1 Matrix of steady state speed and load points

This stage of the testing will run the engine over a period of time stepping the speed and load points as shown in Appendix figure 68.

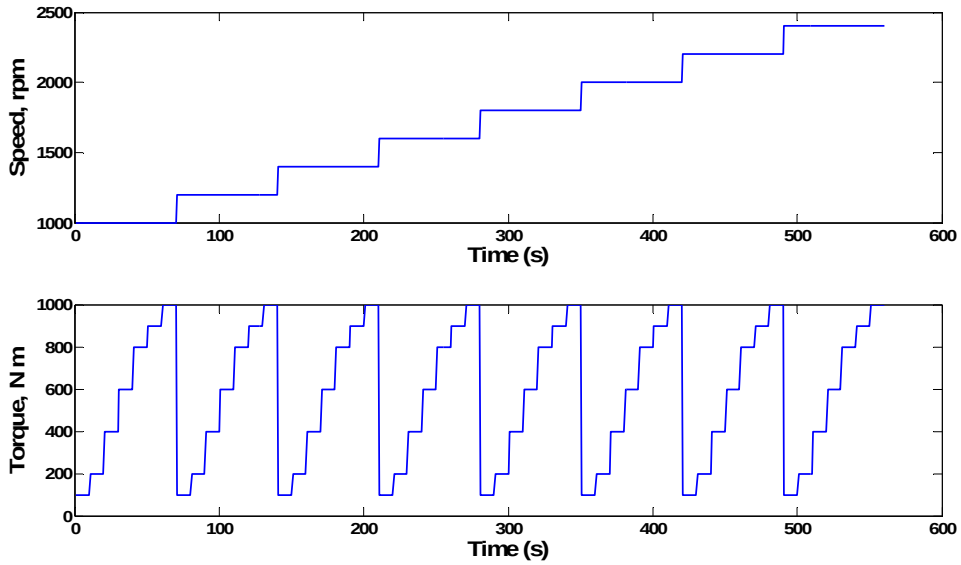

Appendix figure 68 Speed and load points used in experiments

The varying speed and load points are within the maximum and minimum capabilities of the engine, 1000 rpm to 2500 rpm for speed and 100 N m to 1000 N m for load (torque). For each speed step, the engine was run using different torque settings, each step should be held for at least two minutes in order to record the steady state values of acquired data.

For each speed/load point the mass flow rates of exhaust gas and water should be held constant.

I.4.2 Different exhaust mass flow rates

Using the variable geometry turbocharger (VGT) that is connected to the engine's exhaust, the application of different exhaust mass flow rates into the heat exchanger was possible. The VGT setting works on a percentage value that relates the opening of the turbine blades or vanes, with 0% being fully closed and 100% being fully open.

Using a constant speed/load point along with a constant water mass flow rate, the VGT blades should be set at different angles, the more closed the angle, the higher the exhaust mass flow rate will be, as the angle opens for the VGT blades, the exhaust mass flow rate will be reduced. The VGT blade settings should be stepped from 0% to 100%, in 10% step increments, and each step should be held for at least two minutes to record the steady state values of acquired data.

I.4.3 Different water mass flow rates

By controlling the speed of the water pump, different water mass flow rates will be tested. The water pump operating range was between 0.1 L/min and 0.5 L/min (0.001667 kg/s to 0.008333 kg/s).

Using a constant speed/load point along with a constant exhaust gas mass flow rate, the water mass flow rate should be stepped from 0.3 L/min to 0.5 L/min, in 0.05 L/min increments, and each step should be held for at least two minutes to record the steady state values of acquired data.

I.4.4 Transient tests – drive cycles

The drive cycles to be used to perform transient tests are the *On highway drive cycle* (OHDC) [65] and *Non Road Transient drive cycle* (NTRC) [66], these two drive cycles are detailed in this section.

I.4.4.1 On highway drive cycle (OHDC)

The drive cycle OHDC was developed to test heavy duty vehicles such as on highway trucks and large passenger vehicles. The cycle simulates a range of driving scenarios including driving in inner-city (urban) driving and also motorway (highway) driving. A summary of the OHDC characteristics is as follows:

Distance: 10.3 km;

Time: 1200 seconds;

Average speed: 1400 rpm;

Maximum speed: 2603 rpm.

The graphs in Appendix figure 69 show the speed and load points for the cycle.

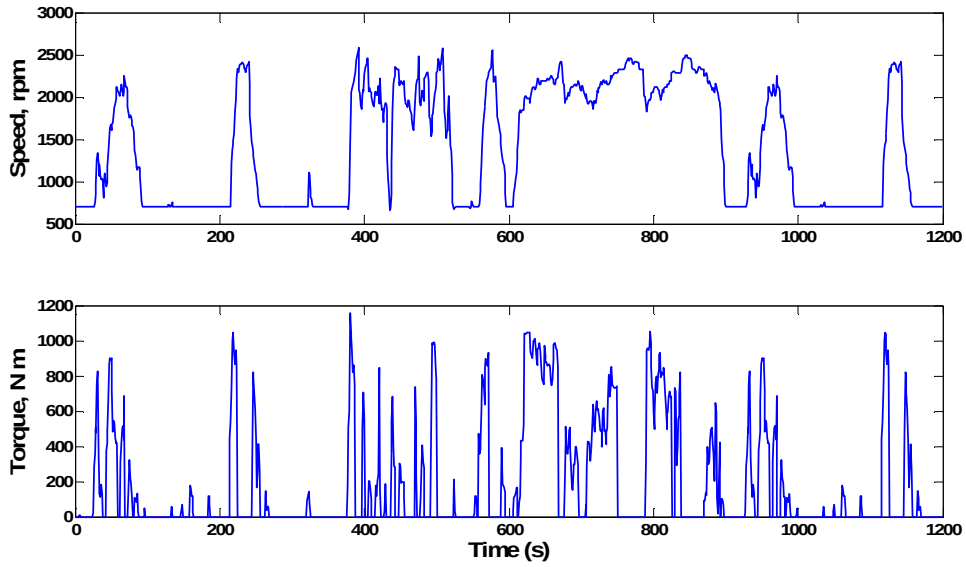

Appendix figure 69 On highway drive cycle

I.4.4.2 Non Road Transient Cycle (NRTC)

This test cycle was developed in the US for non road vehicle engines and is part of a series of tests for both European standards and US standards. A summary of the NRTC characteristics is as follows:

Time: 1200 seconds;

Average speed: 1907 rpm;

Maximum speed: 2480 rpm.

The graphs in Appendix figure 70 show the speed and load points for the cycle.

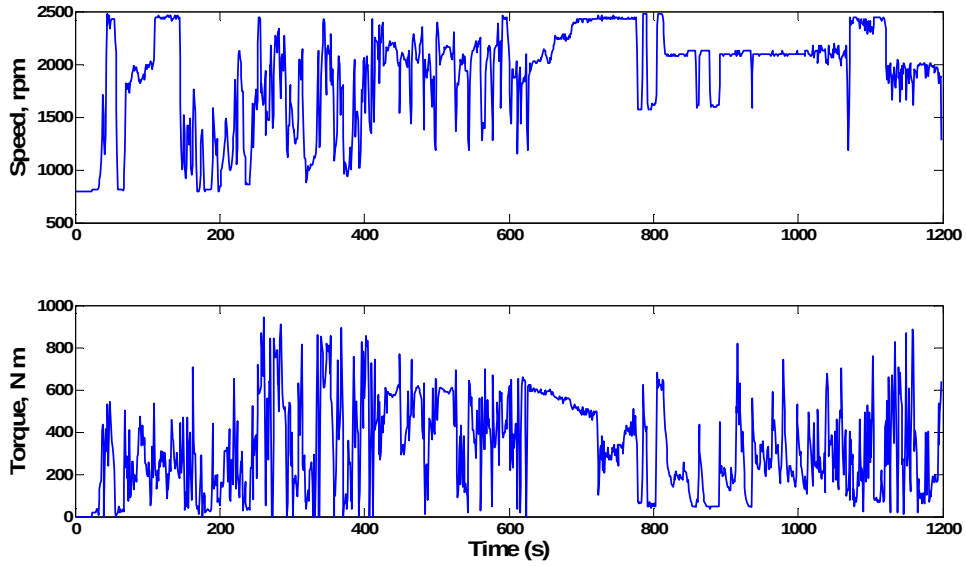

Appendix figure 70 Non road transient cycle

I.5 Future work for heat exchanger test results

The main aim of this part of the project was to use design and demonstrate a working heat exchanger to prove part of the HYSTOR system concept. Additionally the data acquired would be used in the development of the control for the system.

Unfortunately due to some problems with the experimental set up, which included the control of the flow and problem with acquiring steady readings from the pressure transducers, the results from the heat exchanger tests were not available to be included in this thesis. They will be documented in a separate document.

Appendix J: Controller development and test

This appendix contains additional information for the controller development detailed in Chapter 5. Section J.1 describes the individual controller modules that form part of the hierarchical control structure. Section J.2 contains the Simulink SISO control modules and test results. J.3 contains the Simulink blocks that make up the PID controlled system. J.4 contains the results from running the PID controller with QSS and PSAT using the NEDC and US-06 drive cycles.

J.1 Controller modules for the hierarchical control structure

From the hierarchical structure detailed in Section 5.2.1 individual control blocks were developed. The generic control block diagram is as shown in Appendix figure 71, this block diagram will be used as a base on which to develop and describe each control module.

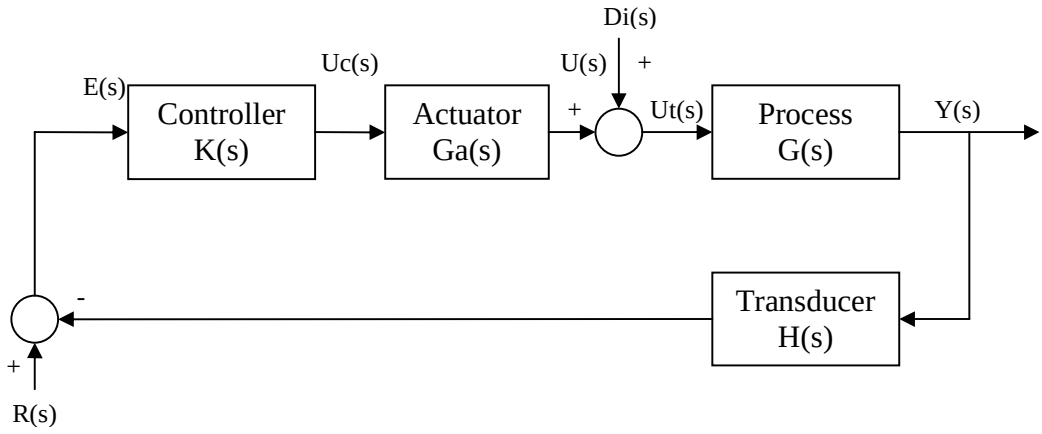

Appendix figure 71 Generic block diagram for control strategies [67]

Referring to Appendix figure 71:

E(s): process error signal;

R(s): reference signal;

Uc(s): controller output signal;

Di(s): input Disturbances;

U(s): actuator output signal;

Ut(s): process input signal;

Y(s): process output.

J.1.1 Water mass flow rate control

The water mass flow rate, or pump, control module will monitor the exhaust gas temperature and mass flow rate into the heat exchanger and control the water mass flow rate so that there is sufficient water supply to generate saturated steam for the expander. The inputs and outputs are visualised in Appendix figure 72.

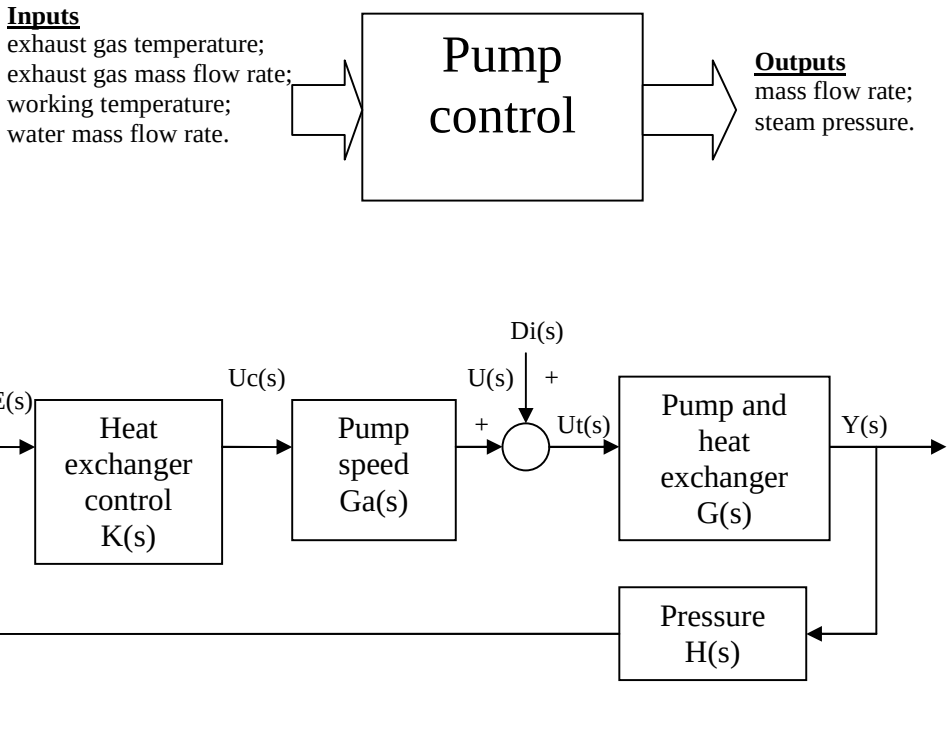

Appendix figure 72 Control block diagram for pump and heat exchanger components

Referring to Appendix figure 72, the following control variables are identified:

Y(s) = steam mass flow rate/pressure;

R(s) = working pressure demand;

Uc(s) = voltage for pump;

Us(s) = mass flow rate water into heat exchanger;

Di(s) = exhaust gas temperature and mass flow rate.

J.1.2 Expander control

The inlet valve will control the speed of the expander and, hence, the torque developed by the expander. The controller will use data obtained on the quality and mass flow rate of the steam available and also the torque demand on the IC engine to determine the cut-off ratio for the inlet valve. The inputs and outputs are visualised in Appendix figure 73.

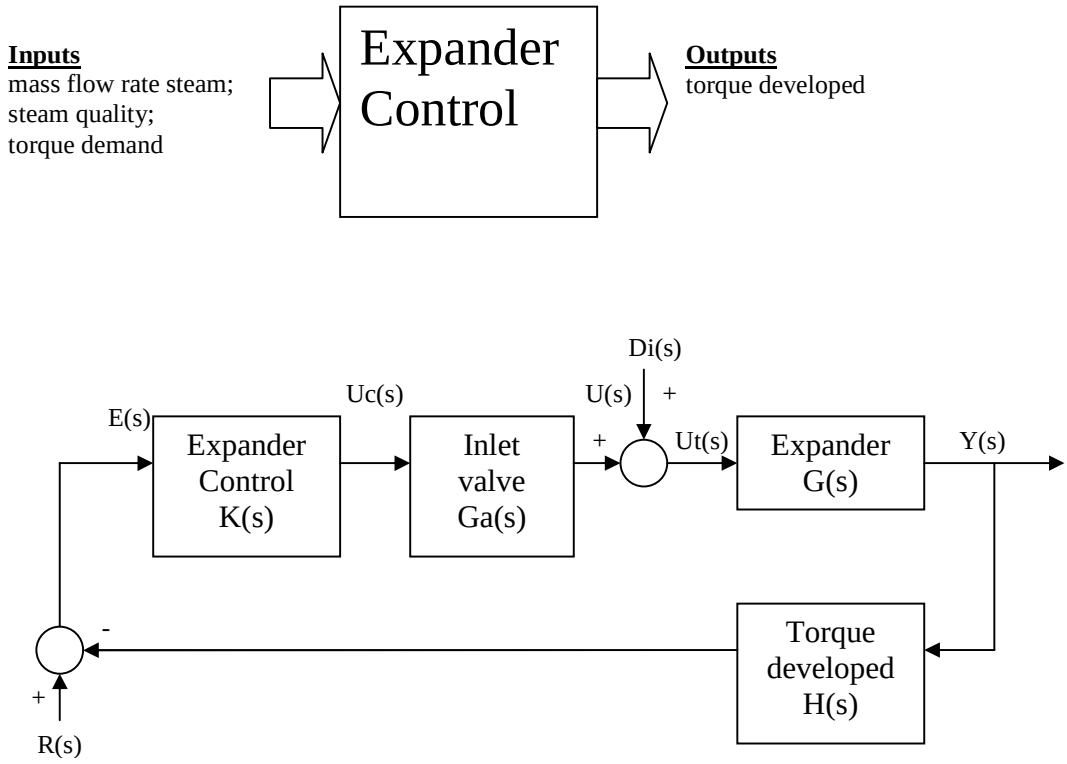

Appendix figure 73 Control block diagram for the expander

Referring to Appendix figure 73, the following control variables are identified:

Y(s) = torque developed;

R(s) = torque demand;

Uc(s) = valve cut-off ratio;

Us(s) = mass flow rate of steam into expander;

Di(s) = torque demand, steam quality and steam quantity.

J.2 SISO control modules and test results

From the control objectives and variables presented in Section 5.3, the following Simulink SISO models were developed and tested.

J.2.1 Pump control module

The pump control module monitors $\dot{m}_w$ and the pressure demanded by the system. The output variable of the controller, n_{dem}, is a voltage that relates to the pump speed requirement. An increase in voltage will increase n and hence increase $\dot{m}_w$ to the heat exchanger. A decrease in voltage will decrease n, and hence decrease $\dot{m}_w$ to the heat exchanger.

Any changes to n or $\dot{m}_w$ will affect the overall pressure of the system, unless coupled with corresponding change in the value of α for the expander.

There is a relation between mass flow rate and speed of the pump, this is in the form of a family of curves (representing k) and the mass flow rate will be k x n. This is shown in the Appendix figure 74 (data obtained from the specification for the water pump referenced in Appendix I).

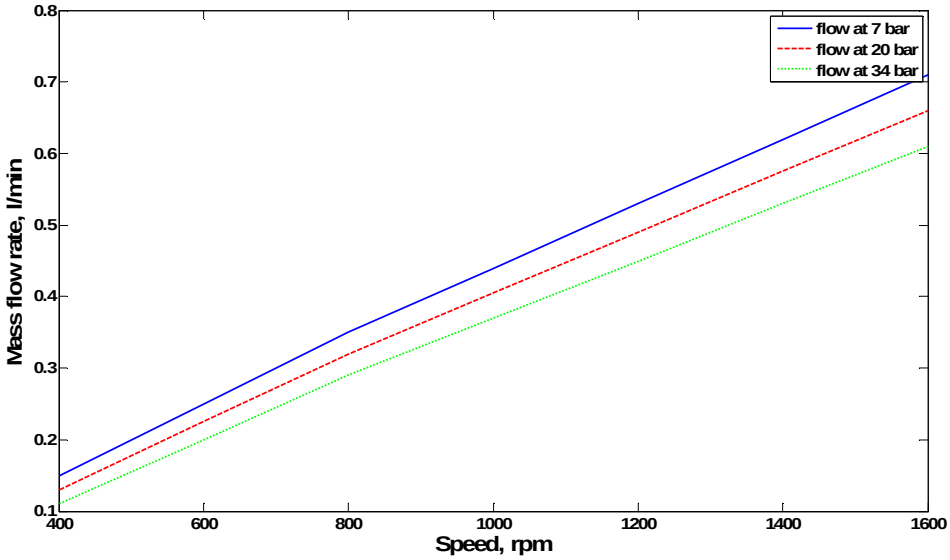

Appendix figure 74 Relationship of mass flow rates and pump speed at different pressures

The control block diagram from Section J.1.1 is further developed as shown in Appendix figure 75. The variables are as follows:

$\dot{m}_w$ - mass flow rate of water;

T_{cond} - Temperature out from the condenser;

P_{dem} - Pressure demanded of system;

P_{sys} - Actual Pressure of the system;

n_{dem} - Demanded speed of pump;

n - Speed of pump.

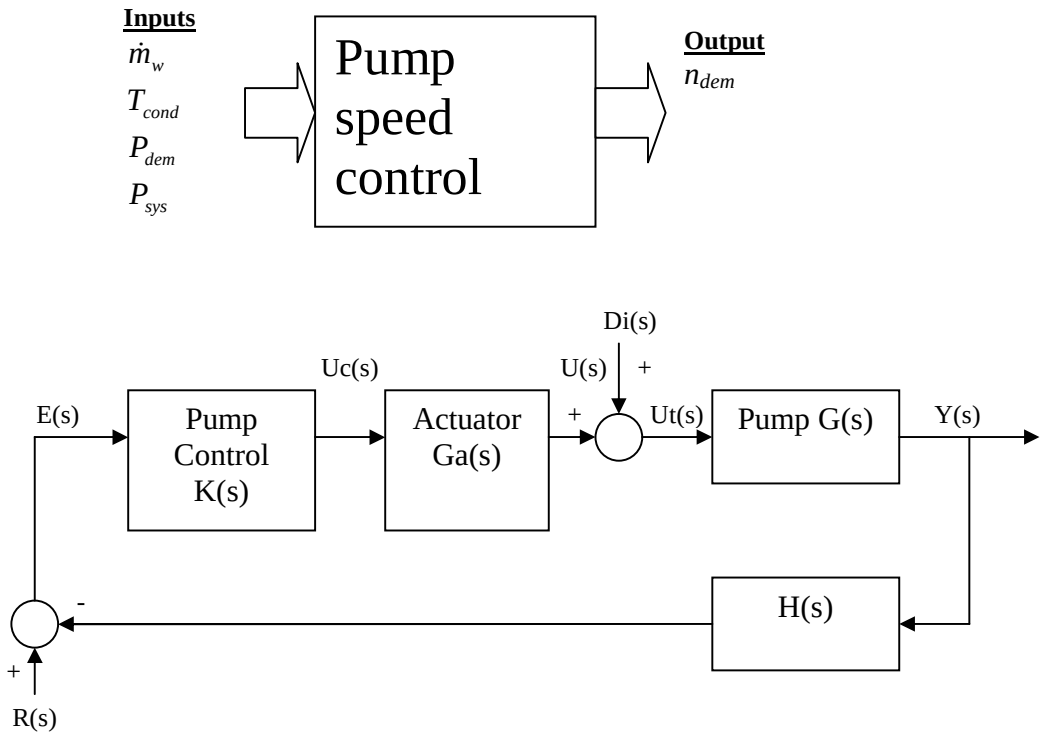

Appendix figure 75 Pump control module

Referring to Appendix figure 75, the control signals are as follows:

R(s) = $\dot{m}_w$ (demand by system);

E(s) = $\dot{m}_w$ (demand) - $\dot{m}_w$ (pump output) or R(s)-Y(s);

Uc(s) = n (output of pump controller);

U(s) = n as a voltage;

Di(s) = monitored speed of pump/pressure change;

Ut(s) = Pump input voltage – U(s)+Di(s);

Y(s) = $\dot{m}_w$ (pump output);

H(s) senses the mass flow rate output and converts it to signal $\dot{m}_w$.

Two Simulink models were developed, one to represent a positive displacement pump and one to represent a centrifugal pump, as these are the two common types of pumps used in industrial applications.

J.2.1.1 Positive displacement pump model

For the positive displacement pump, Equations J.1 through J.3 were used:

Volumetric flow	$F_n = K_s \times n$	(J.1)
Leakage flow	$F_l = K_l \times p$	(J.2)
Total flow	$F = F_n - F_l$	(J.3)

Where n is pump speed, K_s is the speed gain constant, p is pressure and K_l is the leakage gain constant, set to represent a leakage of about 2% of the mass flow. The Simulink model for the positive displacement pump is shown in Appendix figure 76 through Appendix figure 79.

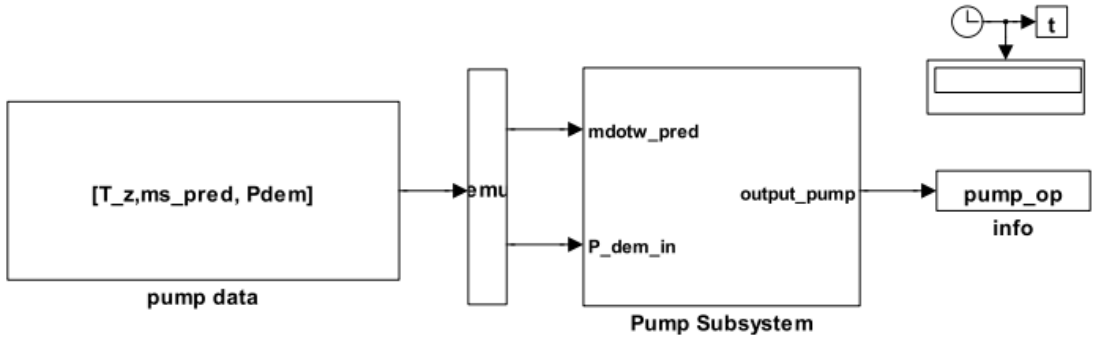

Appendix figure 76 Test harness for the positive displacement pump model

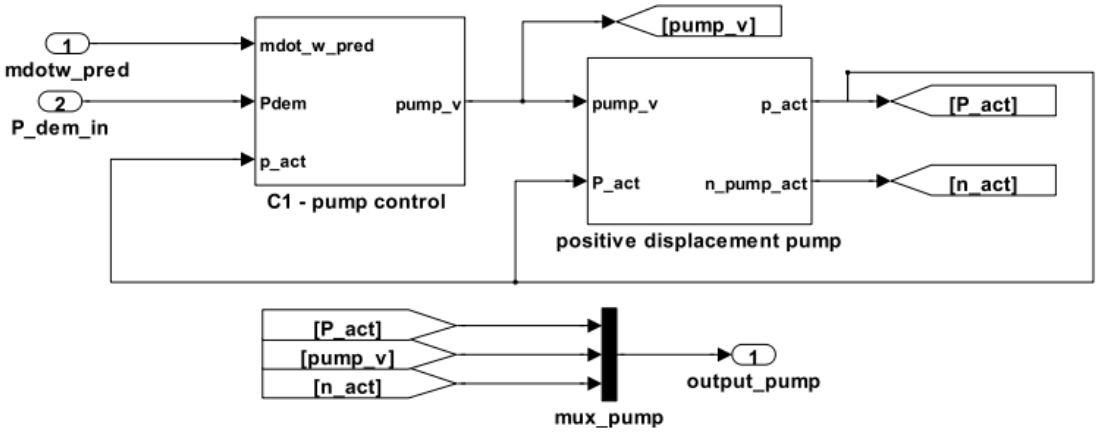

Appendix figure 77 Pump subsystem for the positive displacement pump model

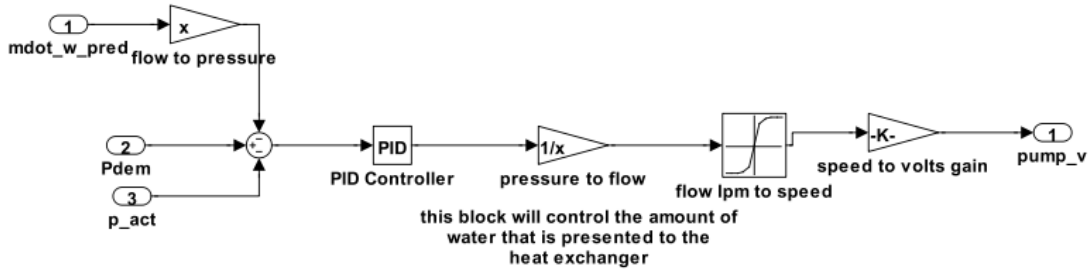

Appendix figure 78 Pump control for the positive displacement pump model

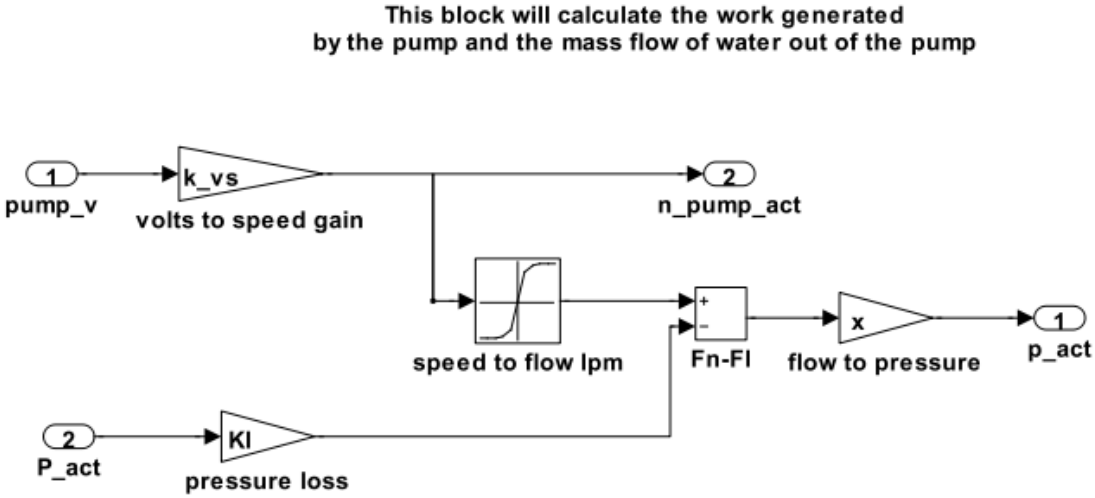

Appendix figure 79 Pump plant for the positive displacement pump model

Using the small test harness developed, as shown in Appendix figure 76, input data was created and output data was recorded. The demanded pressure (P_{dem}) was set at 20 bar; the predicted mass flow rate of water value ($\dot{m}_{wpred}$) was varied over 10 seconds from 0.2 kg/s to 0.1 kg/s, at 4 seconds, and to 0.15 kg/s, at 7 seconds as shown in Appendix figure 80.

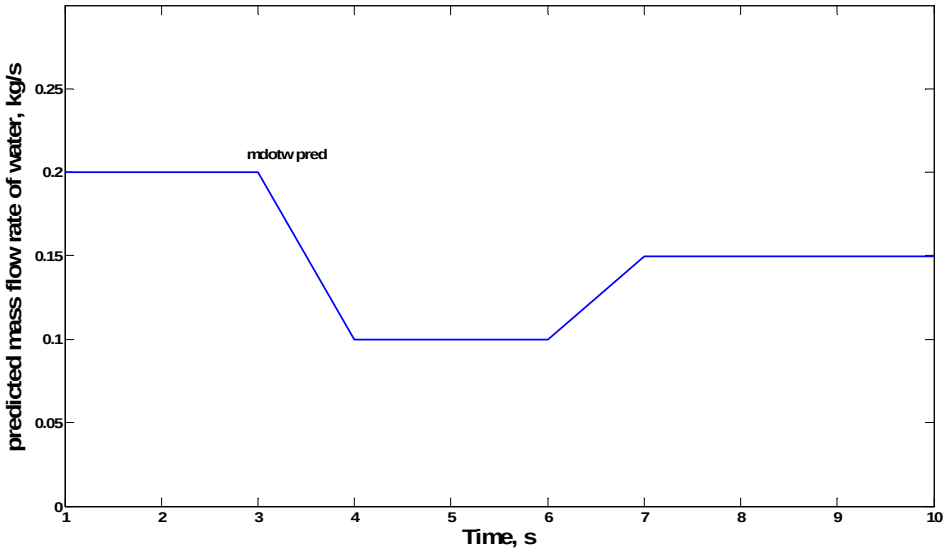

Appendix figure 80 Input to pump model, predicted mass flow water, $\dot{m}_{wpred}$

Appendix figure 81 shows the output of the controller, the pump voltage ($pump_v$), which rises or falls when the predicted mass flow rate of water rises or falls, but is then altered by the control to maintain the correct mass flow rate of water.

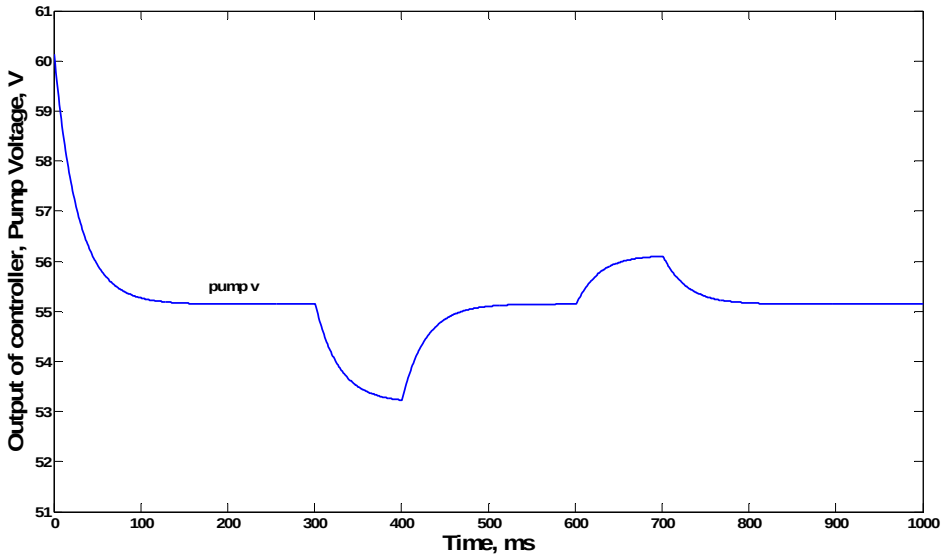

Appendix figure 81 Output of positive displacement pump controller, pump voltage, $pump_v$

Appendix figure 82 further shows the actual pressure (P_{act}) rises or falls momentarily when the predicted mass flow rate of water rises or falls, then returns to the demanded pressure value of 20 bar.

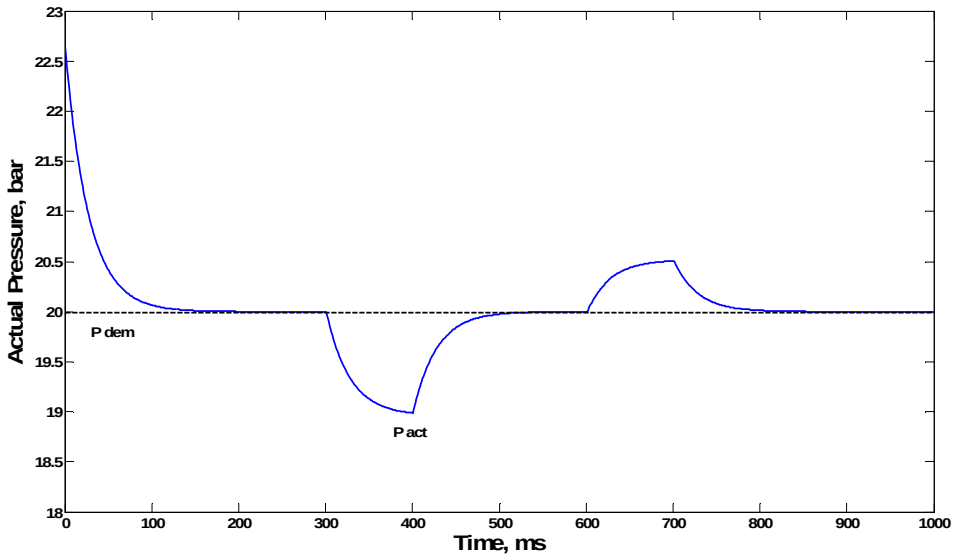

Appendix figure 82 Output of positive displacement pump, actual pressure, P_{act}

The demanded pressure is indicated by the dotted line and using this line it can be seen how quickly the controller acts to regulate the pump output.

J.2.1.2 Centrifugal pump

For the centrifugal pump, Equations J.4 through J.6 were used from [68]:

Blade speed $U_2 = r_p.n$ (J.4)

Total Head $H = \frac{U_2}{g} - \frac{F}{A_2} \times \frac{U_2}{g} Cot\beta_2$ (J.5)

Substituting Equation J.4 into Equation J.5:

Total Head $H = \frac{1}{g}.r_p^2.n^2 - \frac{F}{A_2} \times \frac{r_p.n}{g} Cot\beta_2$ (J.6)

Where n is speed (rad/s), r_p is the radius of the pump (0.1m), g is gravity (9.81), F is mass flow rate (kg/s), A_2 is the acceleration of the pump (0.1m/s), Cot β_2 =0.7 and total head is in Pascals.

The Simulink model for the centrifugal pump is shown in Appendix figure 83 through Appendix figure 86.

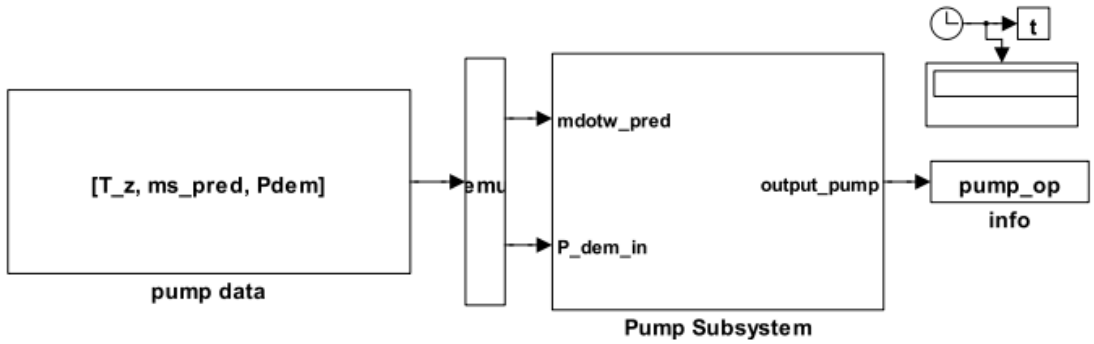

Appendix figure 83 Test harness for the centrifugal pump model

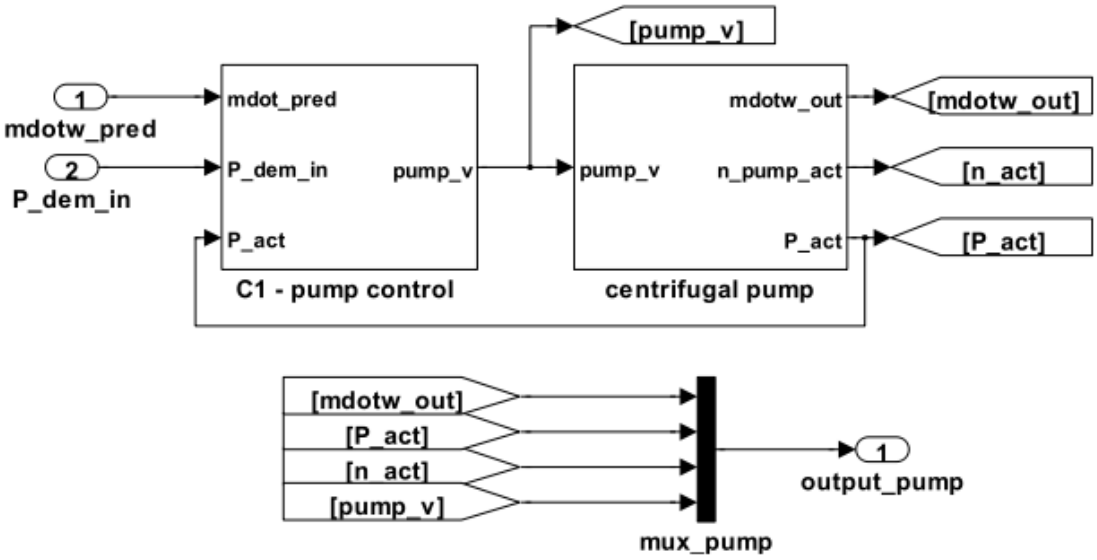

Appendix figure 84 Pump subsystem for the centrifugal pump model

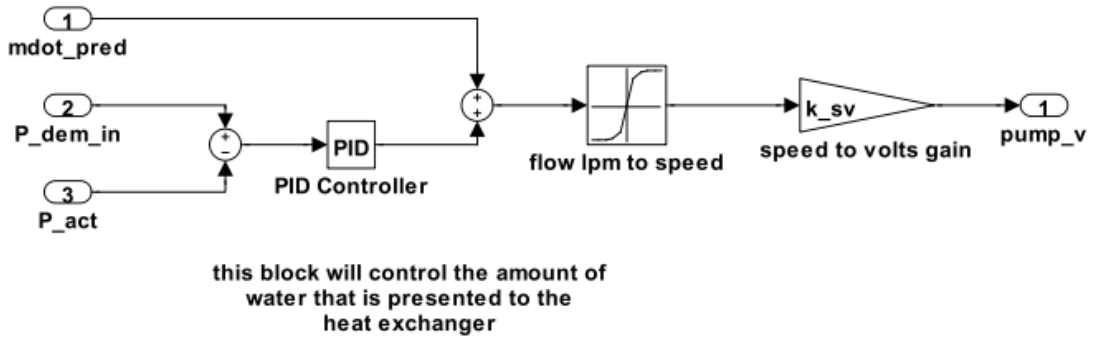

Appendix figure 85 Pump control for the centrifugal pump model

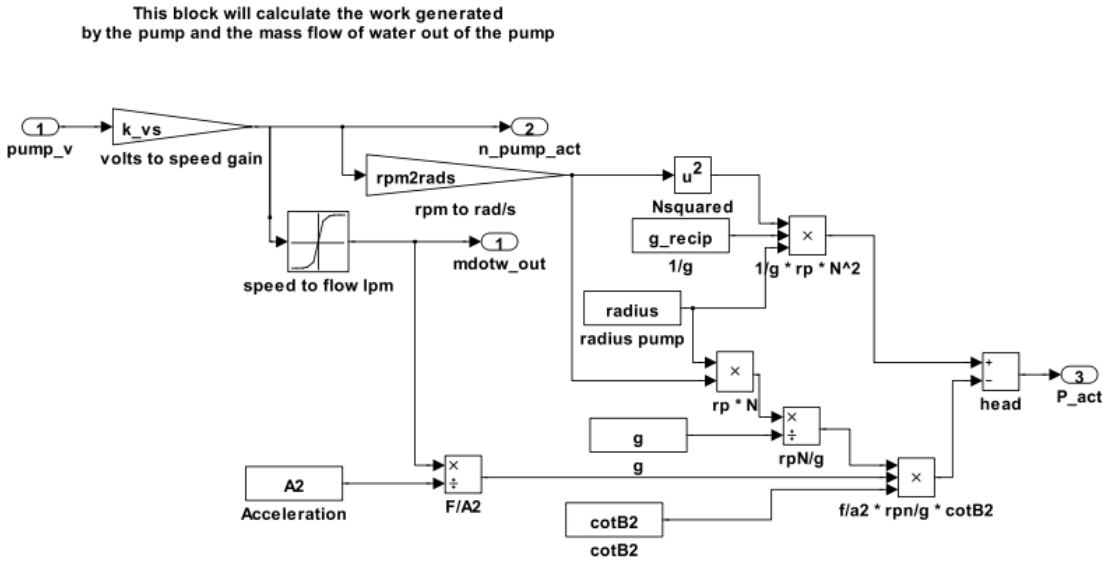

Appendix figure 86 Pump plant for the centrifugal pump model

A small test harness was developed, as shown in Appendix figure 83, input data was created and output data was recorded. The demanded pressure (P_{dem}) was set at 20 bar; the predicted mass flow rate of water value ($\dot{m}_{wpred}$) was varied over 10 seconds from 0.2 kg/s to 0.1 kg/s, at 4 seconds, and to 0.15 kg/s, at 7 seconds as shown in Appendix figure 80 in Section J.2.1.1.

Appendix figure 87 shows the output of the controller, the pump voltage ($pump_v$), which rises or falls when the predicted mass flow rate of water rises or falls, but is then altered by the control to maintain the correct mass flow rate of water.

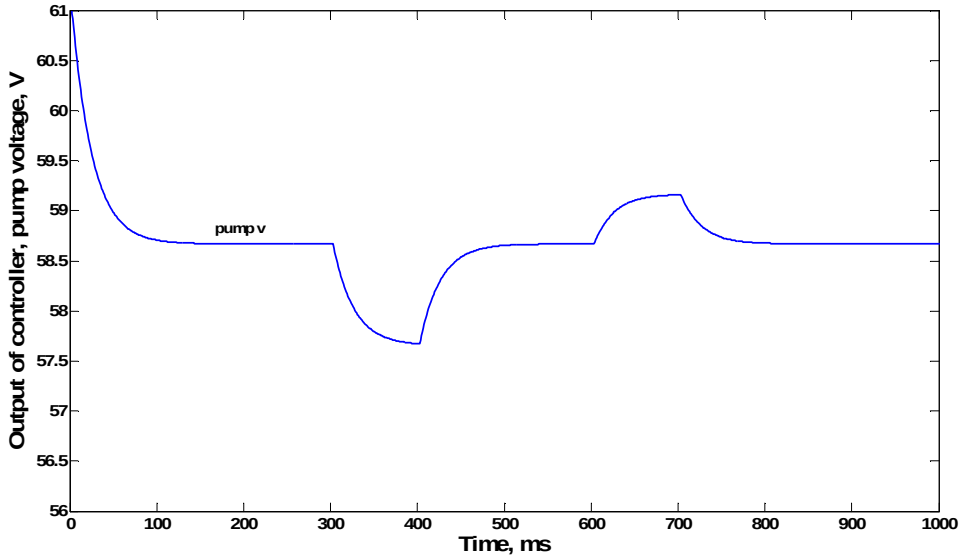

Appendix figure 87 Output of centrifugal pump controller, pump voltage, $pump_v$

Appendix figure 88 further shows the actual pressure (P_{act}) rises or falls momentarily when the predicted mass flow rate of water rises or falls, then returns to the demanded pressure value of 20 bar.

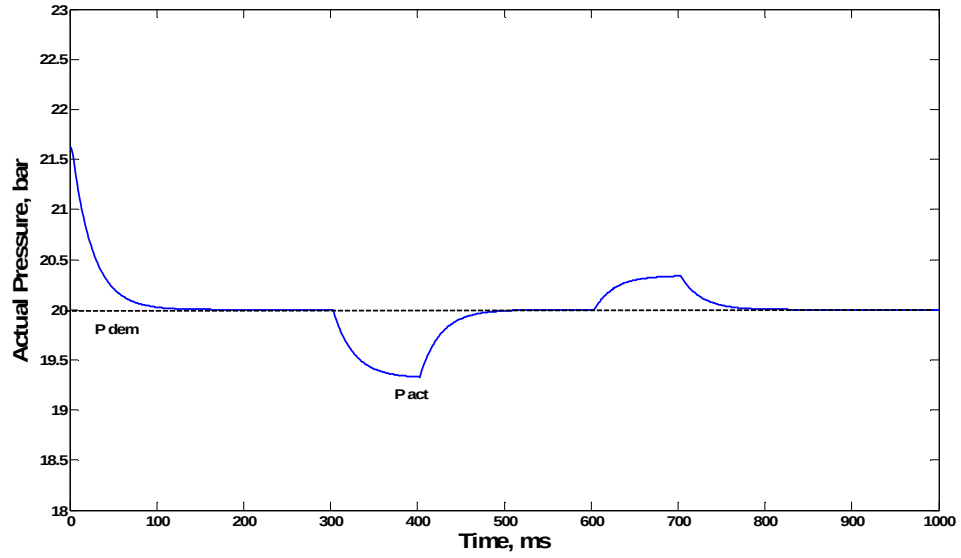

Appendix figure 88 Output of centrifugal pump, actual pressure, P_{act}

The demanded pressure is indicated by the dotted line and using this line it can be seen how quickly the controller acts to regulate the pump output. Appendix figure 88 is slightly different from Appendix figure 82 due to different settings for the PID controller and the behaviour of the two different pumps.

J.2.2 Expander control module

The expander control module controls the expander process by monitoring the torque demanded on the system (from the vehicle driver), the actual torque output from the expander and the pressure drop across the expander. The output variable of the controller, α, is a voltage that relates the opening time, or cut-off , value for the throttle valve to the expander inlet.

The torque output of the expander will be proportional to the upstream pressure, but not necessarily proportional to the value of α. The value of α will affect the work output, an increase in α will relate to an increase in work output and hence a decrease in α will result in less work output from the expander.

Any changes to α will affect the overall pressure of the system, unless coupled with corresponding change in the value of *n* from the pump controller module. Any changes in the upstream and downstream pressure should be monitored and the α altered accordingly so that $\dot{m}_w$ remains constant.

The speed of the expander will be governed by the IC engine speed, as the two will be coupled mechanically using a reduction gearbox.

The power output will need to be kept constant so that

$$P = T_{act}.n_{\exp ander} = K.n_{\exp ander}.\alpha \qquad \text{(J.7)}$$

where K is the proportional gain of the expander controller.

The control block diagram from Section J.1.2 is further developed as shown in Appendix figure 89. The variables are as follows:

T_{dem} - Torque demanded;

T_{act} - Actual torque output from expander;

P_{up} - Pressure upstream of the expander;

P_{down} - Pressure downstream of the expander.

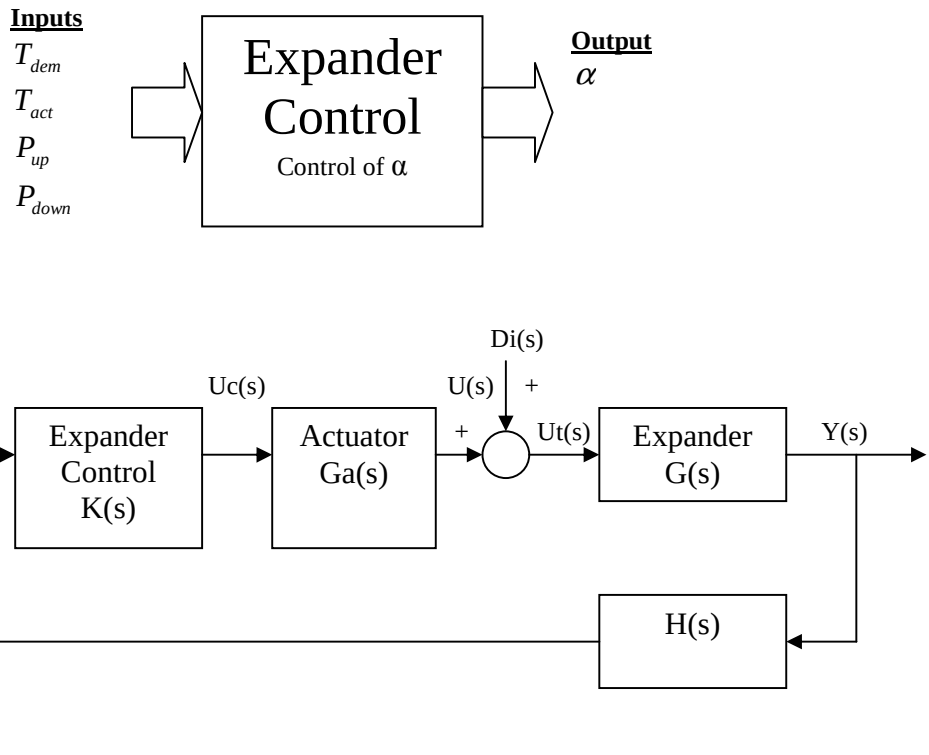

Appendix figure 89 Expander control module

Referring to Appendix figure 89, the control signals are as follows:

R(s) = T_{dem} ;

E(s) = T_{err} = R(s)-H(s);

Uc(s) = α (output of expander controller);

U(s) = α as a voltage;

Di(s) = predicted α voltage according to T_{dem};

Ut(s) = Expander valve input voltage = U(s)+Di(s);

Y(s) = Work (kj - expander output);

H(s) senses the work output and converts it to the T_{act} value.

A Simulink model was developed for the control module; the expander block contained equations to calculate work done, these equations were developed using the standard pv diagram for a steam expander, shown in Appendix figure 90.

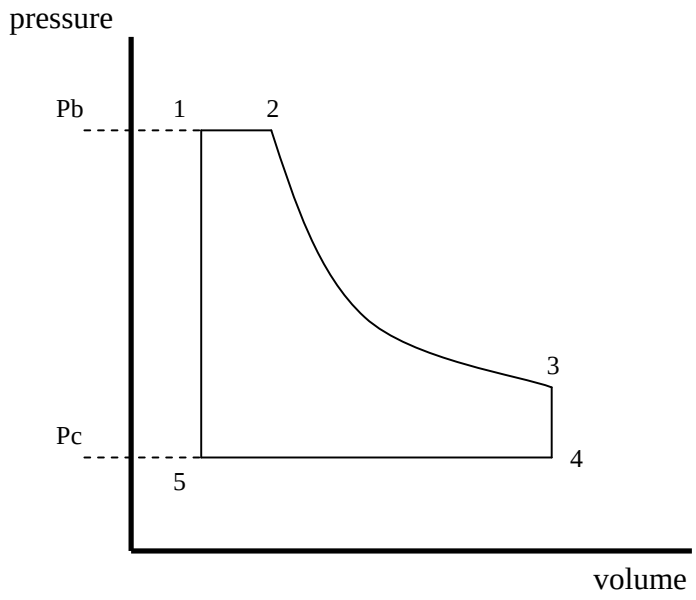

Appendix figure 90 pv diagram for a steam expander

Referring to the numbered points in Appendix figure 90:

$$work = \int p.\partial v \qquad \text{(J.7)}$$

$$= Pb.\alpha_v + \int_{\alpha_v}^{V} \frac{k1}{V^{\eta}}.\partial v - Pc.V_5$$

$$= \left((Pb.(\alpha_v.V)) + \left(\frac{k1}{1-\eta}\right).\left[\frac{1}{V_3^{\eta-1}} - \frac{1}{V_2^{\eta-1}}\right] \right) - (Pc.V_5) \qquad \text{(J.8)}$$

where:

$$k1 = Pb.(\alpha_v.V)^{\eta}$$

η=thermal efficiency of steam (1.4)

V = total Volume

V3=V

V2=V x α_v

V_c=Clearance Volume

The Simulink model for the expander is shown in Appendix figure 91 through Appendix figure 94.

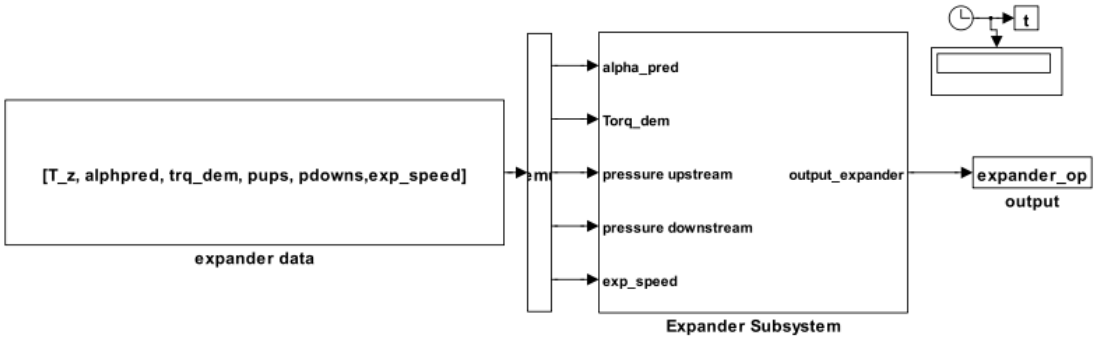

Appendix figure 91 Test harness for the expander model

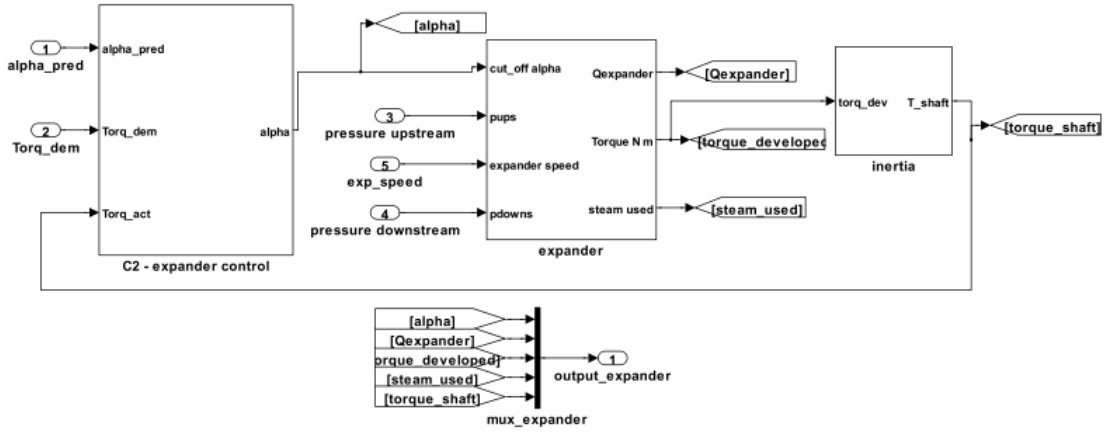

Appendix figure 92 Expander system model

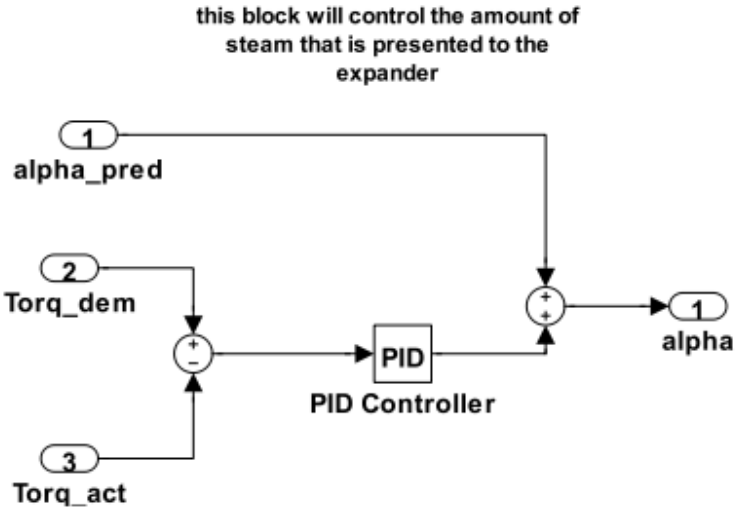

Appendix figure 93 Expander controller model

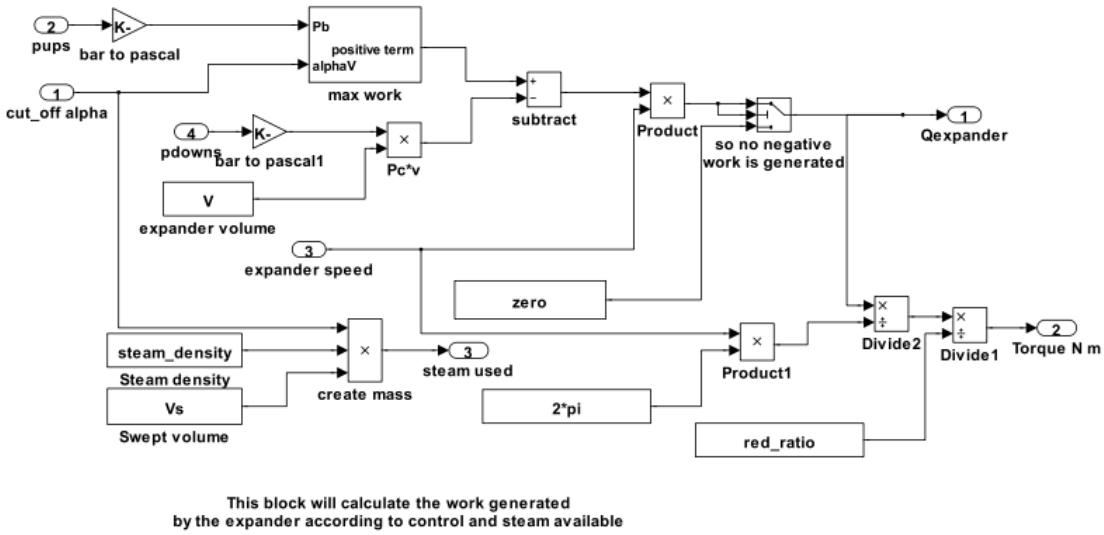

Appendix figure 94 Expander plant model

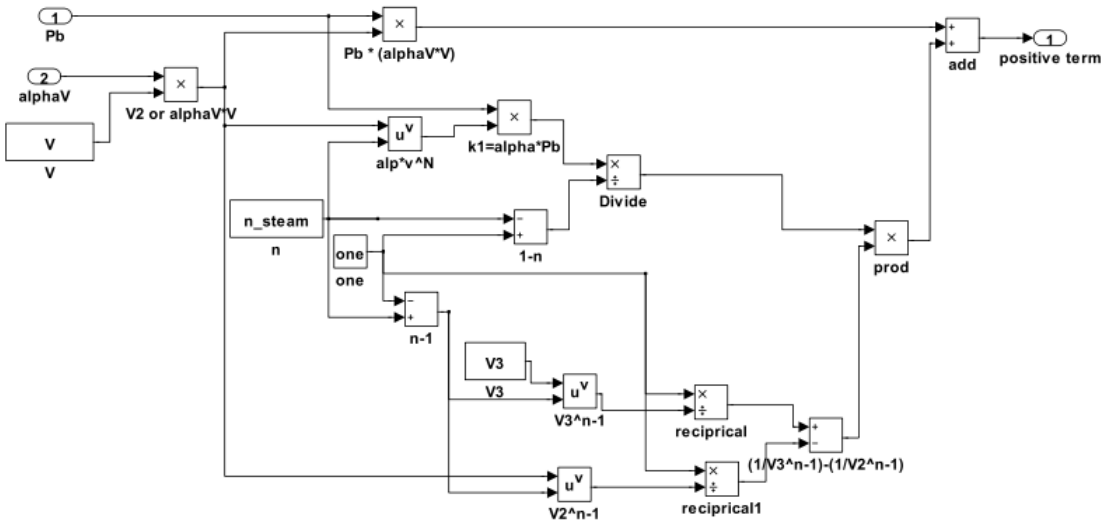

Figure 0-1 Expander plant, work calculation

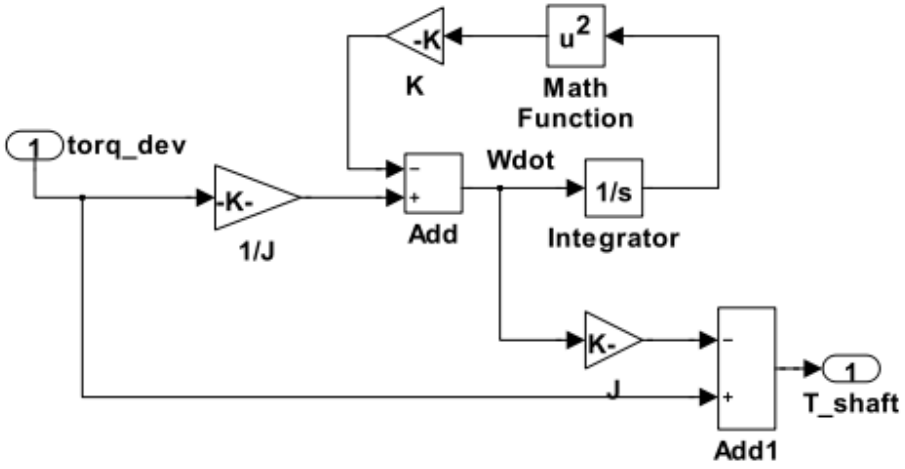

Figure 0-2 Expander model, inertia and shaft torque calculation

A small test harness was developed, as shown in Appendix figure 91, so that input data could be controlled and output data could be recorded. The demanded torque (T_{dem}) was set at 35 N m; the predicted cut-off value (α_{pred}) was varied over 10 seconds from 0.1 to 0.5, at 4 seconds, and to 0.8, at 7 seconds as shown in Appendix figure 95.

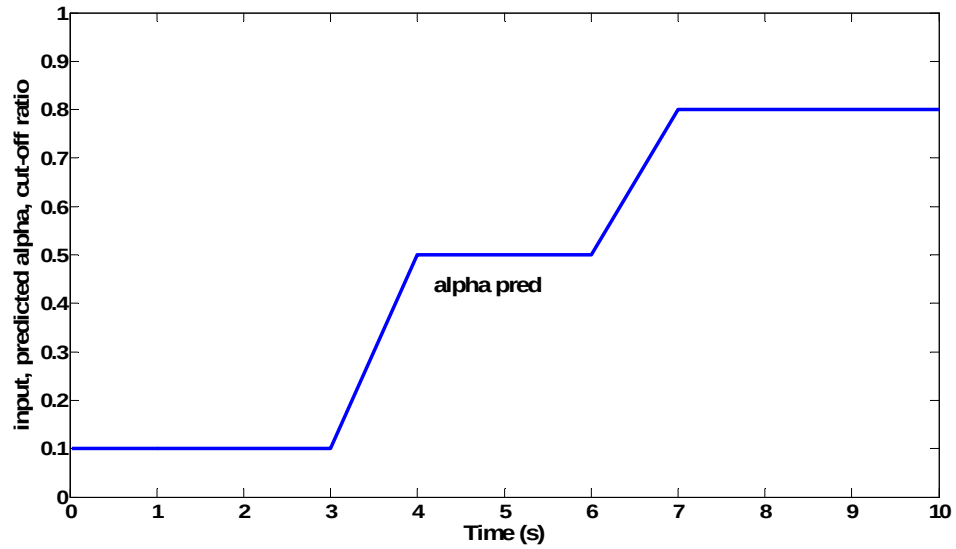

Appendix figure 95 Input to expander model, predicted cut-off ratio, alpha$_{pred}$

Appendix figure 96 shows the output of the controller, the cut-off ratio (α), which rises when the predicted mass flow of water rises, but is then altered by the control to maintain the correct torque output.

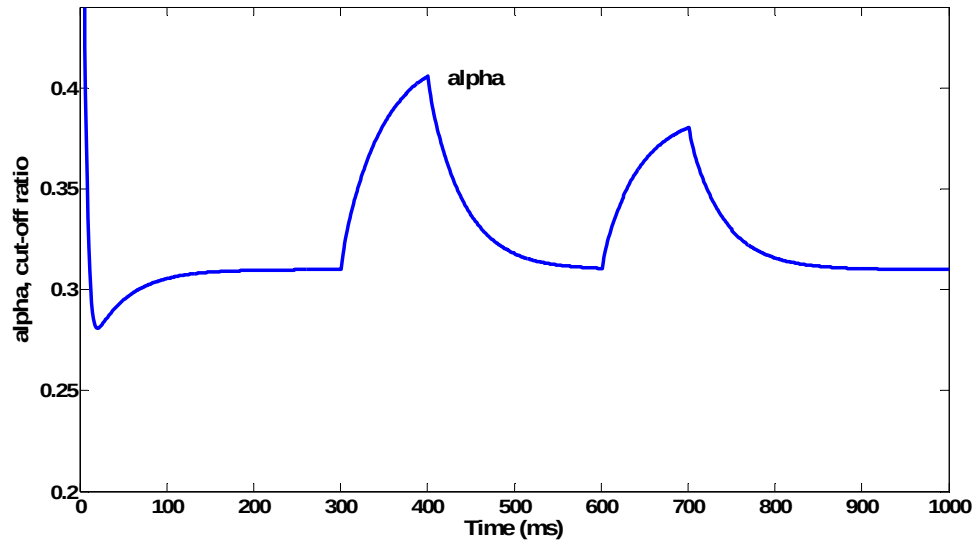

Appendix figure 96 Controller output, cut-off ratio, alpha

Appendix figure 97 further shows the actual shaft torque (T_{shaft}) rises momentarily when the predicted alpha rises, then returns to the demanded torque value of 35 N m.

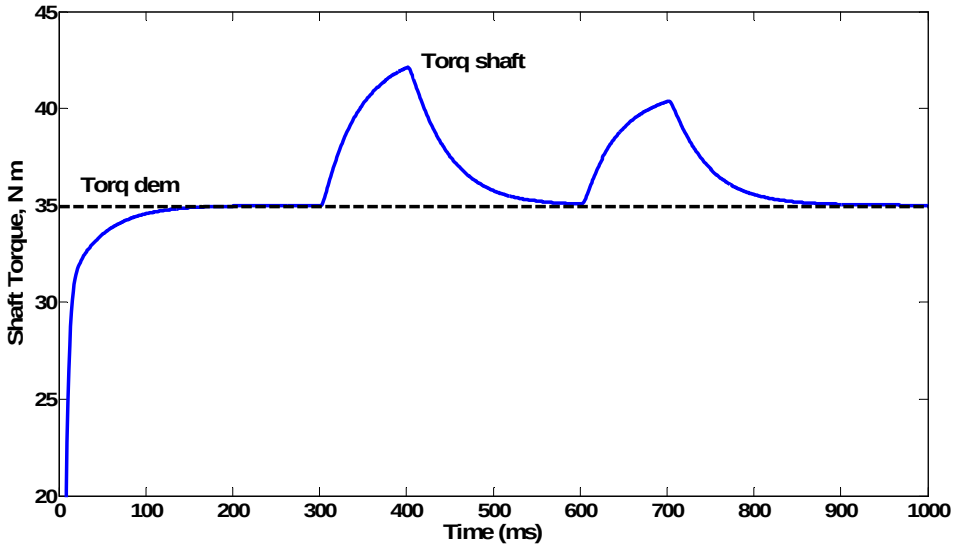

Appendix figure 97 Expander output after inertia, torque on shaft

The demanded torque is indicated by the dotted line and using this line it can be seen how quickly the controller acts to regulate the expander output.

J.2.3 Supervisory controller

The supervisory controller does not directly control a process, but controls the predicted inputs to the pump and expander controllers, $\dot{m}_{wpred}$ and α_{pred}, respectively. This is implemented through a series of algorithms that monitor the systems behaviors and selects the appropriate predicted signals. This is achieved by cross-coupling the response of the pump and expanders in order to stabilize the system so that when one changes and corresponding change is predicted in the other.

To cross-couple any changes in the system pressure to the predicted input to the expander the following equation is used:

$$\alpha_{pred} = K.\frac{P_n}{P_{n-1}} \qquad \text{(J.9)}$$

Where K is an appropriate gain value, P_n is current the system pressure and P_{n-1} is the previous value of system pressure. To cross couple any changes in torque developed by the expander to the predicted input to the pump, the following equation is used:

$$\dot{m}_{pred} = n_{\exp}.\alpha.V.\rho \qquad \text{(J.10)}$$

Where n_{exp} is the speed of the expander, V is the expander volume and ρ is the density of the steam at the system pressure.

Another algorithm for the supervisory control uses the heat exchanger data to monitor the volume and the heat flux information (from exhaust data) to ensure that enough water is flowing to the heat exchanger. This is achieved by monitoring the values of exhaust temperature ($\theta_{\min}$) and mass flow rate ($\dot{m}_{e\_\min}$) to ensure they do not go below the required value for steam generation. In this case the IC engine should be the sole provider of the torque until these values are reached.

J.3 Simulink files for the PID controlled steam system

This appendix contains the Simulink blocks used for the QSS-TB PID controlled steam hybrid model that is described to in Section 5.6.1. The model is divided into levels with level 1 representing the top level of the model and levels 2 through 6 representing the lower levels.

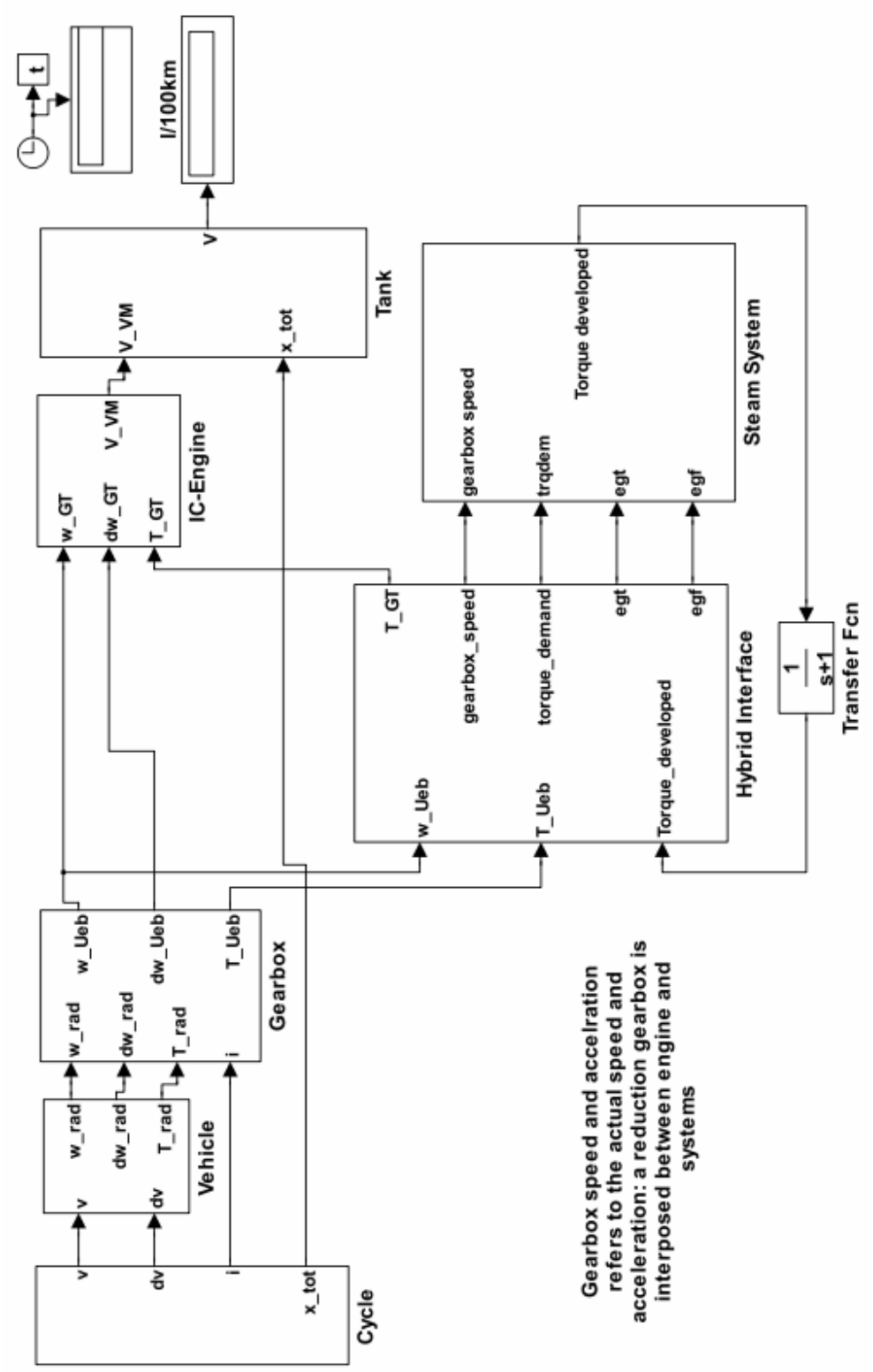

Appendix figure 98 Level 1 – QSS-TB PID controlled steam hybrid

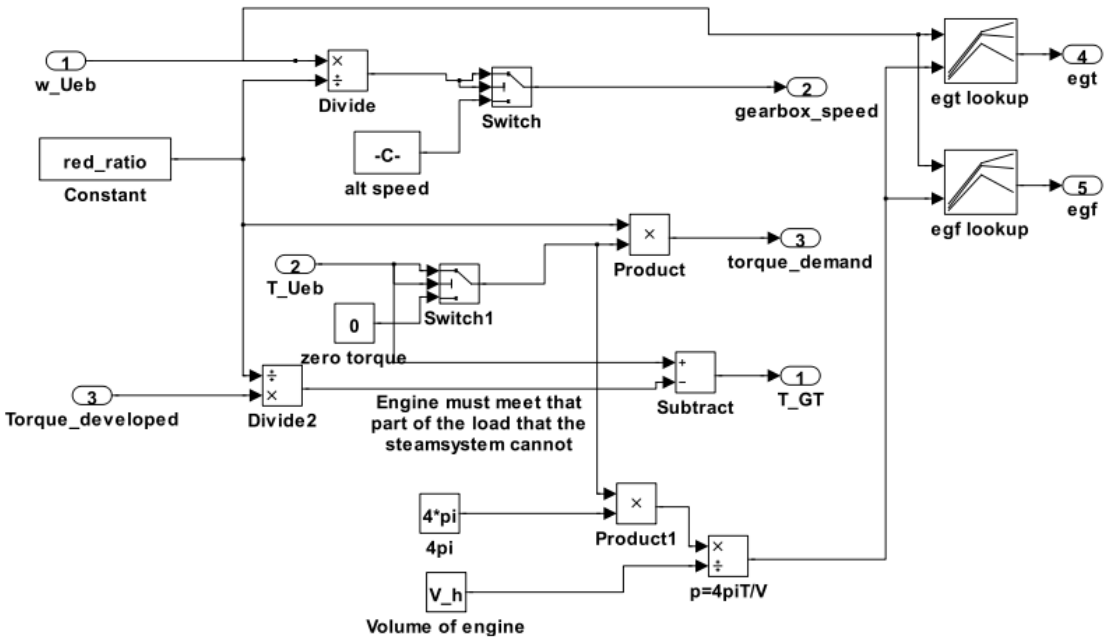

Appendix figure 99 Level 2 – Hybrid interface block

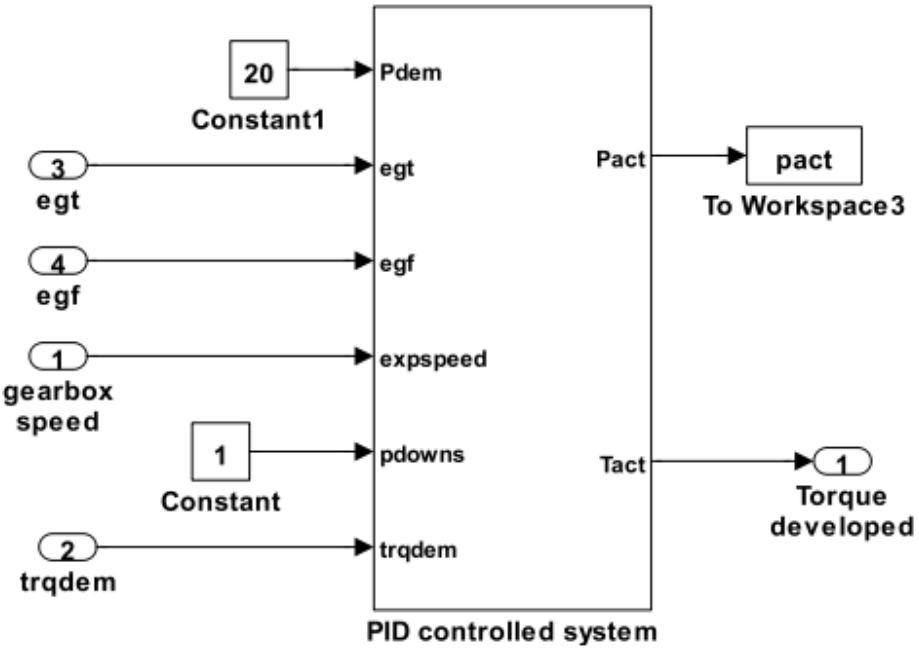

Appendix figure 100 Level 2 – Steam system

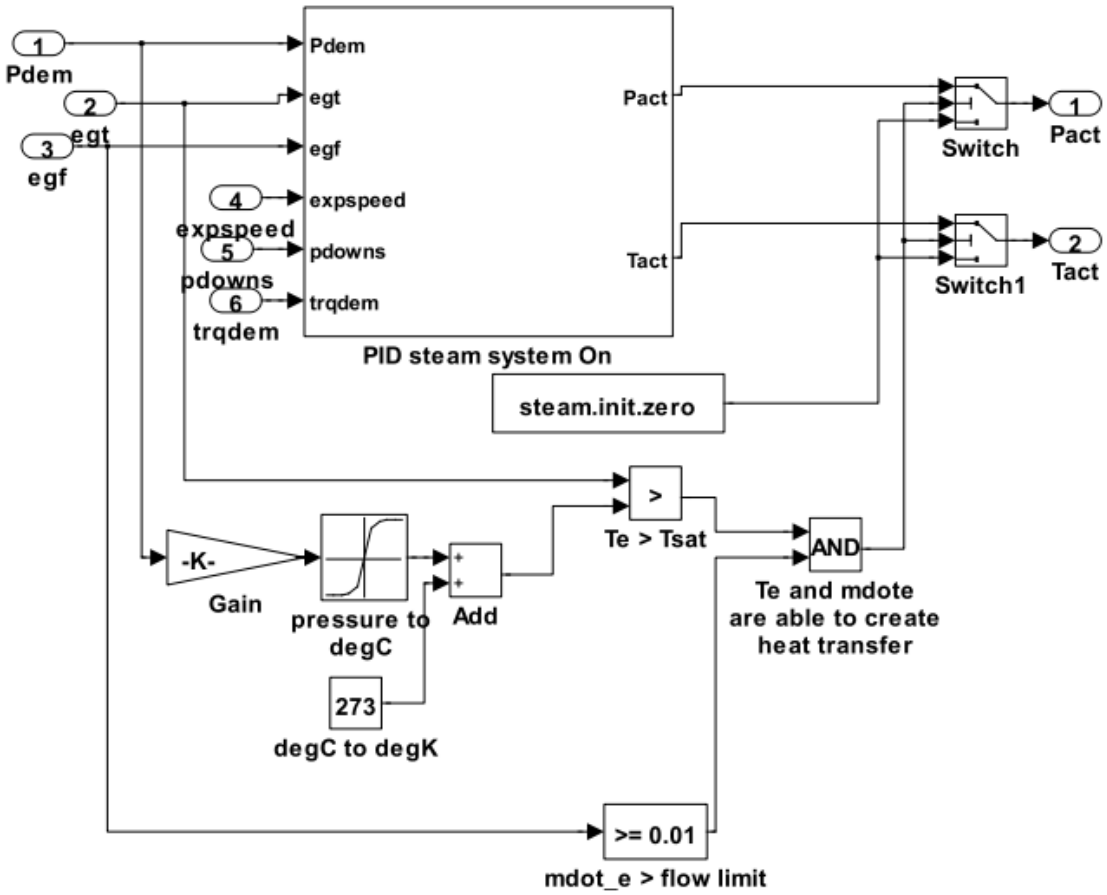

Appendix figure 101 Level 3 – PID controlled system

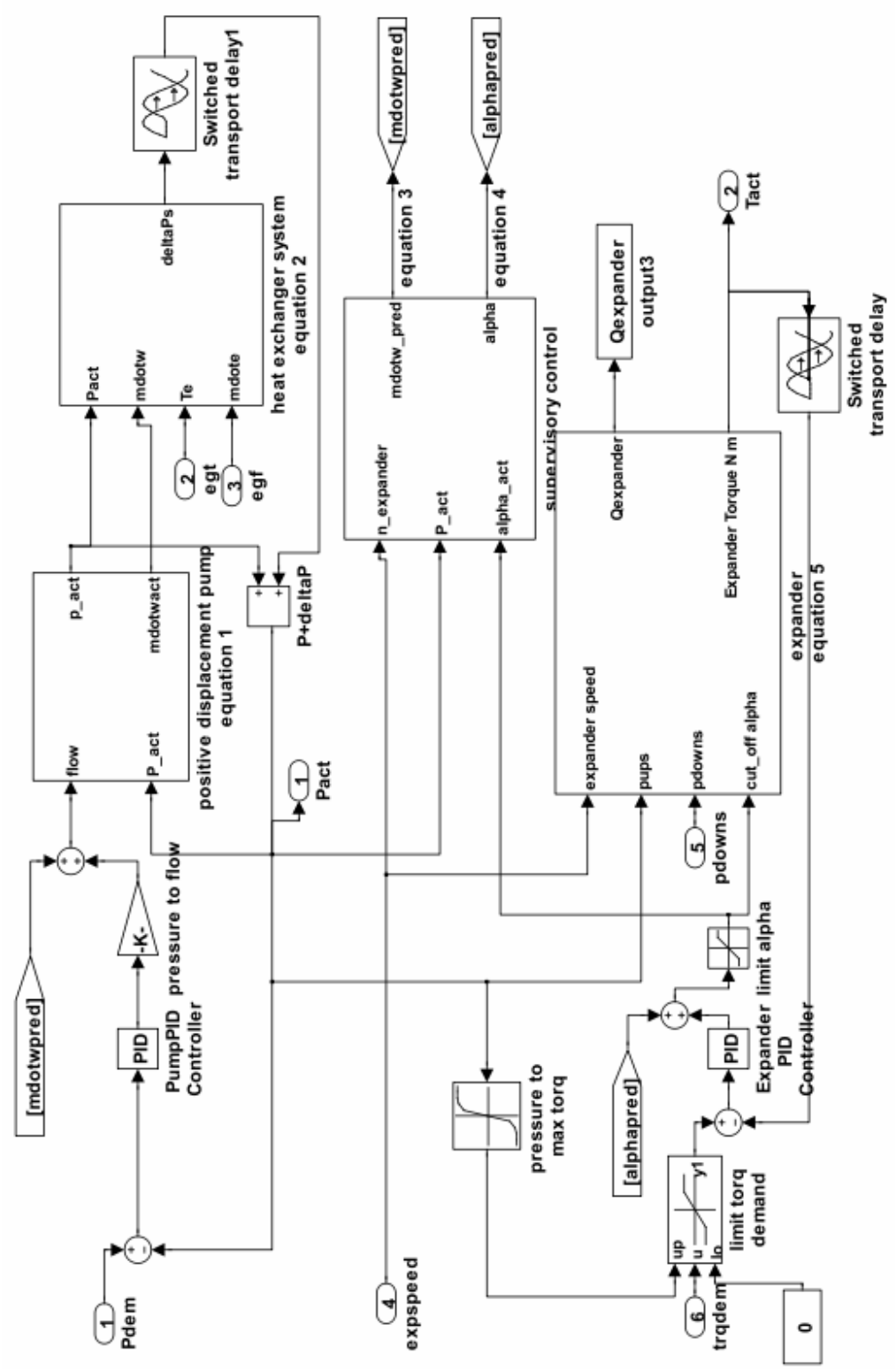

Appendix figure 102 Level 4 – PID steam system on

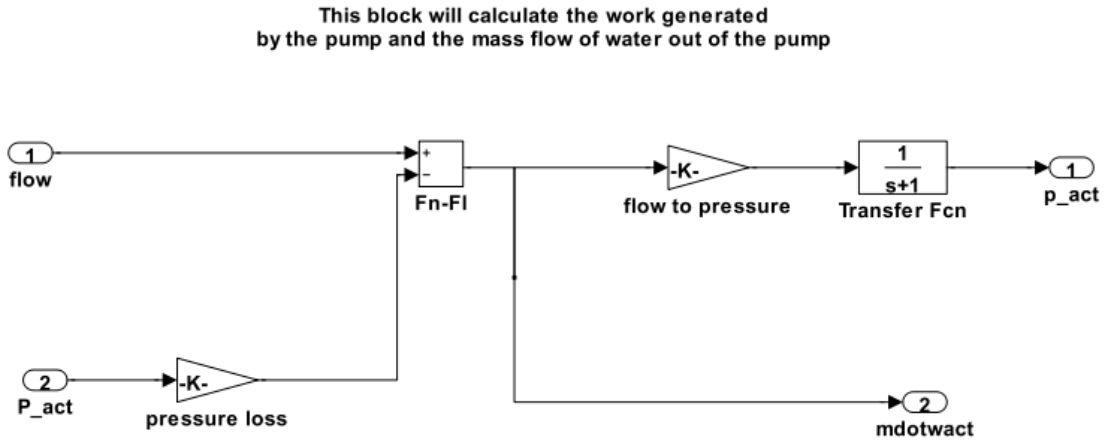

Appendix figure 103 Level 5 – Positive displacement pump

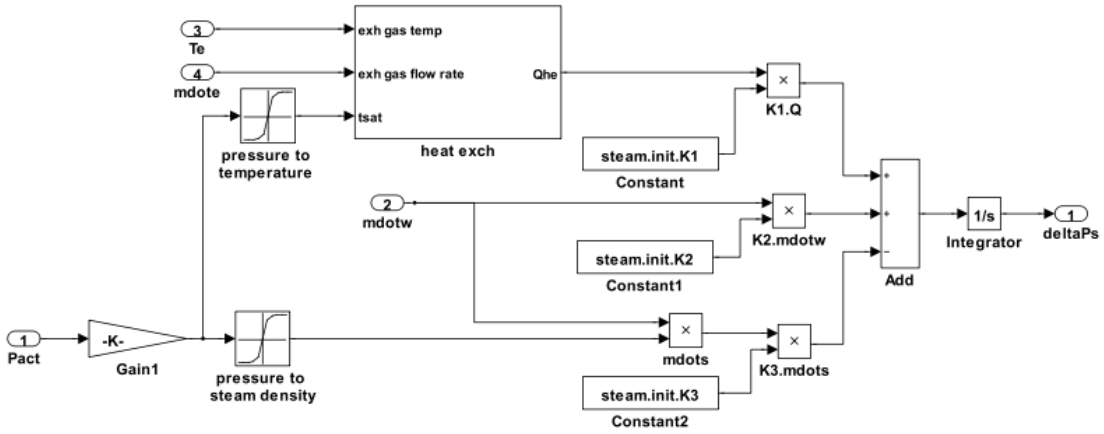

Appendix figure 104 Level 5 – Heat exchanger system

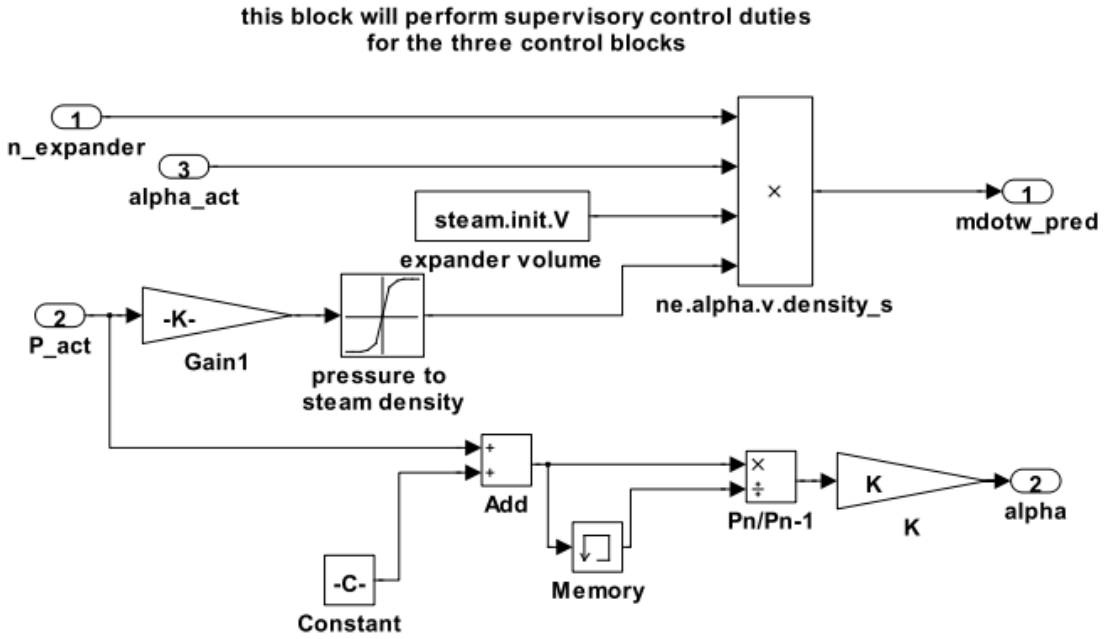

Appendix figure 105 Level 5 Supervisory control

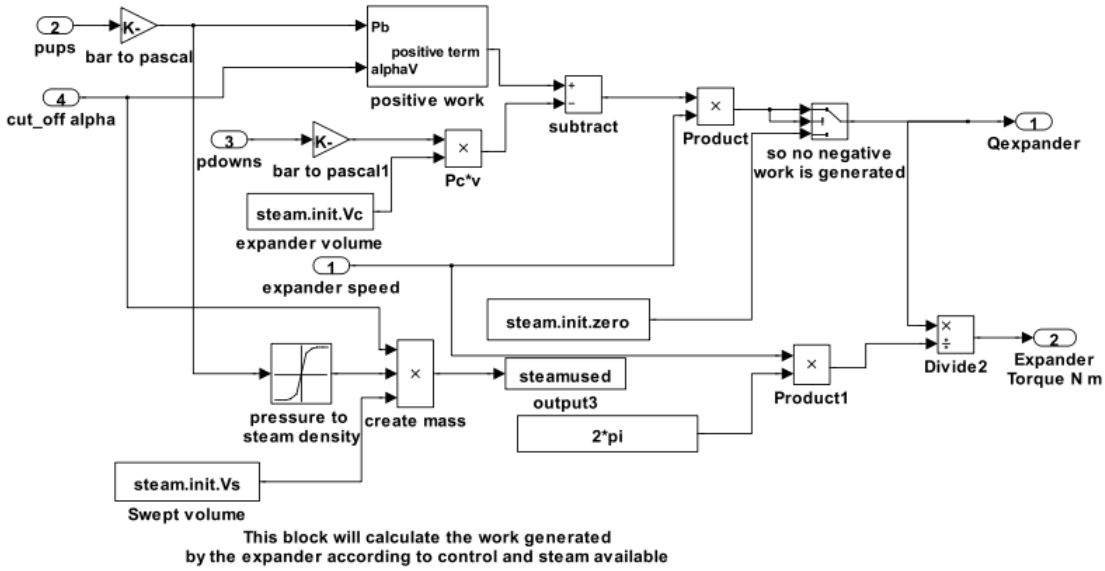

Appendix figure 106 Level 5 Expander

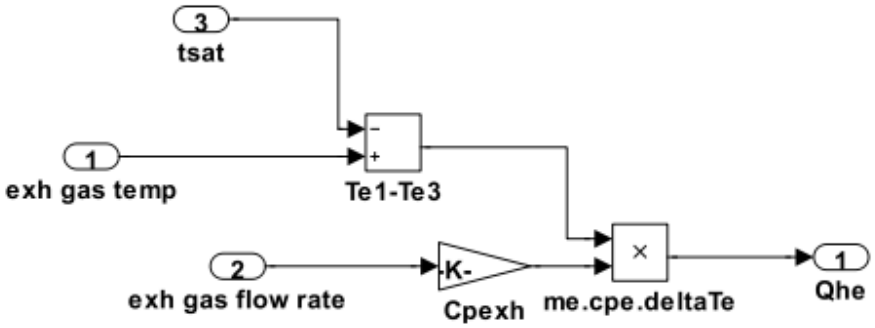

Appendix figure 107 Level 6 Heat exchanger

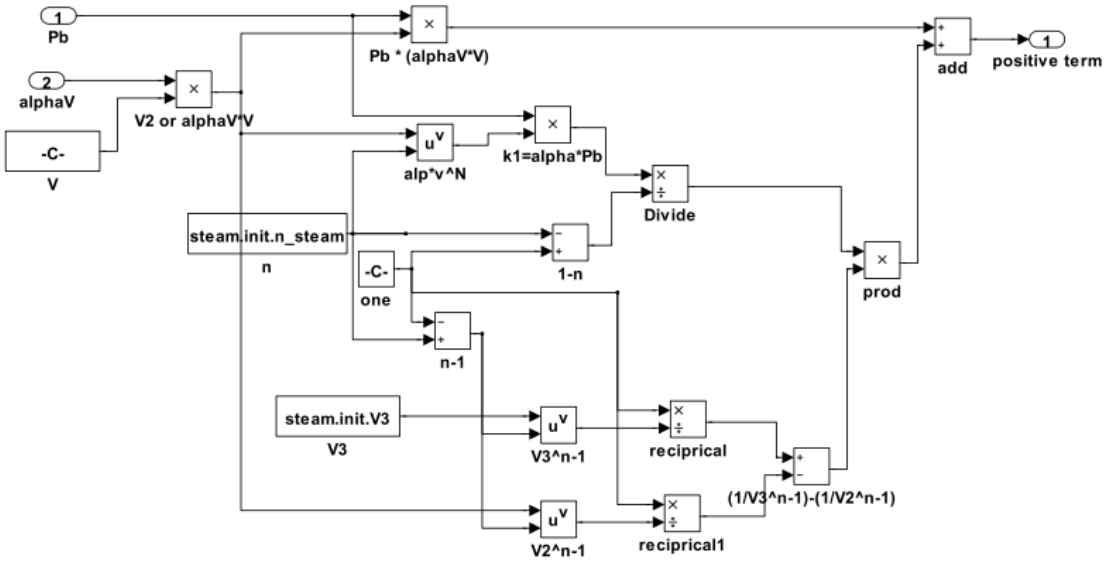

Appendix figure 108 Level 6 Positive work

J.4 PID Controller results

This section contains the results from running the PID controller with QSS and PSAT using the NEDC and US-06 drive cycles.

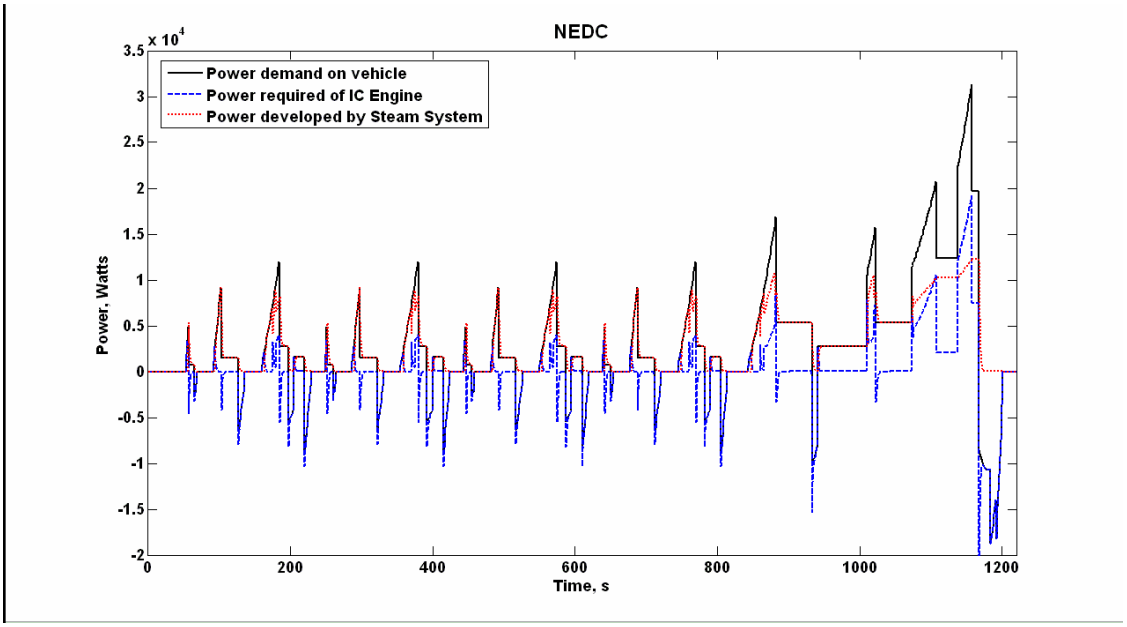

Appendix figure 109 Power comparison for QSS-TB PID controlled model, NEDC

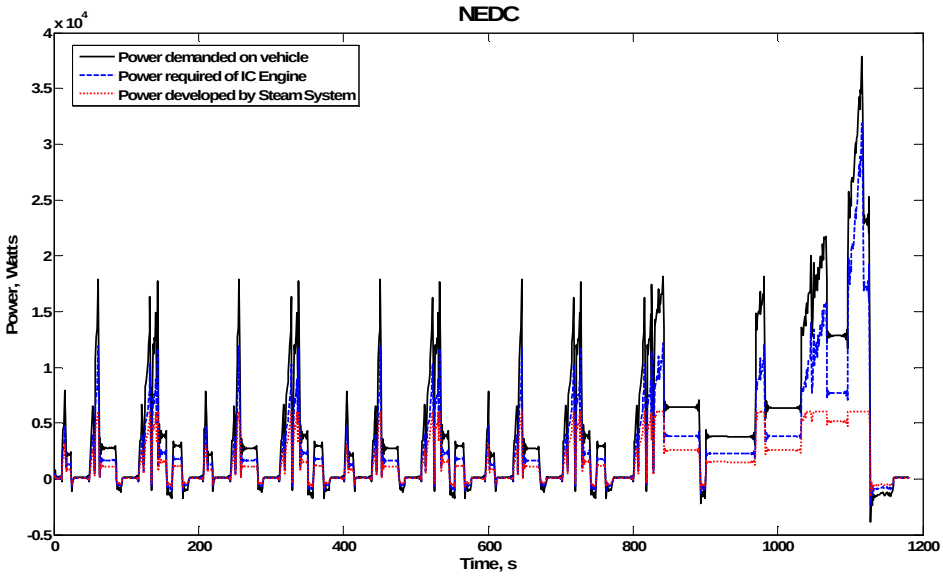

Appendix figure 110 Power comparison for PSAT PID controlled model, NEDC

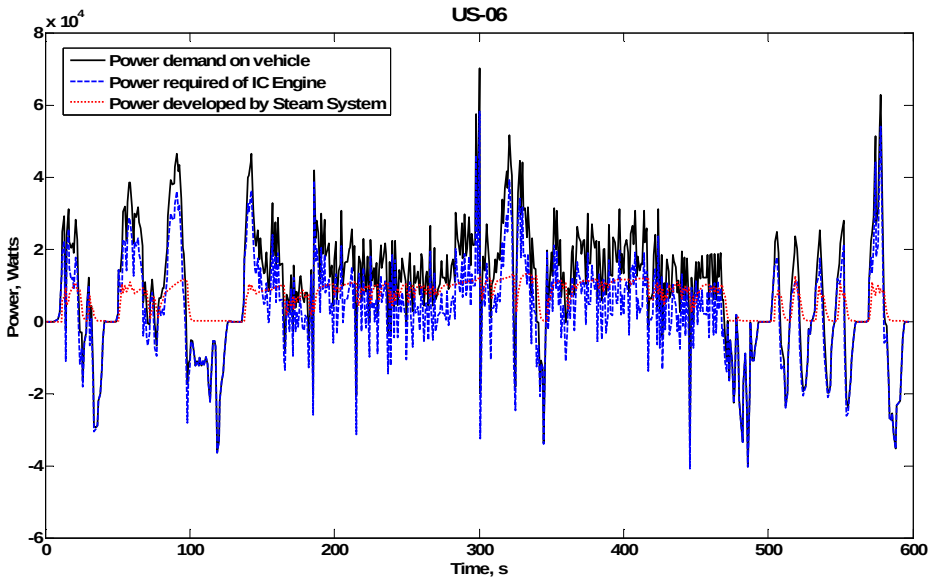

Appendix figure 111 Power comparison for QSS-TB PID controlled model, US-06

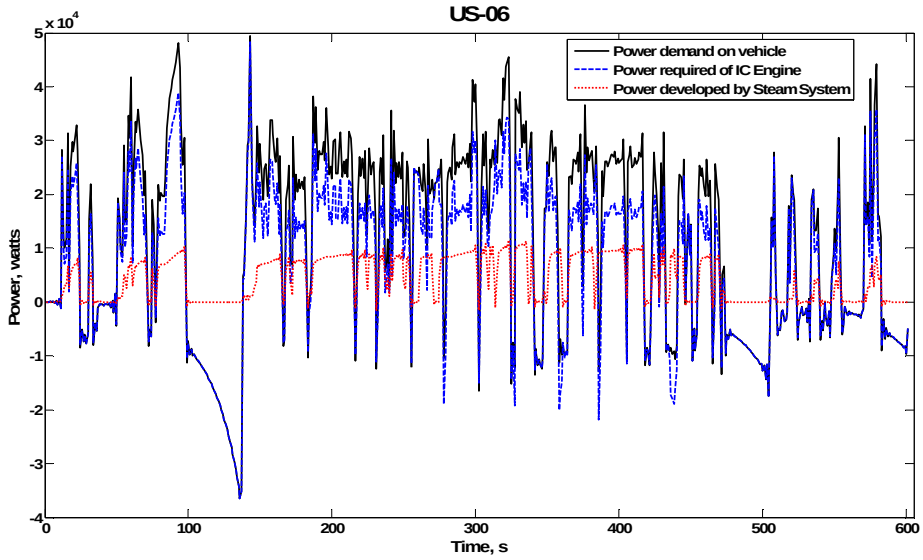

Appendix figure 112 Power comparison for PSAT PID controlled model, US-06